

CZECH TECHNICAL UNIVERSITY

Faculty of Civil Engineering



Diploma thesis

2004

Markéta POKORNÁ

Diploma thesis

EM 2000 Microbathymetric and HYDROSWEEP DS-2 Bathymetric Surveying – a Comparison of Seafloor Topography at Porcupine Bank, west of Ireland

MARKÉTA POKORNÁ

June 2004

Supervisor: Prof. Jan Kostecký, Czech Technical University in Prague
Second Supervisor: Prof. Günter Seeber, University of Hannover

Czech Technical University
Faculty of Civil Engineering
Department of Advanced Geodesy
Czech Republic

Alfred Wegener Institute
for Polar and Marine Research
Bathymetry and Geodesy Section
Germany



České vysoké učení technické v Praze
Fakulta stavební
166 29 Praha 6, Thákurova 7

ZADÁNÍ DIPLOMOVÉ PRÁCE

studijní program: geodézie a kartografie
studijní obor: geodézie
akademický rok: 2003/2004

Jméno a příjmení diplomanta: Markéta Pokorná
Zadávací katedra: katedra vyšší geodézie
Vedoucí diplomové práce: prof. Ing. Jan Kostecký, DrSc.
Název diplomové práce: Aplikace bathymetrie. Porovnání různých typů sonarových měření
Rámcový obsah diplomové práce: Na základě výsledků expedice ARK 19/3a porovnejte výsledky dvou typů bathymetrických měření ve vybraných oblastech

Datum zadání diplomové práce: 1. 3. 2004 Termín odevzdání: 11. 6. 2004

Diplomant bere na vědomí, že je povinen vypracovat diplomovou práci samostatně, bez cizí pomoci, s výjimkou poskytnutých konzultací. Seznam použité literatury, jiných pramenů a jmen konzultantů je třeba uvést v diplomové práci.

.....
vedoucí diplomové práce

.....
vedoucí katedry

Zadání diplomové práce převzal dne: 1. 3. 2004

.....
diplomant

Příloha: Specifikace zadání

MÍSTOPŘÍSEŽNÉ PROHLÁŠENÍ

Závazně prohlašuji, že jsem celou práci vypracovala samostatně s využitím uvedené literatury.

4.6.2004

Mé rodině

PREFACE

This Diploma thesis was written at the Alfred Wegener Institute for Polar and Marine Research in Bremerhaven in the period from January till May 2004, and following the expedition XIX/3a in June 2003 and the evaluation and processing of recorded data. The data were worked on at the Alfred Wegener Institute and partly at the French Research Institute for Exploitation of the Sea in Plouzané and in La Seyne sur Mer.

First of all, for getting the chance to take part in an expedition I would like to thank to Dr. Hans - Werner Schenke of the Alfred Wegener Institute, Bremerhaven.

I would like to cordially thank Professor Günter Seeber from the University of Hannover for his open scientific mind, for his opinions and advice, for his time and his enthusiastic support of my work.

I am very grateful to Professor Jan Kostelecký of the Czech Technical University for the leadership of this Diploma thesis, for his consultations and constructive remarks.

For help with the remedy of raw data problems, my thanks go to Christian Edy of IFREMER, Plouzané. For explanations of systems on the robot and the POSIDONIA navigation system, I am thankful to Severine Beraud and Dr. Jan Opderbecke of IFREMER, La Seyne sur Mer. For sustained answers to my questions I thank to Doc. Miroslav Hampacher from CTU Prague, and Hans Vos of QINSY support, Martin Pronk and Ottokarl Büchschütz-Nothdurft of CARIS support, Peter Gerchow of FIELAX and Dr. Andy Wheeler from University College Cork. I wish to express my gratitude to Hartmut Martens, Dr. Martin Klenke, Andreas Beyer, Dr. Klaus Dittmers, Fred Niederjasper, Daniel Schulte, Rike Rathlau and Jörn Hatzky from the Alfred Wegener Institute and especially to Ralf Krockner for his studious approach to problems, for making my acquaintance with GMT software, and for discussions. My appreciation goes to Dr. Graeme Eagles for responsive help with language corrections.

Finally, I would like to thank my family and friends, namely my grandparents, my parents, especially my caring mother, and also my sister Jitka. My thanks for support and encouragements go to all my friends, for all to Américo Montiel, Jirka Pinkava, Agnieszka Beszczyńska-Möller and Gerárd Laurantin.

I would like to mention the *Leonardo da Vinci programme* and *Nadation of Josefa, Marie a Zdeňky Hlávkových*, and express my thanks for their financial support of my studies, as well as the Geological Survey of Ireland for providing illustrations of Ireland's mapping project, KONSBERG SIMRAD for providing literature about echo sounder EM 2000 and H. von Lom-Keil and V. Spiess from the University of Bremen for the use of SENT software.

Last of all, I would like to thank to Ing. Lena Halounová who was there at the beginning of everything.

Bremerhaven, 27 May 2004
Markéta Pokorná

CONTENT

PREFACE.....	v
CONTENT.....	vi
ABSTRACT.....	ix
1. INTRODUCTION.....	1
2. BATHYMETRY THROUGH THE CENTURIES.....	3
3. NAVIGATION ON THE SEA.....	5
3.1 From Phoenicians to Microwaves.....	5
3.2 Positioning onboard R/V POLARSTERN.....	6
3.2.1 GPS receivers.....	6
3.2.2 Common reference point and local coordinate system.....	7
3.2.3 Global coordinate system and UTC.....	8
3.2.4 Linear transformation.....	8
3.2.5 Inertial navigation.....	9
3.3 How to locate the underwater robot VICTOR 6000.....	12
3.3.1 Local coordinate system and sensors.....	12
3.3.2 Navigation system POSIDONIA.....	13
3.3.2.1 Principles of ultrashort baseline navigation.....	14
3.3.2.2 Calibration.....	14
3.3.3 Dead reckoning.....	16
3.3.3.1 Polygonal parallel	16
3.3.3.2 Transformation between systems.....	17
3.3.4 Computation of coordinates.....	19
3.3.5 Accuracy and errors.....	20
3.3.5.1 Long Baseline and moored transducers.....	20
3.3.5.2 Specific examples by means of screenshots.....	20
4. WORKING AREA, INSTRUMENTS, DATA SAMPLING AND HANDLING	23
4.1 Irish waters and chronological exploration of the Porcupine Bank.....	23
4.2 Expedition ARK XIX/3a.....	26
4.3 Carbonate mounds.....	26
4.4 Research vessel POLARSTERN.....	27
4.5 ROV VICTOR 6000.....	28
4.6 Used mapping instruments.....	30
4.7 Bathymetric software, data circulation and archival.....	31
4.8 Progress of work and problems with XTF format.....	33
4.9 Four microbathymetric surveys.....	35

7. COMPARISON AND INTERPRETATION.....	81
7.1 Data distribution	81
7.2 Differences.....	82
7.2.1 Input and output data.....	83
7.2.2 Interpretation of difference grids.....	84
7.3 Profiles of area SM4.....	87
7.4 Correlation	90
7.4.1 Correlation coefficients.....	90
7.4.2 Regression curvatures.....	90
7.5 Coherence analysis.....	91
7.5.1 Recommendation: grid merging.....	92
7.6 Results and discussion: comparison.....	93
8. CONCLUSIONS.....	95
8.1 Raised queries.....	95
8.2 Recommendations and remarks.....	96
8.3 Comparison and marine methods.....	97
ABBREVIATIONS.....	98
LIST OF FIGURES.....	100
LIST OF TABLES.....	104
REFERENCES.....	105
APPENDIX A: Digital terrain models – overview.....	I
APPENDIX B: Sound velocity profiles used.....	IV
APPENDIX C: Tidal flow applied on microbathymetric measurements.....	VI
APPENDIX D: Track plots of R/V POLARSTERN and ROV VICTOR 6000.....	IX
APPENDIX E: POLARSTERN & VICTOR parameters.....	XIV
APPENDIX F: Digital terrain models - RAW data.....	XVI
APPENDIX G: Visualisation of digital terrain models and their differences.....	XXI
APPENDIX H: Digital terrain models - GMT software.....	XXVI
APPENDIX I: Difference grids - CARAIBES software.....	XXXV
APPENDIX J: Digital terrain models provided by GSI	XXXVIII
APPENDIX K: PARASOUND data images.....	XL
APPENDIX L: Sidescan images.....	XLV
APPENDIX M: Mosaicking images.....	XLVIII

ABSTRACT

One of the latest discoveries in the world oceans are carbonate structures in the North-East Atlantic. In the frameworks of several European projects, the research vessel POLARSTERN and underwater robot VICTOR 6000 were engaged to explore these areas. The data described in this thesis were collected during the expedition ARK XIX/3 between 16 - 19th June 2003. Bathymetric and microbathymetric data in parts of the Pelagia Province, located on the northern Porcupine Bank, west of Ireland, were measured with two multibeam sonar systems deployed at different distances from the bottom. The four compared models come from a KONGSBERG SIMRAD EM 2000 multibeam sonar system and an ATLAS ELEKTRONIK HYDROSWEET DS-2 multibeam sonar system. After necessary corrections of the data, digital terrain models were created, subtracted and correlated using appropriate software.

This thesis begins with a description of the historical background of bathymetry, followed by a description of the principles of navigation and underwater navigation, inertial navigation systems, and the calibration of these systems. Systematic errors will be pointed out. It examines the measurement principles of the echo sounders used on the ARK XIX/3a expedition and accompanying necessary procedures, such as CTD measurements. A discussion of how the data are processed from raw data to edited results, and the effects of the errors, follows. One chapter is dedicated to a comparison and interpretation of the data. Sidescan, mosaic and PARASOUND data from the Hedge and Scarp Mounds are introduced as complementary information.

ANOTACE

Jedním z posledních objevů ve světových oceánech jsou karbonátové hůrky na severovýchodě Atlantického oceánu. Do několika evropských projektů určených k průzkumu těchto oblastí byla zapojena výzkumná loď POLARSTERN a také podmořský robot ROV VICTOR 6000. Data pro tuto diplomovou práci byla naměřena na expedici ARKXIX/3a, která se konala 16.-19.června 2003, na severu Porcupinské pánve, západně od Irska. Batymetrická a mikrobatymetrická měření z oblastí provincie Pelagia byla získána dvěma sonarovými systémy z různých vzdáleností od mořského dna. Čtyři porovnávané modely pocházejí z měření sonaru KONGSBERG SIMRAD EM 2000 a sonaru ATLAS ELEKTRONIK HYDROSWEET DS-2. Po editacích dat byly vytvořeny digitální modely podmořských terénů, které byly odečteny a korelovány v příslušných programech.

Tato práce začíná krátkou historií batymetrického měření, pokračuje popisem navigačních principů, principů inerciální navigace a kalibračních systémů. Jsou zmíněny systematické chyby, které navigaci ovlivňují. Dále jsou uvedeny principy sonarů, kterými bylo měřeno na expedici ARK XIX/3a a další nezbytné procedury, např. měření CTD. Jedna z kapitol pojednává o zpracování dat a efektech, které mohou měření zkreslovat. Další kapitola je věnovaná porovnání modelů terénu a interpretaci výsledků. Metody sidescan, mozaika a PARASOUND jsou představeny jako doplňující informace o oblastech hůrek Scarp a Hedge.

1. INTRODUCTION

More than 100 years ago, the American naval officer and hydrographer Matthew Fontaine Maury failed to foresee the technical developments of coming years. "Man can never see, he can only touch the bottom of the deep sea, and then only with the plummet" (Maury, 1893). At that time, he could not believe that it would be possible to achieve the equivalent of dropping thousands of "plummetts" to the seafloor and so obtain fine scale deep-sea topography in just a few minutes.

The earliest technique of measuring bathymetry involved lowering a heavy rope of known length to the bottom to measure the ocean depth. The accuracy of this principle was improved with the echo sounding method, where the travel time of a sound pulse sent from a vessel, and reflected back to it from the seafloor is noted. This allowed continuous depth measurement, rather than measurements of depth at a single point, to be done (Encyclopædia Britannica, 1987).

Bathymetric data will be handled in this thesis in order to obtain digital terrain models of areas, located on Porcupine Bank, west of Ireland, and these models will then be compared. These areas of unusual seafloor morphology were mapped in detail by two different sonar systems – the KONGSBERG SIMRAD EM 2000 multibeam echo sounder and ATLAS HYDROSWEEP DS-2 multibeam echo sounder.

Irish offshore research has intensified in the last few years. Detailed bathymetry data have been collected over more than 400 000 square kilometres of the continental shelf since July 2000. The purpose of the "Irish National Seabed Survey" is to prepare for the use of Irish marine territory for more commercial purposes and to effectively protect the marine environment; it is one of the largest seabed mapping projects undertaken anywhere in the world (Geughegan, 2003).

In order to explore seafloor areas more accurately and to reduce the risks to divers' lives, underwater robots have been intensively developed in the last 30 years. One of the first simple robots was made in 250 B.C. – the water clock of Ctesibius of Alexandria and one of the latest in a series of miniature submersibles is an undersea robot, ROV VICTOR 6000 (Drogou, n.d.).

ROVs (Remotely Operated Vehicles) are generally used in many fields and many applications. They have proved themselves as a unique aid to ocean exploration. The VICTOR 6000 project started 12 years ago. In contrast to its predecessor - Rebikoff's "Chien Plongeur" of 1954 (Ward, 2003), it can be deployed from aboard a surface vessel into depths of up to 6 000 metres. Equipped with video cameras and lights, it facilitates microbathymetric measurements and is connected to the ship by means a power transmission cable which carries the video signal and other sensor data to the surface.

Bathymetry has been defined as the "measurement of ocean depth"(Encyclopædia Britannica, 1987) and as "the measurement of water depth at various places in a body of water; also: the information derived from such measurements"(Merriam-Webster Online Dictionary, 2004). Microbathymetry is not defined in encyclopædias. Though the root is the

same in both words, their meaning is quite different. Microbathymetry cannot be defined as precise *micro*- measurement of water depths. There is a difference in measurement technique compared to traditional bathymetry developed from plummet measurement: the microbathymetric depth includes components from sonar or altimeter values and pressure sensor values, whereas bathymetric depths come directly and only from sonar.

For the purposes of this thesis, *microbathymetry* will be defined as underwater surveying with the aim of obtaining seafloor information about micromorphology (understood as detailed size, shape, and structure) and human-made features in large, intermediate, fine or ultrafine resolution with video observation scales. Georeferenced video sequences are understood as a new dimension of seafloor topography, or rather microtopography, with centimetre size features per single video image.

The principles of microbathymetry were made use of on projects whose aim was to explore carbonate mounds and deep coral communities in the Porcupine Seabight and Rockall Trough. After spectacular discoveries on the Irish Continental Margin, European scientists became interested in the mounds, with the effect that exploration of the area became part of several European projects (European Communities, 1995-2003, 2000)

As part of various European projects and within framework of a Franco-German co-operation, the ARK 19/3 expedition was organised by the Alfred Wegener Institute for Polar and Marine Research (AWI) and the French Research Institute for the Exploitation of the Sea (IFREMER) in June 2003. The first part was carried out in the area of the Porcupine Seabight and the Porcupine Bank, to study carbonate mounds and deep-water corals. The French deep-sea robot VICTOR 6000 was deployed. The stable platform for the dives was provided by the German research vessel POLARSTERN.

Multibeam echo sounder data collected aboard POLARSTERN was acquired using the ship's HYDROSWEEP DS-2 multibeam system. The multibeam data from the SIMRAD EM 2000 echo sounder, measured a few metres above the sea-floor, was sent from VICTOR to the POLARSTERN by fibre optic cable. Hence, two different types of bathymetric information were obtained during the expedition.

A number of questions arise if we think about comparing different density data originating from instruments deployed at unequal distances from the bottom. How can we compare these data? Does correlation provide sufficient statements about the data? Is the comparison of such small areas conceivable for deep sea sonar? Will the offset between the two grids be close to zero, or will the DTMs of areas have a constant offset? How can we merge the data to get an optimal terrain? What aspects influence the values of differences? Do both systems recognize small mounds of a few meter size? Does it make sense to subtract the data? We can speculate but we cannot clearly answer these questions if we do not try to provide a comparison.

The objectives of this work are to interpret subtracted models of four areas stemming from surveying with the Shallow Water Multibeam Sonar SIMRAD EM 2000 and with the Hydrographic Multibeam Sweeping Survey Echosounder for Deep Sea, to show correlative statistics of these models, and to introduce the other methods of marine surveying.

2. BATHYMETRY THROUGH THE CENTURIES

The first purposeful measurements of the depths were provided by “lead and line”. Theoretical ideas of acoustics in water were probably first introduced by Leonardo da Vinci (1452-1519) when he thought about identifying ships through listening for the noise they make in water. Soundings first appeared on charts around 1550, mostly in shallow waters.

Ocean depths were measured with a device whose origins are in Arabic or Jewish science. A simple system was created with a weight and a float. When the weight hit the bottom, the float broke away and rose to the sea surface. The depth was calculated from the time between launching and emergence. The accuracy of such measurements was influenced by currents, and a true vertical depth was not always found. The open ocean provided many operating complications.

One of the earliest sounding machines with a mechanical “waywiser” and a pressure gauge was developed by Robert Hooke at the end of the 17th century (Deacon, 2003). Experiments, and improvements to sounding machines, followed. The military surveyor Luigi Ferdinando Marsigli ascertained that depths increase with distance from the coast into regions where they were no longer measurable. This led to Marsigli’s conviction that the sea is bottomless. When officer Maury introduced the first bathymetric chart of the North Atlantic around 1850, some sounding values appeared anomalously deep to him.

Improved mechanical sounders got a new view of the world when transatlantic cables were laid for the purposes of submarine telegraphy between Europe and North America; not only the depth, but also the nature of the bottom, temperature, pressure, currents and tide information were observable. The 19th century became an important stepping stone in technological progress in marine research. Among others, even Prince Albert I of Monaco enriched marine and bathymetric knowledge at that time, by undertaking expeditions from the equator to the Arctic. A new generation of vessels used steam propulsion and wire sounding. The greatest oceanic depth, of 5269 fathoms* (9636 meters), known at the end of the 19th century was near Guam (Deacon, 2003).

Continental drift theory and sea-floor spreading observations belong to the 20th century. This century saw two world wars that forced the development of marine technologies such as submarines and bathyscapes, and ushered in a new era in the study of the sea in all its aspects. Research into underwater acoustics was undertaken; seismology, magnetics, sedimentology and long-range navigation to locate vessels far offshore improved, and these techniques were applied to collect more widespread data sets (Monahan, 2003). New instruments were used for recording or photographing at sea. War brought new knowledge of the transmission and reception of sound in the water. Captain Scott used one of the first echo sounders on his cruise to South Georgia in 1924. At that time, soundings were sent from a “circle of inflated rubber tube, with a hammer at its centre striking on a diaphragm” (Ommanney, 1961). This system was lowered into the water, but later systems were incorporated into the ship’s hull. Sonar systems began to be widely used in fishing and also trawling, and for mapping.

* 1 [fathom] = 6 [feet] = 1.8288 meters

Step by step, new innovations were introduced, and at the beginning of the 21st century, steam is replaced by gas, and modern research ships carry a wide range of instruments. Further ingenious sensors are to be found on submarine ROVs, powered by efficient electric engines. It is possible not only to “see the bottom of deep sea” but also to record sub bottom scenes and even remove samples of rocks, plants or animals using robot grabbers. Acoustic methods have come to be used in both depth and sidescan measurements. Lower frequencies output information about the structure of the earth’s crust. Small variations in the earth’s magnetic field and gravity field can be used to detect seafloor rocks and the theory of sediment transportation by currents was developed (Laughton, 2003).

Bathymetry serves primarily for the creation of accurate nautical maps and, for example in industry for the survey of places to lay ocean cables. Bathymetric measurement revealed the presence of the mid ocean ridge, encircling the whole earth for over 50 000 km. The highest mountain in the world is Mauna Kea, with its summit 4 205 m above sea level and its feet on the floor of the Pacific Ocean at a depth of 5 500 meters. Mauna Kea is the highest mountain of the Hawaiian Islands.

Bathymetry constantly makes new discoveries. In 1997, on a crossing from Cape Town to Neumayer station in Antarctica, a sudden elevation in the terrain was recorded. Subsequent research showed that the vessel had surveyed a volcanic cone. The area was christened Heinz-Kohnen Seamount (Schenke, 2001). Another recent discovery is the cluster of carbonate mounds on the Porcupine Bank in Irish waters, discovered by a number of expeditions starting in 1997.

3. NAVIGATION ON THE SEA

„Marine navigational systems may need geodetic accuracy,
but geodetic control is not available to these systems.“
(Mourad and Fraizer, 1967)

Navigation is an important part of bathymetric surveying at sea. The better the navigational accuracy, the more accurate is the bathymetry obtained. In order to improve the accuracy, navigational systems have to be calibrated. The position of a measuring vessel is received mostly through navigational satellites.

Acoustic methods are applied in the positioning of underwater vehicles. Based on one position fix of a vessel or underwater robot, the coordinates of single beams are derived from the distance and angle measurements of the sea-floor mapping system. Contrary to land positioning, an inertial navigation is additionally used at sea. An inertial navigation system serves for the determination of velocity, heading and motion components of the vessel. Every measurement has to be related to some reference system. Every vessel or underwater robot has a local coordinate system which has to be connected to a global coordinate system.

3.1 From Phoenicians to Microwaves

Celestial navigation is the oldest marine navigational method. Phoenicians and Polynesians are known as the first navigators from ancient times. They drove their ships by the guidance of the stars several thousand years ago. Later, the relative motions of the sun, moon, planets and stars were determined as a function of time.

The motion of space objects has attracted the attention of astronomers for centuries. Nicolaus Copernicus in the 15th century, Tycho Brahe and Galileo Galilei in the 16th century, Johannes Kepler in the 17th century and his successor, Isaac Newton, whose equations describe motion in an inertial coordinate system. Motion in inertia is also applicable to the motion of Earth satellites.

Waves are today used as information carriers. Christiaan Huygens argued that light consists of waves. Two centuries later, James Clerk Maxwell created the electromagnetic theory (Encyclopædia Britannica, 1987). It was discovered that electromagnetic waves could carry information too. Electromagnetic energy is transversal and is spread perpendicular to the direction of propagation of the wave, whereas acoustic energy is longitudinal and spread mechanically by compression or expansion of the medium. The mechanical vibrations of acoustic waves work well in water, and are hence utilized in underwater navigation. Electromagnetic waves cannot propagate in liquid media (Lurthon, 2002).

The properties of the electromagnetic waves used by radio, telephone or television have been known since the 19th century. The development of radio signals in the 20th century opened up a new dimension of communication. Radio waves were used by Sputnik 1, the first satellite, launched in 1957 (Encyclopedia.com, 2004).

In satellite geodesy, electromagnetic waves are used as a means of base communication, especially in the visible light and microwave domains. In 1973, a precise three dimensional navigational system was developed. The NAVSTAR GPS (NAVigation System with Time And Ranging Global Positioning System) time and ranging system is nowadays composed of 24 satellites moving in six orbits 20 200 kilometres above the earth (Seeber, 2003).

3.2 Positioning onboard R/V POLARSTERN

Sometimes it is impossible to navigate with respect to any useful coastal reference point on polar missions or on the open sea. In the case of high northern or southern latitudes, GPS performance is strongly affected by multipath effects because the satellites are closer to the horizon, and their geometrical constellation is not optimal. Relative positioning between two stations achieves better results than absolute measurements. In the navigation of vessels, the differential GPS method (DGPS) is hence often used (Figure 3.1).

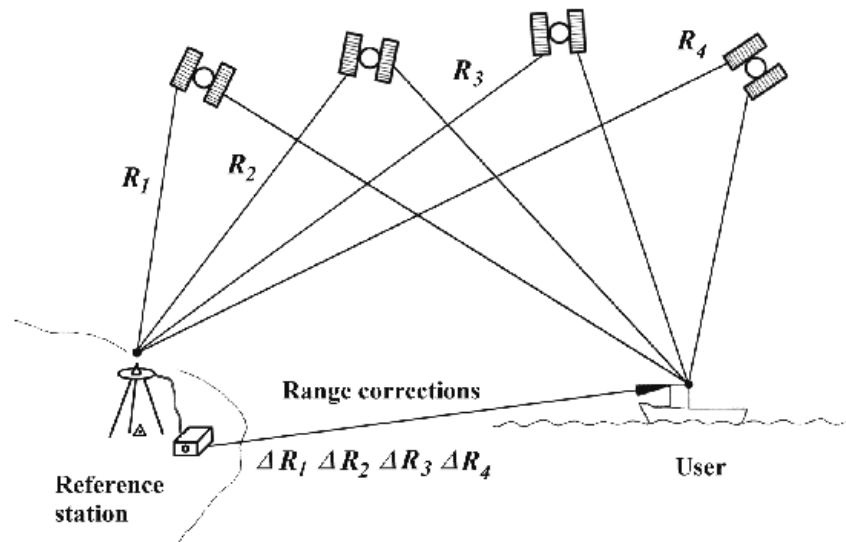


Figure 3.1: Outline of the DGPS principle (after Seeber, 1993).

3.2.1 GPS receivers

R/V POLARSTERN employs different GPS receivers for various purposes. Measurements on two frequencies, L1 and L2, are performed using MS750 TRIMBLE receivers. Together with ASHTECH and LEICA MX400 receivers they are mounted on the upper part of the ship (see Figure 3.2).

Data obtained from the TRIMBLE receiver are posted to the MINS (Marine Inertial Navigational System) system. The MINS inertial navigation accuracy on POLARSTERN is ± 25 meter (pers. comm. Peter Gerchow, FIELAX, 2003). Positions of bathymetric soundings are transferred to the HYDROSWEEP device from MINS. The MINS system gathers the position from TRIMBLE 1 by default and, if problems occur, TRIMBLE 2 is activated.

Theoretically, the accuracy of a single position made with a dual frequency-receiver is ± 10 – 50 meters. The relative positioning accuracy of TRIMBLE receiver was, after examination in the

Lloyd shipyard in Bremerhaven, even less than 1 meter (pers. comm. Peter Gerchow, FIELAX, 2003).

The LEICA receiver works in differential mode (DGPS). Data from this receiver serve as positioning information to navigate the ship. The DGPS method, with single frequency measurement on the ship and UHF waves broadcasting corrections from reference stations on land output positions with an accuracy of ± 25 meters (pers. comm. Peter Gerchow, FIELAX, 2003).

The ASHTECH receiver is used in order to support the onboard time system.



Figure 3.2: One of the TRIMBLE antennas (left) and the LEICA antenna (right) on board POLARSTERN (2002).

3.2.2 Common reference point and local coordinate system

Computation of longitude, latitude and depth is related to the reference point of the ship. The origin of this defined local Cartesian coordinate system, also referred to as the navigation reference point, is at the HYDROSWEEEP unit on the hull of the ship (see Figure 3.3). The X and Y axes are defined so that the pitch angle is positive when the bow of the vessel is down side, and roll angle is positive when the port of the vessel is upside.

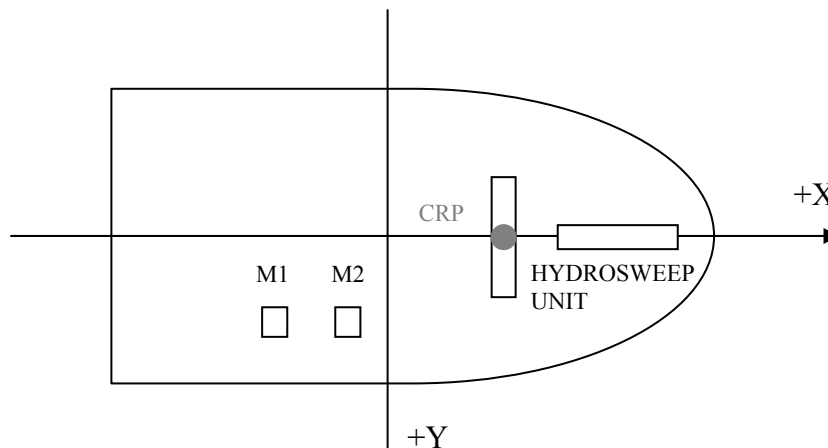


Figure 3.3: Common reference point on POLARSTERN in one of HYDROSWEEEP units.

The MINS devices are placed parallel to the X axis, separated from one another by a distance of 80 cm. Their computations are registered as one input, but it is not recorded from which aperture the data come.

The coordinates of the individual instruments used for navigation of the ship can be seen in Table 3.1. The acoustic array of the POSIDONIA (see Chapter 3.3.2) navigation system was centred in a special place on the ship, in the well.

Table 3.1: Local coordinates of several facilities (February 2001).

Instrument	Y (m)	X (m)	Z (m)
HYDROSWEEP unit	0	0	0
Well	1.655	-6.048	-0.008
MINS	3.160	-18.800	10.340
GPS ASHTECH	-0.123	-5.129	44.817
GPS TRIMBLE 1	8.627	3.221	34.027
GPS TRIMBLE 2	-10.474	-3.032	34.062
GPS LEICA	-9.200	-6.000	32.000

3.2.3 Global coordinate system and UTC

The geocentric coordinate system WGS 84 (World Geodetic System 1984) is a frequently used reference frame for many civil and scientific applications all over the world. Its parameters were first introduced in 1984 (Burša and Kostelecký, 1999). GPS orbits refer to this Conventional Terrestrial Reference System (CTRS). WGS 84 is used as a global system of many local systems. For navigation purposes, the Conventional Terrestrial Reference System WGS 84 is used together with the Universal Time Coordinated (UTC) time scale. UTC is atomic time which differs from GPS time by 13 seconds (at epoch 2003).

3.2.4 Linear transformation

The corrected GPS coordinates of the vessel are obtained from the TRIMBLE antenna at regular intervals. Local coordinates of the 59 single sonar beams are derived from the distance and angle measurements. The stored positions of the vessel are sent from MINS to the HYDROSWEEP (HYDROgraphic multibeam SWEEPing Survey Echosounder) system every second. Linear transformation of local (HYDROSWEEP) coordinates to the global (geographic) system is shown algorithmically and graphically in the formulas and figure below (Schenke, 1992).

$$\varphi_i = \varphi_S - \Delta\varphi_i = \varphi_S - d_i \cdot \sin A_S, \quad (3.1)$$

$$\lambda_i = \lambda_S - \Delta\lambda_i = \lambda_S + d_i \cdot \cos A_S. \quad (3.2)$$

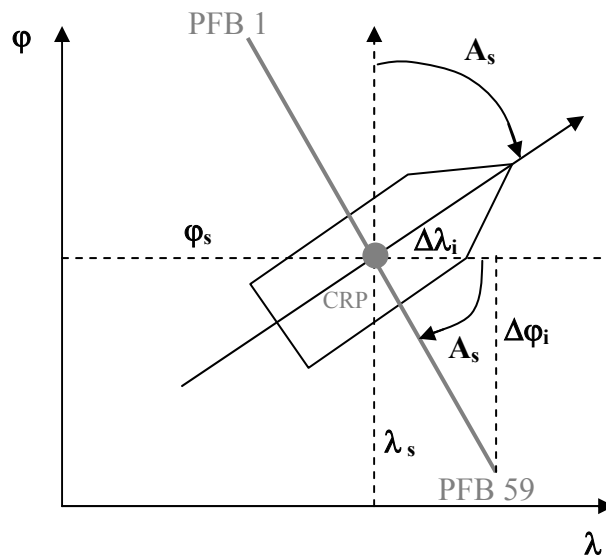


Figure 3.4: Computation of coordinates (after Schenke, 1992).

3.2.5 Inertial navigation

The basic principles of inertia were stated by Newton in 1687 when he formulated three laws of motion. The principles of inertia are embraced in his first law: “A body remains in its state of rest unless it is compelled to change that state by a force impressed on it” (Encyclopædia Britannica, 1987). The six degrees of freedom of an abstract body are shown in a Cartesian system in Figure 3.5.

The rotation motions of a ship is described as the roll (θ), pitch (ψ) and heading = yaw (ϕ) angle and translation motions are called surge (ΔX), sway (ΔY) and heave (ΔZ). The roll and pitch angles, along with heave, are measured and included in the computation of depth and position of every beam. These measurements are conducted by MINS accelerometers and gyroscopes.

Inertial navigation keeps the ship in an imaging fixed position (Merriam-Webster Online Dictionary, 2004). On board POLARSTERN, the fixed position is held by inertial systems called MINS (Marine Inertial Navigation System). One of the base components of MINS is an integrated strap down laser assigned mainly for vessels and submarines. MINS supplies longitude and latitude, heading, pitch and roll angles, heading-, roll- and pitch- rates, velocity components and log speed. From the angular information of gyroscopes and linear information of accelerometers, the three dimensional motion of the ship with respect to an inertial frame of reference is obtained (Verplaetse, 1995). The integrated navigation package is displayed in Figure 3.6.

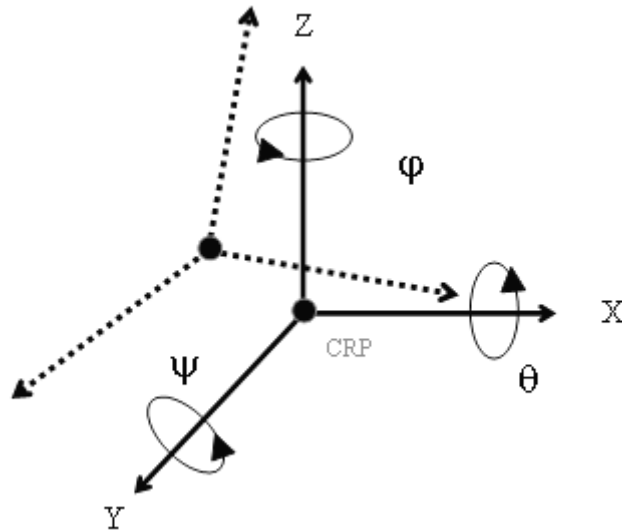


Figure 3.5: Six degrees of freedom.

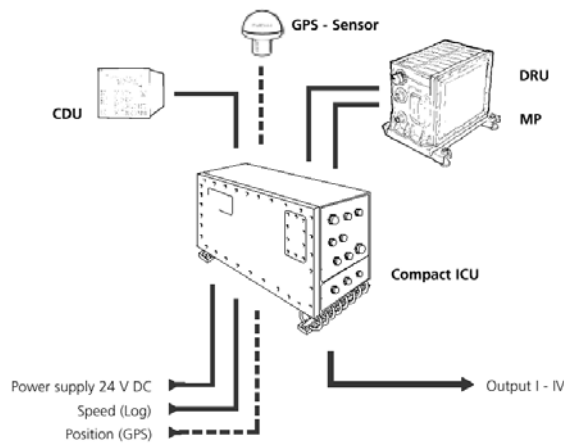


Figure 3.6: MINS – device configuration (CDU is Control and Display Unit, indicating all data of the platform, DRU is Dynamic Reference Unit, incorporating the laser gyros, the accelerometers and the gyro electronics, MP is Mounting Plate, mechanical interface for the DRU establishing a defined horizontal plane relative to the ship’s bench marks, ICU is Interface and Connection Unit, modular built interface to connect the MINS with log, GPS, ship’s mains and the signal users) (after Raytheon Electronics).

Ring laser gyroscope

An optical ring laser gyroscope is an important part of marine navigation system. The device for rotation measurement based on laser properties was first found useful by Clifford V. Heer from Ohio State University (Anderson, 1986). Unlike a mechanical gyroscope, with its locomotive parts, the size of light photons in an optical gyroscope allows faster measurements of angles.

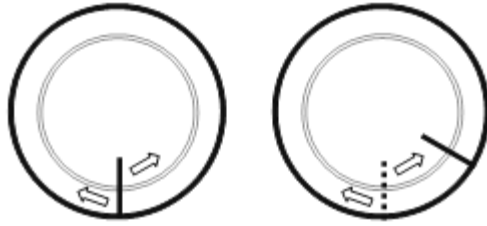


Figure 3.7: Two travelling pulses of light in a static (left) and rotating (right) body.

A ring laser gyroscope is composed of a small glass block, mirrors and electrodes and is filled with helium-neon gas. The measurement of roll and pitch angles is based on the phase shift of two light wavelengths ($0.6 \mu\text{m}$). Initially, the laser wave is split into two pulses which travel in the block-circuit in both clock directions (Anderson, 1986).

The pulses in the circuit are of the same length if the body does not move (see the left side of Figure 3.7). Their addition is ascertained as a constructive interference (Figure 3.8). Since the time needed for light travelling in the circuit depends on the rate of rotation, any rotary motion will provoke modifications to the beams' paths (see the right side of Figure 3.7). The difference of arrival times of beams in the output detector is directly proportional to the angular velocity (Anderson, 1986). The different lengths of pulses will result in a phase difference or destructive interference (see Figure 3.8).

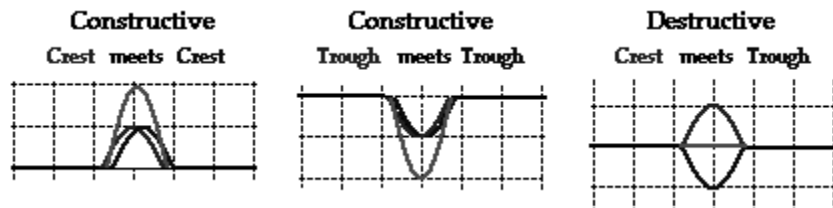


Figure 3.8: Addition of wavelengths - absent rotation (after Henderson, n.d.).

Heave compensator

Heave is the vertical acceleration along the Z axis of a body. Heave compensation is one operational task of HYDROSWEEP system. The actual heave value is immediately aligned with depth measurements from the sounder, so that the final depth corresponds to mean sea level. Onboard POLARSTERN, heave is measured by the compensator TSS 330 (Figure 3.9).



Figure 3.9: Heave compensator.

3.3 How to locate the underwater robot VICTOR 6000

Acoustic methods are frequently applied to the task of navigating objects within water, because radio signals can not penetrate deeper water layers. Water remains almost inaccessible for electromagnetic waves. Vice versa, water does not block the acoustic signals. Mechanically perturbed acoustic signals are nowadays the only practical way to carry information under water (Lurton, 2002).

3.3.1 Local coordinate system and sensors

As can be seen from Figure 3.10, the remotely operated vehicle VICTOR 6000 has a local coordinate system with the origin at the front of the vehicle. The orientations of its axes are: X positive forwards, Y positive out the right side, Z positive downwards. Roll, pitch and heading values issue from a gyroscope (Photonetics Octans). The echo sounder SIMRAD EM 2000 provides the microbathymetry. The acoustic antenna of the transponder is placed on top of the vehicle and the second part of the transponder is mounted at the rear of the vehicle (marked grey). Sensor outputs are sent through serial port RS 232 and are saved together with the POLARSTERN outputs in NMEA file (see Table 4.3). VICTOR sensors and their coordinates are listed in Table 3.2 and Table 3.3.

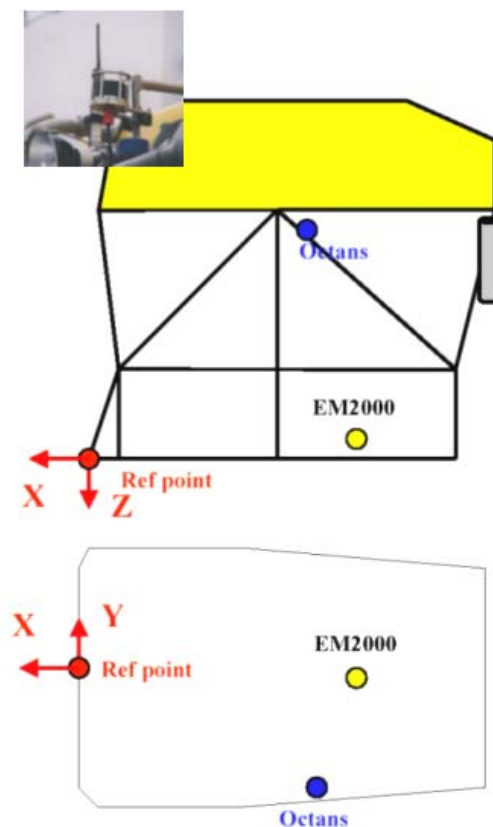


Figure 3.10: VICTOR coordinate system and details of the transducer antenna.

Table 3.2: VICTOR sensors (pers. comm. Jan Opderbecke, IFREMER, 2003).

Sensor	Value, unit	Time interval	Placement	Precision
Altimeter (200kHz)	height VICTOR-bottom, m	200 ms	rear	~10 cm
Doppler Log (DLV)	velocity, kn	1 sec	rear	Few mm/sec
Pressure sensor	pressure, dBars	< 1 sec	centre	0.1 m(relative) 0.5 m(absolute)
Temperature sensor	temperature, °C	-	in DLV	-
Octans	heading, °	100 ms	centre	-

Table 3.3: Coordinates of sensors from Figure 3.10.

metres	X	Y	Z
Reference point	0	0	0
Octans	-1.58	-0.85	-1.67
Sonar EM2000	-1.98	0.00	-0.10

3.3.2 Navigation system POSIDONIA

The acoustic array of the ultrashort baseline system POSIDONIA (Figure 3.11), mounted below the ship's hull, is composed of two ultrashort baselines with one transmission transducer, four reception and four transmission channels per hydrophone. Each of the hydrophones can detect an acoustic pulse at a frequency from 8.5 to 16 kHz.



Figure 3.11: POSIDONIA acoustic array – flush version, \varnothing 80 cm (after Bellier, 2002).

POSIDONIA operates in electric and acoustic mode. The electric signal travels through the fibre optic cable from the ship to the robot every five seconds and invokes the acoustic pulse in the beacon which is immediately transmitted to the ship. There are four receiving hydrophones in the antenna, placed in the ship's hull, with maximal reception from an opening angle of thirty degrees.

In the case of ROV VICTOR 6000, the beacon is placed on top of the robot and its absolute coordinates with respect to the ship are computed after decoding of the phase and time of the arrived frequencies (Bellier, 2002).

3.3.2.1 Principles of ultrashort baseline navigation

One of the acoustic techniques in marine positioning is the ultrashort baseline technique (USBL). USBL is suited for short range navigation delivering the position of one or more submerged vehicles. Acoustic signals are exchanged in both directions between an acoustic beacon on the vehicle and an array system on the ship. Signals between the ship and the vehicle can be sent electrically via cable in order to avoid noise in the water.

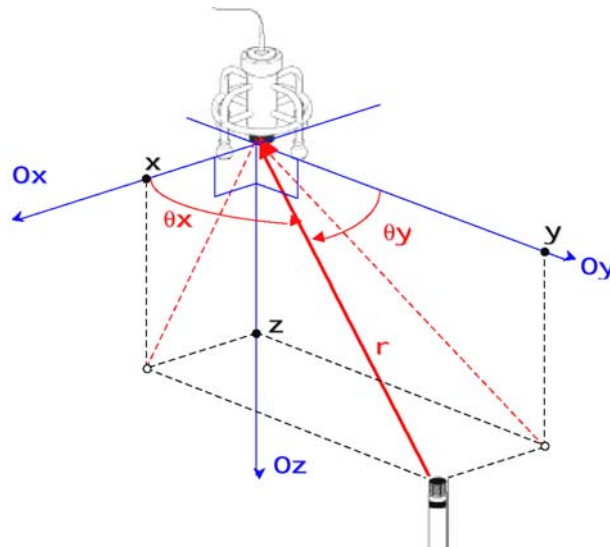


Figure 3.12: USBL calculation principle (after Bellier, 2002).

Ultrashort baseline (shorter than 0.5 m) is established on the principles of range bearing. The distance “ship’s array - vehicle’s beacon” (see in Equation 3.3) is computed by multiplication of the sound velocity c by the time delay of the pulse Δt , and the phase shift, φ , between hydrophones is computed as shown in Equation 3.4 where θ is an incidence angle, l is the length of a baseline, and λ is a wavelength. The calculation principle is displayed in Figure 3.12.

$$r = c \cdot \Delta t, \quad (3.3)$$

$$\varphi = \frac{2\pi \cdot l}{\lambda} \cdot \sin \theta. \quad (3.4)$$

3.3.2.2 Calibration

To calibrate the POSIDONIA system, a transponder that is about 70 cm long has to be moored on the sea bottom (Figure 3.13).

After mooring the construction, the transducer transmits acoustic signals. At the same time the ship sails a figure “8” (see Figure 3.14) and the transmitted signals are registered from all directions.

The calibrated values of heading, roll and pitch are computed with regard to the vertical and horizontal axis of the ship by the method of least squares (Figure 3.15). Calibration offsets from the expedition ARK 19/3a are: -0.46° for heading, -0.26° for roll and -0.16° for pitch.

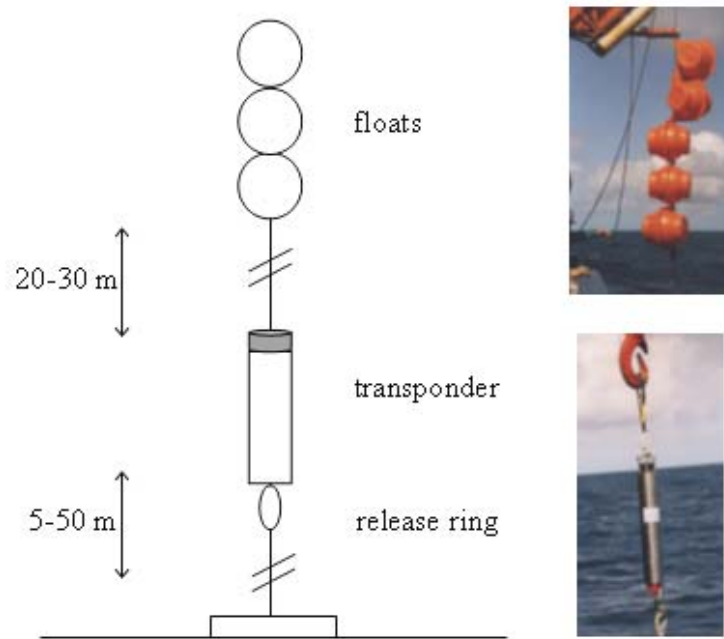


Figure 3.13: Outline of moored transponder (left), transponder (bottom right) and floats (upper right).

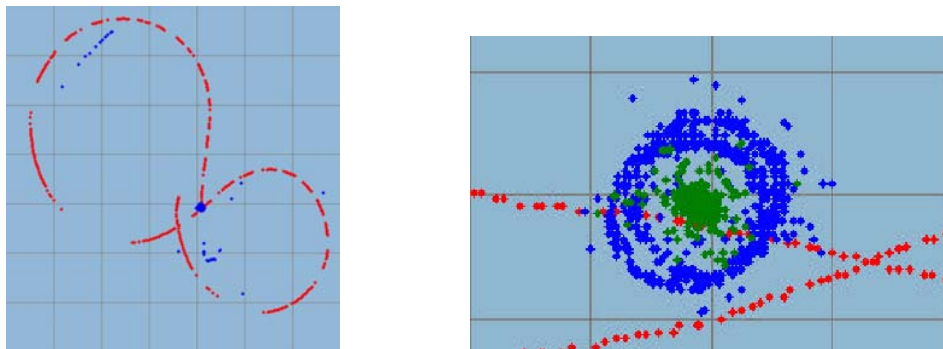


Figure 3.14: POSICAL calibration (after Bellier, 2002) – calibrated positions are marked green.

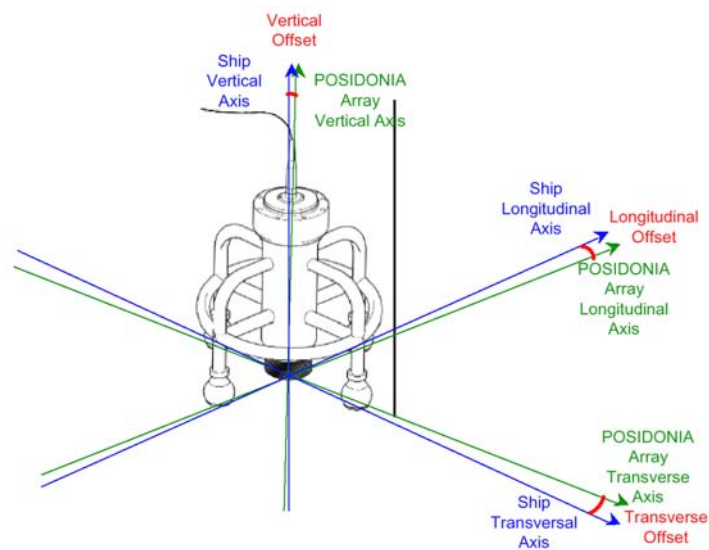


Figure 3.15: Calibration offsets (after Bellier, 2002).

3.3.3 Dead reckoning

Since the 18th century navigators have calculated a ship's future position with the help of the dead reckoning method. Dead reckoning is a process of determining an object's position by applying a speed and direction to the last established position. Vectors represent all true courses and speeds (Garrison, 1999). The first point of dead reckoning method has to be initialized by another navigation method. In the case of VICTOR, the position of the first point is given from POSIDONIA acoustic navigation.

The Octans Inertial Unit indicates a direction and the Doppler Log measures changes in speed. The initialisation is actually the resetting of offsets to zero. Inertial navigation causes undesirable drifts. To reduce these offsets, initialisation is manually done almost every hour.

Table 3.4: Commonly used underwater vehicle navigation sensors (after Kinsey and Whitcomb 2003) – VICTOR sensors written bold.

INSTRUMENT	VARIABLE	PRECISION
Acoustic altimeter	Z – Altitude	0.01 – 1.0 m
Pressure sensor	Z – Depth	0.01 %
12 kHz LBL	XYZ – Position	0.01 – 10 m
16 kHz USBL	XYZ – Position	± 30 m
Inclinometer	Roll and Pitch	$0.1^\circ - 1^\circ$
Magnetic compass	Heading	$1^\circ - 10^\circ$
Gyro compass – conventional	Heading	0.1°
Gyro Compass – 3 axis, optical, north seeking	Angular position and velocity	0.1°
Bottom-lock Doppler sonar	XYZ – velocity	1%

3.3.3.1 Polygonal parallel

As shown in Figure 3.16, dead reckoning on the sea can be considered equivalent to an open polygonal traverse in land surveying. Both methods are derived from measurements of distance and angle. In dead reckoning, coordinates of subsequent points can be calculated as a coordinate difference added to the position of a known initial point. Coordinate differences are acquired as sines and cosines of adapted angles multiplied by their respective distance. In polygonal traverse, differences dx and dy increase with every added polygonal point. The coordinates are based on adjusted differences.

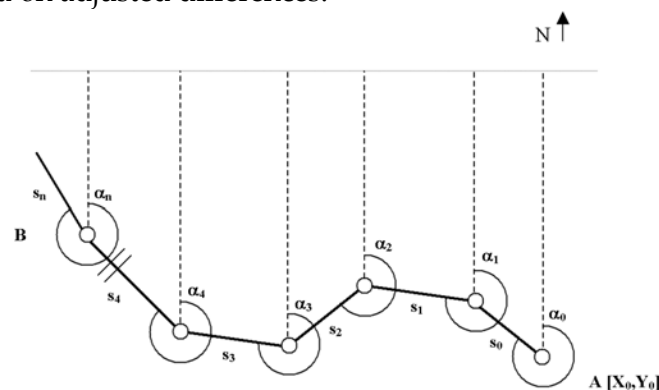


Figure 3.16: Open polygonal traverse, or inertial navigation.

In Figure 3.17, two open polygonal traverses are marked black. The initialization positions are expressed by circles. If we suppose that initialized position (3) is correct, the polygonal traverse between the first (1) and the last point (3) can be adjusted. The offset value (marked red) will be split and assigned to every point depending on the distance from (3). If initialization (3) is wrong, the adjustment between points (1) and (4) could be performed in order to get continuous positioning (green). It is also possible to shift the first polygonal traverse (blue) to link it to the second one.

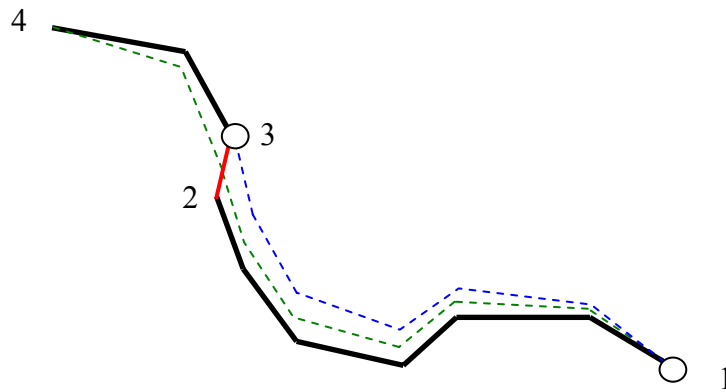


Figure 3.17: Adjustment possibilities of VICTOR track line.

The problem of some tens of meters of drift under the water is solved by initialization. The dead reckoning drifts are not adjusted. In post-processing, the rough navigation errors are manually shifted in order to give a continuous robot track. It still has to be considered that land surveying methods undergo different environmental conditions than navigation methods in the water do.

3.3.3.2 Transformation between systems

By transformation between systems we understand here the transformation between the Doppler Log related coordinate system, Instrument related coordinate system (ROV) and World related coordinate system (POSIDONIA).

The Doppler Effect is often explained by a car's horn or siren which is first higher-pitched and then lower-pitched with the passage of the car. The change in the pitch of the siren is actually a shift in the frequency of sound waves and is called the Doppler Shift. By the measurement of the rate of change of pitch, the vehicle's speed can be estimated.

VICTOR's Doppler Velocity Log (DVL) emits pulses from four beam transducers in all directions. Transducers look down with an inclination angle of thirty degrees from the vertical axis of log.

$$f_R = f_T \cdot \left(1 + \frac{v_R}{c_0}\right) \quad (3.5)$$

As seen from Equation 3.5 (MathPages, n.d.), the apparent bottom velocity v_R along each beam can be derived from the transmitted and received frequencies reflected by the bottom.

The transmitted frequency, f_T , is 200 kHz, the received frequency f_R is measured and c_0 is the speed of sound in water.

In Figure 3.18, two coordinate systems are displayed. The velocities are measured in the Doppler coordinate system and afterwards transformed to velocities in the directions of the X,Y and Z axes of the instrument coordinate system. The inclination angle has to be taken into account in the calculation and the directions of the four velocities have to be re-counted to velocities in the directions of the X and Y axes.

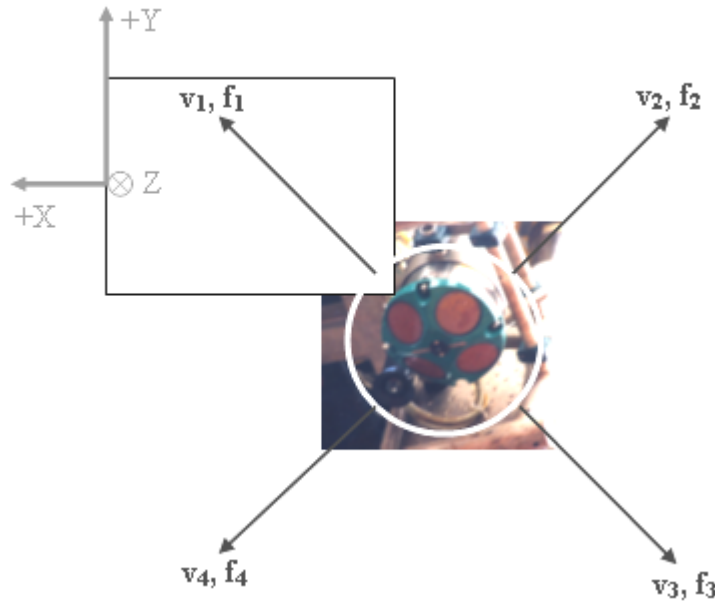


Figure 3.18: Doppler log and instrument coordinate systems.

Kinsey and Whitcomb (2003) describe the calculation for “Doppler to Instrument to World” transformations. Instrument coordinates are the coordinates of the vehicle and the World coordinate system here is the higher-level geodetic system referring to the POSIDONIA array on R/V POLARSTERN.

Four ping responses enter the computation as a 4×1 vector of velocities $v_{(beam)}$ from the Doppler Log. Beam velocities are converted to instrument (local) XYZ velocities ${}^i \dot{p}_d(t)$ where matrix T is a 3×4 constant matrix converting the four beam velocities into a 3×1 vector (3.6):

$${}^i \dot{p}_d(t) = T \cdot v_{(beam)} = \begin{bmatrix} \dot{x}(t) \\ \dot{y}(t) \\ \dot{z}(t) \end{bmatrix}. \quad (3.6)$$

The instrument velocity is transformed to the World frame considering the shift “Doppler to Instrument” with the rotation matrix R_2 and “Instrument to World” (roll, pitch and heading of instrument) with the rotation matrix R_1 (Equation 3.7):

$${}^w \dot{p}_d(t) = R_1(t) \cdot R_2 \cdot {}^i \dot{p}_d(t). \quad (3.7)$$

The world velocities are integrated to allow the calculation of the bottom track position. Vector ${}^w \hat{p}_d(t)$ is initialised using the POSIDONIA estimated position at time t . The computation of position in the world coordinate system follows, as shown in Equation 3.8:

$${}^w \dot{p}_d(t) = {}^w \hat{p}_d(t_0) + \int_{t_0}^t R_1(\tau) \cdot R_2 \cdot {}^i \dot{p}(\tau) d\tau. \quad (3.8)$$

3.3.4 Computation of coordinates

Precise three-dimensional navigation of the robot depends on the position of the vessel, or better, on the Common Reference Point and roll and pitch ascertainment. It is obvious that if the ship's positioning fails, neither the depressor nor the robot's position can be determined.

Besides the "underwater coordinate systems", two further coordinate systems have to be taken into account in relation to the ship. In Chapter 3.3.2, three coordinate systems were mentioned: the Doppler related coordinate system, the Instrument (ROV) coordinate system and World coordinate system, where World coordinates were received from the POSIDONIA positioning.

Furthermore, another set of transformations, namely "World (POSIDONIA) – Ship – WGS84" has to be realised. The POSIDONIA coordinate system lies in the ship's coordinate system and the ship's coordinate system depends on GPS positioning in the world geodetic system WGS 84. Summing up, to get the coordinates, X , Y , of a bottom point, we have to transform through five coordinate systems.

With regard to Figure 3.4, the position of the underwater vehicle is deduced from Equation 3.9. The first matrix characterizes the ship's coordinates (GPS) corrected for pitch and roll errors (MINS output). The POSIDONIA coordinates and conventional offsets between the acoustic array and the ship's reference point are rotated in order to identify their coordinate systems. Matrix R_3 is a rotation matrix (3.10) with roll, pitch and heading angles including calibration corrections (pers. comm. Jan Opderbecke, IFREMER, 2003).

$$\begin{bmatrix} X \\ Y \\ Z \end{bmatrix}_{ROV} = \begin{bmatrix} x \\ y \\ z \end{bmatrix}_{MINS+GPS} + R_3 \cdot \left(\begin{bmatrix} x \\ y \\ z \end{bmatrix}_{POSIDONIA} + \begin{bmatrix} \Delta x \\ \Delta y \\ \Delta z \end{bmatrix}_{CRP} \right), \quad (3.9)$$

$$R = \begin{bmatrix} 1 & 0 & 0 \\ 0 & \cos \theta & \sin \theta \\ 0 & -\sin \theta & \cos \theta \end{bmatrix} \cdot \begin{bmatrix} \cos \psi & 0 & -\sin \psi \\ 0 & 1 & 0 \\ \sin \psi & 0 & \cos \psi \end{bmatrix} \cdot \begin{bmatrix} \cos \varphi & \sin \varphi & 0 \\ -\sin \varphi & \cos \varphi & 0 \\ 0 & 0 & 1 \end{bmatrix}. \quad (3.10)$$

3.3.5 Accuracy and errors

The accuracy of the POSIDONIA System is ± 30 meters in the X and Y directions, and its vertical accuracy is approximately 1% of altitude (Bellier, 2002). That means that ROV deployment in a depth of 600 meters allows a vertical accuracy of about 6 meters. Hence, it can be deduced that although the Doppler Log measures the distance from the bottom with an accuracy of 0.1 meters, this accuracy is not appropriate to the final data.

Generally, the main errors in acoustical positioning are: uncertainty in baseline-determination, uncertainty in determination of the sound velocity and propagation path, instrumental errors, acoustical noise, motion of the sensor platform during measurements, and bad geometric conditions (Seeber, 2001).

The positioning of underwater vehicles is strongly affected by currents and the attenuation of higher frequencies. Multipath effects can be minimised by the use of correlative techniques but the ship's internal noise or reflected and scattered signals from the hull, engines and propellers of the vehicle itself are unavoidable (Peyronnet and Person, 1998).

3.3.5.1 Long Baseline and moored transducers

One possibility to navigate VICTOR more precisely is to use a Long Baseline System. At present, the best positional accuracy can be obtained from a 300 kHz Long Baseline System but unfortunately, attenuation limits the range of this higher frequency (Kinsey and Whitcomb 2003).

The positioning of the ship and the underwater vehicle with respect to an acoustical network offers better accuracy. For this, three or more transponders moored on the sea bottom are required. The position of the vehicle with respect to the transponder network would bring superior results; however, it is worthwhile only in experiments with long-term observations. Unfortunately, for large areas of the ocean, these systems are not available for navigation.

3.3.5.2 Specific examples by means of screenshots

Every dive of the underwater robot has to be planned, especially with respect to key coordinates of tracks, in order to navigate VICTOR to desired areas of interest. There are a few internal requirements for correct navigation. In Figure 3.19, optimal dive configuration is shown by a circle with a diameter of about 200 meters. The depressor, underwater robot and ship are supposed to remain inside this safety circle for the duration of a dive in order to prevent the separation of cables or loss of the vehicle. The vehicle is connected with the ship via the depressor.

The blue and red points are POSIDONIA fixes of, respectively, VICTOR and the depressor. The green dots are dead reckoning navigation points. Theoretically, the acoustic and inertial lines should be identical. But there is a constant distance of a few metres and tracks slowly deviate from each other with time.

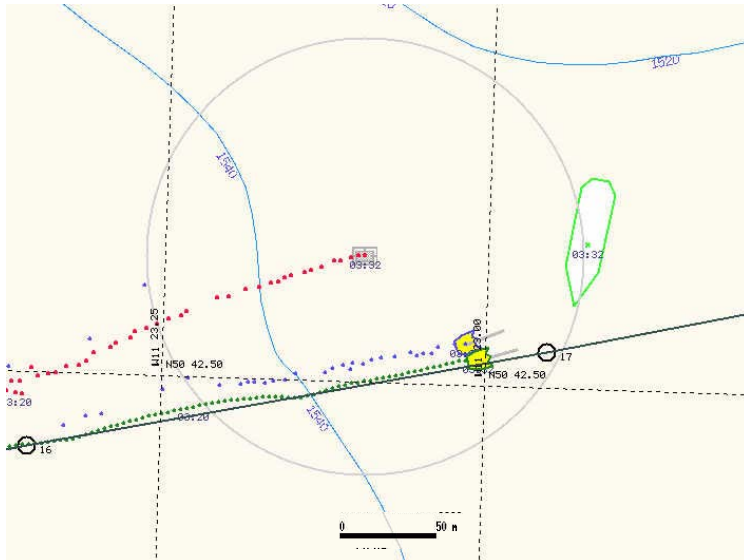


Figure 3.19: Transponder's acoustic signals from VICTOR (blue), depressor (red) and protocol with sensor information (green).

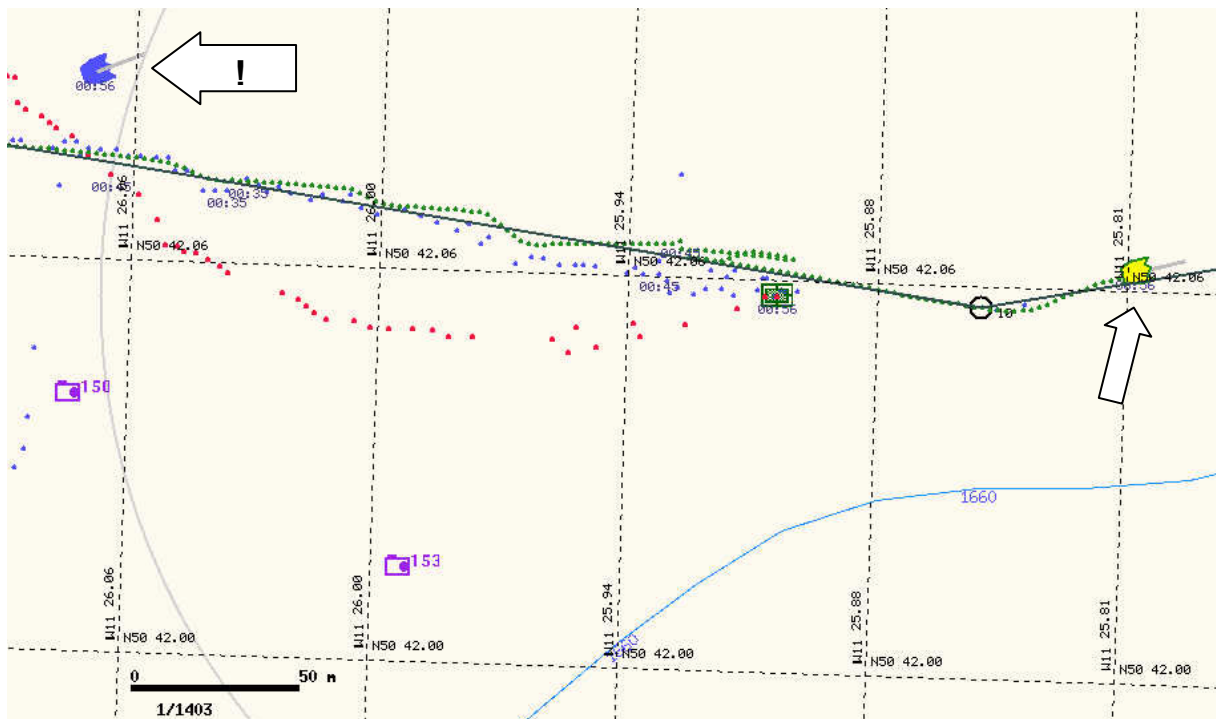


Figure 3.20: Incorrect acoustic navigation (marked blue).

As revealed by Figure 3.20, the difference between acoustics and dead reckoning can be as much as about 300 metres. Sometimes, the acoustic position is very erroneous and differs by hundreds of metres from the physical object. The reason for erroneous navigation could be strong attenuation in the deep sea during period of strong wind. The weather situation on the day after Figure 3.20 was made, $50^{\circ} 42.30' N$ and $11^{\circ} 26.54' W$, included a strong wind of about force 10 (SW10) on the Beaufort scale, what means very high waves and heavy rolling. The next influence can be currents or features in the topography.

It is not recommended to initialise dead reckoning if acoustic navigation is not working properly. If microbathymetry is acquired, every navigation error leads to shifts in the mapped area which have to be corrected in the post-processing (see Chapter 6).

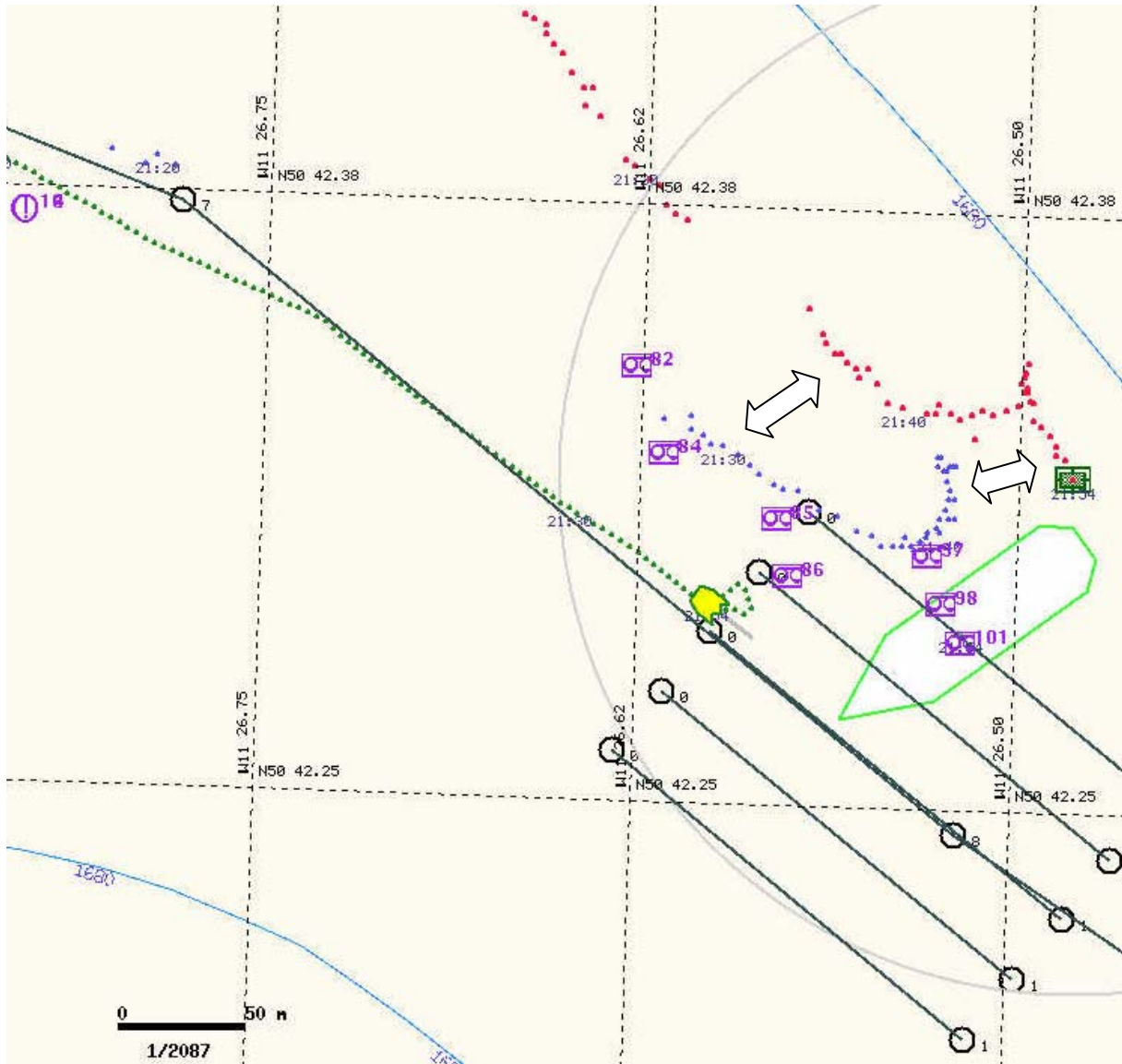


Figure 3.21: Incorrect POSIDONIA navigation.

Figure 3.21, shows incorrect POSIDONIA navigation. Dead reckoning fails most often because of currents which change the direction of vehicle (Garrison, 1999). Inertial navigation works with the respect to the bottom and could be affected also by geoid errors. The Doppler Log fails to send any information from about 100 meters above the bottom.

4. WORKING AREA, INSTRUMENTS, DATA SAMPLING AND HANDLING

Irish territorial waters extend mainly to the west of Ireland. In the last decade, detailed exploration of the sea floor there brought new scientific knowledge about the morphology of the seafloor and surprising relations with corals were found. Porcupine Bank was explored during the expedition ARK XIX/3a by the German icebreaker POLARSTERN and by the French underwater robot VICTOR 6000. One of the main tasks of the expedition was seafloor mapping by HYDROSWEEP and EM 2000 sonar systems. The measured data had to be processed onboard the vessel and prepared and saved for postprocessing onshore. Data storage is an important aspect of an expedition if the data are to be useful onshore later. If problems in data conversion occur, this may lead to data being unusable. In some cases the data from ARK XIX/3a could be corrected and used in later analysis. The corrected data were used for the calculation of grid differences from areas measured by both sonars.

4.1 Irish waters and chronological exploration of the Porcupine Bank

Irish waters cover an area of about 1 400 km², separated into three major zones (Figure 4.1). The first area is mostly coastal, the second one is continental shelf and the third includes Porcupine Bank, Porcupine Seabight and Rockall Trough.

Ten vessels and one airplane were involved in carrying out the National Seabed Survey, intensive program of bathymetric data acquisition with a commercial and environmental background. A Lidar survey with Laser Airborne Depth Sounder (LADS) was undertaken near the coasts. Mapping of Zone 2 is still underway, around 16% is finished. Surveying of deepwater Zone 3 was finished in 2002 (The Irish National Seabed Survey).

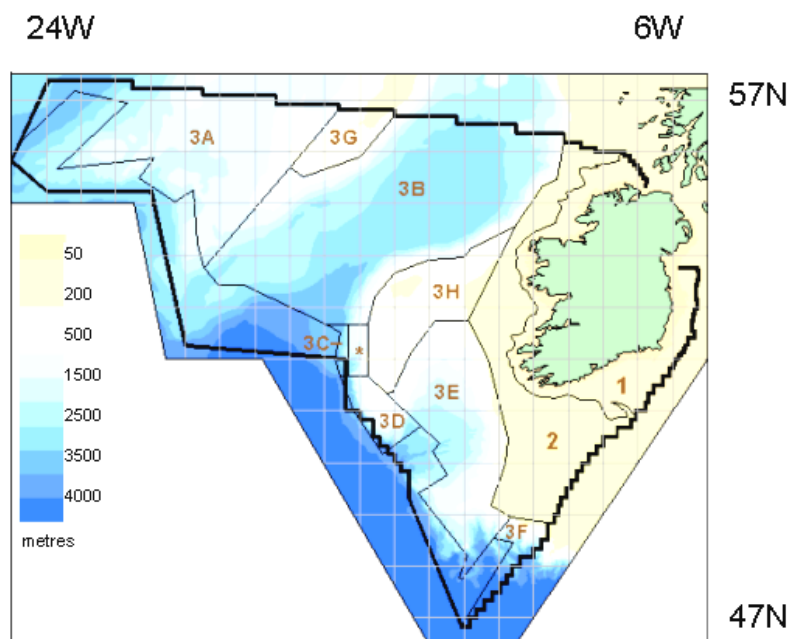


Figure 4.1: Borders and zones of Irish waters (after GSI Seabed Mapping 2001).

The most dominant part of Zone 3 is the continental hook of Irish Continental margin, called Porcupine Bank. Porcupine bank carries the name of the naval survey vessel HMS (Her Majesty's Ship) Porcupine, known for her first ever deep ocean dredge in 1869 (Evans, 2001), and is the location of recently discovered carbonate structures. Scientists recognised hundreds of oval mounds (Figure 4.2) on sonar images of the bank in 1997 and an occurrence of corals on video recordings made at depths of about 600-700 m over a 1200 km² area (Costello, 1999).

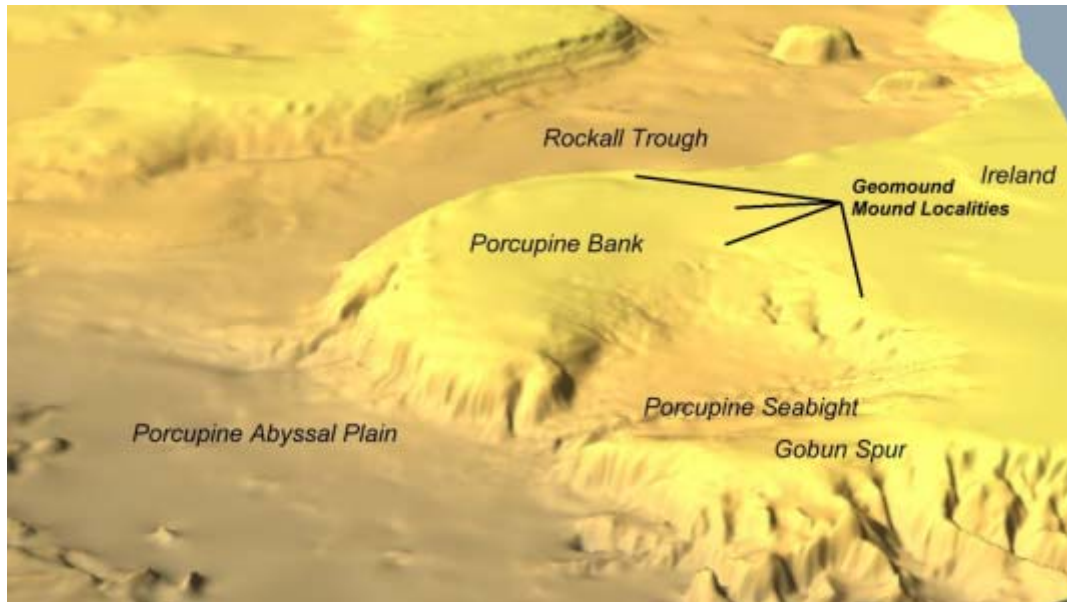


Figure 4.2: Mounds localities in Irish waters (after Vikran Unnitham, n.d.).

Porcupine Bank formed during tectonic rifting of the area between North America and Europe 180 million years ago. Basins on the margins of the bank were the site of clastic deposition and restricted circulation (Smee, 2003) at this time. A diversity of small fauna is preserved in these sediments, about which Maury wrote: "They probably lived and died near the surface, where they could feel the genial influences of both light and heat, and were buried in the lichen caves below after death" and "It is not probable that these animals lived at the depths where these shells are found, but I rather think that they inhabit the waters near the surface; and when they die, their shells settle to the bottom" (Maury, 1893).

A century later, scientists find out that the dark and cold waters off the west coast of Ireland are the site of surprisingly large live coral colonies; containing around 60% of European deep water coral (Siggins, 2003) mainly settled on the tops of odd small hills - clustered, circular or elongated mounds growing above faults.

A series of vessels explored the Porcupine area and Rockall Trough in recent decades: R/V BELGICA (BE) in 1996-98, R/V PROFESSOR LOGACHEV (RU), R/V PELAGIA (NE) in 1999, R/V L'ATALANTE (FR) in 2001, R/V POSEIDON (GE) in 2000-04, R/V POLARSTERN (GE) in 2000 and 2003 and R/V METEOR (GE) in 2004.

During the French cruise CARACOLE (CARbonate Mound and COLd Coral Research) by R/V L'ATALANTE in 2002, five mound locations were reached and observed by ROV VICTOR 6000: Therese Mound (Belgica Province), Propellor and Persistence Mounds

(Hovland/Magellan Province), the R1 Mound complex (Pelagia Province) and the R2 Mound Complex (Logachev Province). Trawling damage was seen on the mounds. Seismic profiles from Magellan Province showed many buried mounds (Huvenne, 2003). The few meters high Darwin Mounds were discovered in British waters on north-east Rockall Trough in 1998.

The names of the mound provinces originate from the ships which discovered them. The following Irish ones are known:

Belgica Province - Therese Mound, Galway Mound, Challenger Mound and Moira Mounds, Twin Mounds, Giant Mounds

Hovland Province - Propellor Mounds

Magellan Province - Persistence Mounds

Pelagia Province - Hedge and Scarp Mounds (also R1 Mound complex)

Logachev Province - R2 Mound complex

The formation of these mounds is still under debate. There are two hypotheses: that the mounds are seafloor depositional structures formed under the influence of currents, or that their genesis is related to ongoing fluid seepage (methane, sulphur) from the subsurface. Hence, according to De Mol (2002) the principal controls on the Porcupine coral banks geology are "oceanic circulation and dynamics in water masses and nutrient supply", but Sager (2003) writes that "topographic mounds are common features at cold seeps on the continental margins". Active and inactive mound assemblages have also been found in the northern Gulf of Mexico where petroleum-producing basins and authigenic carbonate, gas hydrate, and mud mounds were defined (Sager, 2003).

Because of this, the presence of mounds could be an indicator of hydrocarbon reservoirs. Unfortunately, recent research appears to eliminate this theory: "no evidence for suggested link to methane seepage has been found so far" (Kenyon, 2002).

To answer the questions, Ireland became part of the Ocean Drilling Programme in 2000. The aim of this is to take deep cores of carbonate mounds in order to analyse their structure in chemical detail. Drilling should take place in 2005 (pers. comm. Andreas Beyer, AWI, 2004).

Many of the expeditions were connected within the EU Fifth framework programme, issued by the European commission in March 1999. For the study of sustainable measurement of marine ecosystems, 19 projects were chosen and allocated with a budget of 26.9 million Euros. Three proposals related to the mounds were submitted: ACES (Atlantic Coral Ecosystem Study), ECOMOUND (Environmental Controls on Mound Formation along the European Margin) and GEOMOUND (Geological evolution of carbonate mounds) (European Communities, 1995-2003, 2000) which epitomized parts of the Ocean Margin deep-water Research Consortium (OMARC).

4.2 Expedition ARK XIX/3a

The expedition ARK XIX/3a took place from 1st to 21st June 2003 in the framework of a French – German co-operation. The key areas were Belgica and Pelagia Mounds, on the eastern part of the Porcupine Seabight and the Porcupine Bank. These areas occur in the north-east of the Atlantic Ocean and were reached by R/V POLARSTERN to launch the ROV VICTOR 6000 to depths of around 600 meters.

The international expedition was represented by scientists from all over the world. Apart from German and French scientists there were representatives from Ireland, Belgium, England, Russia, Nepal, Mauritius, Bulgaria, India and the Czech Republic who were members of EU funded research groups from universities and institutes, in particular from the German Alfred Wegener Institute for Polar and Marine Research (AWI) and the French Research Institute for the Exploitation of the Sea (IFREMER).

4.3 Carbonate mounds

The goal of ARK XIX/3a was to explore the special carbonate mounds and interrelated occurrence of cold-water coral. The following questions dominated the expedition: How and when did deep sea coral colonies appear in such an inhospitable area? Where do these mounds grow from? Could these areas be used as an indicator of hydrocarbon reserves? Are there some marks of damaging trawling on the bottom and, if yes, how long until the coral areas become protected?

Firstly, the morphological structure of Gollum Channel was observed, then the Belgica Province and the 5 metres high Moira Mound, then the trawler-damaged Twin Mound, and the 100 meters high the tallest-known Giant Mounds. The Pelagia Province - Scarp and Hedge Mounds – were the focus of the second part of the expedition.

The mounds are commonly hard, oval shaped bodies surrounded by a ring feature. They are influenced by physical erosion, scoured by currents, covered with a layer of sand or mud and coral fragments. The seafloor surrounding the mounds is mostly sandy with embedded stones (dropstones) or rock outcrops and diverse microfauna (crabs, asteroids, sea spiders, worms etc.)

The Scarp Mounds exist on a scarp, and probably overlie a deep fault. The Hedge Mounds are, with Giant Mounds, the highest of the Porcupine Bank mounds. They consist of a cluster of 26 mounds placed on a "slight topographic high between the upper heads of a canyon". (Expeditionsprogramm Nr.66, 2003) and are 60 meters high. These mounds are solitary objects positioned in an area of strong currents, 10s to 100s meter high and several kilometers long (Wheeler et al., 2003), occurring in depths of around 600 meters. The Scarp and Hedge Mounds, together covering an area of 20 x 40 km, were discovered during a 30 kHz TOBI Side-scan sonar survey in 2002 by the Royal Netherlands Institute of Sea Research. After the TOBI cruise, the Scarp and Hedge Mounds were next surveyed by R/V POLARSTERN (pers. comm. Andy Wheeler, University College Cork, 2004) and the robotic submersible VICTOR two dives between 16th – 19th June 2003 and have been surveyed over the course of other cruises (Royal Netherlands Institute for Sea Research, United Kingdom's Southampton

Oceanography Centre, French Research Institute for the Exploitation of the Sea, Russian State Hydrometeorological University etc.)

The occurrence of mounds has been assessed through both systematic and “continuous” surveys executed by sonars. Continuous surveying means that sonar device was working without certain aim. The coordinates of systematic VICTOR surveys were computed in advance and saved to the VEMO+ software as a reconnaissance pattern for VICTOR’s pilots. A detailed scientific survey of Porcupine territory was made with two sonars in June 2003.

For the purposes of this thesis, five separate systematically surveyed areas from the northern Porcupine Bank margin were chosen – two areas from Hedge Mounds and three areas from Scarp Mounds. These areas are covered by both POLARSTERN and VICTOR bathymetric surveys.

4.4 Research vessel POLARSTERN

Research vessel POLARSTERN (Figure 4.3) has over “twenty years of shuttle service between North- and South- Pole” (dpa, 2002). The 118 meters long double-hulled icebreaker, nicknamed a “floating university”, has been used for German polar and marine research activities since 1982. It is owned by the German Ministry for Education and Research and run by the Alfred Wegener Institute.



Figure 4.3: Research vessel POLARSTERN.

The ship has six decks and an under-deck with engine-room. All decks are equipped with laboratories. Bathymetric, biological, chemical, geophysical, geological, glaciological and oceanographical work is done in the laboratories on deck E. Deck F houses the gravimeter and magnetometer room, navigational system MINS (Marine Inertial Navigation System) and refrigerator rooms for samples. The meteorological station and radiotelegraphy office are on deck B and the control centre of the ship – “bridge” – is on deck A.

External communication is provided by IMMARSAT satellites. The computer system PODAS serves as an interface for gathered data like the current latitude and longitude, heading, depth, air and water temperature, salinity, strength of wind, visibility etc.

POLARSTERN surveys at speeds of up to 16 knots. The stability of the ship is ensured by the MINS system with pitch and roll co-ordination and underway adjustment of the heel and trim of the ship. The ship's position is determined with the satellite Global Positioning System (GPS). Winches and crane device are at scientists disposal to launch sonds, corers and other devices. Some expeditions are accompanied by helicopters.

During the expedition ARK XIX/3a, the VICTOR laboratory was set up in the winch room on the D deck (microbathymetry, navigation, video management) and in a container (pilot's room, recording apertures, video inspection) stowed in the vessel's loading space.

4.5 ROV VICTOR 6000

The deep teleoperated system VICTOR 6000 (Figure 4.4) was developed after approval in 1992. Its abilities for large scale optical surveying and local observation were first tested in September 1997 (Nokin, 1999).

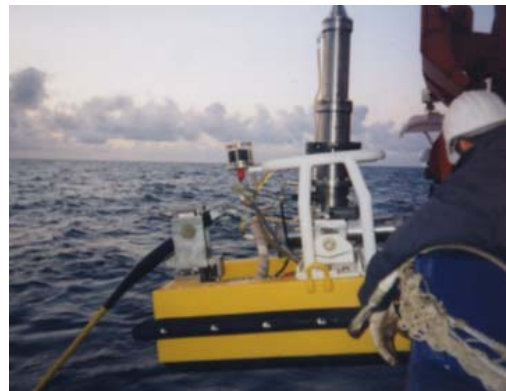


Figure 4.4: Remotely operated vehicle VICTOR 6000. **Figure 4.5:** Depressor of VICTOR 6000.

VICTOR 6000 is a complex system with dimensions 3.1 x 1.8 x 2.0 m providing optical data acquisition, microbathymetry and capabilities for physical and chemical sampling and depositions of markers. VICTOR operates at maximum depths of 6000 m and is the world's only commercial robot for work at such depth. VICTOR is connected to the ship by about eight kilometres of cable which is interconnected with a depressor (Figure 4.5) at about 300 m from the robot (Figure 4.6).

VICTOR navigation with the aid of its gyroscope (heading), pressure sensor (depth), altimeter (altitude), Doppler log (velocity, currents) and temperature sensors mounted. Data

from these measurements are transmitted through fibre optic cable and saved in a “real-time” database on the ship.

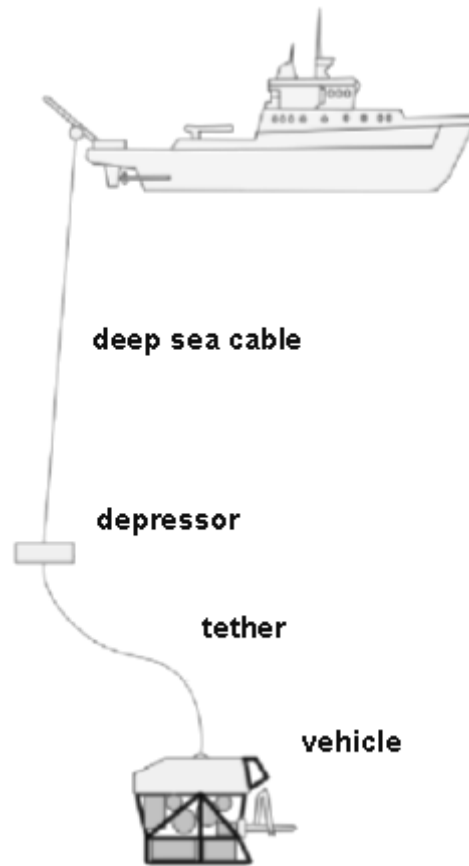


Figure 4.6: Constellation of ship, depressor and underwater vehicle.

Videocameras mounted on VICTOR provide a view of the deep environment. Four red laser beams are integrated with the main videocamera to give a scale on the recorded images. There is a possibility to explore bottom sediment structure with the high resolution vertical camera or take geological or biological samples with mechanical arms. The arms, two propellers, and all the electronic are operated from the pilot’s room. Appendix E lists some technical data for VICTOR 6000 and R/V POLARSTERN.

VICTOR follows the planned trajectory with a maximum velocity of 1.5 kn. The vehicle can work in two modes. If collecting samples, a sampling basket has to be installed in place of the microbathymetric instrument.

The ROV is piloted from the ship. The roll, pitch and heading values are output in octans inertial unit, and saved before corrections are applied in postprocessing. The vehicle’s position was determined by an ultrashort baseline system called POSIDONIA (more in Chapter 3) and inertial systems.

4.6 Used mapping instruments

On R/V POLARSTERN

Continuously operating Seabeam sonar has been used on POLARSTERN since 1982. An echosounder for depths of up to 10 000 metres was developed at KRUPP ATLAS ELEKTRONIK in Bremen between 1984 and 1986. The new swath mapping system was named HYDROSWEET (HYDROgraphic Multibeam SWEEPing Survey Echosounder). A prototype of the system with 59 preformed beams (PFB) and an opening angle of 90° was first tested on the R/V Meteor. The roll, pitch and heave are included in the computations so that “omega” and “tunnel” effects (see Section 5.1.5.2) are automatically avoided (Gutberlet and Schenke, 1989). A HYDROSWEET DS-2 system has been placed on POLARSTERN’s keel since 1997. The variations of sound velocity profiles (SVP) in water are implied in cross-fan calibration computations. The technical parameters of the sonars used are shown in Table 4.1.

Table 4.1: Technical parameters of sonars used during the expedition ARK XIX/3a.

Multibeam sonar	HYDROSWEET DS-2	SIMRAD EM 2000
Fan aperture	90°(120°)	120° (150°)
Beam spacing	2.3°	1.5°x2.5°(3.5°)
Number of beams	59	110
Frequency	15.5 kHz	200 kHz
Depth range	10 – 11 000 m	250 m
Pulse length	1-10 ms	0.05-0.25 ms
Bathymetric accuracy	0.5% of water depth	0.2% of water depth
Swath width	200% of water depth	350% of water depth

On ROV VICTOR 6000

Two sonars were applied in VICTOR microbathymetry measurement: RESON SEABAT 8125 and SIMRAD EM 2000. The SIMRAD EM 2000 system was used during the second half of the expedition.

The EM 2000 is a short range, high resolution multibeam echo sounder with up to 110 narrow beams which was developed by KONGSBERG SIMRAD in Norway. The system consists of a Sonar Head and a Transmit Transducer. It is a precision instrument for bathymetric swath mapping with a vertical precision of 0.2 % of the water-depth.

The HYDROSWEET system’s sending head preforms the ping according to the ship’s attitude so that pings are always sent perpendicularly to the seafloor. The direction of beam shooting in the EM 2000 system depends strongly on the movement and inclination of vehicle. Roll and pitch values are not corrected until postprocessing.

EM 2000 data were only collected by VICTOR when sonar was mounted for work in microbathymetric mode. POLARSTERN’s sonar measured continuously. Because of the different operating depths of the two systems, VICTOR’s swath width covers just 3% of

POLARSTERN swath width in the same area. The functioning of both systems is described further in Sections 5.1.4 and 5.4.1.

4.7 Bathymetric software, data circulation and archival

POLARSTERN has both PC and UNIX networks with software for numerous applications. CARIS HIPS (for HYDROSWEEP) and QINSY (for EM 2000) were utilized for multibeam data editing. ADELIE software was used to process video sequences. Configuration of acoustic navigation was displayed in the ABYSS software. POSICAL served for calibration of acoustic navigation. CARAIBES (CARTography Adapted to Imagery and Bathymetry of Sonars and multibeam echosounders) and GMT (Generic Mapping Tool) were utilized to work with the microbathymetric and bathymetric data. GMT was used to produce georeferenced maps, CARAIBES for navigation corrections, and TERRA MODEL and FLEDERMAUS were utilized for 3-D visualization.

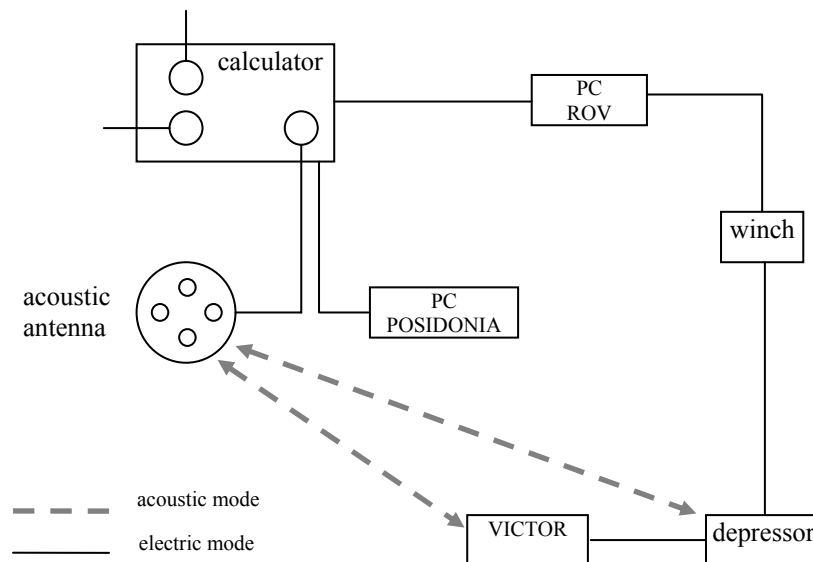


Figure 4.7: Circulation of acoustic and electric pulses between the ship and vehicle (pers. comm. Severine Beraud, IFREMER, 2003).

Raw data logged by the workstations were backed up each day on 8 mm DLT tapes (Digital Linear Tape) and some were transcribed to CD-ROMs. The map products and processed data files were also saved onto 8 mm tapes. Unfortunately, microbathymetric data were not saved in raw format, but only after reformatting to DB format in QINSY (see Chapter 4.7).

Figure 4.7 gives an overview of acoustic and electric data circulation. The network illustrates the POSIDONIA acoustic mode used for positioning of vehicle. When the data are received by the acoustic antenna, a position vector is calculated and the data are saved.

Table 4.2 shows the different manner of data storage used to produce maps (example from areas of Scarp and Hedge Mounds). It demonstrates the differences in the quantity of data, which depends on the distance to the bottom (10 meters for the EM 2000 echo sounder and 600 metres for the HYDROSWEEP echo sounder).

Table 4.2: Overview of sonar data from the different depths.

Area	HYDROSWEEP data	Start time	MB (HIPS)	EM 2000 data	Start time	MB (DB)					
SM2	167_ark06160800	8:00 15:59	42	0022_0001	12:30	265.8					
				0022_0002	12:35						
				0022_0003	13:03						
				0022_0004	13:10						
				0022_0005	13:21						
				0022_0006	13:42						
SM3	167_ark06161600	16:00 23:59	42	0026_0001	18:50	414					
				0026_0002	19:20						
				0026_0003	19:42						
				0026_0004	20:06						
				0026_0005	20:41						
				0027_0001	21:01						
SM4	168_ark06170800	8:00 15:59	46	0034_0003	6:42	379.2					
				0034_0004	7:11						
				0034_0005	7:27						
				0034_0006	7:56						
				0034_0007	8:21						
				0034_0008	8:31						
				0034_0009	8:52						
				HM1	170_ark06190000		0:00 7:59	32	0004_0001	3:16	178.6
									0004_0002	3:31	
0004_0003	3:46:20										
0004_0004	3:46:52										
0004_0005	3:57										
0004_0006	4:10										
0004_0007	4:18										
HM2	170_ark06190800	8:00 15:59	24	0005_0002	10:08	147.4					
				0005_0003	10:18						
				0005_0004	10:26						
				0005_0005	10:29						
				0006_0001	10:45						
				0006_0002	10:56						
				0006_0003	11:08						
0006_0004	11:12										

All sensor data from VICTOR are sent via fibre optic cable to the ship, where they are connected with the ship's navigation data and related to the time stamp. Table 4.3 displays a part of NMEA datagram (National Marine Electronics Association) from 17th June 2003.

The message RVGEN is sent every second and contains miscellaneous VICTOR data: respectively date, time, dive number, latitude, longitude, heading, status of data storage (on), status of high speed digital link (ok), heading in degrees, trim value in degrees, immersion, altitude above seafloor, longitudinal and lateral speed in knots, horizontal orientation of pan main camera, orientation of tilt vertical 3CCD main camera, 3CCD focal length, 3CCD iris opening, 3CCD focus; unwind cable length, winch speed per second, cable tension;

depressor heading and depressor immersion; CTD temperature, salinity and pressure value from Doppler log and some other subsidiary information (ESI/IE, 2003).

The message PSGEN comes every second from POLARSTERN and includes date, time, latitude, longitude, DGPS latitude, DGPS longitude, longitudinal and lateral speed in knots, heading, depth, roll, pitch and other components (ESI/IE, 2003).

Table 4.3: Part of NMEA file: \$RVES/ RVGEN - dead reckoning, \$PSGEN POLARSTERN, \$PTSAG – POSIDONIA navigation

```

NMEA VICTOR 6000
$PIFM,POPSN,17/06/2003,08:59:52.389,273.04,+00.11,-
00.04,RVES,01,17/06/2003,08:59:52.389,N,53,41.7715,W,014,04.1274,0615,F,2,0615
$PIFM,PSGEN,17/06/2003,07:59:59.000,N,53,41.802,W,014,04.205,N,53,41.803,W,014,04.206,-0.1,-0.1,230.16,641.1,305.9,
0.4,0.6,0.2,-0.03,
$PIFM,RVGEN,17/06/2003,08:59:52.839,00000217,+53,43.000,-,14,05.000,N,L,273.00,-0.5,-1.7,614.29,0.107,-0.038,-
8.70,-30.50,,,-447,0.00,-1000,363.70,489.98,138.88,10.600,35.000,1502.000,273.00,273.00,8,6,,
282.48,-999.00,10.03,-0.159,
$PIFM,POPSN,17/06/2003,08:59:53.389,273.02,+00.12,-
00.05,RVES,01,17/06/2003,08:59:53.389,N,53,41.7715,W,014,04.1276,0616,F,2,0616
$PTSAG,#42638,080001.199,17,06,2003,01,5341.828,N,01404.147,W,F,0495,1,9999*28
$PIFM,RVGEN,17/06/2003,08:59:53.839,00000217,+53,43.000,-,14,05.000,N,L,273.09,-0.2,-1.6,614.39,0.117,-0.035,-
8.70,-30.50,,,-447,0.00,-1130,364.20,489.98,138.75,10.600,35.000,1502.000,273.09,273.09,8,6,,
282.81,-999.00,9.88,-0.138,
$PTSAG,#42640,080001.199,17,06,2003,00,5341.802,N,01404.205,W,F,0790,0,0000*23
$PIFM,PSGEN,17/06/2003,08:00:00.000,N,53,41.802,W,014,04.205,N,53,41.803,W,014,04.205,-0.1,-0.0,230.18,641.1,320.2,
0.3,0.7,0.1,0.08,
$PIFM,POPSN,17/06/2003,08:59:54.389,273.13,+00.13,-
00.05,RVES,01,17/06/2003,08:59:54.389,N,53,41.7714,W,014,04.1277,0616,F,2,0616
$PIFM,RVGEN,17/06/2003,08:59:54.839,00000217,+53,43.000,-,14,05.000,N,L,273.19,-0.2,-1.4,614.58,0.134,-0.034,-
8.70,-30.50,,,-447,0.00,-1130,364.10,489.88,131.38,10.600,35.000,1502.000,273.19,273.19,8,6,,
282.90,-999.00,9.84,-0.130,
$PIFM,PSGEN,17/06/2003,08:00:01.000,N,53,41.802,W,014,04.205,N,53,41.803,W,014,04.205,-0.1,+0.0,230.06,641.1,8.0,
0.3,0.8,0.0,0.31,
$PIFM,POPSN,17/06/2003,08:59:55.389,273.23,+00.12,-
00.02,RVES,01,17/06/2003,08:59:55.389,N,53,41.7714,W,014,04.1278,0616,F,2,0616
$PIFM,PSGEN,17/06/2003,08:00:02.000,N,53,41.802,W,014,04.205,N,53,41.803,W,014,04.205,-0.1,+0.0,229.86,641.1,50.4,
0.4,1.0,-0.0,0.61,
$PIFM,RVGEN,17/06/2003,08:59:55.839,00000217,+53,43.000,-,14,05.000,N,L,272.99,0.3,-1.4,614.63,0.123,-0.024,-
8.70,-30.50,,,-447,0.00,-1060,365.10,489.29,140.50,10.600,35.000,1502.000,272.99,272.99,8,6,,
283.02,-999.00,9.59,-0.126,
$PIFM,POPSN,17/06/2003,08:59:56.389,272.44,+00.12,-
00.03,RVES,01,17/06/2003,08:59:56.389,N,53,41.7714,W,014,04.1279,0616,F,2,0616
$PIFM,RVGEN,17/06/2003,08:59:56.839,00000217,+53,43.000,-,14,05.000,N,L,271.90,1.3,-1.7,614.82,0.111,-0.007,-
8.70,-30.50,,,-447,0.00,-1060,366.10,488.89,141.38,10.600,35.000,1502.000,271.90,271.90,8,6,,
281.98,-999.00,9.44,-0.105,
$PIFM,PSGEN,17/06/2003,08:00:03.000,N,53,41.802,W,014,04.205,N,53,41.803,W,014,04.205,-0.1,+0.0,229.72,641.1,67.9,
0.6,0.9,-0.1,0.72,
$PIFM,POPSN,17/06/2003,08:59:57.388,271.45,+00.14,+00.01,RVES,01,17/06/2003,08:59:57.388,N,53,41.7714,W,014,04.1281,
0616,F,2,0616
$PIFM,RVGEN,17/06/2003,08:59:57.838,00000217,+53,43.000,-,14,05.000,N,L,271.23,1.1,-1.9,614.88,0.108,0.020,-
8.70,-30.50,,,-447,0.00,-980,366.10,488.10,146.50,10.600,35.000,1502.000,271.23,271.23,8,6,,
280.90,-999.00,9.50,-0.099,

```

4.8 Progress of work and problems with XTF format

The work began partly already during the expedition when the data were processed from raw binary data recorded on DLT tapes to SURF, DUX, new DUX, HYD, NAK and finally

XYZ formats. Necessary conversions and editing of navigation data, tide application and coarse editing of single beams was performed onboard POLARSTERN.

Smooth functioning of HYDROSWEEP system was ensured by a 24 hour watch in the "Bathymetry Laboratory". CTD (Conductivity-Temperature-Pressure) measurements of the sound velocity in the water column were applied to take account of attenuation in the water profile.

Although the microbathymetric data are mainly handled late in the postprocessing, observations of the VICTOR systems were made in the winch room and container during all dives. Microbathymetric data were loaded and saved by QINSY software direct to hard disk (in DB format). The raw sonar data were not saved, which caused problems with data-export afterwards.

In post cruise processing, data were first downloaded from magneto-optical media. Both POLARSTERN and VICTOR bathymetric data had to be postprocessed. It was envisaged to process all echo sounder data using the CARIS because HYDROSWEEP data are commonly processed in that way, and because QINSY can export to XTF format. It seemed to be a trouble-free solution because CARIS can normally import XTF format data. Nevertheless, XTF files could not be opened in CARIS. A solution for this problem was sought together with the suppliers of QINSY and CARIS, KONGSBERG SIMRAD and in cooperation with IFREMER.

The echo sounder data were incompatible due to the way they were recorded during the expedition. The DB data were saved on hard disk in raw datagrams (run time). To export the data in XTF format, however, the DB data should be recorded in a depth datagram (with depths and offsets). It is not possible to change the format of the datagram.

After a few months of effort it was submitted that the XTF format is not readable by CARIS and could not be exported in any other way from QINSY to CARIS. Raw SIMRAD data were not saved, so nothing more could be done in order to arrange the exporting.

In November, the data from POLARSTERN were cleaned and prepared for comparison, but the preparation of VICTOR data stagnated. The rough corrections made in QINSY were not sufficient for the planned comparison.

Often, things get worse before getting better. Christian Edy (IFREMER, Plouzané) mentioned in Email sent to AWI that the CARAIBES software is able to read XTF files and fully process the VICTOR microbathymetry data. A journey to France followed on 8th December 2003, in order to use CARAIBES.

Some further problems were found in Plouzané:

- there is a gap in the data (bad time synchronisation between the SIMRAD Computer and QINSY Computer).
- there are a few incorrect dates in the bathymetry packet

A one hour delay was corrected, incorrect dates were eliminated, and navigation TXT files were used to extract the time. Required immersion, which was zero in all the XTF files, was put at the right place in the XTF file and, after that, the data could be opened.

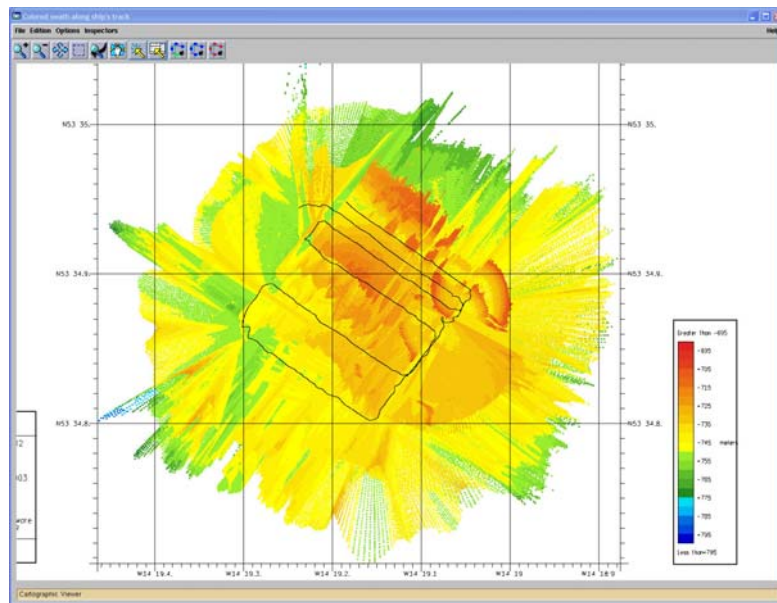


Figure 4.8: Erroneous microbathymetry

The bathymetry was erroneous in the first area (Figure 4.8), but useful data were saved in the other files.

An import of one meter raw grid files to ARC VIEW was successfully made in La Seyne sur Mer. However, uncorrected shifts remained in the navigation, which could lead to a doubling of features in an image (Figure 6.34): NO TIDE correction was applied, NO SHIFTS were corrected for and NO FILTERING was applied.

Finally, the corrections for tide, navigation offsets and manual editing of microbathymetric data was made in CARAIBES in Plouzané.

4.9 Four microbathymetric surveys

Five areas were microbathymetrically mapped around Scarp Mounds. Two of these were too small to make a useful comparison with HYDROSWEEP data. Hence, only three areas from Scarp mounds were compared.

In the Hedge mounds, two areas were surveyed. The first one appeared highly erroneous and was eliminated from the analysis. The second microbathymetry from Hedge mounds was surveyed on the last expedition day. The microbathymetric survey was taken into account despite its planned systematic survey not being quite finished. The main criterion for a choice of areas about 0.1 km² for comparison was their topography. Table 4.4 presents five selected areas with extent of 40 x 20 kilometres.

Table 4.4: Microbathymetric measurement of Hedge and Scarp Mounds.

40 x 20 km	Scarp Mounds			Hedge Mounds	
Areas	SM2	SM3	SM4	HM1	HM2
Dive No.	217	217	217	218	218
Date	16.6.2003	16.6.2003	17.6.2003	19.6.2003	19.6.2003
Time	92 min	149 min	132 min	77 min	71 min
Longitude (track)	13°59.85' – 14°0.20' W	14°1.30' - 14°1.65' W	14°4.05' - 14°4.35' W	14°19.05' – 14°19.30' W	14°21.14' - 14°21.45' W
Latitude (track)	53°43.57'- 53°43.81' N	53°43.20' - 53°43.40' N	53°41.75' - 53°41.98' N	53°34.80' – 53°34.95' N	53°33.45' - 53°33.64' N
Diameter	500 m	450 m	350 m	-	350 m
Km ²	0.25	0.2	0.1	-	0.1
Topography	part of mound	mound	plain slope	indistinguishable	part of mound
Note	mosaicking	+ feature for correlation	- feature for correlation	not used	survey not finished

5. THEORETICAL BACKGROUND

It is known that sound travels in water five times faster than in air. Because of this, sonars have been applied for a variety of purposes. Multibeam sounders, sidescan sonars, sediment profilers, acoustic Doppler systems, acoustic navigation systems, backscattering, microbathymetry and mosaicking are all examples of marine applications (Figure 5.1) developed in the last century. These applications provide information about the seabed from various angles. Sonar data have been used with other information in interdisciplinary studies to explore seafloor reflectivity, roughness, topmost sediment layering or for detailed exploration and video recording of the sea bottom.

At the moment a range of frequencies is used in marine exploration by echo sounders. The HYDROSWEEP multibeam echo sounder sends pulses of 15 500 Hz, single-beam PARASOUND echo sounders shoot pulses of 4 000 Hz and pulses of 200 000 Hz are sent by the multibeam echo sounder EM 2000. For comparison, the human ear can recognise the vibrations at frequencies of 20 to 20 000 Hz.

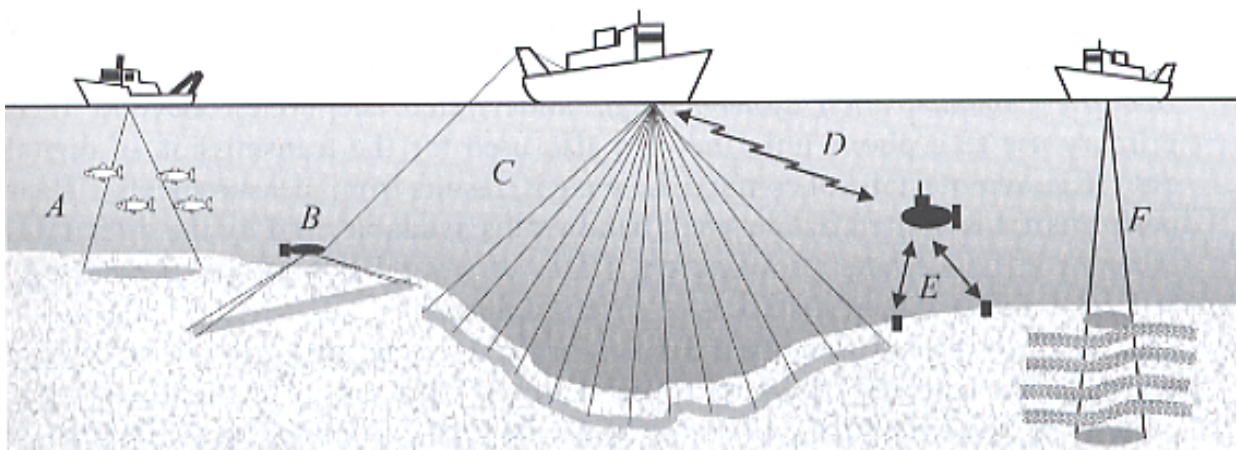


Figure 5.1: Examples of civilian application of sonar: bathymetry or fishery sounder (A), sidescan sonar (B), multibeam sounder (C), data transmission system (D), acoustic positioning system (E), sediment profiler (F) (after Lurton, 2002).

There are many influencing factors that disturb, absorb, attenuate or reflect emitted signals in the marine space. Many of these are unavoidable and can be only eliminated by manual postprocessing or filtering. Such factors source from the water or from the geometry of the measurement itself.

Sonar activities are partly restricted. Sonars have to be switched off south of 60 degrees as a part of an Antarctic agreement of 1988. Their acoustics may be disturbing for sea organisms e.g. whales communicating on the distances of 10 – 100 kilometres.

5.1 Bathymetry

The word “bathys” comes from Greek and means “profound”. Bathymetry is information derived from the measurement of water depth. Bathymetric charts are one of the most frequently requested marine data products and are used to provide depth input to navigation charts. They have aided the safety of navigation, the laying of trans-oceanic telephone cables, exploration and drilling for offshore oil, locating important underwater mineral deposits, and have improved our understanding of geological processes (Ng’ang’a, n.d.).

5.1.1 Snell’s law and the sonar equation

In the ocean environment, a sound wave spreads with a velocity close to 1 500 meters per second. The most exact models of sound motion through water were created by Chen and Millero in 1977. Contrary to sound waves, electromagnetic waves travel at around 300 000 000 meters per second. Electromagnetic waves are, by their form, transverse to their direction of propagation whereas acoustic waves are compressional. Acoustic waves propagate from point to point by compressions and dilations in gas, liquid or solid. The domain from 10 Hz to 1 MHz is used by acoustic applications.

The basic principles of echo sounder measurement are encapsulated in several mathematical and physical principles. One of the most important is the law of refraction defined by Snellius in 1621. This Law says that the angle of incidence is equal to the angle of reflection at an interface (Figure 5.2). Acoustic waves do not move linearly in water that consists of layers of different physical characteristics. Snell’s law also says (Equation 5.1) that the grazing angles β_1 , β_2 are proportional to the sound velocities (c_1 , c_2) in the different layers bounding an interface and the quotients are equal to a constant. Refraction therefore happens at interfaces where differences in sound velocity occur.

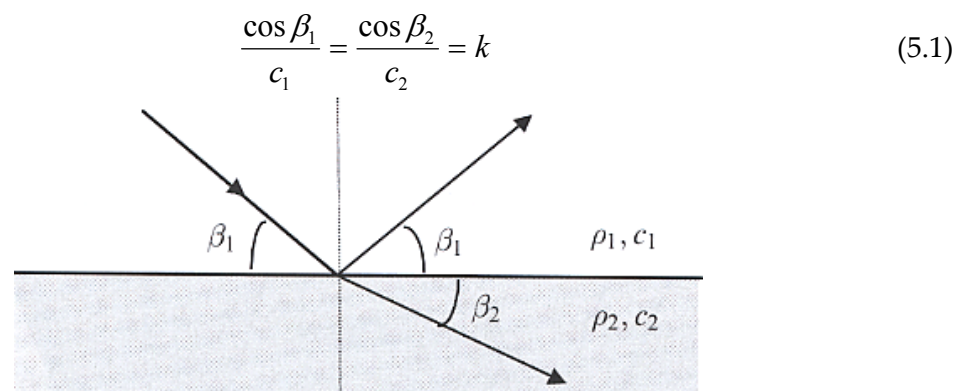


Figure 5.2: Snell’s Law (ρ is density) (after Lurton, 2002).

The sound waves generated by the sonar piezoceramic¹ projector travel through water to the bottom, are reflected (dependent on the sea floor) and return to the receiver, which converts the sounds into an electric signal, which is processed. Afterwards, the time needed for

¹ Piezoelectric Effect: a property of materials that respond to stress (such as squeezing) by producing a voltage.

passing the distance between the transmitter and the sea bottom is evaluated. The following equations are needed:

$$c = f \cdot \lambda, \quad (5.2)$$

$$s = \frac{1}{2} \cdot c \cdot t, \quad (5.3)$$

where c is mean sound velocity, f is frequency and λ is wavelength, s is the distance from the transmitter to the bottom and t is the run time of the beam.

An acoustic wave spreads in the water at a speed that is dependent particularly on salinity, pressure and temperature. Echo excess is determined as difference between the actual beam-former output and the detection threshold. Disturbances are included in the so called sonar equation for 1 Hz band (from Nielsen, 1991):

$$EE = SL + 2TL + TS - (NL - DI) - DT, \quad (5.4)$$

where EE is echo excess, SL is source level (dB), TL is transmission loss, TS is target strength, NL is background noise level, DI is directivity index of receiver array, DT is detection threshold. In the case of a reverberation from the sea surface, RL is written instead of $(NL - DI)$.

A wave of 12 kHz loses (TL), by attenuation, a half of its energy after 3,000 meters (ATLAS HYDROSWEEP DS, 1988). Every transducer in a multibeam array is sensible to one particular direction (DI). Target strength is related to objects on the sea floor, reverberation level and its effect on marine life, and sea surface conditions. More information can be found in Nielsen (1991).

The propagation velocity of an acoustic wave is imposed by the density and elasticity factor of the medium (Lurton, 2002). For the accurate measurement of these properties in water, measurements of temperature and pressure relating to depth, captured by CTD, has to be taken into account, and calibration of middle beams is also provided.

5.1.2 CTD measurement

The CTD sonde (Conductivity-Temperature-Pressure) is an important piece of equipment for the calibration of bathymetric measurements. The sizes differ. In Figure 5.5, one CTD cylindrical device is shown to be around 1 meter high, with a diameter of 20 centimetres and is covered with meters and probes. As it is lowered and raised in the ocean, nearly continuous profiles of temperature, salinity, and other properties are provided. On each CTD station, position, date, time, sampling interval, meteorological and sea surface conditions are reported.

The velocity of the propagation of sound is different at different depths, and the CTD record demonstrates the temperature, salinity or conductivity, density, and possibly dissolved

oxygen or transmission at specified depth or pressure levels in the water column that determine this velocity.

The recorded data are immediately applied to computation algorithms in order to improve or calibrate the measurement of actual depths.

Results of CTD deployments can be found in Appendix B. Graphs of sound velocity in relation to depth are displayed in Figure 5.3. The curvature is characteristic for the North-East Atlantic as can be seen in Figure 5.4.

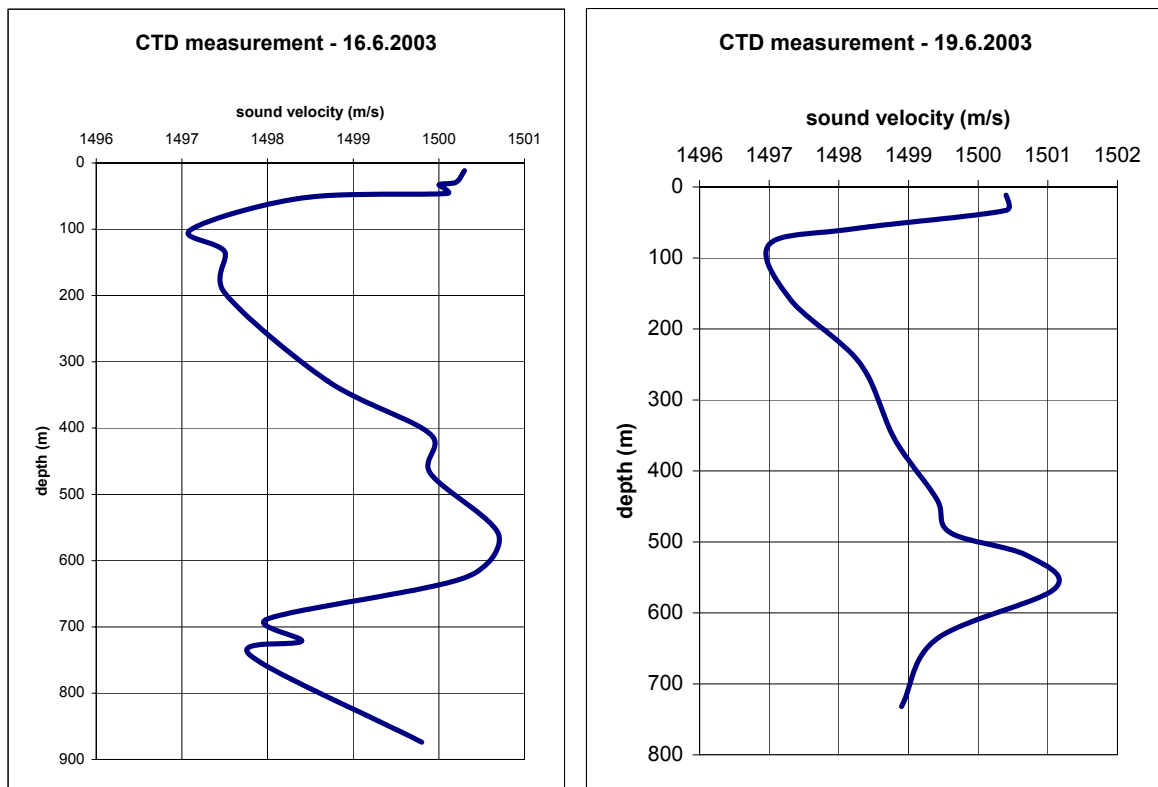


Figure 5.3: Sound velocity profile from 16 and 19th June 2003, ARK XIX/3a.

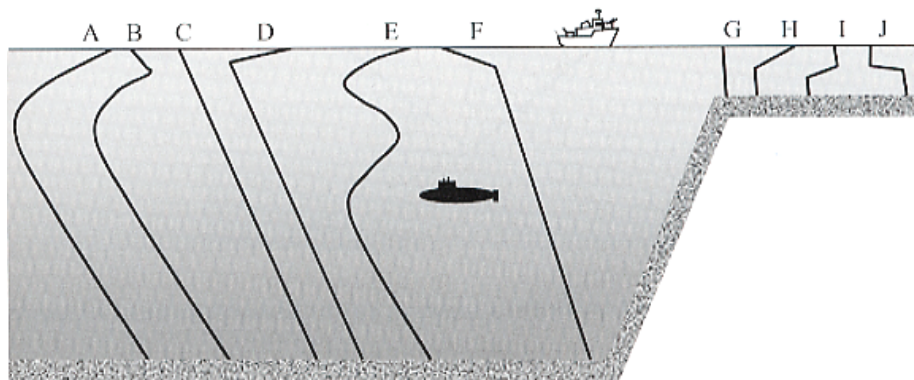


Figure 5.4: Different sound velocity profiles for deep and shallow waters: North-East Atlantic (E), polar (F), winter (C, G), summer (D, H) (after Lurton, 2002).

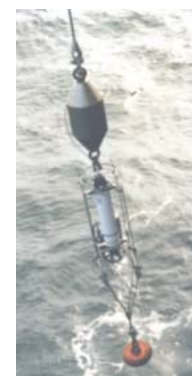


Figure 5.5: CTD sonde.

5.1.3 The geometry of multibeam sonar

Exact terminology is used to describe the angles and lengths within multibeam geometry. Figure 5.6 demonstrates the most important angles and distances used in the calculations of the run times of single beams. The angle of incidence θ_i , grazing angle θ_g , angle of arrival θ_a and slope angle θ_s are counted with reference to nadir. The double slant range, s , can be computed as time t multiplied by wave speed c (Equation 5.3).

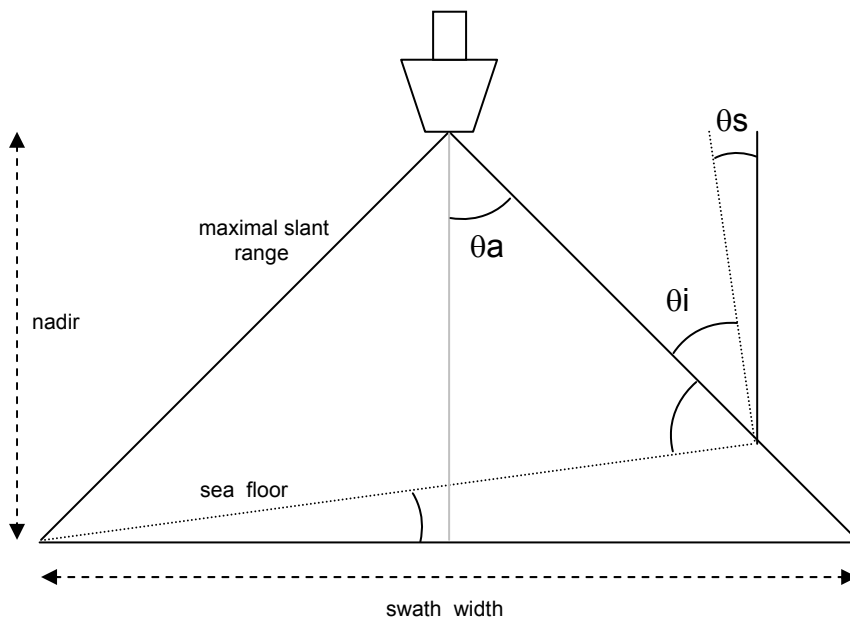


Figure 5.6: Multibeam geometry over rough terrain (after Jacobs, 2002).

5.1.4 Cross-Fan Calibration

Beams are preformed (PFB) in the digital beam former, and sent to the bottom through 72 amplifier channels. Signals are transmitted (or received) at three arrays (Figure 5.7 right). Each array is composed of 3 identical transducers each of which consists of 96 elements arranged in 4 by 24 matrices, so that 72 channels receive signal echoes.

For each of 59 channels, a memory area is filled with the received amplitude vs. time signal. The return signal is received from the sea bed from a fairly large area of the seabed, defined by depth, slant angle and swath width (Krupp Atlas Elektronik, 1988).

The cross-fan calibration principle stems from the suggestion that two different paths of sound propagation should yield the same result if the water sound velocity, c_m , is correctly applied. The calculation of depths is based on the adjustment of c_m . After a least-squares comparison between two profiles ($\sum d = \min$), a mean sound velocity is calculated which can be used for surveying. The mean water sound velocity formula, c_m , (Equation 5.5) makes the slant beam profile fit best with the vertical beam profile (Gutberlet and Schenke, 1989).

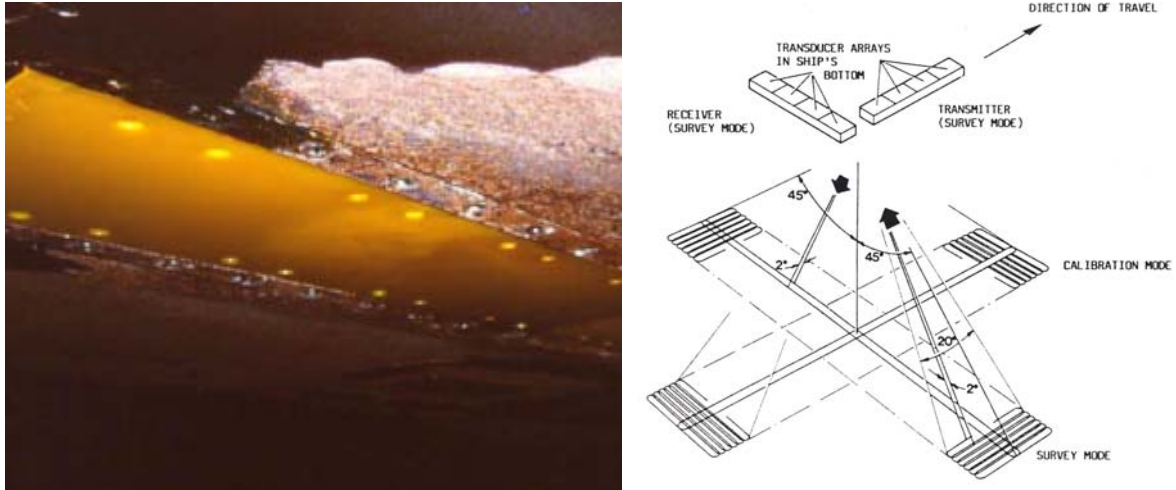


Figure 5.7: Transmitting part of HYDROSWEEP (left) and surveying principle (right).

Maul and Bishop (1970) represents one of possible the formula as:

$$c_m = \left[\frac{1}{z} \sum_{i=1}^n \frac{\Delta z_i}{v_i} \right]^{-1}, \quad (5.5)$$

where z is the depth, Δz is vertical distance of one layer and v is sound velocity in single layer and i, n a water body of n layers.

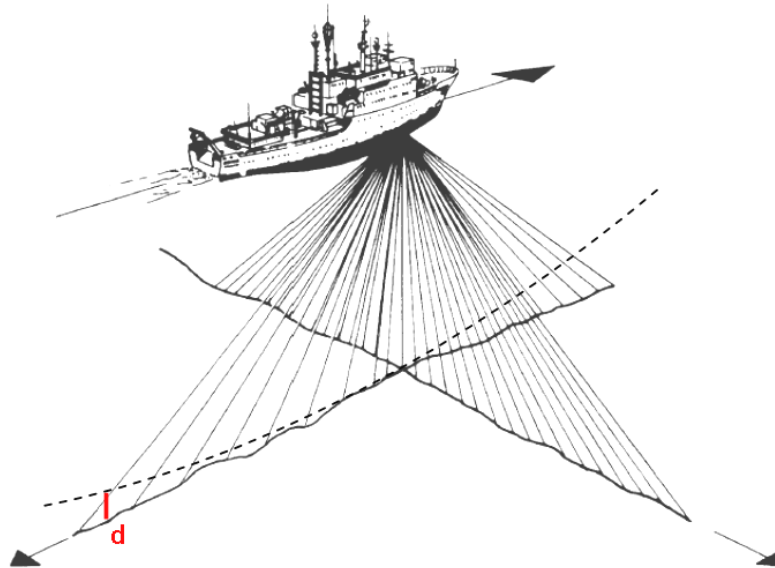


Figure 5.8: Principal of cross-fan calibration HYDROSWEEP (d is difference) (after Krupp Atlas Elektronik, 1988).

A new kind of calibration algorithm without fan crossing was developed by Atlas Hydrographics, with the main idea to record just the vertical slant beams (Büchenschütz-Nothdurft, 2002).

5.1.5 Systematic and random errors

Generally, bathymetric measurement is influenced by external errors (sound velocity and refraction), internal errors (movements of platform) and errors in the acoustic measurement itself.

The fifty-nine coordinates in a swath depend mainly on correct time and angle measurement for their accuracy. Time and angle measurements are affected by many removable (R) or irremovable (I) factors. Application of a sound velocity profile (R) considers the effects of layering of ocean water, but there are still disturbances due to propeller noise, backscattering at the seafloor and motions of the ship (R). Sea water absorbs part of the energy of the radiated wave (I). Further errors which influence the travel and reception of the signal in the water are caused by attenuation of waves (I) in water with dissolved salt (NaCl, $MgSO_4$), propagation loss of beams (I), air bubbles in upper water layers (I), multiple paths (I), Doppler effect (lengthening of a time signal) (I), ocean noise (I), seismic activity (I), weather conditions (I) or movement and noise of sea organisms (I). Attenuation loss depends on frequency and depth (Lurton, 2002).

In this chapter, only systematic errors concerning the movements of ship and system geometry will be described. The consequences of certain errors will be further discussed with practical examples in Chapter 6 and 7.

5.1.5.1 Movements of the ship

Forward motion causes a horizontal shift between the transmitter and receiver. The run time of a beam aiming from the ship to the sea floor differs from the run time from the sea floor to the moving ship after reflection. Figure 5.9 illustrates motion of the ship from the position A to the position B, and how this affects the run time.

Assuming a situation like the one described in Section 5.1.6, the time, t_{AB} , between two successive transmissions will be 3 seconds. At a speed of 29 km/h, HYDROSWEEP covers a distance of 24 meters in 3 seconds.

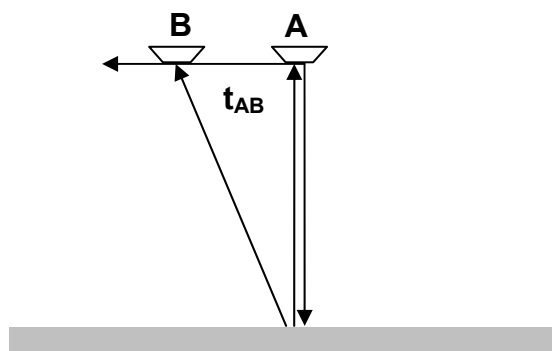


Figure 5.9: Forward motion of the vessel.

The heave values are compensated by HYDROSWEEP device (Figure 5.7). The correction is not always necessary because heave motions in mild weather may not exceed few meters, and the absolute vertical accuracy in 600 meters is 6 meters (1% of depth). The problem is

more complicated when measuring the distance between two changing surfaces (Figure 5.10): the topography of the seabed and the dynamic sea surface.

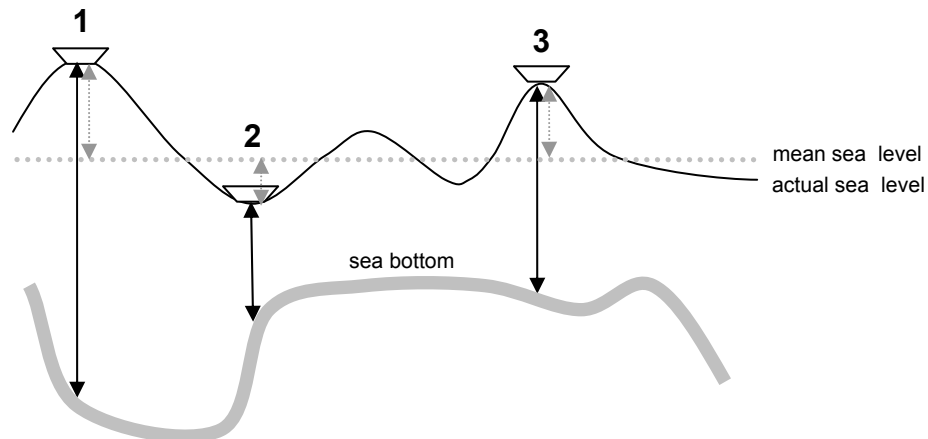


Figure 5.10: Different heave motions about the mean sea level (MSL): above MSL (1), below MSL (2), above MSL with different depth (3).

The beams are preformed to the nadir direction by HYDROSWEEP. Therefore, correction for non-vertical beams is not necessary except for corrections for roll and pitch of ship itself.

5.1.5.2 Errors caused by geometry

As can be seen from Figure 5.11, the different beams are detected with different time offsets and with different strength signals. The reflection of the middle beam has the highest amplitude but has a smaller footprint than the lobe beam. Lobe parabolic reflections are weaker and do not bring such high quality information as the vertical beam. In postprocessing editing, the lobe beams have highest probability of being evaluated as erroneous. The more distant from the middle beam, the greater the area that is covered. The difference in the sizes of footprints can also be seen in the time signals axis (Figure 5.11).

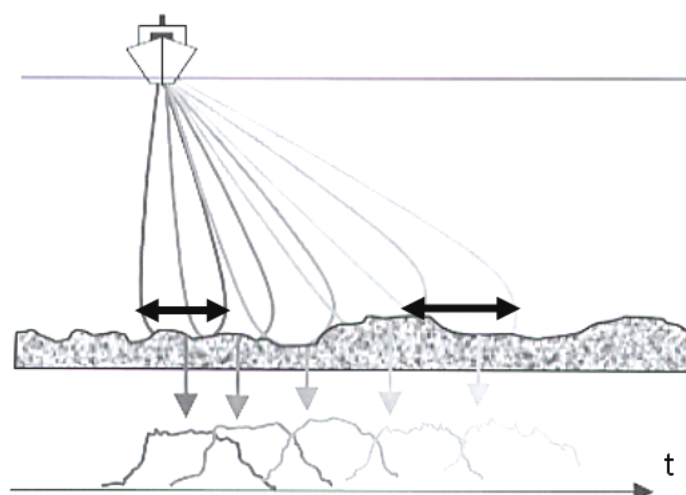


Figure 5.11: Formation of sonar image, stressing the relative geometries of the vertical and boundary beams (after Lurton, 2002).

The error caused by side lobe echoes received prior to the main echo is called the omega effect. The omega effect occurs if the middle beam has to travel a longer distance than the lobe beam.

If the middle beam is strongly reflected, then the tunnel effect can occur. The amplitude of a neighbouring signal is weak in comparison with the nadir beam, with consequence that the estimated nadir beam run-time seems to be deeper than the true bottom.

The detection of shapes on the seafloor is shown in Figure 5.12. If a feature has a diameter less than the footprint (24 meters at a depth of 600 meters), it will not be detected by an echo. The shape of detected feature will be therefore the preciser the higher the horizontal resolution of the sounder is. Errors are larger if just a single echo sounder is used.

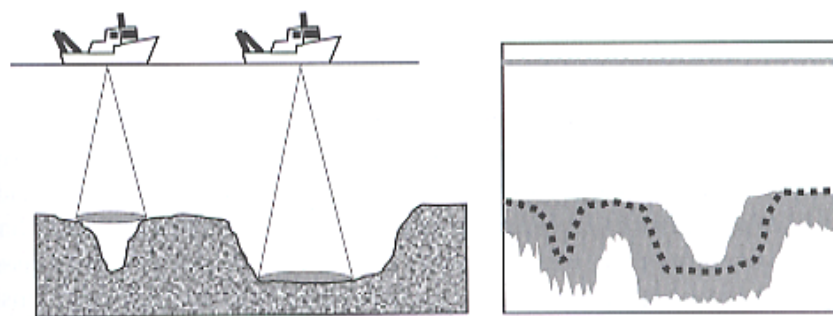


Figure 5.12: Seafloor trough detection and respective echogram (after Lurton, 2002).

The layering of water as described in Section 5.1.2, influences the paths of beams. Figure 5.13 illustrates the path of the lobe side beam through the water medium compared with an estimate based on an erroneous layering model. The error is the higher the more water layers occur.

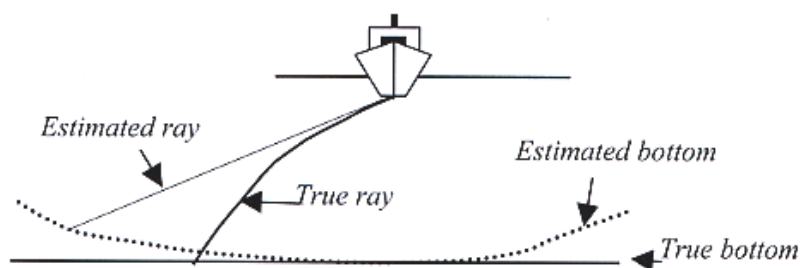


Figure 5.13: Errors associated with sound velocity profiles (after Lurton, 2002).

5.1.6 Preparation for systematic surveying

On every expedition the bathymetry is measured almost continuously. Sometimes, a systematic bathymetric surveying is needed. The first step is a check on maps for regions that were not surveyed in previous expeditions. If surveying will take two days, then the topographer counts with 48 hours (= 2 880 minutes = 172 800 seconds). Forecasting is another task for HYDROSWEEEP operators, namely of likely depths in the area to be surveyed. From the predicted depth, the swath width can be calculated simply as

$$w = 2 \cdot d \cdot \operatorname{tg} \frac{\alpha}{2}, \quad (5.6)$$

where w is the swath width, d is depth and α is the opening angle of the echo sounder. Depths are usually approximately known, for example from satellite altimetry. Mainly, IBCAO (International Bathymetric Chart of the Arctic Ocean), ETOPO5 (Earth TOPOgraphy - 5 minute) or GEBCO (GEneral Bathymetric Chart of the Oceans) is used as information sources (see Figure 7.13). For HYDROSWEEP multibeam sonar, which has an opening angle of 90 degrees, Equation 4.6 allows us to expect a swath width of 1,200 meters in 600 meters of water.

The next task is to estimate the speed of the ship during the surveying in order to overlap two following swath lines. If we take an average speed of sound in water of 1,500 m/s, then, two-way travel time of the middle beam is 0.8 second, and of the side beam (hypotenuse is equal to 1,698 meters) is 1.1 seconds. A further 1-2 seconds should be added for the HYDROSWEEP device to calculate and save the received signals. Afterwards, next signal can be sent. In a depth of 600 therefore a seabed profile will be measured every 3 seconds.

One profile of beams of 2.3 degrees covers a width of about 24 meters in the direction of motion. To survey with an overlap of 5 meters, POLARSTERN has to move at 8 m/s (19 meters per 2 seconds for necessary calculations), that is at 16 knots² (29 km/h). Surveying a 600 meters deep surface of 10 × 1.2 kilometres will take 21 minutes at this speed. Overlapping of the swaths gives a better resolution in the resulting map. The overlap is necessary in order to avoid “holes” which might have appeared during interpolations.

5.2 Sidescan

Sidescan (Figure 5.14) is another way of visualising the seafloor and, together with acoustic backscattering and sediment profiling, is also based on sonar measurement. Sidescan sonar data are not used in the measurement of depths, but are an appropriate supplement to bathymetric data.

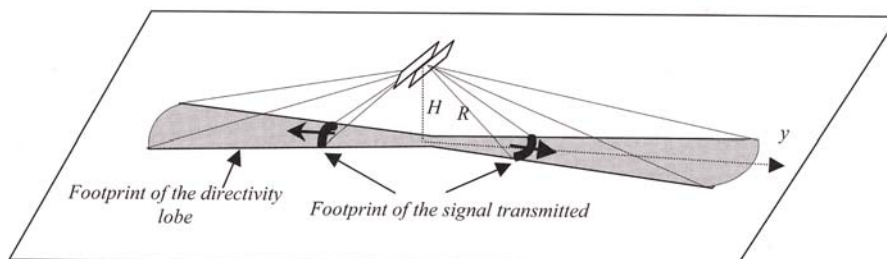


Figure 5.14: Sidescan sonar principle (R for range and H for depth) (after Lurton, 2002).

Usually, sidescan devices are mounted on a “fish” which is towed close to the bottom. The HYDROSWEEP system has a sidescan capability. Through a Max-PFB filter, the amplitudes of the received signal are cut and stored in 1024 equidistant pixels within the fan sweep

² 1 [knot] = 0.514444444 [m/s] = 1.852 [km/h]

(Hohmann, 2002). Angles of incidence are taken into account and grazing beams are thus converted to orthogonal directions and amplified.

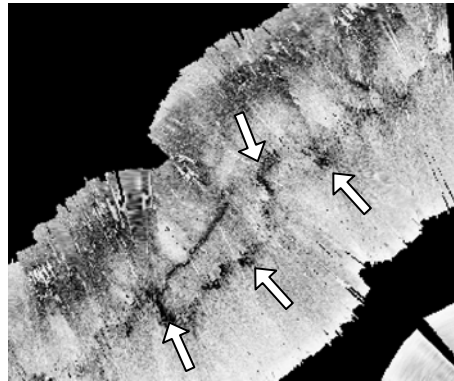


Figure 5.15: Higher reflectivity areas relating to carbonate mounds on Porcupine Bank.

Sidescan's difference to bathymetry (see Figures 5.16 to 5.19) is that signal is recorded laterally. A sidescan image shows contrasts in seafloor reflectivity (Figure 5.15). Soft materials like mud do not reflect all of the energy of beam but absorb a part of it. In such cases the low intensity reflection signal received by the sonar is coloured light grey on the image. Maximum reflection occurs off hard smooth materials like rock. The high reflectivity is displayed dark grey.

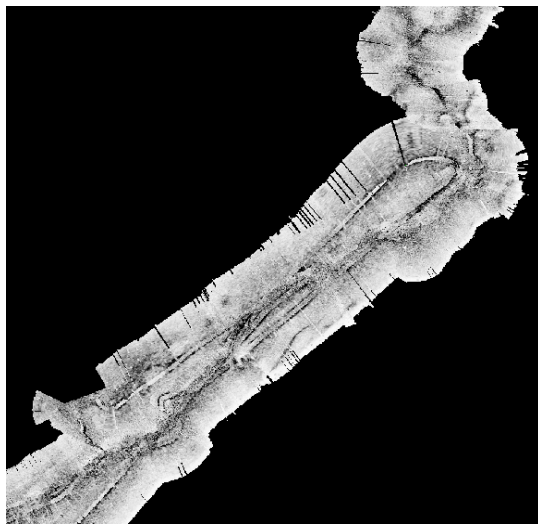


Figure 5.16: Sidescan image of Scarp Mounds area (HYDROSWEEP).

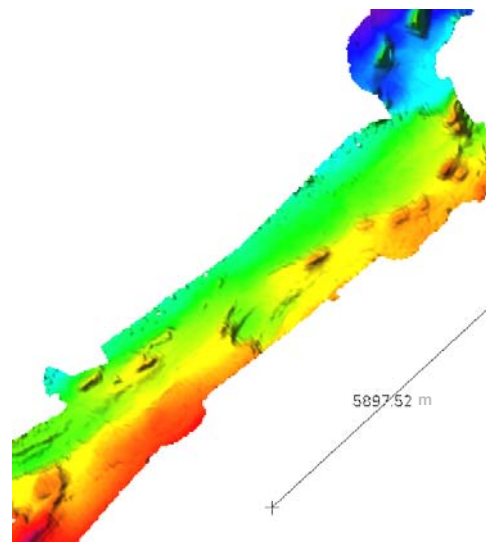


Figure 5.17: Bathymetry of the same Scarp Mounds area as in Figure 5.16 (HYDROSWEEP).

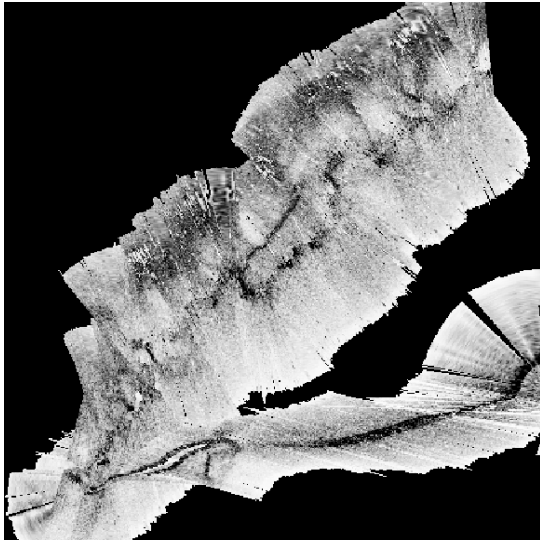


Figure 5.18: Side Scan image of Hedge Mounds (HYDROSWEEP).

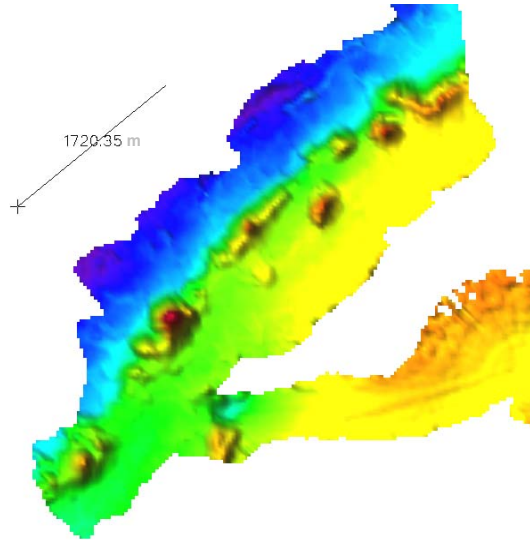


Figure 5.19: Bathymetry of the same part of Hedge Mounds as in Figure 5.18 (HYDROSWEEP).

5.3 Parametric echo sounder on POLARSTERN

The single beam system PARASOUND (PARAMetric echoSOUNDer) also penetrates and reveals shallow geological layers beneath the seafloor (Figure 5.20). The PARASOUND echo sounder (STN Atlas Elektronik GmbH, Bremen) allows the improvement of lateral and vertical resolution of seabed. Imaging the higher frequency than seismic systems allows a higher vertical resolution that provides more detailed information about the upper layers of sediment. PARASOUND measures with an opening angle of 4 degrees. Its footprint at a depth of 600 meters will be about 42 meters, and in general is about 7 % of the water depth. The high resolution is a result of the parametric effect, when two frequencies are radiated simultaneously. The 18 kHz, and the secondary varies from 20.5 up to 23.5 kHz.

The two slightly different frequencies interact and their sum or difference generates information about the sub-bottom layers. High frequencies determine the water depth.

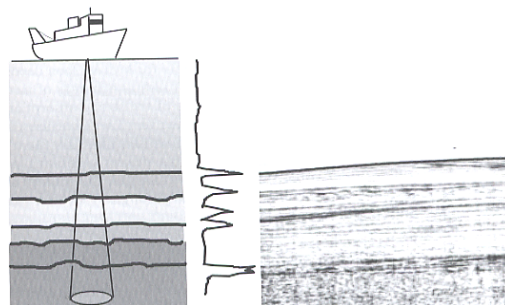


Figure 5.20: Profile obtained with the PARASOUND system and time domain signal (middle).

Because of the ship's movement, the transmitter has a different position than the receiver. Hence, hub compensation is additionally included, through run time correction, in order to refer the beam to a common point (Bergmann, 1996).

PARASOUND data are output in two ways. Digital output is stored in a PS3 format and analog output is drawn by a DESO 25 (Atlas Hydrographics) recorder on a roll of paper.

During expedition ARK XIX/3a, the movement of POLARSTERN was dependent on the status of VICTOR. If VICTOR was deployed, its umbilicus did not allow POLARSTERN to steam at more than 1.5 knots. Such slow movement is advantageous for the collection of PARASOUND data because continuity of layers in the imaged sediment pattern was guaranteed. Internal structure can hence be seen in the resulting digital images of Pelagia Mounds (see Appendix K). Bathymetric data and PARASOUND images are clearly useful as complements to one another.

5.4 Microbathymetry from ROV VICTOR 6000

Microbathymetry is the micromorphological measurement of sea topography connected with video recording and photographing of sea life and the sea bottom. Microbathymetric charts provide an opportunity to study the detailed size, shape, and structure of the seafloor. Examples of its utilization are in archaeological research, documentation of shipwrecks, detailed mapping of hydrocarbonate or methane mud volcanoes, study of sites where cables have to be laid, and site surveys for drilling or other engineering activities.

5.4.1 Sonar EM 2000

The EM 2000 high resolution multibeam echo sounder (Figure 5.21), transmitting 110 signals operate typically in depths of 250 meters. On subsea vehicles, the sonar can be deployed at depths of up to 3000 meters. The instrument has a vertical precision of 0.2% of its altitude. A combination of phase and amplitude detection is employed, resulting in a measurement accuracy of 8 centimetres RMS (Root Mean Square), independent of beam angle (EM 2000, 2002). Nevertheless, the horizontal accuracy drops to ± 30 meters through positioning (see Section 3.3.2).

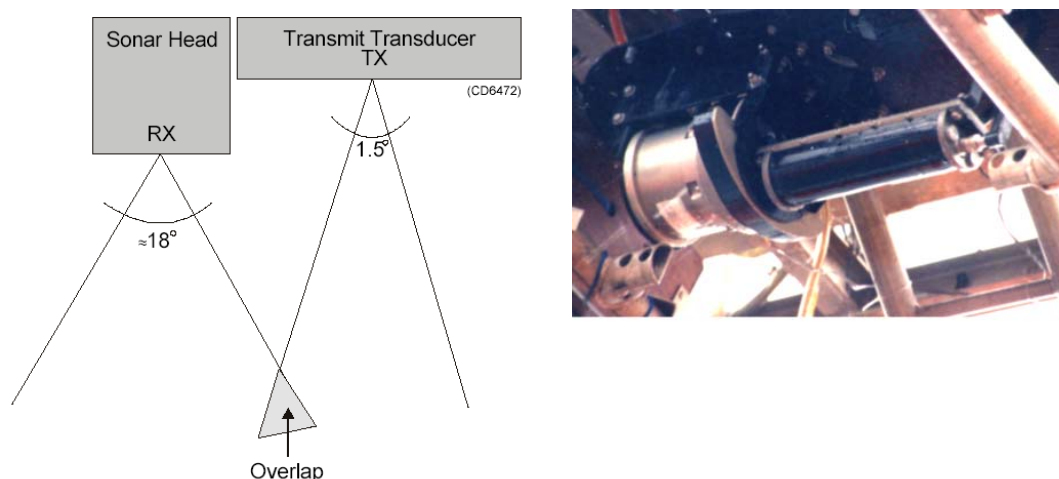


Figure 5.21: SIMRAD EM 2000 sonar (figure on the left after EM 2000, 2002).

The construction of the multibeam EM 2000 is different than the HYDROSWEEP. The EM2000 Sonar Head contains the receiver transducers and all transmitter and receiver electronics. A separate Transmit Transducer has 120 degrees coverage. The Transmit Transducer is connected to the Sonar Head via a short underwater cable (EM 2000, 2002).

5.4.2 Roll calibration through selected lines

“The best check of gyro is done with theodolite in the harbour.” (EM 2000, 2002)

For shallow water bathymetry, calibration of the system is less important than for deep water surveying. At any rate, a few errors always occur and so it is necessary to establish the offsets to the system.

Calibration should be done at the start of every survey. The SIMRAD EM 2000 system has to be calibrated separately for roll, pitch and heave. Figure 5.22 demonstrates then roll calibration procedure.

Firstly, two survey lines have to be selected in the calibration display, in order to discover their systematic errors and the time delay of the positioning system. These lines are measured several times in opposite directions and the results along two selected lines are analyzed. Finally, the output is the mean of values determined in a calibration corridor.

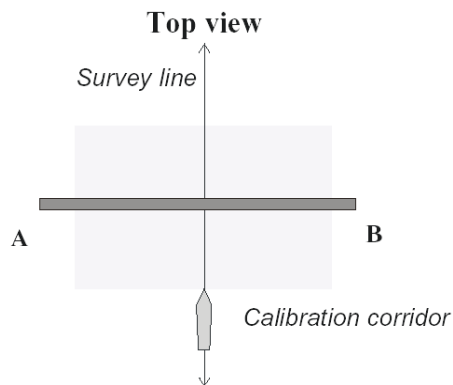


Figure 5.22: Roll procedure (right) (after EM 2000, 2002).

Roll calibration can be done over a flat area. For pitch calibration, a fairly steep slope is ideal. Offsets enter the system and the calibration is once more reprocessed to control the correctness of the calibration.

The calibration of systems is beyond the scope of this thesis. For detailed information about calibration procedures for sound speed, pitch and time delay see EM 2000 (2002).

5.4.3 A comparison of the two sonar's geometries

During the expedition, the HYDROSWEEEP sonar operated with an opening angle of 90 degrees, and the EM 2000 with an opening angle of 120 degrees. HYDROSWEEEP received echoes from 600 meters above the seafloor and EM 2000 about 10 - 30 meters above it. At the operating distance of 10 meters above the bottom, VICTOR's swath width covered 3 % of POLARSTERN's swath. Between the footprints there was a relation of 26 centimetres to 24 meters; a proportion of 1:92. Figure 5.23 emphasizes the different opening angles of the sonars and shows the ideal configuration for acoustic positioning of VICTOR from the ship. In the next figure, correct mapping of sea floor is displayed. Quasi footprints of EM 2000 beams are shown in the form of black points, and the direction of surveying is shown by an arrow on the center beam, number 55. Just 18 are displayed in the window.

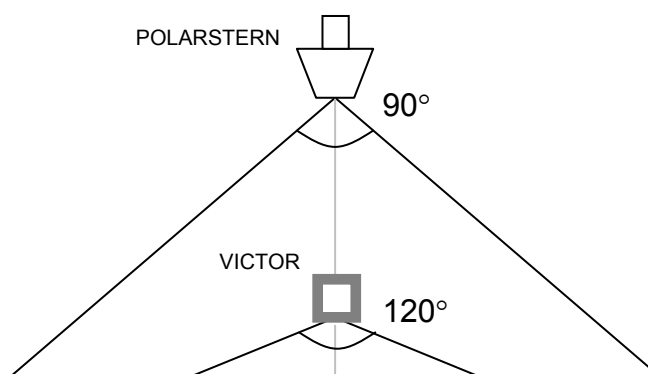


Figure 5.23: Ideal mapping sonar constellation of POLARSTERN and VICTOR sonars.

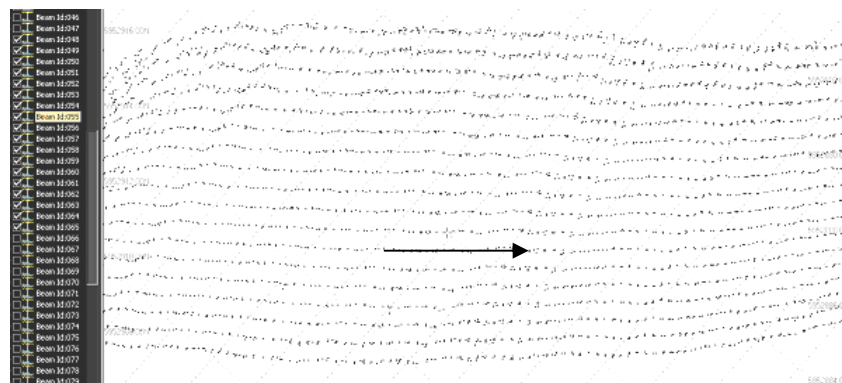


Figure 5.24: Beams measuring the seafloor, arrow pointing in the center beam.

5.4.4 Different depth measurement

Microbathymetry is not the precise measurement of water depths at all. There is a difference in measurement compared to traditional bathymetry developed from plummet measurement: the microbathymetric depth consists of added components from sonar or altimeter values and pressure sensors values, whereas bathymetric depths come directly and only from sonar.

In Figure 5.25, depth C is measured by altimeter and can be also derived from sonar measurement, (Equations 5.3 and 5.8). Distance B expresses the length between the sonar and the ROV's pressure sensor, which is countable from the local coordinate system (see Section 3.3.1).

The depths measured on POLARSTERN are counted as addition of the depth b, from HYDROSWEEP unit to the seafloor, and heave value a corrected to mean sea level.

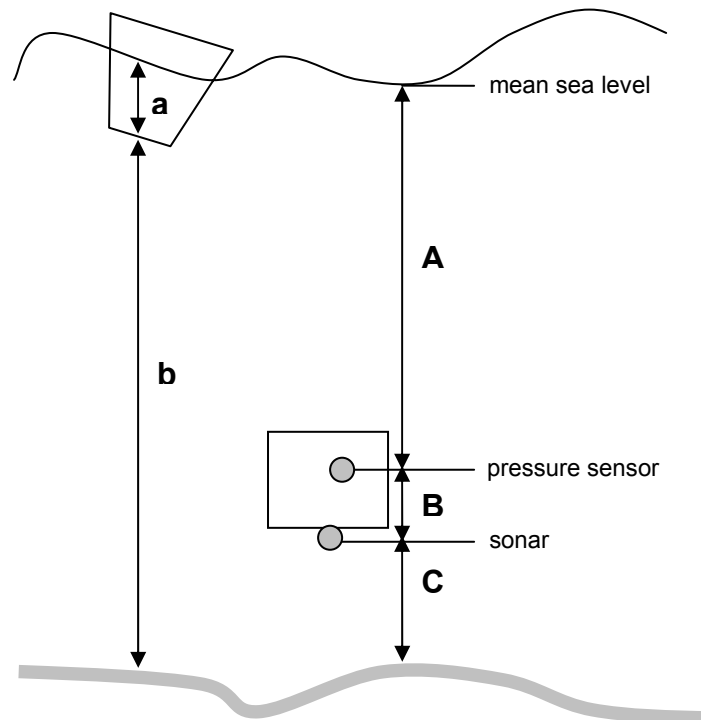


Figure 5.25: Microbathymetric and bathymetric determination of depths.

5.4.5 Microbathymetric errors

Some of the surveying errors that were outlined in Section 5.1.5 are partly valid also for microbathymetry. It has to be added that microbathymetry is not as heavily influenced by disturbances as bathymetry, whose signals travel much greater distance in the water. Internal errors have to be adjusted by calibration offsets. Disturbances from propellers, transmission loss, absorption or attenuation of water are not significant either air bubbles do not occur. Sound velocity could be an influence but the same sound velocity profiles (Figure 5.3) from CTD sonds are applied to avoid bias due to this factor. Uncoordinated motions of the vehicle and refraction of beams cause the most problems and these may be provoked by currents. The Operator Manual (EM 2000, 2002) states that the 200 kHz frequency is tolerant to turbid waters.

VICTOR's movement is stable in Figure 5.26a, the track line is straight, and hence reliable microbathymetry can be measured. An unstable motion is depicted in Figure 5.26b. Such movement may occur during changes of direction, is the presence of side currents, or by acceleration or deceleration of the ROV.

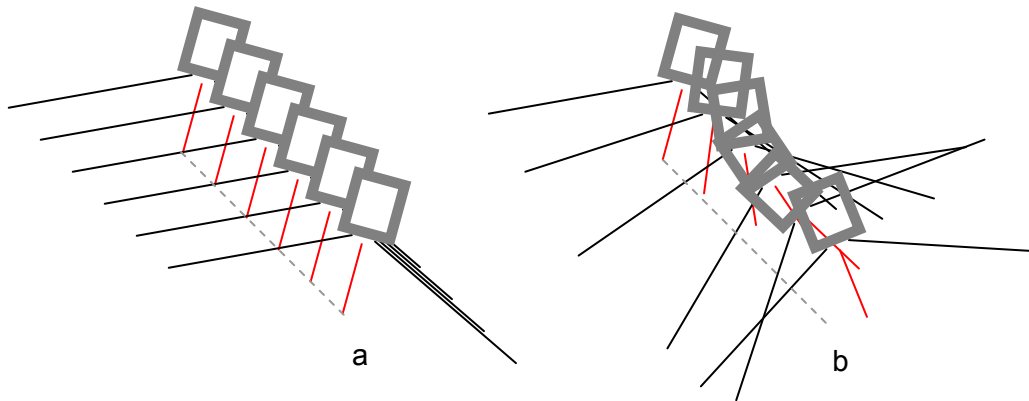


Figure 5.26: Motion of VICTOR: stable (a), unstable (b).

Heave is achieved with the help of hydraulics. Sinking is achieved by filling water into VICTOR's tank and runs relatively smoothly. Roll and pitch are determined in Octans Inertial Units.

Generally, errors in range and angle translate into vertical errors. Roll is one of unwanted angular change. Rolling disturbs the continuity of surveying and complicates positioning from the ship. A simple situation with roll movement is shown in Figure 5.27, where it is supposed that the transmission and reception of signals occurs in water of constant velocity of 1 500 m/s. Change of the roll angle means that the calculated distances from run time do not output the vertical depth, v , but slant distances, a_s , a_b , a_c . Roll angle, θ , is measured by Octans. The verticals v_s , v_b , v_c can be additionally calculated from the known values of time, via the slant distance and angle of arrival, θ_a , as:

$$v_c = a_c \cdot \cos \theta_a, \quad (5.7)$$

$$v_s = a_s \cdot \cos(\theta_a - \theta), \text{ and} \quad (5.8)$$

$$v_b = a_b \cdot \cos(\theta_a + \theta). \quad (5.9)$$

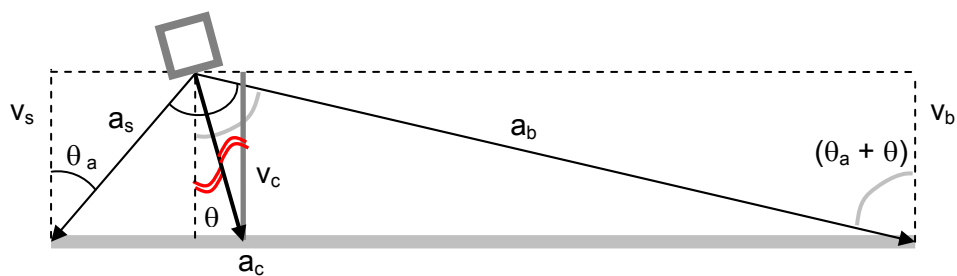


Figure 5.27: Rolling geometry with roll angle θ .

In the case of a flat sea bottom the values v_s , v_b , v_c will be equal one another. Recomputation of depths received from Equation 5.3, to "real" depths is not realized until postprocessing the VICTOR data. A fuller description of this problem is to be found in EM 2000 (2002).

5.4.6 Planning of surveying

Like bathymetric surveying (4.1.6), microbathymetric surveying is planned before its execution. The bridge officer as well as the ROV's pilots receive the coordinates of the planned survey and they try to follow them. Microbathymetry can not be planned as precisely as bathymetric surveying. VICTOR's movement is not as stable as POLARSTERN's, and therefore the planned lines cannot be followed exactly. Figure 3.19 illustrates the influence of acoustic navigation as a visible "shaking" of the track. VICTOR can move at a maximum of 1.5 knots, and is often disturbed by currents, so that overlap of neighbouring swath widths is also not quite guaranteed.

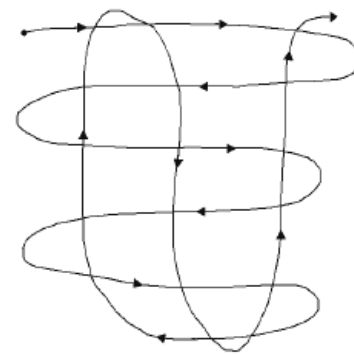
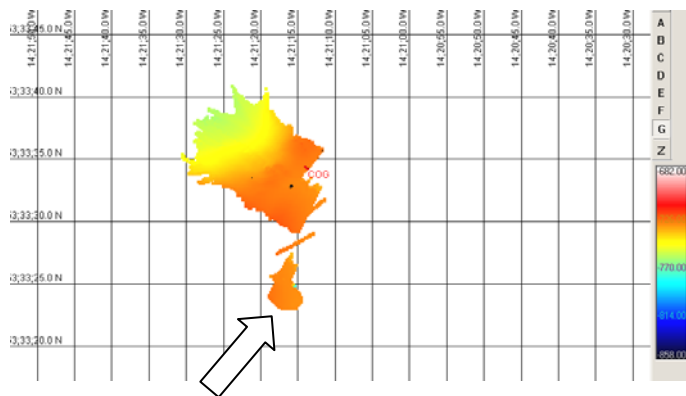


Figure 5.28: Beginning of surveying of Hedge Mounds (HM2). **Figure 5.29:** Usual microbathymetric surveying trajectory.

A pilot gets the coordinates to follow. The minimum operating altitude for the EM 2000 is 2.5 meters, but microbathymetry is done at around 10 metres. Microbathymetric operators observe the whole mapping online. Important observations are the correctness of acoustic navigation, dead reckoning navigation and continuity of sonar measurements. Almost every hour, the resetting of acoustic navigation has to be done manually. The division of files has to be done mainly before and after the vehicle's turns and in the event of a navigation jump. Available software does not allow for correcting the navigation inside one file. The CARAIBES software is able to shift single files.

In Figure 5.28, the error due to bad navigation can be seen. If this happens, storage of the file has to be immediately finished, dead reckoning navigation has to be initialized and a new file has to be initialised. The storage of single files depends on the correctness of the POSIDONIA navigation, the Doppler Log, and other systems. Figure 5.29 shows a theoretical microbathymetric survey and Figure 5.30 demonstrates the systematic surveys of areas in Pelagia Province. The centre beam is displayed in blue.

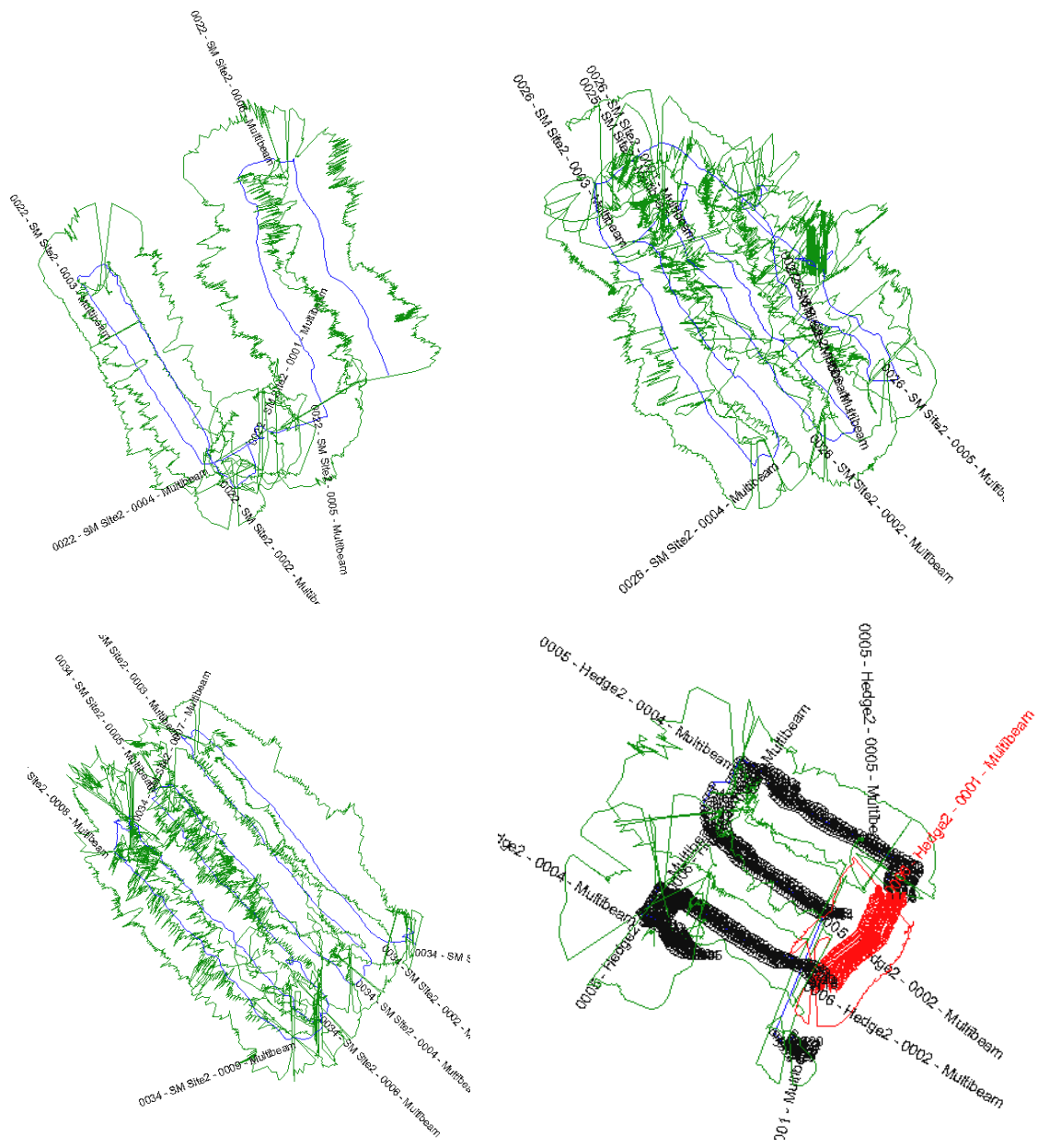


Figure 5.30: Surveying of SM2, SM3, SM4 and HM2 areas – one of the survey files is displayed in red.

5.5 Mosaicking

Video observations are commonly switched on a few minutes before the dive. Video recording is used during every dive and is of use for movement of the ROV on the bottom. A camera is mounted vertically underneath vehicle and records video sequences of the sea floor at the speed of VICTOR. The recordings from the vertical camera are stored on DVDs on the ship.

A mosaic is a composite image of several aligned video images from a sequence (Garcia, 2001). Video sequences are processed in the ADELIE or MATISSE software with a feature tracking method or robust optic flow algorithm. Advantage of this approach is the possibility of georeferencing.

Processing is accomplished in four steps. Firstly, image processing, secondly, computation of the geographical size of the mosaic, thirdly, lighting correction, and finally, the image trajectory is corrected with navigation in order to obtain georeferenced data.

Mosaicking is of interdisciplinary use. This imaging method helps to classify diverse features on the sea bottom. Primary research is usually done by parametric and multibeam echo sounders, seismic echo sounders or by drilling and biological sampling. Findings, discoveries, or thoughts can be further investigated using mosaicked images.

Figure 5.31 shows mosaicking image from the area of Scarp Mounds. Further images of the Scarp and Hedge Mounds areas, generated in ADELIE, can be seen in Appendix M.

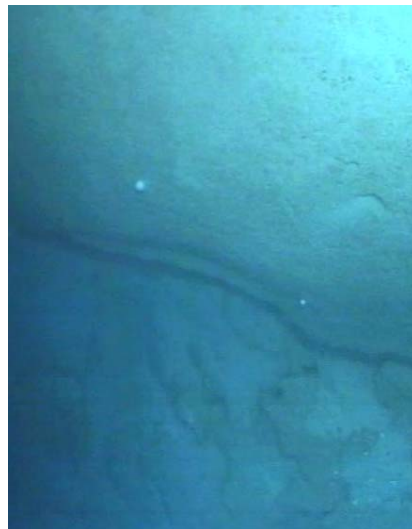


Figure 5.31: Mosaic of part of Scarp Mounds.

6. PROCESSING AND POSTPROCESSING OF DATA

The quality of a DTM is heavily influenced by data processing procedures. Processing is the most important part in the life of the data. In processing, the signals are filtered, converted, transformed and variously edited in many ways. Processing can be thought of as the signal travelling from one format to another.

The basis for further work with the data is to have correctly received signals. Properly processed data from complex topographies are often the result of long editing. In cases of incorrectly recorded data, processing can not rescue useful information. Before we have “clean” data in order to generate digital terrain models, files of many different formats have to be worked with. Often, also the software companies have their own formats which other software may or may not be able to read.

In this chapter, an overview of the processing of HYDROSWEEP and EM 2000 data is given. For a more detailed description of the postprocessing of HYDROSWEEP data see Christen (1999) or Jacobs (2002).

A short note about formats

A long time was spent exporting to XTF format in specialists from IFREMER in La Seyne sur Mer, but mainly with Martin Pronk and Hans Vos from QINSY support and Tolgrim Eldevik from KONGSBERG SIMRAD. Even with actualized and reprogrammed versions, the desired XTF format was not reached.

The CARAIBES software gave hope. However, only IFREMER experts can immediately work with the software, and 2 days of my visit there was not enough to learn all the functions to continue in Bremerhaven. Data were corrected and exported from CARAIBES, and differences were mediated. Further work with the program would require many experiments. CARAIBES is still developing, and to read and correct EM 2000 data both the older and new versions were used. The older version was even slightly reprogrammed in order to read the XTF data.

More time was invested in the preparation of data to specific formats with the aim to realise the cross correlation in ARCVIEW software. Nevertheless, time was too short to become familiar with this comprehensive software. Because no AWI nor ARCVIEW support was available for help and explanation, it was decided to work only with the data as received and to provide those analyses which were available in other software by working with the ASCII format in GMT (Generic Mapping Tools), FLEDERMAUS, TERRAMODEL and MATLAB 6.0.0.

Additional formats were necessary to prepare the PARASOUND data and for the Mosaicking software which required specific information from internal VICTOR files to generate the continuous seafloor image. Also basic backscatter data were prepared and processed, but the time for their evaluation and interpretation would take a month or more, so that in the end only sidescan data were evaluated.

6.1 Processing and postprocessing of ATLAS HYDROSWEEP data

Signals are received at 72 elements placed on the ship's hull. Each is sent to a matching circuit, amplifier and beamformer, where the elements are converted to 59 output channels. Data processing begins for bathymetric surveyors with these 59 signals.

Data are processed and, partly, also postprocessed during the cruise. Most postprocessing takes place back on land. HYDROSWEEP data are postprocessed at AWI in the CARIS HIPS (Computer Aided Resource Information System - Hydrographic Information Processing System) program which was developed in Fredericton, Canada.

The steps are as following: navigation correction, application of zero tide, depth editing, and export to a general format which is readable in other visualising programs.

6.1.1 From raw data

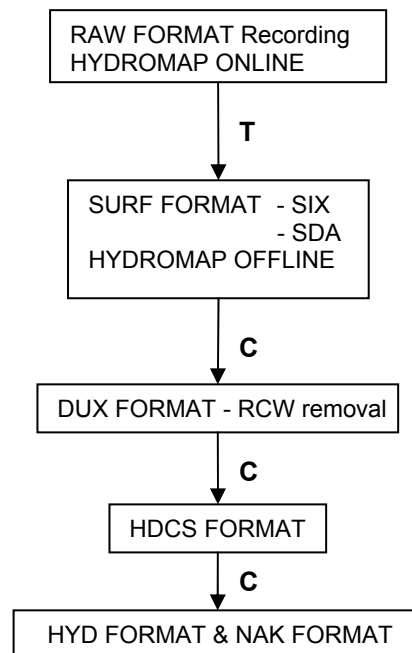


Figure 6.1: Processing of HYDROSWEEP data.

Raw data are stored both in an analogue form on DLT (Digital Linear Tape) and digitally on hard disk every 10 minutes. For later work with the data, a transformation from RAW to SURF is provided three times daily during measurement. SURF (from German *Sensor Unabhängiges Rohdaten Format*) is an export format which is divided into binary data (SDA) and index (SIX) files.

SURF files can be opened in the HYDROSWEEP OFFLINE Navigation Editor, within which possible navigation errors can be eliminated manually. After navigation correction, the data are converted to the DUX format.

Firstly, the starting RCW (Record Control Word) of each line has to be deleted, and the DUX file is converted to an internal HDACS file which is readable in CARIS HIPS (UNIX) where

important edits of the data are investigated. Sometimes, DUX files are summed into binary HYD files or into NAK, AWI's own bathymetry and navigation formats. Figure 6.1 displays all of these steps.

6.1.2 Navigation correction

The postprocessing of navigation is mainly done immediately on board in the HYDROMAP OFFLINE software. Navigation errors appear as outlier points with respect to the continuous navigational line of vessel positions. At such points, incorrect position X and Y is assigned to the correctly measured depth. These outliers are either deleted or assigned an interpolated position. It can happen that a line of points, jumps a few hundred meters away from the track. The line can be shifted or rotated back into its correct position. During the expedition, west of Ireland, no outliers occurred. The vertical accuracy is one hundredth of the water depth, hence, 2 meters of error in 600 meters of water are negligible.

6.1.3 Tides

Tidal information is important for mapping depth information. Depths are usually referenced to mean sea level. The world's highest tidal range is recorded in Nova Scotia, at Minas Basin, where the water level at high tide is as much as 16 metres higher than at low tide (Bishop, 2004). In the North Atlantic, the few meters of tidal range does not have a significant influence if we consider the vertical accuracy of HYDROSWEET. Hence, a tidal correction was not applied.

In the CARIS HIPS software, geographic coordinates are not assigned to single pings until *zero tide* is applied to the data. Zero tide is also referred to as the "chart datum" on hydrographic charts. The tide values are interpreted in specific units above zero tide.

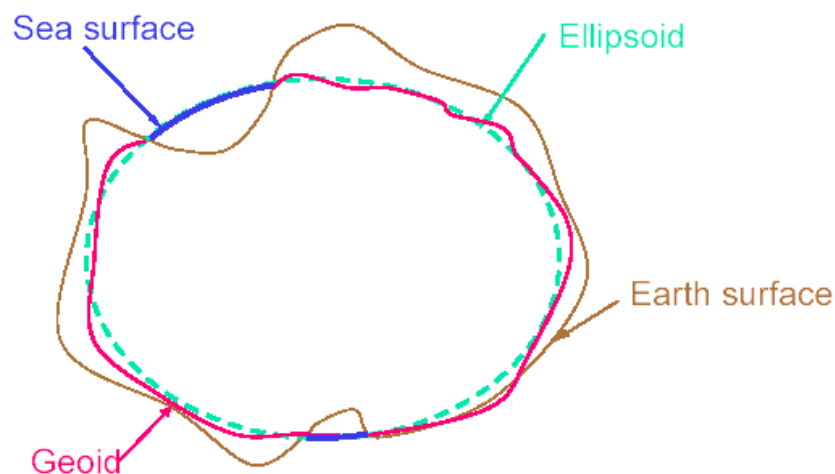


Figure 6.2: Sea surface is almost identical to the geoid.

The coordinates received by GPS are conformed to the WGS 84 Ellipsoid. The measured depths are corrected to the depth of the HYDROSWEET array (11 meters below the water line). Because sea level is proportionally divided on the Earth and differs from geoid maximally by a few meters, it can be asserted that the depths from HYDROSWEET are with

the added constant of 11 meters, closely related to the geoid (Figure 6.2). In connection with the GPS coordinates, a value of geoid undulation has to be added.

6.1.4 Depth corrections within CARIS HIPS

Before the data are opened in Swath Editor, they have to be assembled using the merge function. The merge step combines all of the horizontal and vertical offset information needed to produce a depth and location for the soundings. This information includes:

- Observed Depth
 - Navigation
 - Gyro
 - Tide or GPS Tide
 - Calibration Parameters
 - Refraction Coefficients
 - Motion Data (Heave, Pitch, and Roll)
 - Waterline
 - Dynamic Draft
- (CARIS HIPS, 2001)

The geographic references of soundings can be examined in Swath Editor. In Swath Editor (Figures 6.3 - 6.7), single beams are editable as points in single profiles. Three editor windows show the data in side, rear and plan views, and bad data can be treated using keyboard combinations. Data can be rejected, interpolated, or marked as outstanding. Special attention should be given to the correction or elimination of swath outliers, roll errors or badly reflected lobe beams.

Figure 6.3 shows a relatively unnoisy stripe of swath bathymetric data. Figure 6.4, to the contrary, demonstrates noisy beams. The cause of the noise could be roll error, backscattering, or multipath effects of beams.

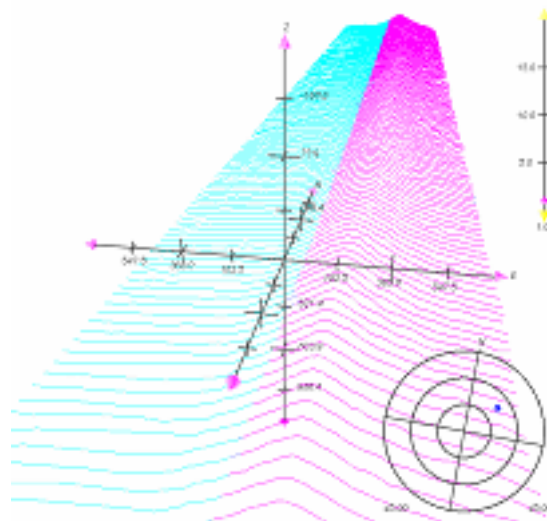


Figure 6.3: Editor window – swaths with little noise.

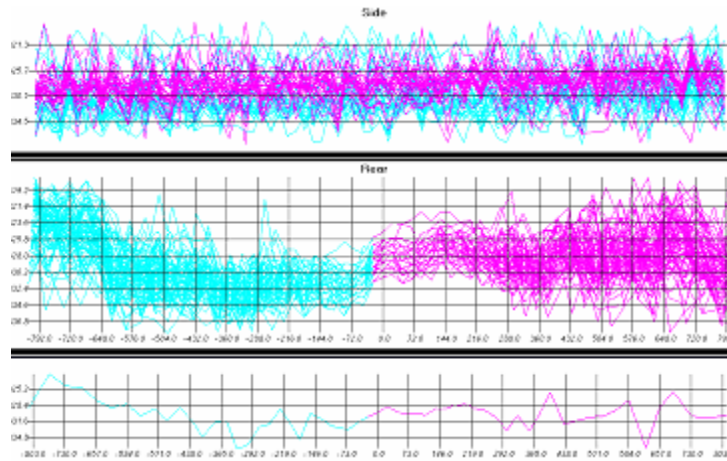


Figure 6.4: Side, rear and single beam window – noisy data.

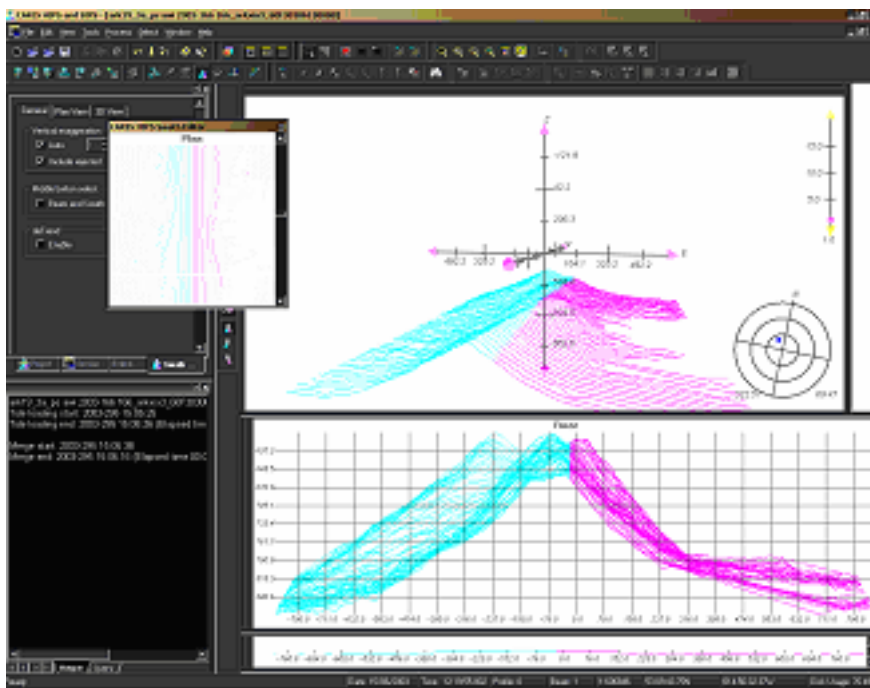


Figure 6.5: Swath Editor – missing data caused by bad reflectivity.

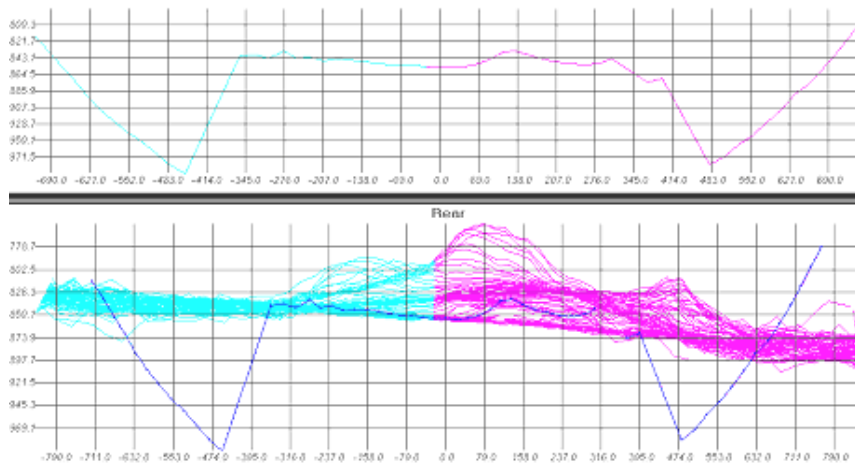


Figure 6.6: Incorrect lobe beams.

Figure 6.5 illustrates missing data on the slope of a mound caused by bad reflectivity. Figure 6.6 shows peaks of lobe beams, which have to be deleted. The beam area in the centre of the swath is reliable and can be retained.

During the editing of file „168_ark_06170800“ (Figure 6.7), an interesting reflection was noticed. HYDROSWEEP sonar recognised a moving object, apparently 5-10 meters long and 10-15 metres high. At the same time (on 17.6.2003), VICTOR was operational (dive No. 217). It can be guessed that the object was VICTOR, as POLARSTERN moved at the same speed (0.1 - 0.5 knots) and on the same heading. At a depth of 670 meters, the accuracy of HYDROSWEEP sonar accuracy is around 7 meters, but it is clear that the robot, with dimensions of 3x2x2 meters and a highly reflective surface (synthetic paint) could be recognised travelling a few meters above the sea bottom.

After editing of pings, final fine edits are made in the Subset Editor (Figure 6.8), where single soundings are seen and data are corrected in a three-dimensional view.

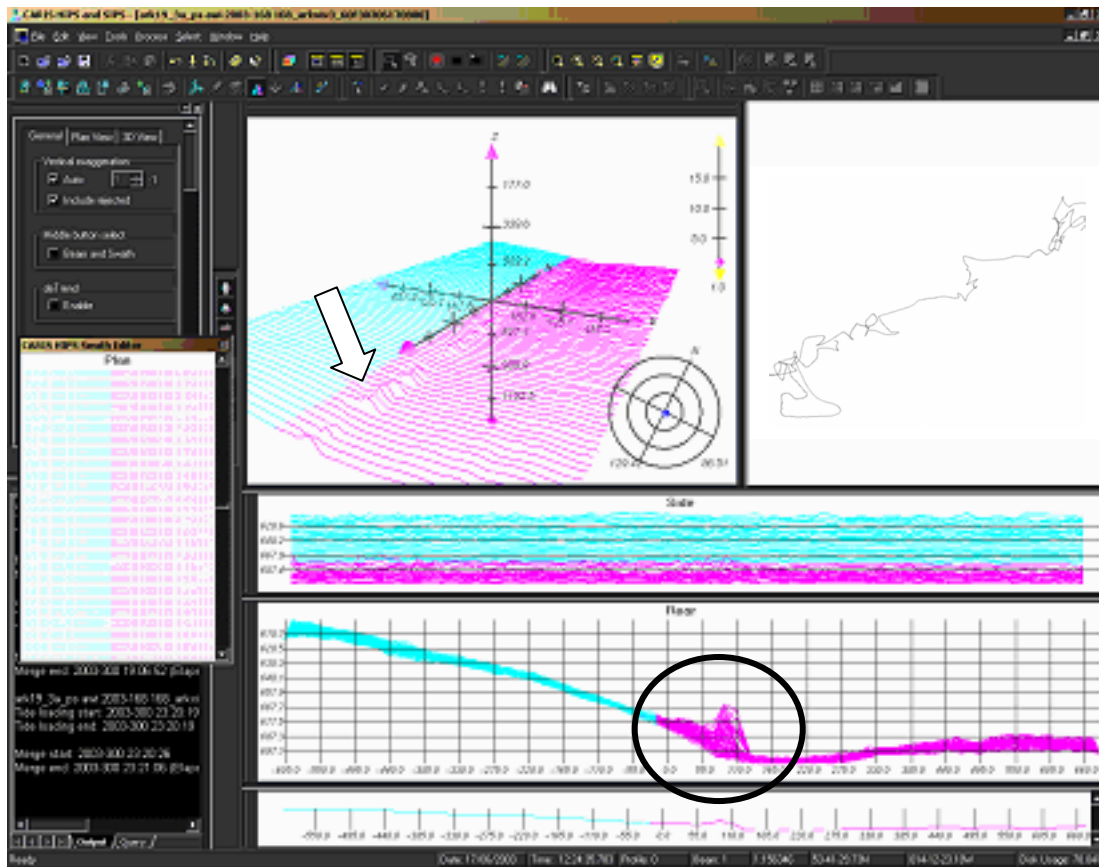


Figure 6.7: ROV VICTOR was detected by the HYDROSWEEP system.

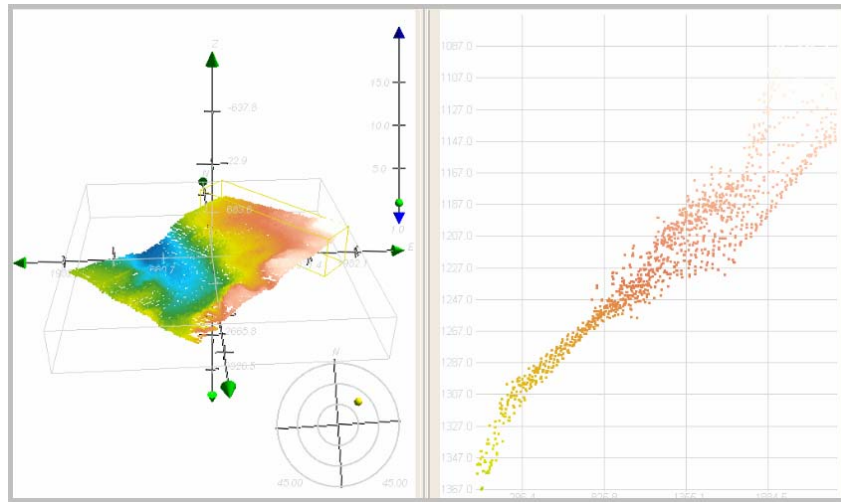


Figure 6.8: Screenshot of Subset Editor.

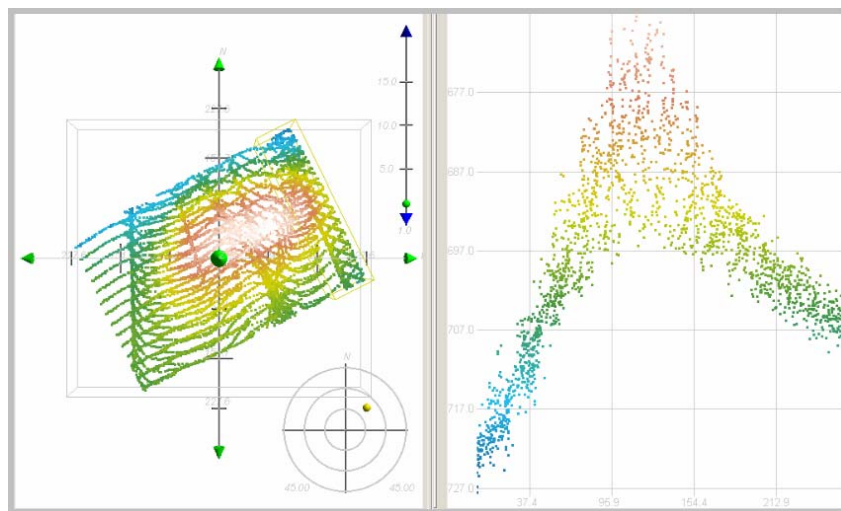


Figure 6.9: Striped features of HYDROSWEEP measurement.

The stripy terrain imaged in the left part of Figure 6.9 is an unusual feature. One reason for this feature could be a HYDROSWEEP system error (arrays were partly switched off), another could be an inappropriate pixel resolution in the display: in shallower areas, beams are closer to each other and are displayed as a smooth surface. In deep areas, conversely, there is a distance between neighbouring beams. Christen (1999) writes in his thesis about a calculated 0.37 % error in beam editing of Hydrosweep data. One HDCS file of eight hours has records of a few thousand beams. Manual editing in Swath Editor is therefore the most time-consuming and demanding task of postprocessing.

6.1.5 Gridding and pixel registration

After editing of data comes the creation of a DTM. To produce the contours which represent the best estimate of the mean seabed surface, a grid of mean depth values can be generated (Gourley, 2000).

For generating a weighted mean seabed surface within a Field Sheet area, it is necessary to preset the UTM zone of the area, the scale of the requested map, and the dimensions of the DTM area. The Field Sheet is afterwards converted to a grid. Before the gridding process, the grid cell size and beam spacing (1.3 degrees for ATLAS HYDROSWEEP) of the sonar should be entered into the processing option formula.

Several grid modes exist. Figure 6.10 and Equations 6.4 – 6.7 introduce two of them. The difference is in the placement of nodes. A DTM is constructed by generating mean depth values over a defined grid interval (Gourley, 2000). In the left hand side of the figure, the node values are allocated to the corners of cells. This method is used in the CARIS software. In the right hand side of the figure, node values are placed in the centres of cells; such an approach can be taken with GMT.

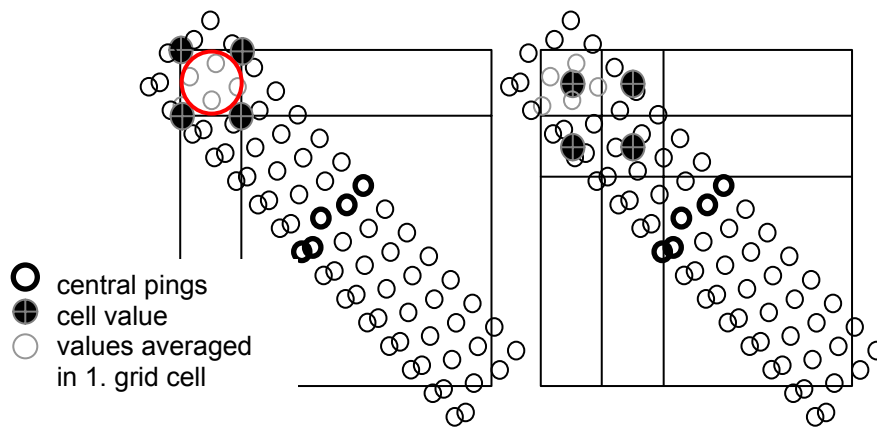


Figure 6.10: Gridding modes – pixel and grid registration.

Gridding in CARIS

Gridding in CARIS is achieved with the Inverse Distance Weighting method. The selected area is assigned a block of memory and each sounding is gradually added to the grid. The depth at each node is a weighted mean of all soundings surrounding it. One sounding can affect many nodes. The weighting is based on the distance within an accepted circle of influence (red in Figure 6.10).

The further the beam is from nadir, the more elliptical the form of the footprint. For gridding in CARIS HIPS, the following computation is used. Firstly, formula (6.1), for a circular area of influence and an elliptical function, is calculated as:

$$r = \frac{d \cdot \tan\left(\frac{a}{2}\right)}{\cos^2(90 - \beta)} \quad (6.1)$$

where r is the circle's radius, d is depth, a is beam width, and β is the grazing angle. Next, the double – weighting is realized.

The weight of the sounding depends on the grazing angle (Figure 6.11). In an area with overlapping survey lines, the grazing angle weight ensures that a higher priority is given to

data from beams from the inner part of a swath. Soundings near to nadir will be maximally enhanced, and minimum weight will be assigned to the external part of the swath (Gourley, 2000).

The second weight decreases linearly with the distance from the node and is assigned to soundings in inverse proportion to their distance from the node, raised to the power n:

$$\frac{1}{d^n} \quad (6.2)$$

Range weight is added as shown in Figure 6.11 (right).

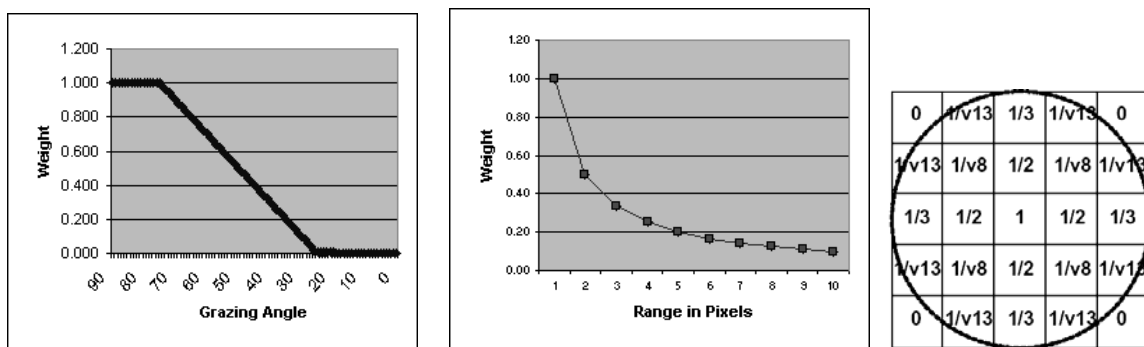


Figure 6.11: Grazing Weight Model (left), Range Weight Model (centre), and circle of influence (right) (after Gourley, 2000).

Grids are displayed as geo-referenced images that can be enhanced with sun-illumination and vertical exaggeration. Usually, a grid size of 50 or 70 meters is used to display bathymetric data from the HYDROSWEEP system. In the case of mounds, at first, a grid size of 2 meters was experimented with. It was calculated that the footprint of HYDROSWEEP beams at a depth of 600 meters is 25 meters. The grid size should always be larger than the actual footprint to avoid aliasing and hence, a grid of size of 30 meters was afterwards used.

A comparison of two grids can be seen in Figure 6.12. A grid spacing of 2 meters shows artefacts that arise from the interpolation of soundings shown, in the right hand frame, which was created in GMT. The track line reveals that POLARSTERN moved slowly, and partly stopped, waiting for VICTOR from time to time. Many pings were transmitted to the same places, and so a stripy beam pattern developed in the survey lines.

In CARIS, various profiles of all the explored areas of mounds were created. They can be seen with different vertical exaggerations in Figure 6.13. Figure 6.14 shows them placed in the map created from HYDROSWEEP measurements made on 16 -19 June 2003.

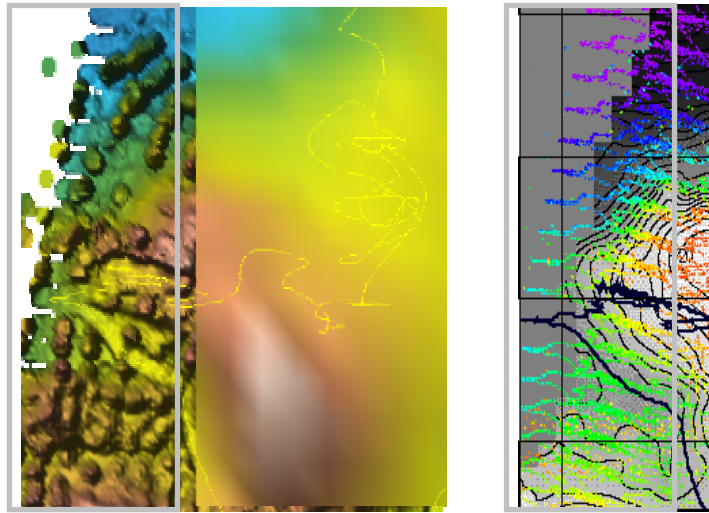


Figure 6.12: HYDROSWEEP measurements - grid size of 2m (left), grid size of 30m (centre), and the single soundings in colour (right). POLARSTERN's track is shown by a black (right) or yellow (left) line.

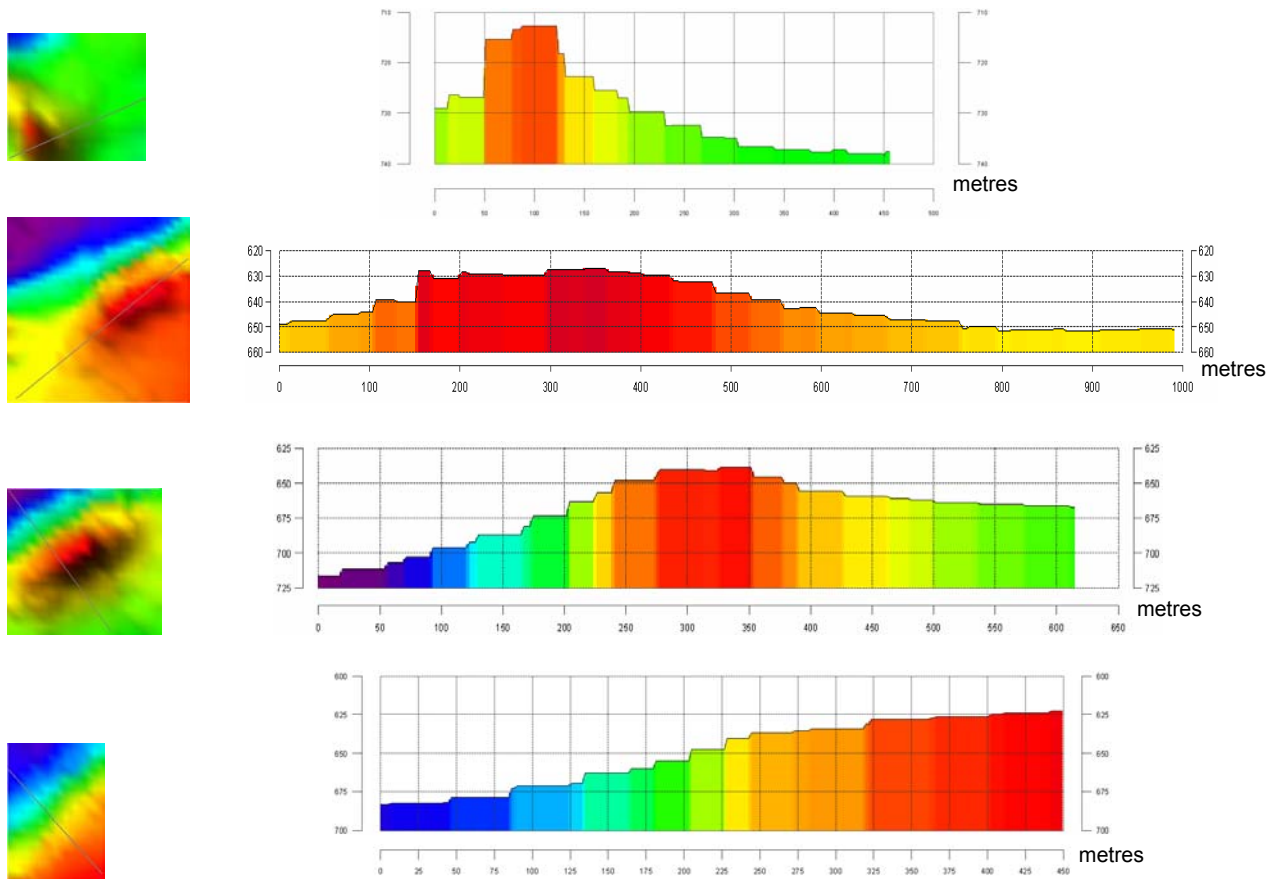


Figure 6.13: Profiles of Mounds HM2, SM2, SM3 and SM4, grid size of 30 m, in HYDROSWEEP data.

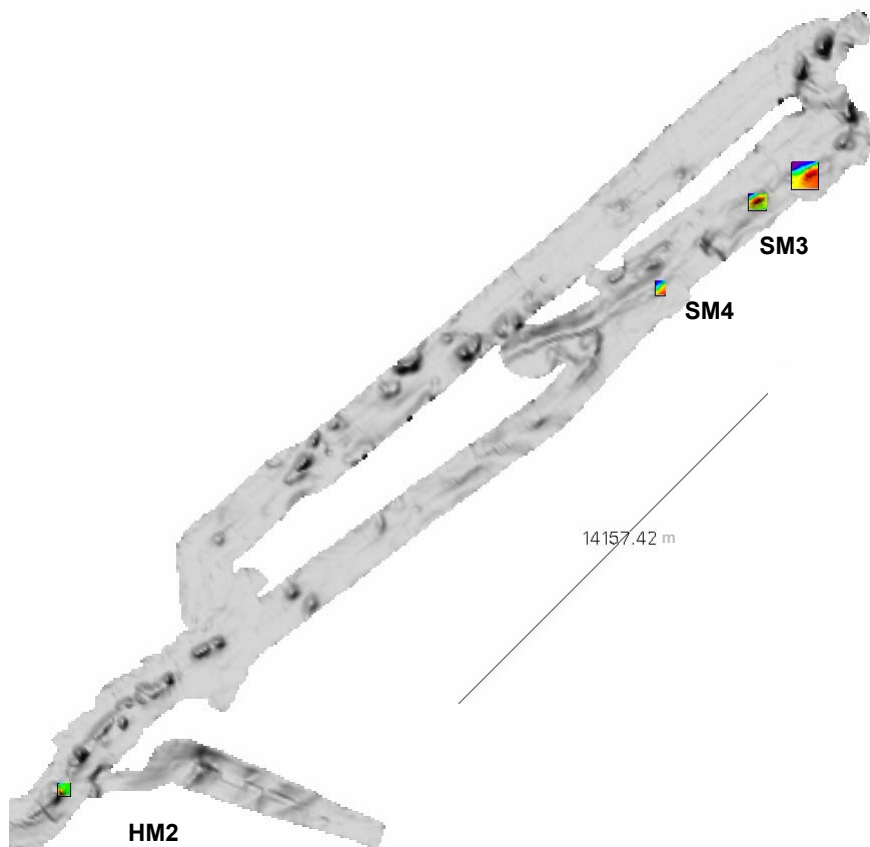


Figure 6.14: Northeast part of Porcupine Bank – Scarp and Hedge Mounds – grid size of 30 m (HYDROSWEEP).

Gridding in GMT

The first version of the Generic Mapping Tools (GMT), running on a UNIX platform, was developed at Columbia University in 1988. Gridding routines in GMT differ from those provided in CARIS. One modeling function that can be applied to data is called “Splines in Tension” (Wessel and Smith, 1999) and is a form of bicubic spline interpolation. Examples of the spline principle are shown in Figure 6.15.

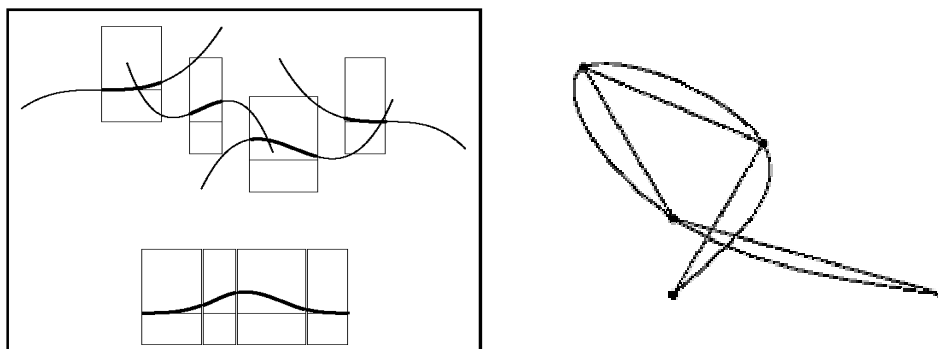


Figure 6.15: Model of cubic B-spline (four polynomials) demonstrating the principle of spline creation (left) (after The Math Works, 2000) and spline curvature (right) (after Weisstein, n.d.).

By analogy, the minimum curvature algorithm with surface tension is like bending an elastic sheet in such a way that it passes through all the data, and then measuring it at places where it intersects the grid pattern.

In GMT gridding, the spline in tension technique is realized using the command “surface”. An example of “surface” is as follows:

```
surface FILE.xyz
  -GGRID_FILE.grd -I0.044672727m/0.02592m -R-14.3592/-14.35101/53.5571/53.56142 -T1 -V
```

where -G is the flag for the name of the resulting grid, -I ascertains the resolution of grid in minutes of longitude/latitude, -R indicates the borders of grid, -T is the tension factor (0 for minimum tension) and -V is the flag for “verbose” mode, which reports progress in gridding.

The resulting grid value $z(x,y)$ is counted from X,Y,Z coordinates as:

$$(1 - T) \cdot L(L\langle z \rangle) + T \cdot L\langle z \rangle = 0, \quad (6.3)$$

where L indicates the Laplacean operator, the three-dimensional generalization of the one-dimensional curvature operator d^2/dx^2 . The tension factor $T=0$ means that minimum of tension is adopted in the surface, which hence has no local minima or maxima that are not defined by input data.

If there are many values in one grid cell, an aliasing effect can occur. To avoid aliasing during the gridding process, the “blockmean” command can be utilized in order to rank the soundings equally.

Grid or pixel registrations

The resulting grids can be registered in different ways. Figure 6.10 shows the difference between pixel and grid registration. In the case of grid line registration (used in CARIS and GMT), the number of nodes are related to the region and grid spacing by

$$nx = (xmax - xmin) / xinc + 1 = 4 \quad (6.4)$$

$$ny = (ymax - ymin) / yinc + 1 = 4, \quad (6.5)$$

while for pixel registration (used in GMT only) :

$$nx = (xmax - xmin) / xinc = 3 \quad (6.6)$$

$$ny = (ymax - ymin) / yinc = 3 \quad (6.7)$$

Gridded DTMs generated in programmes CARIS HIPS and GMT are shown in the Appendix A.

6.2 Sidescan data in CARIS HIPS

Sonar data from the HYDROSWEEEP device are output to the HYDROMAP ONLINE software. In the processing of backscattering signals, the CARIS software full fills all the requirements for creation of sidescan images. After loading and internal conversions, the corrected and amplified signal is stored as an ASCII file together with the bathymetric data in DUX format, and is modulated to HIPS data during postprocessing.

Data can be examined in the HIPS Sidescan Editor (Figure 6.16). Field Sheets are produced from the examined data and, after application of the slant range correction, they are gridded using the Weighted Inverse Distance method.

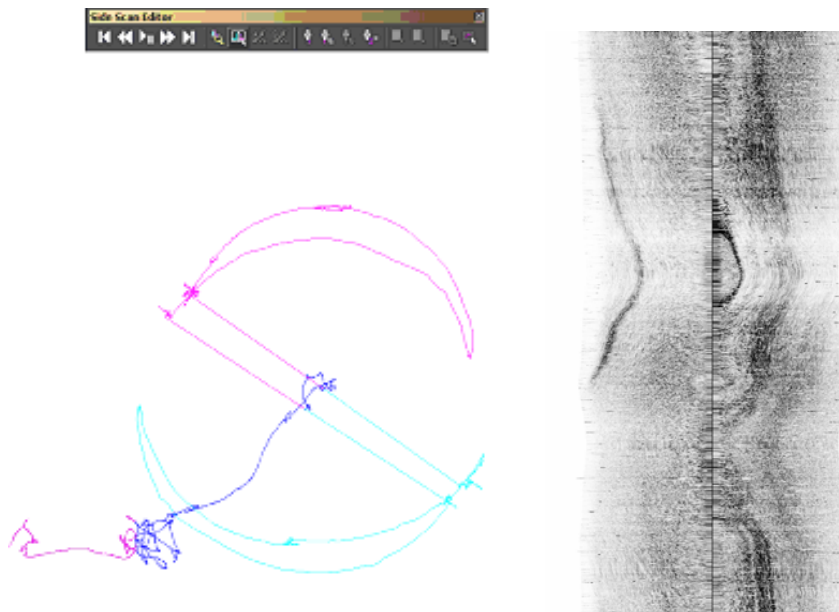


Figure 6.16: CARIS Side Scan Editor, with an example showing a mound.

For four parts of the Porcupine Bank, sidescan images were generated with the help of the HIPS command *mosaic*. The areas of Scarp and Hedge Mounds are shown in bathymetric and sidescan data in Figures 5.16 – 5.19. The images yield only coarse/rough information about seafloor reflectivity. The reception on the big distances deteriorates the quality of images resolution. The gridding results of single areas are displayed in Appendix L.

6.3 Processing of PARASOUND data with the SENT program

During the ARK XIX/3a expedition, PARASOUND data were recorded both on paper and digitally in PS3 format. For postprocessing of the PS3 data, the SENT software, developed at the University of Bremen by H. von Lom-Keil and V. Spiess was used to display the sedimentary structure of the sea bed.

First of all, the CPS control file has to be created. Then, appropriate parameters for data display have to be chosen. The most important steps are to choose the type of processing, and not to forget a colour palette (black and white is the default) and the scales of axes (pers. comm. Klaus Dittmers, AWI, 2003). If needed, the header lines can be filled.

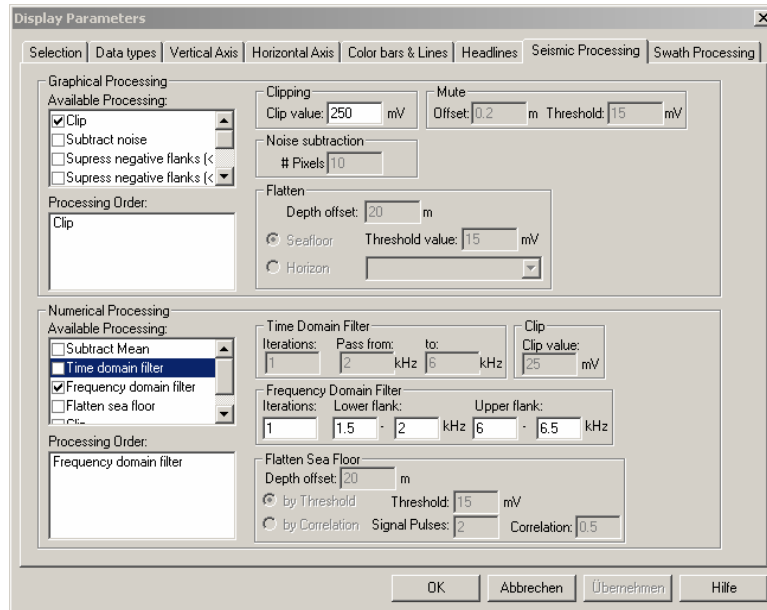


Figure 6.17: Menu of SENT software for processing PARASOUND data.

In the case of data from the Porcupine Bank area, a frequency domain filter was selected with a clipping value 250 mV for the highest reflectivity. The PARASOUND data reveal that the bigger mound (particularly in area SM2) is composed of milli mound features and bowls (Figure 6.18).

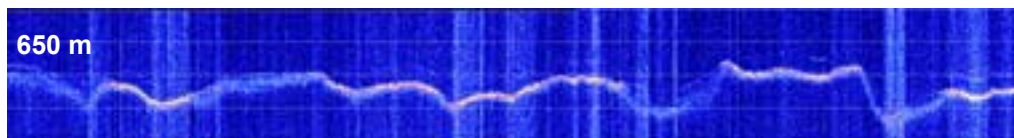


Figure 6.18: Scarp milli mounds (SM2).

Strong reflections, shown by bright colors (Figures 6.18, 6.19), are delivered from hard bottom surfaces. The faint line above the bright reflection in Figure 6.19 probably indicates a younger sedimentary layer lying over a hard surface that could be harder rock. Figure 6.20 shows the similarity of forms resulting from PARASOUND measurement to the microbathymetric profile of Figure 6.21.

For a detailed analysis, a deeper knowledge of marine geology, and also drilling corer samples would be necessary. PARASOUND imagery outputs from areas SM2, SM3, SM4 and HM2 (partly in Figure 6.19) are shown in Appendix K. The profiles refer to the POLARSTERN track lines attached in Appendix D.

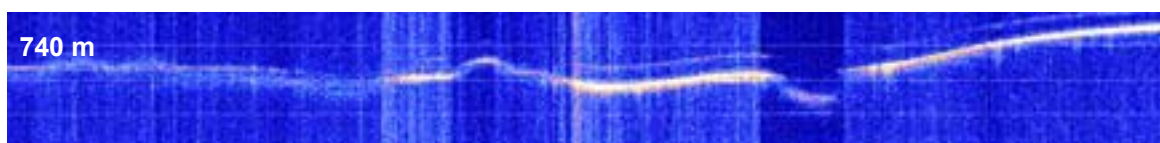


Figure 6.19: Hedge Mound (HM2).

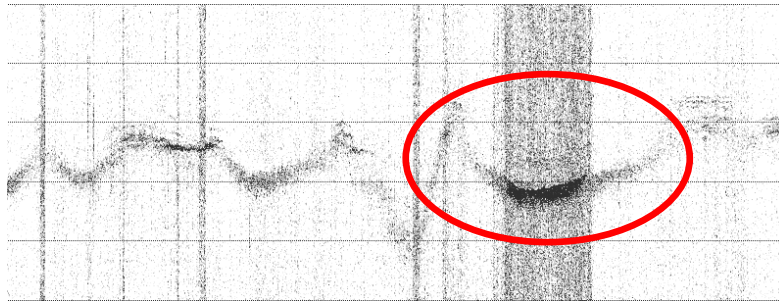


Figure 6.20: PARASOUND of Scarp Mound in SENT (SM3).

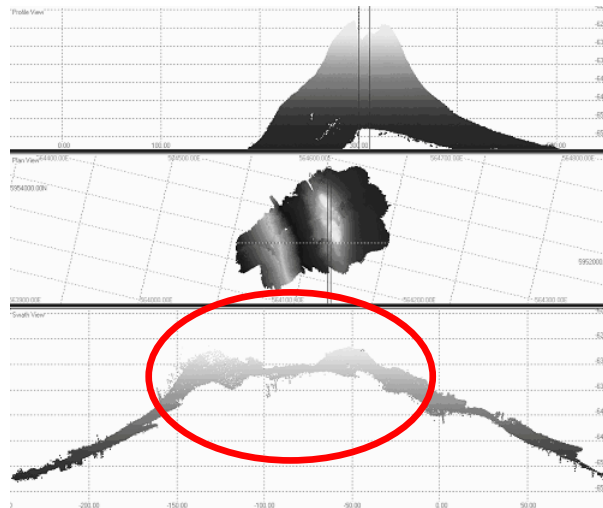


Figure 6.21: Microbathymetry of Scarp Mound in QINSY Validator (SM3).

6.4 Microbathymetric processing and postprocessing

The microbathymetric processing flow onboard R/V POLARSTERN during the ARK XIX/3a expedition, and the postprocessing of data after the cruise was as follows: The data sent from VICTOR were separated into files of navigation, depth soundings and sound velocity information. Bad data that were outside expected depth ranges were rejected and navigation correction was done. Anomalous multibeam soundings were edited, and tidal information was applied to the corrected data files.

At first, it was thought that data will be worked up in CARIS HIPS, through the XTF format, which was offered as an export and import option in both the CARIS and QINSY software. Unfortunately, after many attempts this possibility failed. It was not possible to read the exported QINSY XTF data into the CARIS software. These complications were described in Section 4.8. Postprocessing was instead done in the CARAIBES software.

Data were postprocessed in QINSY and CARAIBES software and visualised in TERRAMODEL, GMT and FLEDERMAUS software.

6.4.1 Processing of EM 2000 data

Multibeam sonar data, X and Y coordinates from the POSIDONIA system, Z coordinate information from the pressure sensor (distance from ROV to sea level) and ship navigation information (PSGEN) were mixed in PCs onboard POLARSTERN (the multibeam sonar processor PC, multibeam sonar logging PC, navigation TRIADE PC and the POSIDONIA PC). Microbathymetric data were stored in DB files in the QINSY software. The data flow is shown in Figure 4.7.

6.4.2 Editing within QINSY and CARAIBES

Filtering, manual editing and data analysis and interpretation was mainly undertaken in the QINSY software. The postprocessing steps are shown in abbreviated form in Figure 6.22. A gridded DTM can be generated using the Sounding Grid Utility. In this module, standard deviations (RMSs) of four areas of interest were computed. High RMSs were analysed based on the visualizations in TERRAMODEL.

6.4.2.1 Filtering

First edits were made through filtering, where zero value data are deleted and coarse errors and strong noises were eliminated. The structure of the filter algorithm is optional, and it is possible to filter various sensors. The mean among seven and median among nine values were used in case of VICTOR sensor's data as seen in the Table 6.1.

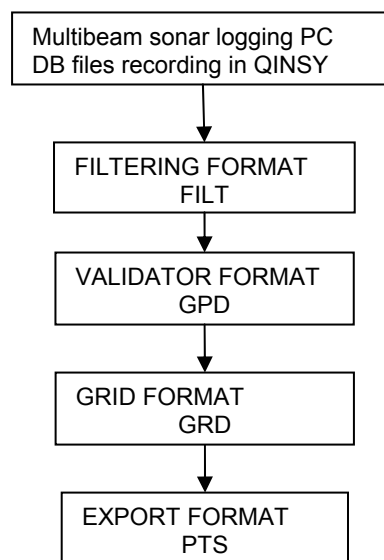


Figure 6.22: Steps in QINSY postprocessing.

Table 6.1: Sensors and selected filters.

sensors filters	Gyros	Echo sounders	Motion sensors	Position LAT/LON	Position heights	Multibeam
Raw Value	x		x	x	x	
Median 9	x	x	x	x	x	
Mean 7	x	x	x	x	x	
Remove zero data		x				x

6.4.2.2 Validation and interpretation of errors

Filtered files were manually corrected in Validator. In Figures 6.23 to 6.29, examples of noises and errors are introduced, with possible explanations. A turn of the ROV in the left part of Figure 6.28, and acoustical navigation, in Figure 6.26, are influences which could conspicuously deteriorate microbathymetry measurement. The sound velocity profile used can be seen from graphs in Figure 5.3. As revealed by the “bowl U-effect” in the right side of Figure 6.28, an incorrect speed (too high) of sound was used for computation of the depth across the track. CTD measurement may not be effective in areas of strong variable currents.

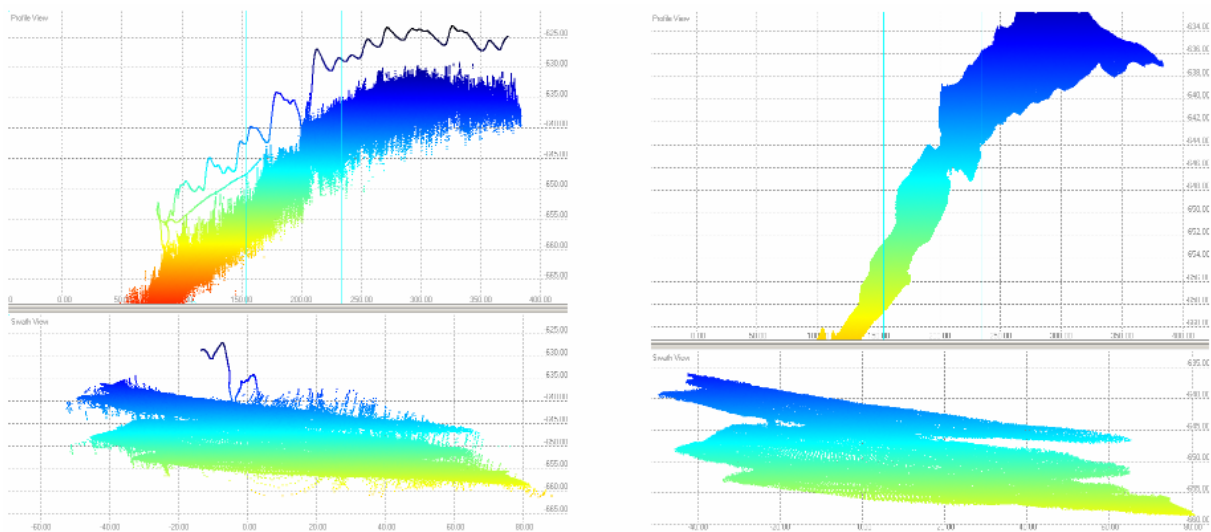


Figure 6.23: Cuts of raw (left) and corrected (right) data in swath and profile views.

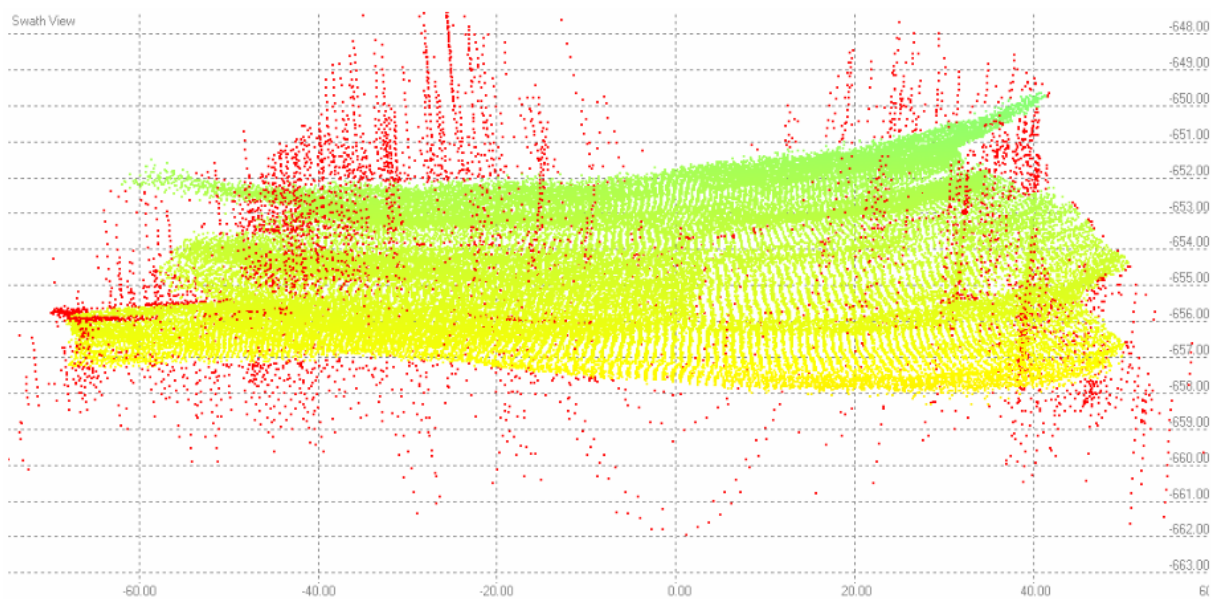


Figure 6.24: 30 meters of terrain mapped from ROV VICTOR 6000.

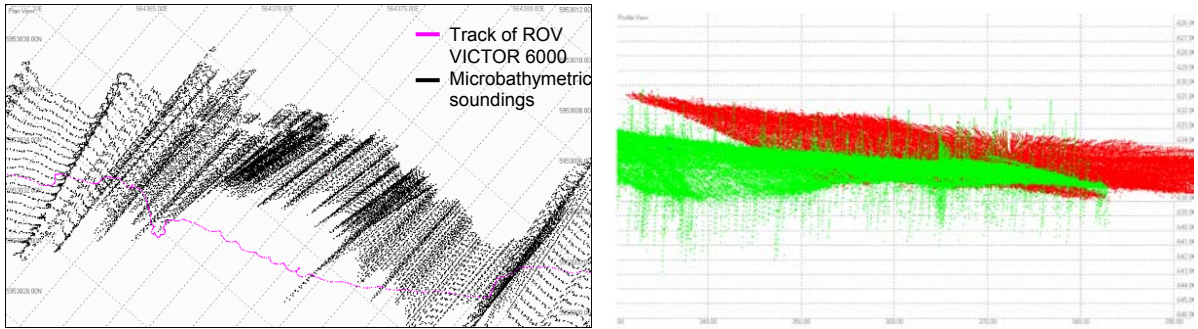


Figure 6.25: Roll error (left) and its consequence in mapping (right).

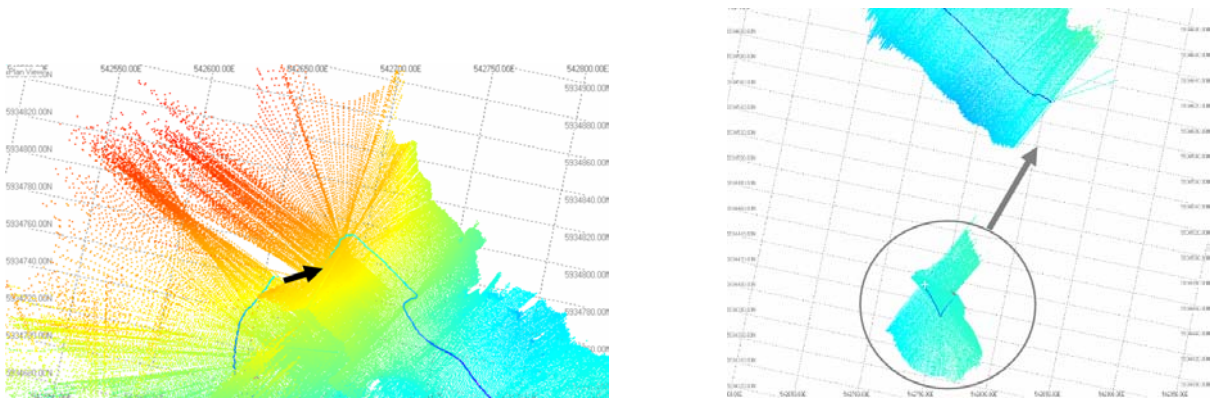


Figure 6.26: Navigation jumps in HM2.

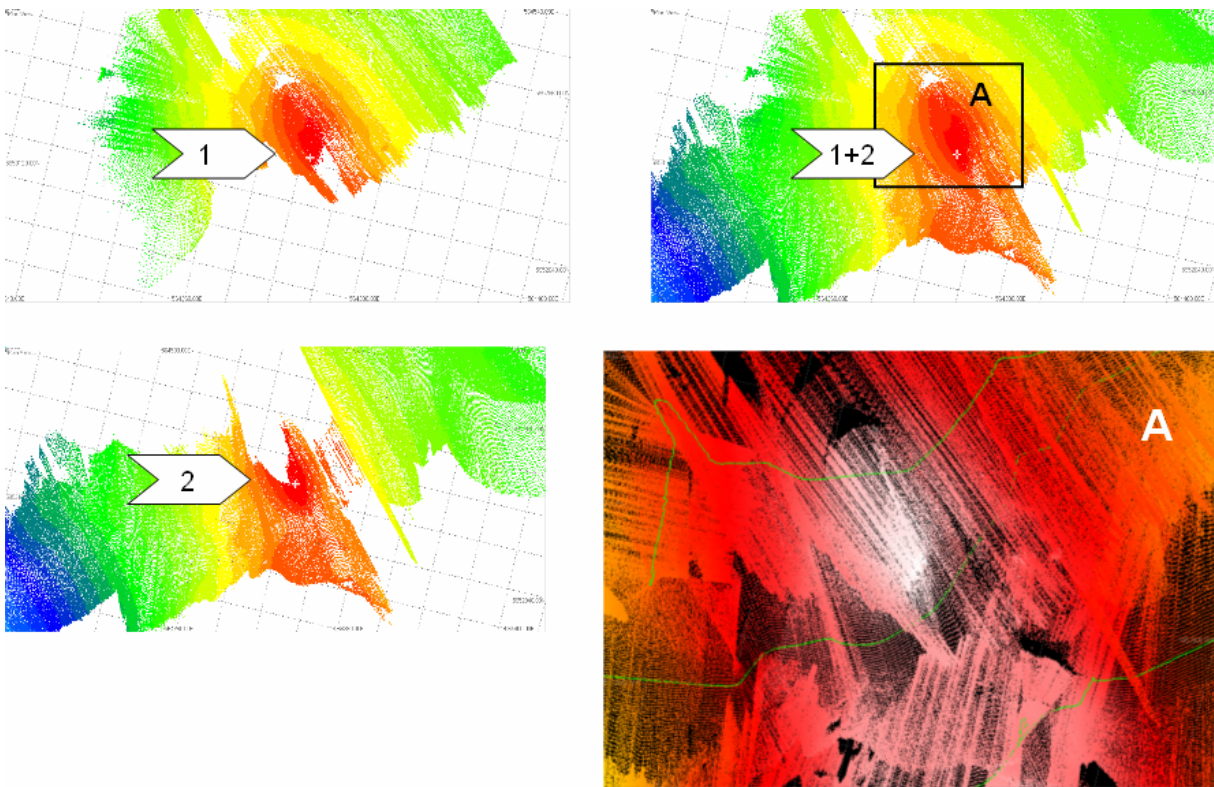


Figure 6.27: Overlaps of files 1 and 2 with roll effects in SM3 (detail at bottom right).

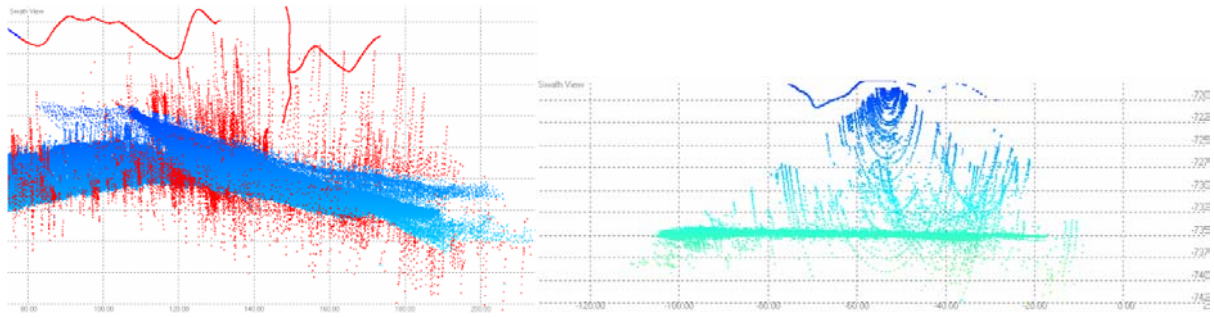


Figure 6.28: Discontinuity caused by turning (left) and “U” errors caused by use of an incorrect sound velocity in calculations (right).

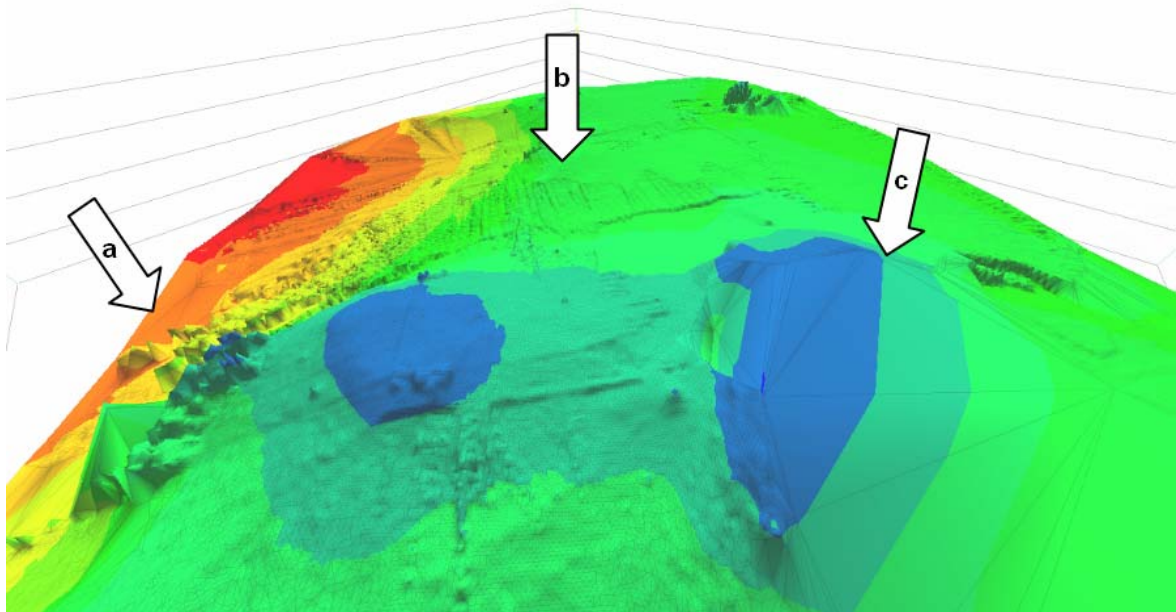


Figure 6.29: Artefacts: bad reflectivity in slanting terrain (a), roll and navigation errors (b) and extrapolation into an area with no data measured (c).

6.4.2.3 Interpretation of terrain using standard deviations of micro- areas

Typically, as a consequence of acoustical navigation, two data files do not fit exactly in their overlaps. In some places, we can observe steps, instead of a continuation of the terrain from the neighbouring file. These trends often have higher RMSs. In Figure 6.30, RMSs are imaged with a scale interval from 0 to 1 meter. Deviations higher than 1 meter are coloured in violet.

In area HM2, there is a stripe of data with $RMS > 1$ m. By comparison with Figure 6.29, the connection between arrows a and b point exactly to the same area. Artefacts that follow a way path are caused by roll movement. Spikes are caused by reflective material at the sea bed, or by multipath effects. All TERRAMODEL figures were generated before any editing of data. What is seen in Figure 6.31 are raw data.

By comparing, the tracks indicate the continuity of single files in Figure 5.30, or in Appendix D, it is clear that the highest RMSs occur in areas of overlap (see SM4) and at boundaries (see HM2).

Even though there is a navigation jump (detail in right hand of Figure 6.26) in the HM2 area, the values are correct. Obviously, acoustic navigation jumps do not influence the quality of microbathymetric measurement.

High RMSs were found also in the areas around the mounds, in the transition areas between the tops of mounds and the surrounding seafloor. These ellipses of higher deviations can be well seen in areas SM3 and HM2 and are emphasised by arrows.

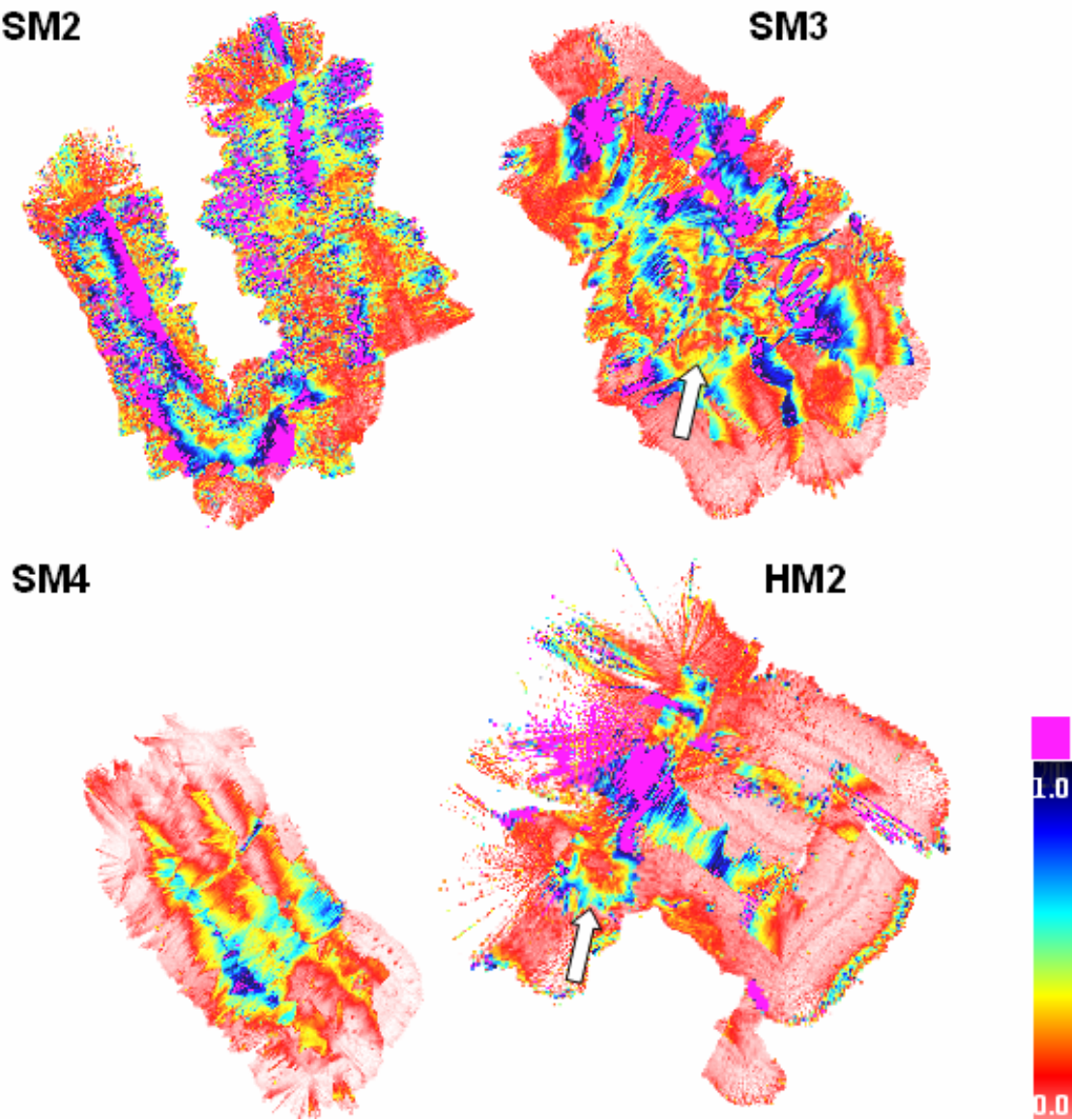


Figure 6.30: Standard deviations of SIMRAD EM 2000 measurements.

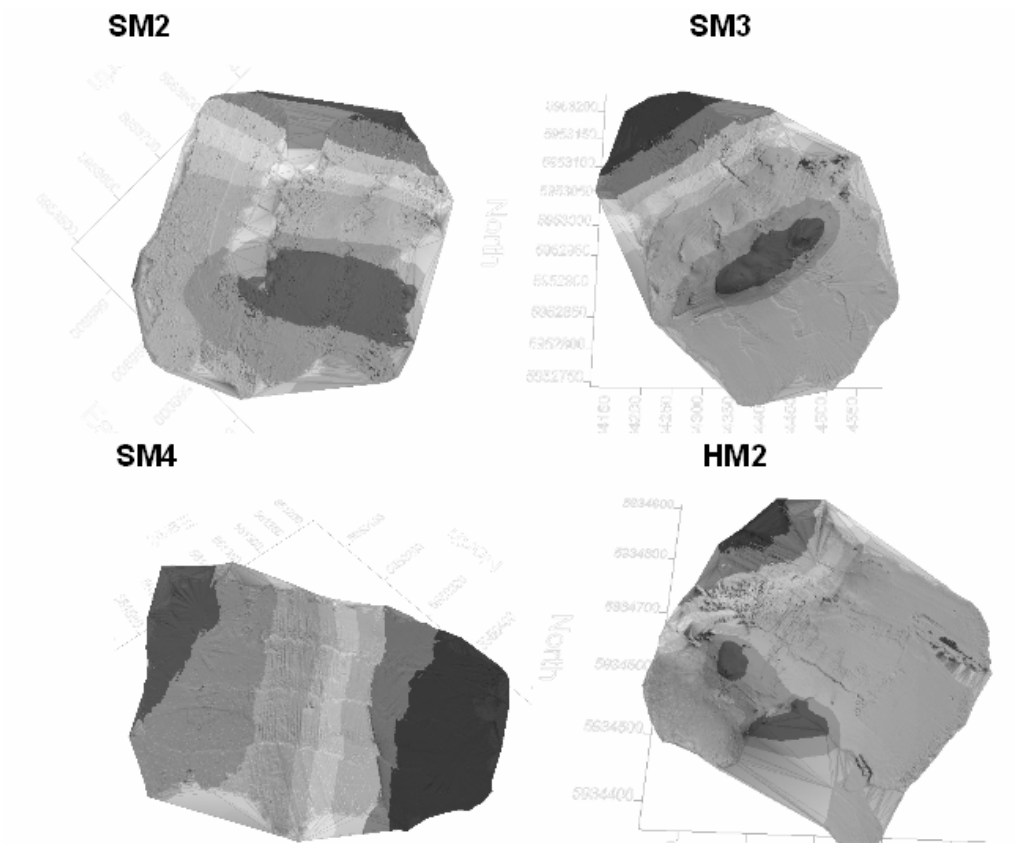


Figure 6.31: Visualisation of uncorrected microbathymetric data.

6.4.3 Roll calibration and pitch correction

Roll and pitch errors are important values, which are measured by Octans during microbathymetric surveying and stored for later processing.

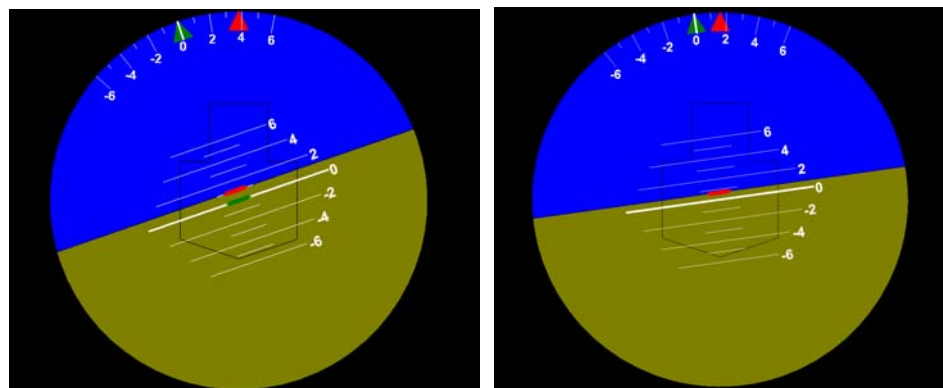


Figure 6.32: Roll (green) and pitch (red) movement in QINSY.

In order to provide roll calibration, two profiles are surveyed in opposite directions. For EM 2000, a roll bias of 0.3° was found. Roll error is shown in Figure 6.32.

Due to the mounting of the multibeam echo sounder on VICTOR, and its position with regard to VRU (Vertical Reference Unit), a pitch correction is needed. In Figure 6.33, two images demonstrate the need for this correction. In microbathymetry of the Pelagia Province,

the pitch influence is obvious. A coarser resolution was used in order to smooth out all systematic bias.

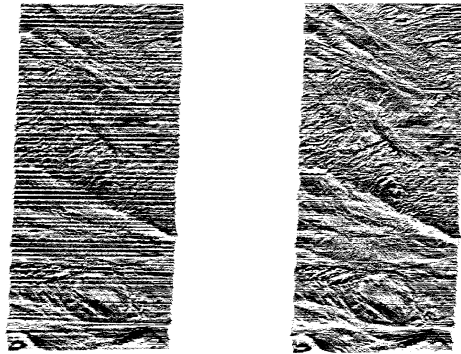


Figure 6.33: Before and after pitch correction (after Edy, 2003).

6.4.4 Tide and navigation edits

During VICTOR operations, navigation errors happen which have to be corrected in postprocessing. Bad initialization of the starting point can cause a shift of the mapped area by up to a few tens of meters away from other mapped parts. Such navigation jumps are impossible to correct in the QINSY software. Navigation jumps are usually corrected in CARAIBES software.

The arrows in Figure 6.26 imply the places where the jumped area has to be returned to, in order to follow the data time line. If a navigation jump is observed on the monitor during online mapping, the file has to be immediately stopped, acoustic navigation has to be re – initialized, and the next recorded data are saved in a new file.

In the CARAIBES module REGINA, bathymetry was displayed by contour lines along the ship’s track, in order to detect identical structures surveyed on different profiles. An automatic adjustment of navigation was computed to position the identical structures at the same location (Edy, 2003). Doubling of features occurs in the microbathymetric data displayed in Figure 6.34. To avoid this doubling effect, the data should be worked on as single files.

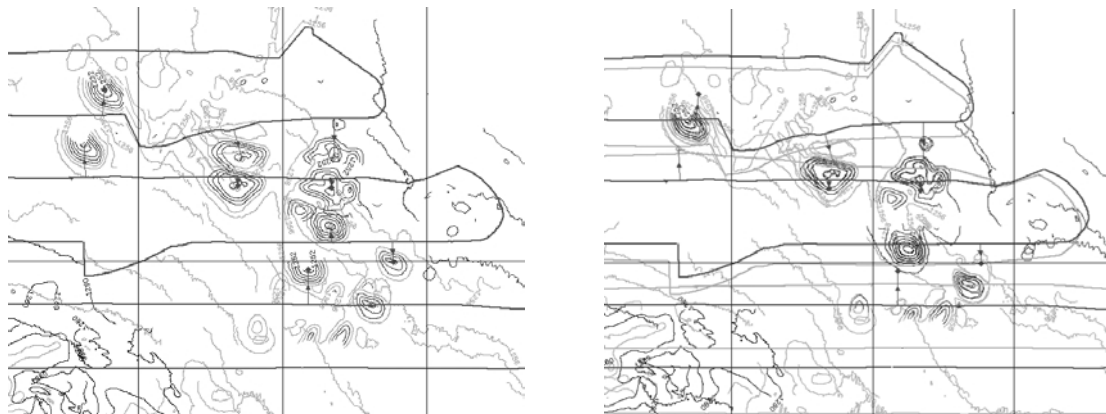


Figure 6.34: Doubling effect caused by navigation error before (left) and after (right) correction (after Edy, 2003).

After navigation correction, manual edits and tidal corrections were realised. In Germany: coastal waters, BSH (Bundesamt für Seeschifffahrt und Hydrographie) Hamburg is responsible for tidal information. The French SHOM (Service Hydrographique et Océanographique de la Marine) was consulted for information about tides on the open ocean. The information provided was applied to microbathymetric data from four measured areas of Pelagia province. The applied differences between low and high tide were 175 to 280 centimeters. Tidal data are attached in the Appendix C.

6.5 Mosaicking processing

The mosaicking software ADELIE (Figure 6.35) was used for processing. The creation of a mosaicked image is accomplished after selecting a video sequence to be mosaicked, choosing a time interval between adjacent tiles, or video snapshots, and choosing the kind of mosaicking (2D,3D) and lighting. Mosaicking begins in the moment of clicking the PLAY button.

Regrettably, the mounds microbathymetry is measured a few metres above the sea floor, from which position the bottom not visible by video cameras. Hence, no area exists with both mosaicking and microbathymetry coverage. The areas mosaicked are close to the mound areas whose microbathymetry is introduced in this Diploma thesis.

Mosaic files were selected at every 10 seconds. The mosaics were not georeferenced, and the only unit is UTC time. All mosaicked images are attached in Appendix M. The video sequences from Hedge Mounds stem from expedition DVD No. 218-205, the sequences from Scarp Mounds are from DVDs No. 217-207 and 217-203.



Figure 6.35: Mosaicking in ADELIE software.

6.6 Discussion: processing

Soundings in the close with surrounding of the nadir of the multibeam sonar yield mainly correct measurements of depth. In the computation of bathymetry in CARIS software, such soundings are given a weight of 1.0, and the more distant soundings from nadir are assigned decreasing weight. GMT software cannot work with the data in this way as there is no possibility to define the beams by their grazing angles. Gridding works using the bicubic spline method.

In order to explore data properly from all sides, various methods were investigated to discover similarities and differences in topography and to reveal the real features and artefacts. If bathymetric and microbathymetric data are taken together, a good overview of seafloor topography can be obtained. If we add sidescan data, we find that the top of mound HM2 has a high reflectivity and that mound area SM4 has a bowl with absorbing characteristics. From mosaicking data, even details of a few millimetres size can be observed, fauna can be detected and sediments roughly determined and, with reflectivity from bathymetry, sidescan or PARASOUND, more precisely identified.

The quality of measurement with both sonar systems depends on several factors. Firstly, the characteristics of the water column epitomised in sound velocity profiles. Secondly, the morphology of the sea bed, which influences backscattering. Incomplete reflection below around the mounds can be caused by steep seafloor surfaces. On the other hand, a certain part of the signal is absorbed depending on the sedimentary structure of the mound province. Thirdly, external noises can be caused by the weather conditions, other systems (ship's propeller) or waves and currents, and in polar areas also by ice. Effects caused by the geometry of the emitted impulses e.g. tunnel or omega effects also have an impact on the bathymetric data, but ATLAS algorithms can detect and eliminate these effects. In microbathymetry, special problems related to platform movement have to be solved. Besides this, acoustical navigation has to be additionally corrected for. It is moot point if is necessary to apply a tidal correction.

There are a few more acoustic systems mounted on the hull of R/V POLARSTERN. In addition to the 15.5 kHz HYDROSWEEP, the particular 12/13 kHz DWS frequency, 50/150 kHz NAVLOT frequency, 38 kHz NBS frequency, 18/21.5/24.5 kHz PARASOUND frequencies and 8.5-16 kHz POSIDONIA frequency. Theoretically, it is supposed that these frequencies do not disturb each other (pers. comm. Roger Verhoeven, FIELAX, 2003).

Last, but not least, there is a human factor that enters into the important decisions made both during the measurement on the vessel and during postprocessing of data. There are a lot of conversions and transformations, and during the manual editing one has to decide which signal will be eliminated and which is correct.

7. COMPARISON AND INTERPRETATION

Areas of four mound locations in Pelagia Province were measured by the two different swath instruments. The challenge was to compare two DTMs from the two systems. In order to explore the similarities between structures and their forms, other methods providing information about sea floor morphology were also used.

Visual comparison is the first step done, but the human ability to compare two areas visually is limited. Conversely, correlations between two datasets can be calculated, but the value of correlation coefficients does not locate the differences. In order to obtain the spatial location of differences, models can be subtracted and visualized. One of the other possibilities is frequency analysis. Such results give information about how single waves correlate. In order to make further comparison, the coherences could be investigated. The next chance to compare the datasets is cross correlation, in which areas are translated and rotated in order to best fit their form. This possibility could give new information about navigation offsets.

To undertake all the above described analyses, experience with mathematical functions and defined formats of specific software are necessary. In the short time available for this Master's degree, just a few of the methods were realized. Grid differences and correlation coefficients were calculated and regression curves generated. Coherence curves were generated without appropriate interpretation being done.

7.1 Data distribution

The distribution of data with an area plays an important role in the generation of DTMs. In Figure 7.1, 59 sounding points over grey-shaded topography from HYDROSWEEP beams can be seen. Soundings are displayed perpendicular to the POLARSTERN track. The further the distance from the nadir beam, the more scattered points are, as can be seen in upper part of Figure 7.1. POLARSTERN moved slowly during dives of VICTOR, and hence soundings were frequently sent to the same points.

POLARSTERN's HYDROSWEEP system has a vertical beam footprint with a diameter of 25 meters in 600 metres water depth, whereas VICTOR's SIMRAD system footprint at 10 meters from the bottom is 24 centimeters in diameter. POLARSTERN's footprints at nadir are, at this depth, almost 10 000 times larger than VICTOR's.

Area SM4 in Figure 7.2 illustrates the distributions of HYDROSWEEP and EM 2000 data. The black compact area composed of points stems from EM 2000 measurement. These data are visibly much denser than HYDROSWEEP data. In inset a, track lines of VICTOR centre beams are displayed together with point soundings from HYDROSWEEP.

The data density is an important factor for interpolation algorithms. The denser the depth information, the more fluently data can be interpolated among the points.

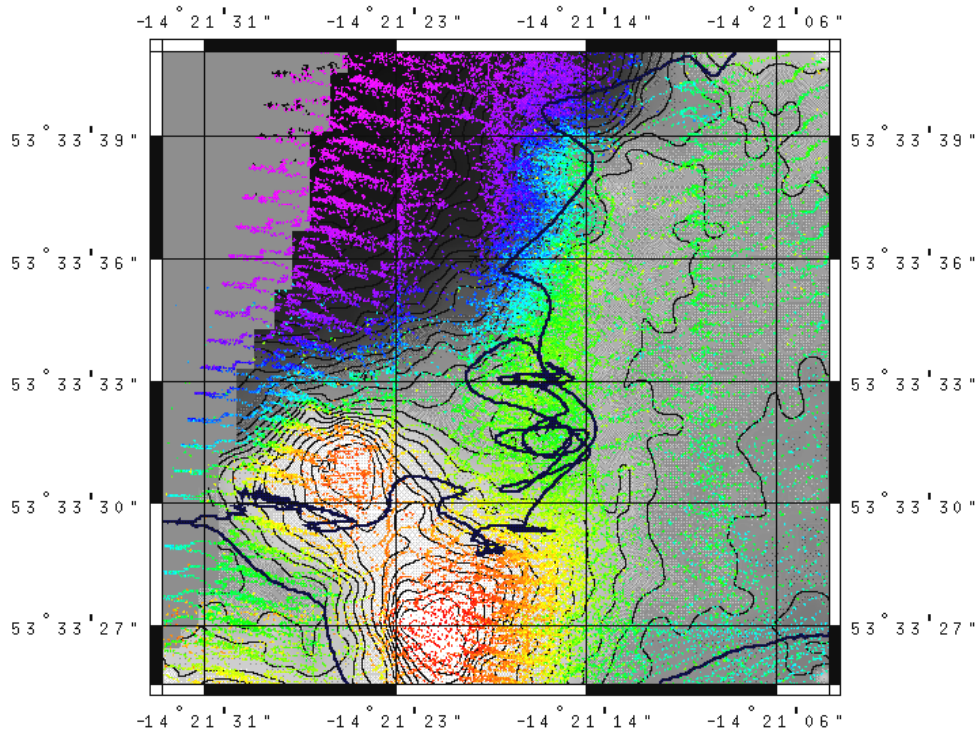


Figure 7.1: Data density for POLARSTERN tracklines (black lines) and HYDROSWEEP soundings (in colour).

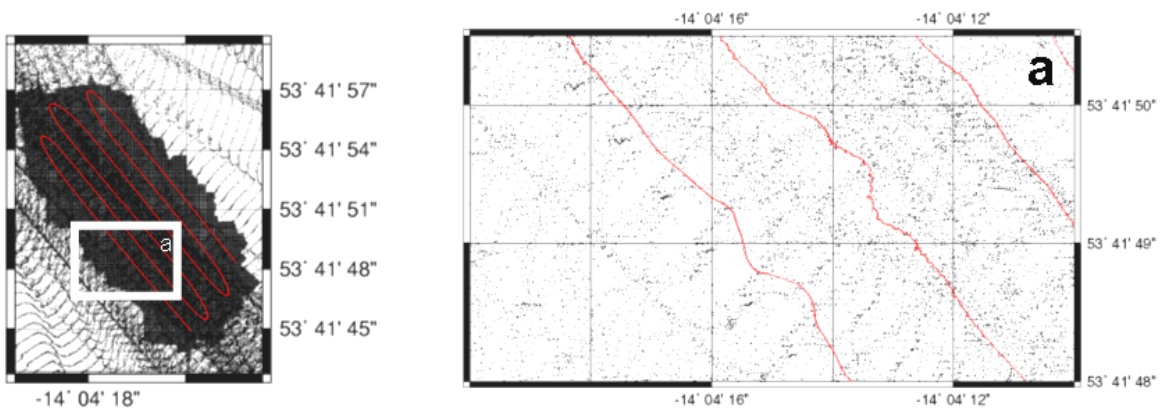


Figure 7.2: Distribution of data – EM 2000 (red tracklines) and HYDROSWEEP (black points).

7.2 Differences

After weighing up which software to use to provide differences, GMT was decided upon. GMT's diverse options for work with grids, and broad spectrum of commands allow gridding and regriding of models in different resolutions, georeferencing and annotation. Grids of identical resolution were generated for all areas and afterwards they were subtracted.

7.2.1 Input and output data

Digital terrain models were generated based on data obtained from VICTOR and POLARSTERN. After manual editing of beam reflections, and the application of tidal and navigation correction, the data were prepared for visualization. GMT and MATLAB were used to process the data and to make statistical comparisons. FLEDERMAUS software was used for the visualization of profiles.

GMT was utilized in order to work with grids. After a few experiments, it was decided to create grids with a cell size of around $0.0446' \times 0.0259'$ (Mercator projection), or approximately 80x50 metres. In the calculation of differences, grids were regrided to $0.00091' \times 0.00054'$ (approximately 2x1 m) in order to obtain finer details.

In a Mercator projection, the distance between lines of latitude increases with increasing latitude. To display a grid with square resolution grid cells, latitudinal grid cell size must be the cosine of latitude: $0.00054' : (\cos 53^\circ 33' 33'') \cdot 0.00091'$.

$$\text{MINUEND}_{\text{EM2000}} - \text{SUBTRAHEND}_{\text{HYDROSWEEP DS-2}} = \text{DIFFERENCE}_{(\text{EM2000} - \text{HYDROSWEEP DS-2})} \quad (7.1)$$

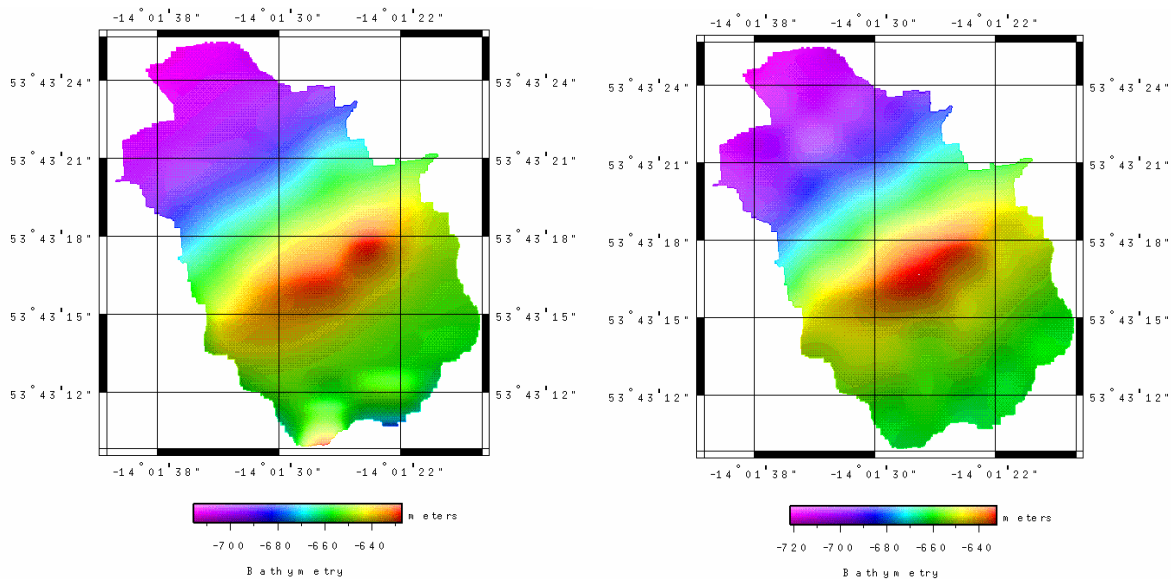


Figure 7.3: Scarp Mound SM3 – minuend EM 2000 (left), subtrahend HYDROSWEEP DS-2 (right).

Grid cell sizes were chosen based firstly on the basis of the different densities of soundings in swaths and, secondly, the size of the two systems' footprints at the seafloor. The differences of grid files were derived with relationship (7.1) and an example of input grids is demonstrated in Figure 7.3. The resulting difference statistics are demonstrated in Table 7.1, and residual grid parameters in Table 7.2. Difference grids are displayed in Figure 7.4. The histograms in Figure 7.5 are used to analyse the distribution of differences in the gridded models.

Table 7.1: Parameters of grids and their differences.

	[m]	Z_min	Z_max	Median	Mean	Standard deviation
SM2 _{EM 2000}		-687.732	-624.106	-641.445	-647.689	17.6034
SM2 _{HYDROSWEEP DS-2}		-687.783	-626.916	-641.715	-647.431	15.5951
SM2 _E - SM2 _H		-21.9948	11.0111	0.524719	-0.258392	3.36475
SM3 _{EM 2000}		-715.715	-627.145	-654.566	-662.954	23.6928
SM3 _{HYDROSWEEP DS-2}		-721.692	-632.382	-659.527	-666.273	22.3119
SM3 _E - SM3 _H		-17.9732	35.6855	3.16348	3.31879	2.99916
SM4 _{EM 2000}		-682.014	-620.283	-657.573	-653.799	21.5547
SM4 _{HYDROSWEEP DS-2}		-686.445	-623.445	-660.13	-657.032	21.4401
SM4 _E - SM4 _H		-50.3983	6.99103	3.63867	3.23253	2.26918
HM2 _{EM 2000}		-765.937	-715.906	-733.519	-736.069	10.7641
HM2 _{HYDROSWEEP DS-2}		-769.5	-718.844	-735.772	-738.574	10.7767
HM2 _E - HM2 _H		-15.681	12.4333	2.70111	2.50449	2.59555

Standard deviations were calculated using this relationship:

$$\sigma = \sqrt{\frac{\sum_{i=1}^n (\bar{x} - x_i)^2}{n-1}} \quad (7.2)$$

$$\bar{x} = \frac{\sum_{i=1}^n x_i}{n} \quad (\text{Hampacher and Radouch, 2003}). \quad (7.3)$$

Table 7.2: Parameters of grids and their dimensions.

both EM + HYD.	nX × nY (approx. 80 x 50 m)	nX × nY (approx. 2 x 1 m)	X_min (west longitude)	X_max (east longitude)	Y_min (south latitude)	Y_max (north latitude)	NaN (zero nodes)
SM2	18×19	819×857	-14.0075	-13.9951	53.7241	53.7318	565722
SM3	11×11	476×490	-14.0283	-14.0211	53.7194	53.7238	103478
SM4	9×12	391×513	-14.0734	-14.0675	53.6952	53.6998	114496
HM2	12×11	541×481	-14.3592	-14.3510	53.5571	53.5614	135935

7.2.2 Interpretation of difference grids

Negative differences are marked violet and positive differences are colored red in Figure 7.4. Positive differences mean that higher topography was measured by VICTOR, and negative differences mean that VICTOR measured deeper seafloor than POLARSTERN.

The biggest differences occur in the flattest area, SM4, which does not contain any mound feature, but instead a depression. Here, a systematic error was suspected. Extreme differences are also to be found in area SM3 which has the strongest relief. Area SM3 shows an extreme positive difference of 35 metres and SM4 shows an extreme negative difference of -50 metres. Comparing with the histograms, we can see that the most frequent differences have a magnitude of 3 meters, hence, the extreme values might be here caused by gridding method.

It could seem that high positive differences occur over mounds themselves, but after detailed searching in the input DTM (Figure 7.6), it was found that the higher differences actually occur over the inclined surfaces of mounds. This, and other observed features, are analysed and summed up in Table 7.3. The areas where the features are best developed are marked in bold type.

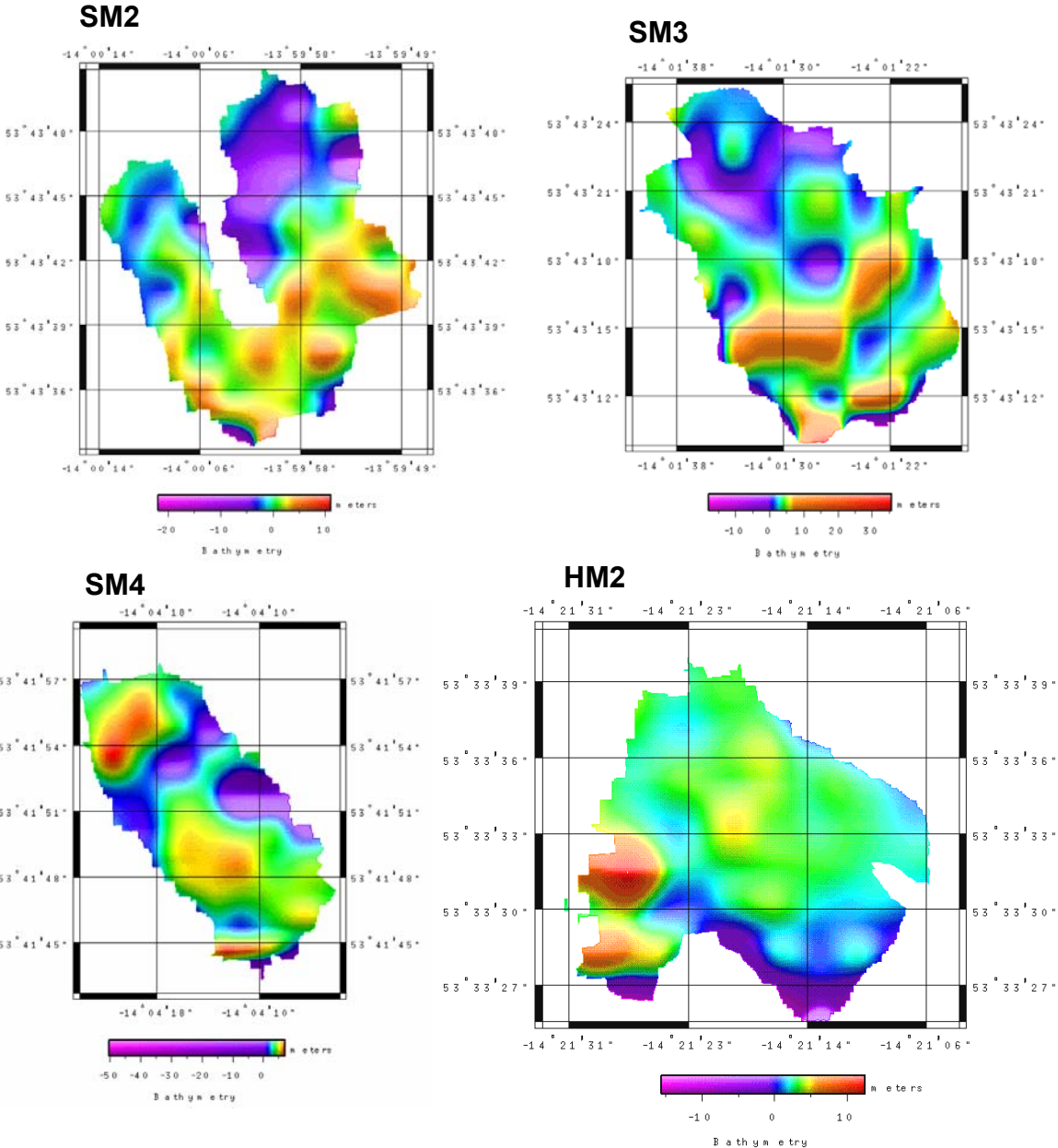


Figure 7.4: Difference grids for the explored areas of Hedge and Scarp Mounds.

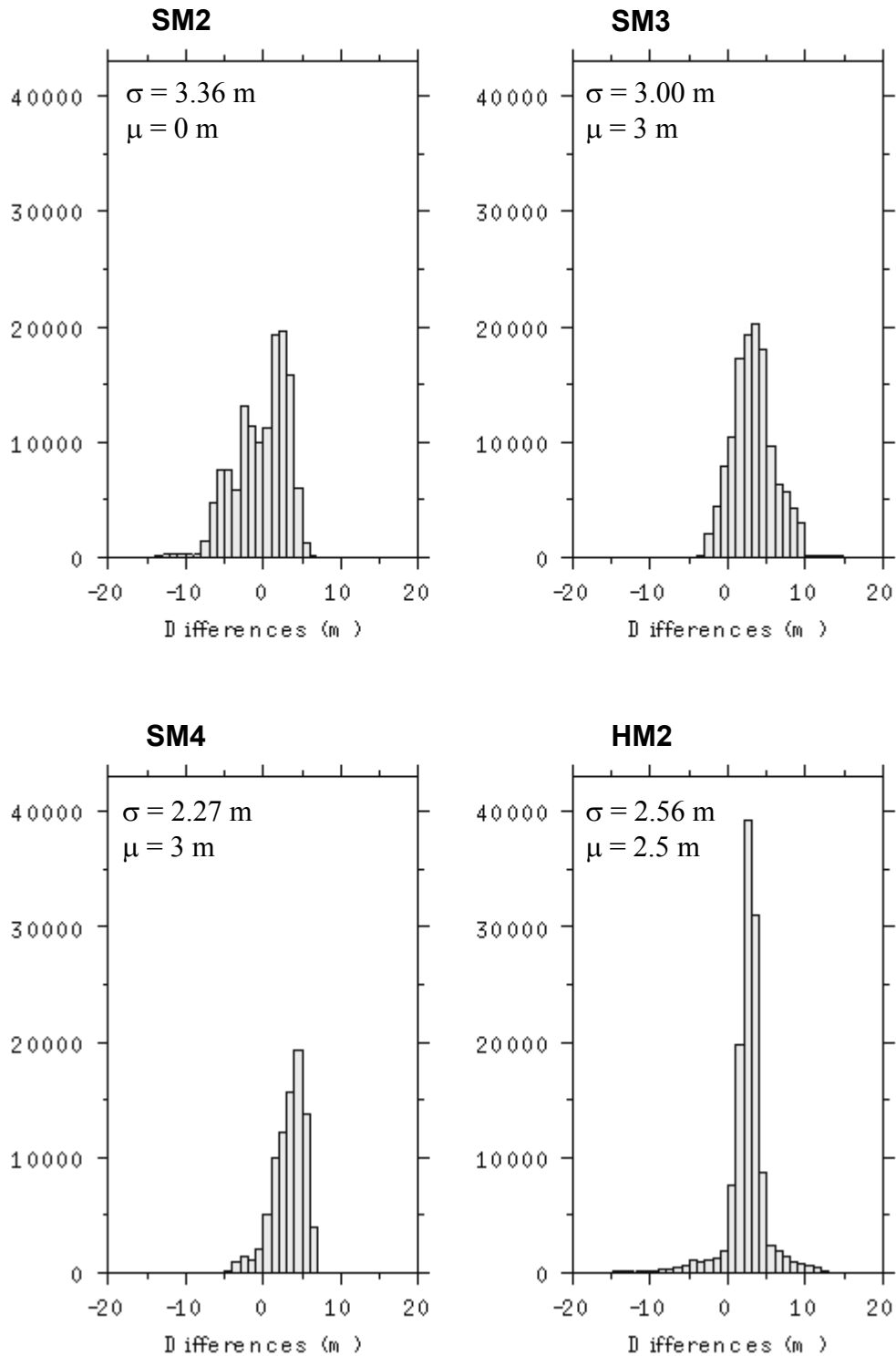


Figure 7.5: Histograms of difference grids from Scarp and Hedge Mounds (σ = standard deviation, μ = mean).

The systematic difference of 3 meters in all areas, with the exception of SM4, can be seen in the histograms (Figure 7.5). Minimum and maximum values of differences are listed in Table 7.1. Standard deviations of difference grids vary in interval from 2.27 to 3.36 meters.

Table 7.3: Features in difference grids and their explanations.

Observation	Area	Cause
Circular positive anomalies	SM2, SM3, SM4, HM2	Sparse signal reflections of deep sea sonar
Large negative anomaly	SM2	Violet “iceman” feature continues to the second arm of mapped area, lower terrain measured with deep sea sonar is probably a consequence of rounding
Small differences on top of mounds	HM2, SM3	Strong topography is well recognized by both sonars
Extreme positive differences in the areas around the mounds	SM3, HM2	Deep sea sonar rounds the mound forms (Figure 5.12) and shallow sonar does not notice steep terrain (bad reflection)
Boundaries negative features	HM2, SM3, SM2, SM4	Incorrect reflected lobe beams in microbathymetry, roll error
Doubling of mound features	SM3, HM2	Incorrect acoustic navigation of ROV
High amplitude negative anomaly	SM4	Deep water sonar measured 50 meters higher terrain – high frequency feature
Dominant negative differences	SM2, SM4, HM2	Deep sea sonar measures terrain higher than it might be in reality - omega effect (Section 5.1.5.2)
Dominant positive differences in transition areas between mound and underground	SM3	Shallow water sonar does not notice steeper terrain from the side
Offset μ	SM3, SM4, HM2	In different cases, may be HYDROSWEEP or EM 2000 system offset or different sound velocity profiles.

Figure 7.6 displays one area mapped by both EM 2000 and HYDROSWEEP. The mound position was mapped differently by the two systems. A possible reason for this may be a doubling effect (see Figure 6.34) in microbathymetry or of the interpolation algorithm. EM 2000 recognised more mass, but with the terrain steeply inclined down whereas HYDROSWEEP’s algorithms calculated a smoother terrain from the highest to the lowest part of mound. The difference mound in the third part of the picture is actually a feature recognized by the EM 2000 system and rounded by HYDROSWEEP gridding.

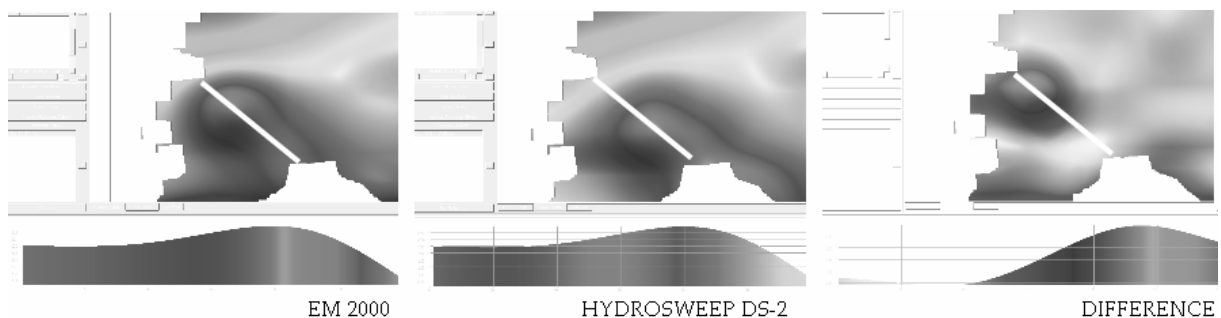


Figure 7.6: Profiles of certain parts of HM2 area and in the difference grid.

7.3 Profiles of area SM4

The most interesting differences were seen in area SM4. It was supposed that the area is a flat, sloping, landscape with occasional small hills. However, the PARASOUND image

showed a 140 meters long by 30 meters deep depression there (see Appendix K). The area was cut by six profiles (Figure 7.7) in order to analyse the differences and similarities in bathymetric and microbathymetric measurements. The profiles are displayed in Figure 7.8. Longitudinal profiles are over 500 meters long and the lateral profiles over 200 meters long in water depths of between 680 and 630 meters.

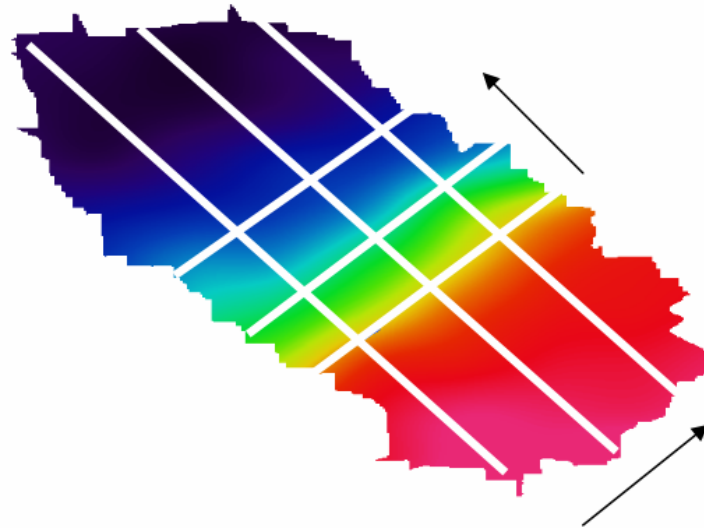


Figure 7.7: The lines of profiles in the SM4 area, arrows imply the order of profiling.

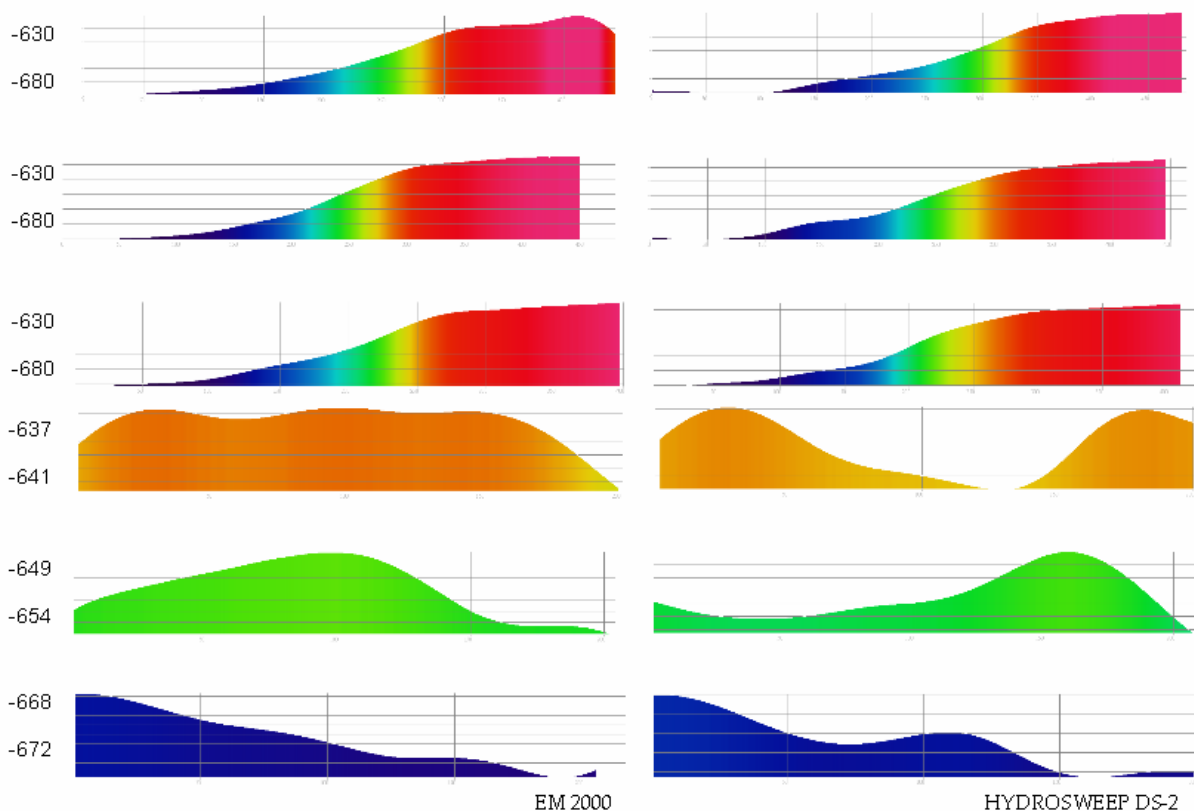


Figure 7.8: Three longitudinal (top) and three lateral (bottom) profiles of the SM4 area (depths in meters).

It can be observed that the longitudinal and lateral profiles from HYDROSWEEP and EM 2000 systems are not the same. Longitudinally, the profiles show a similar tendency. Differences are stronger in lateral profiles, and hence these will be more closely analysed.

The reliefs of the lateral profiles are 4, 5, and 4 metres. In the first lateral profile over EM 2000 data, three small mounds can be seen, whereas in the other measurement a depression is seen. The highest points differ by one meter. It is remarkable that gridding of the HYDROSWEEP data image a depression in the some place where gridding of the EM 2000 predicts a mound. Interpolation, data density, or size of the footprint could be possible explanations. HYDROSWEEP's vertical accuracy is in such depths about 6 meters, so that the imaged features are in HYDROSWEEP's accuracy limit.

The second lateral profile shows a similar phenomenon, with EM 2000 gridding showing a mound and HYDROSWEEP a depression. Although the depth of the shallowest point agrees in both profiles, the two locations are separated by a distance of 70 meters.

The third lateral profile has the same trend as the others – up left to down right. The profiles conform in their display of a flat area. In the EM 2000 profile, there is just a hint of a mound, but the HYDROSWEEP landscape contains exaggerated waved as a consequence of spline interpolation.

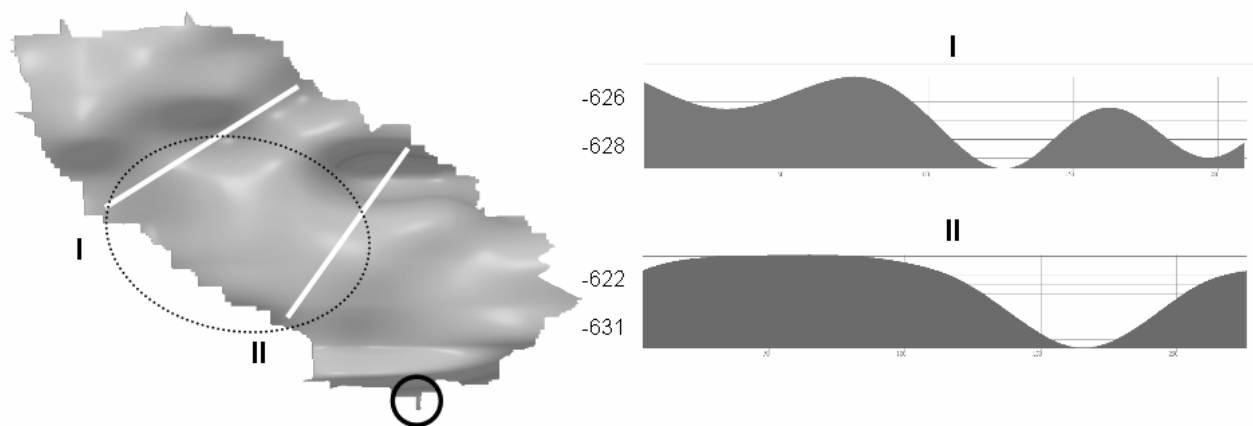


Figure 7.9: Difference profiles: Profile I is 200 meters long, Profile II is 250 meters long, circle displays the location of minimum difference value, ellipse borders a depression.

Two profiles in the difference grid SM4 (Figure 7.9) were generated, in order to focus on areas with extended differences. The mean difference in SM4 is around 3 meters (Table 7.1), and the extreme differences are -50 meters and 6 meters. Close examination of Figure 7.9 shows that the extreme negative difference is to be found in the circled area, in a peripheral part of a swath that therefore has a high likelihood of error occurrence.

Profile I demonstrates a difference interval of around 2 meters, and Profile II displays up to 9 meters of difference. A depression some 30 meters deep appears on a PARASOUND image of this area. If the theory about inaccurate detection of the slopes of mounds is correct, the same theory seems to be applicable for slopes within depressions. One suggestion could therefore be the negative differences in area SM4 can be caused by inaccurate mapping of the sloping walls of depressions.

Figure 7.10 shows profiles over the detected depression. It can be seen that a broad depression (the ellipse in Figure 7.9) with a diameter of about 140 meters was recognised by both systems. However, a horizontal shift of 70 meters and a vertical shift of 1 meter was recognised between the representations. The dotted line in Figure 7.10 illustrates the different diameters of the depression at a same depth of 663 m. Models of areas and differences were visualized in FLEDERMAUS and are attached in Appendix G.

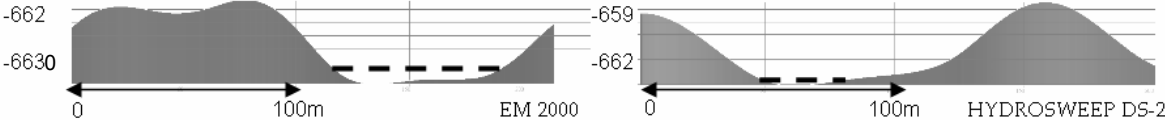


Figure 7.10: Broadness of a detected depression at the same depth.

7.4 Correlation

A correlation coefficient is a measure of dependence between the results of two different measurements. Identical objects have a correlation coefficient of 1.00. Variations of images of features (mounds, bowls, rock outcrops etc.) decrease the level of correlation. A correlation coefficient equal to 1 would be the best result of a comparison of areas mapped by two systems.

7.4.1 Correlation coefficients

Correlation coefficients were calculated in order to prove the linear relationship strength between variables (Hampacher and Radouch, 1998); using

$$r = \frac{n[xy] - [x][y]}{\sqrt{(n[xx] - [x]^2)(n[yy] - [y]^2)}} \tag{7.4}$$

where n is the number of measurements , x is the depth measured with the ship’s sonar and y is the depth measured with the robot’s sonar. The resulting coefficients reveal significant linear relationships in all areas:

- r_{SM2} = 0.987
- r_{SM3} = 0.993
- r_{SM4} = 0.994
- r_{HM2} = 0.971

The highest degree of correlation is in the area of smoothest seafloor SM4, and the lowest is in area HM2. The correlation coefficients provide one number, the information about adherence of two models to each other. However, correlation do not provide sufficient statement about the details, it does not give evidence about points in models with are the minimal or maximal adherence values.

7.4.2 Regression curvatures

The correlation of grid differences and depths, as was found in the previous section, will be investigated in this section. In order to underline the correlation results, depths measured by HYDROSWEEP and EM 2000 systems were cross-plotted on, respectively, the X and Y axes in Figure 7.11. The regression curves demonstrate the overall linear dependence except for small variation in the right parts of the graphs. To explain these anomalies, further exploration of possible distortions and the influences of measurement would be necessary.

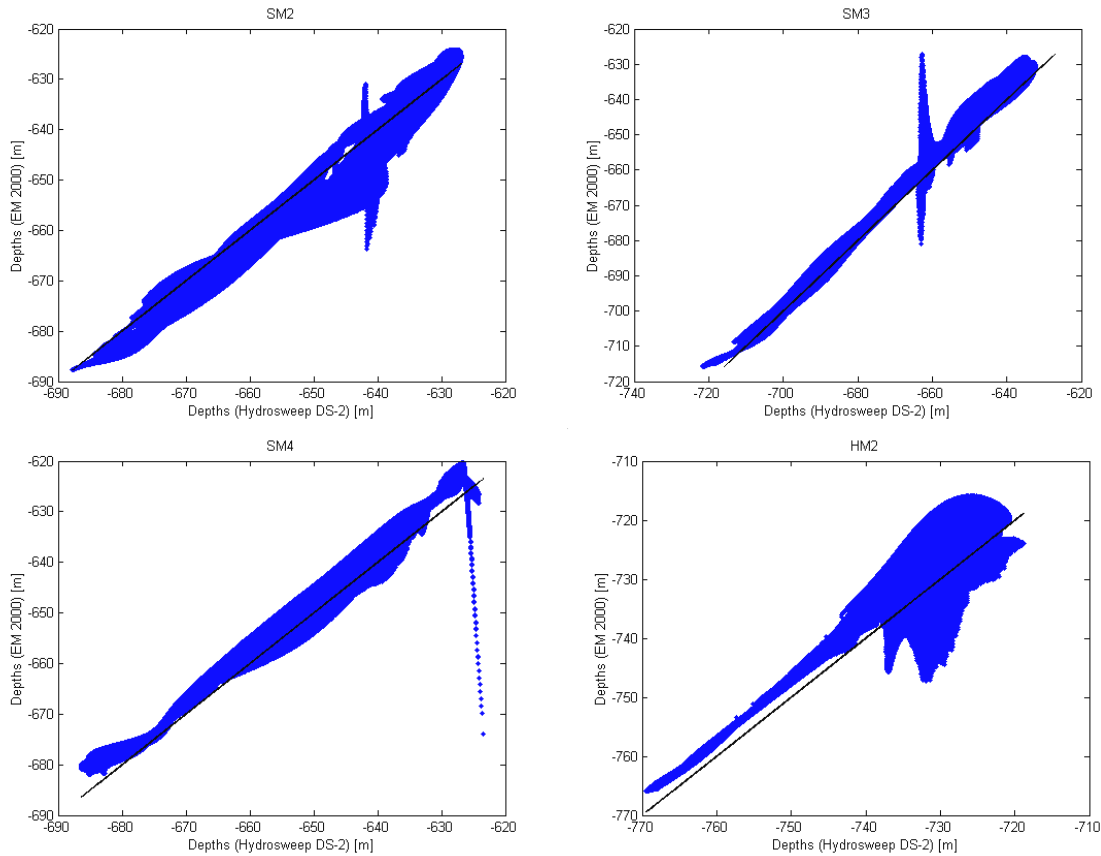


Figure 7.11: Regression of depth values.

7.5 Coherence analysis

A coherence function implemented in MATLAB's `cohere` command was used in order to display the relationship between depths measured with the EM 2000 and HYDROSWEEP sonars from a different point of view – in the frequency domain.

The magnitude-squared coherence between two signals, $x(n)$ and $y(n)$, is given by

$$C_{xy}(\omega) = \frac{|S_{xy}(\omega)|^2}{S_{xx}(\omega)S_{yy}(\omega)}. \quad (7.5)$$

The default values were: $nfft = \min(256, \text{length}(x))$, $fs = 2$, *window is a periodic Hann window of length $nfft$* and $numoverlap = 0$ (MATLAB Help 6.0.0).

The *cohere* command takes sequences of x and y , computes their power spectra and cross spectral density, and returns the quotient of the squared magnitude of the cross spectral density and the product of the power spectra. The quotient displayed on the Y axis is a measure of the correlation between $x(n)$ and $y(n)$ at the frequency ω .

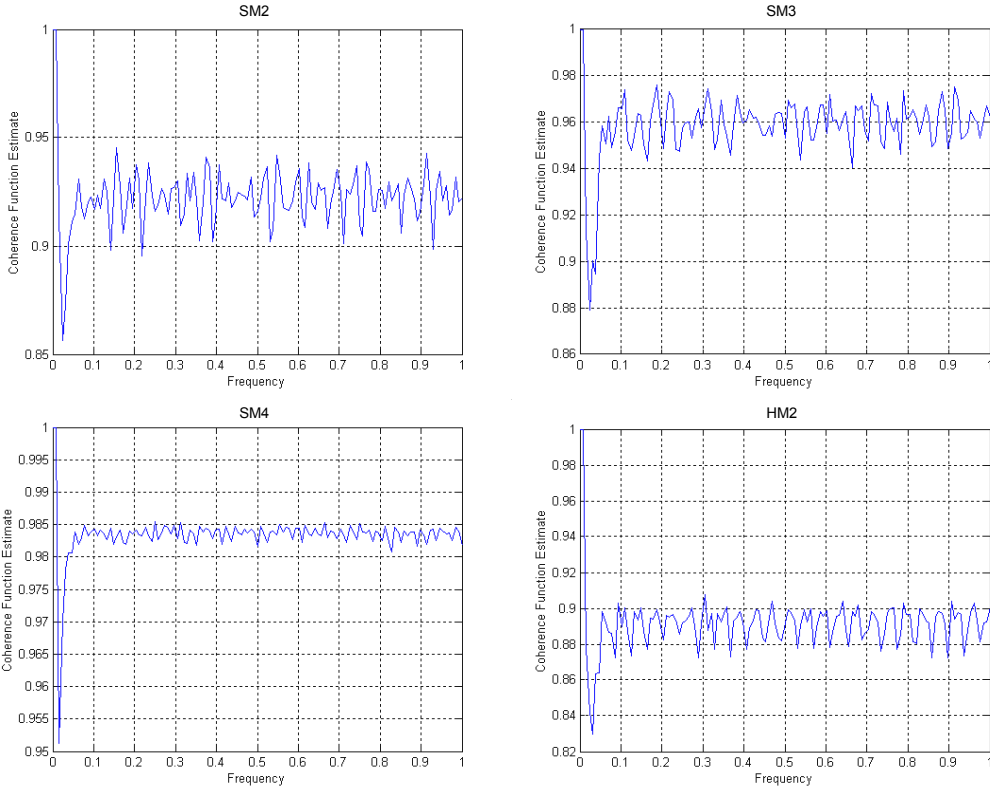


Figure 7.12: Coherence graphs.

The coherence quotient equals approximately 0.92 for area SM2, 0.96 for area SM3, 0.98 for area SM4 and 0.89 for area HM2. These values are in proportion to the correlation coefficients shown in Table 7.4.

Table 7.4: Correlation and coherence coefficients.

	SM2	SM3	SM4	HM2
Correlation	0.987	0.993	0.994	0.971
Coherence	0.925	0.960	0.984	0.890

7.5.1 Recommendation: grid merging

Grids in the space domain can be transformed to the frequency domain by a two dimensional fast Fourier transformation. What we would get is a matrix of values in the frequency domain for EM 2000 and HYDROSWEEP. The next step is an empirical ascertainment of variances of the frequencies which are applied to the frequency values in an appropriate grid cell as weights. In the case of HYDROSWEEP, elements with lower frequencies would be given higher weights, because HYDROSWEEP recognises the long wavelength topography better. In the case of EM 2000, a higher weight would be assigned to

higher frequencies elements because EM 2000 works well at short wavelength and covers better the detailed topography. The weighted mean of the HYDROSWEEP and EM 2000 frequency grids is transformed by an inverse 2D FFT back to the space domain, thus yielding a frequency dependent merged grid of HYDROSWEEP and EM 2000 sonar measurements (pers. comm. Ralf Krocker, AWI, 2004).

This work could not be performed because of a lack of time due to problems with reformatting of the data (see Section 4.8).

7.6 Results and discussion: comparison

For the initial interpretation, the GEBCO Digital Atlas was utilized. The GEBCO chart fits well in the series of data distribution described at the beginning of this chapter. The distances between data from altimetry are bigger than those in HYDROSWEEP's soundings. The GEBCO chart offers too coarse a scale for closer analysis of mound structures (Figure 7.13 b), and was used just as an overview image.

In order to avoid generating grids with artefacts caused by data distribution, appropriate interpolation methods and grid resolutions were selected (Table 7.2) for each data type.

The grids were subtracted and visualized using the GMT and CARAIBES software (IFREMER), and additionally visualized using the FLEDERMAUS software (see Appendix G). GMT georeferenced difference grids can be seen in Figure 7.4, and a systematic difference of 3 meters in all areas (except area SM4) can be seen in histograms in Figure 7.5. The difference grids are displayed together with the EM 2000 and HYDROSWEEP DS-2 terrain models in Appendix H. Grids were also subtracted in CARAIBES software, but they were not used for more detailed analysis. The difference grids are overlaid on the original grid of EM 2000 measurement using CARAIBES, and with that the resulting grids are not distorted. The results are attached in Appendix I.

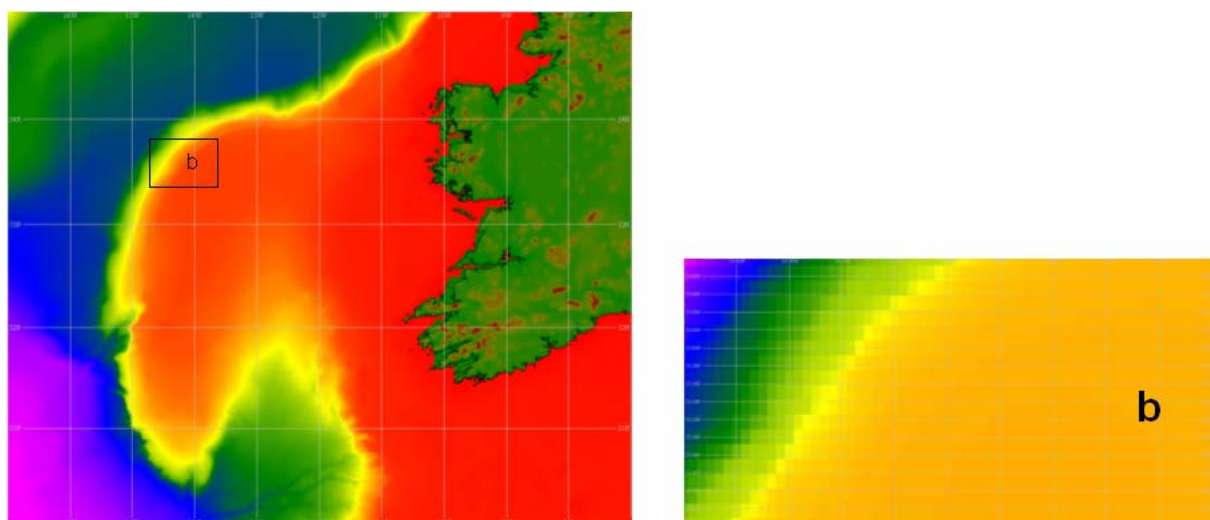


Figure 7.13: Porcupine Bank, and detail of Pelagia Province (GEBCO, 2003).

Profiles over the difference grids were also analysed in area SM4. In order to explain the differences there, the PARASOUND method contributed by imaging a depression on the seafloor. Hence, it was shown that other methods are useful in controversial areas when it is not known if an object is part of the seafloor topography or an artefact.

The correlative analysis confirmed a high linear dependence between the DTMs of the areas, and their relationship was displayed in the form of regression curves. The strongly correlative relationship was also confirmed by means of coherence analysis.

8. CONCLUSIONS

This thesis begins with history, continues with descriptions of navigation principles and data handling, goes through marine measurement methods, provides an overview of data processing and postprocessing steps, and finally makes a comparison of bathymetric and microbathymetric models. The focus of this thesis is a comparison of measurements made by two sonar systems, but other themes are also handled which are closely associated with ocean mapping. Marine surveying is an exotic subject for research in the land-locked Czech Republic and for these reasons the thesis is somewhat large than many.

The three most important sections are *Navigation on the sea*, *Methods of marine surveying* and *Comparison*. The navigation chapter contains a detailed description of systems, principles of inertial and acoustic navigation, the calibration of systems and methods of acquisition of navigation data. Chapter 5 is thematically related to Chapter 6, but Chapter 5 handles the theoretical bases of marine methods and Chapter 6 the practical aspects of working with the data, in order to show how the finished product (e.g. a DTM) is created ready for interpretation. The penultimate chapter compares the microbathymetric and bathymetric DTMs by means of differences, profiles, correlations and coherences.

8.1 Raised queries

The following questions were posed in the introduction: *How could we compare these data? Does correlation provide sufficient statements about the data?* and were answered in Chapter 7. In the following lines, some of the remaining queries from the introduction will be answered, and some recommendations will be given.

Is the comparison of such small areas conceivable for deep sea sonar?

Deep sea sonars are normally not used for sea floor mapping at such fine scales. Their vertical accuracy depends on depth. HYDROSWEEP's vertical accuracy in depths of 600 meters is approximately 6 meters. On the other hand, although the shallow sonar EM 2000 does resolve detailed features, it does not recognize steep escarpments very accurately.

Will the offset between the two grids be close to zero, or will the DTMs of areas have a constant offset? How can we merge the data to get an optimal terrain?

As shown in Figure 7.4, the differences are not constant. The offsets vary over the different morphologic features on the bottom. A systematic error of 3 meters (see histograms in Figure 7.5) is important knowledge before any attempt to merge the models together is made. Merging of the survey data from VICTOR and POLARSTERN can be done if the HYDROSWEEP data are gridded with a grid size of 50 meters in order to interpolate the gaps between sparse signals and afterwards regridded to 1 meter grid size. The EM 2000 data are dense enough to create a 1 meter grid size immediately without interpolation. With this grid cell size, and with a correction for the 3 m constant offset, a merged DTM can be visualized, for example in the FLEDERMAUS program.

What aspects influence the values of differences?

The largest impact on differences was sparse coverage of signals. Poorly distributed data lead to the need for interpolation, and this introduces inaccuracies. Also, gridding methods can cause artificial local minima or maxima. Time and angle measurements of signals travelling in liquid media are also affected by many factors that may give rise to unwanted differences. There are disturbances due to propeller noise, backscattering at the floor and rotational motions of the ship. Further errors may be caused by bad reflections from the seabed, multiple paths, change of duration of path during transmission, or lengthening of a time signal, ocean noise, seismic activity, weather conditions, or the movement and noise of sea organisms (Lurton, 2002). Errors may also occur in the application of corrections for density variations in layered ocean water. Some of these causes are invoked for the differences described in Table 7.3.

Do both systems recognize small mounds of a few meter size?

Both sonars are able to recognize small mounds. However, the sonars vary in their estimation of the mound's boundary. The deep sea sonar rounded the details, as shown in Figure 5.12, and the shallow sonar did not properly receive reflections from the sloping terrain. Generally, beams at nadir bring better results and are often noise-free because of the slight influence of refraction in layered water or their geometry.

Does it make sense to subtract the data?

The DTMs are better used as complements to each other because they do not concur in many details. HYDROSWEEP mapping cannot offer detailed topography and EM 2000 cannot cover such a wide swath as HYDROSWEEP. If some spectacular feature appears in normal surveying, a robot can be deployed to explore in detail.

It can be concluded that the differences in the measurements by the two methods are consequences of multiple factors such as incorrect acoustic attitude, varying topography, different density of the sonar data, different swath widths and the geometry of measurements in the swath boundaries. The vertical errors of HYDROSWEEP DS-2 are dependent on depth. Positioning errors of VICTOR are dependent on acoustic positioning accuracy.

8.2 Recommendations and remarks

Microbathymetry was predicted to be more accurate, nevertheless, the accuracy is strongly deteriorated by the difficulty of correctly navigating the vehicle, and such errors are difficult to correct. The positioning accuracy of the vehicle is around 30 meters, so that fine structure could be mapped a few tens of meters away from its real seafloor position. VICTOR navigation can be assessed from the differences between POLARSTERN and VICTOR positions. In order to eliminate these positioning errors, transducers on the sea bottom, or long baseline positioning would certainly improve the placement of microbathymetric data in a coordinate system. None of the study areas was measured twice, so it is not possible to make a comparison of the variance in microbathymetry measurement due to navigational problems.

The vertical accuracy of HYDROSWEEP sonar must be taken into account in the relation to the relief of the generated DTMs. A depth of 600 meters allows a vertical accuracy of 6 meters. Contrary to bathymetry, the accuracy of microbathymetric depths consists of three summands. The EM 2000 sonar has accuracy 0.2 % of altitude, pressure sensors generally have an accuracy of around 0.25% full scale and the third summand is error in the vertical distance calculated between the sonar and pressure sensor on ROV.

It is important to realise that the quality of the data depends on reliable functioning of the systems. Many systems work together in acquisition and it is almost impossible to maintain all of them in an unerroneous state at all times.

Microbathymetry cannot be planned in the same way as bathymetry. Differences in scales determinate HYDROSWEEP as a reconnaissance tool in relation to the EM 2000 placed on VICTOR, which is a device for measuring the finest scale structures of the seafloor.

HYDROSWEEP is not suitable for microbathymetry, and the EM 2000 sonar mounted on VICTOR can not map such large areas in such a short time. Hence, an ideal opportunity for future research would be further ship cooperation with ROVs or AUVs, which will slowly replace manned submersibles.

8.3 Comparison and marine methods

Bearing a mind that the ideal difference between measurements would be equal to zero, we can be satisfied with an approximately constant systematic error which can be ascribed to the respective processing software and corrected far so that a zero difference is reached. In the end, the systematic difference of about 3 meters was seen as satisfactory because it is within the limit of HYDROSWEEP's vertical accuracy.

A correlation coefficient of at least 0.971 was acquired for all areas, and this correlation could be repeated using the coherence method. A more sophisticated approach could use cross correlation or fast Fourier transformation. Nevertheless, in the frame of this thesis, difference grids were sufficient for an interpretation.

Other marine surveying methods can serve as a complement to bathymetry and microbathymetry as well as to the other fields such as geology, geophysics, oceanography or geography. These methods include sidescan data, backscattering, PARASOUND and video mosaicking, and may be obtained from focussed studies of significant areas, as in the case of the mysterious mounds.

LIST OF ABBREVIATIONS

ACES	Atlantic Coral Ecosystem Study
AWI	Alfred Wegener Institute for Polar and Marine Research
BSH	Bundesamt für Seeschifffahrt und Hydrographie
CARACOLE	CARbonate Mound and COLd Coral Research.
CARAIBES	CARtography Adapted to Imagery and BathymEtry of Sonars and multibeam. echosounders.
CARIS	Computer Aided Resource Information System
CDU	Control and Display Unit, indicating all data of the platform
CDU	Control and Display Unit
CTRS	Conventional Terrestrial Reference System
DGPS	Differential GPS method
DLT	Digital Linear Tape
DRU	Dynamic Reference Unit
DVL	Doppler Velocity Log
ECOMOUND	Environmental Controls on Mound Formation
ETOPO5	Earth TOPOgraphy - 5 minute.
GEBCO	GEneral Bathymetric Chart of the Oceans
GEOMOUND	Geological evolution of carbonate mounds
GMT	Generic Mapping Tools
GPS	Global Positioning System
HIPS	Hydrographic Information Processing System
HMS	Her Majesty's Ship

HYDROSWEEP DS-2	HYDROgraphic multibeam SWEEPing Survey Echosounder for Deep Sea
IBCAO	International Bathymetric Chart of the Arctic Ocean
ICU	Interface and Connection Unit
IFREMER	French Research Institute for the Exploitation of the Sea
LADS	Laser Airborne Depth Sounder
MINS	Marine Inertial Navigational System
MP	Mounting Plate
MSL	Mean Sea Level
NAVSTAR GPS	NAVigation System with Time And Ranging Global Positioning System
NMEA	National Marine Electronics Association
OMARC	Ocean Margin deep-water Research Concortium
PARASOUND	PARAmetric echoSOUNDer
PFB	Preformed Beams
RCW	Record Control Word
ROV	Remotely Operated Vehicle
SURF	Sensor Unabhängiges Rohdaten Format
USBL	Ultrashort baseline
UTC	Universal Time Coordinated
WGS	World Geodetic System

LIST OF FIGURES

FIGURE 3.1: Outline of the DGPS principle.....	6
FIGURE 3.2: One of the TRIMBLE antennas.....	7
FIGURE 3.3: Common reference point on POLARSTERN.....	7
FIGURE 3.4: Computation of coordinates.....	9
FIGURE 3.5: Six degrees of freedom.	10
FIGURE 3.6: MINS – device configuration	10
FIGURE 3.7: Two travelling pulses of light	11
FIGURE 3.8: Addition of wavelengths	11
FIGURE 3.9: Heave compensator	11
FIGURE 3.10: VICTOR coordinate system	12
FIGURE 3.11: POSIDONIA acoustic array	13
FIGURE 3.12: USBL calculation principle	14
FIGURE 3.13: Outline of moored transponder.....	15
FIGURE 3.14: POSICAL calibration.....	15
FIGURE 3.15: Calibration offsets.	15
FIGURE 3.16: Open polygonal traverse, or inertial navigation	16
FIGURE 3.17: Adjustment possibilities	17
FIGURE 3.18: Doppler log and instrument coordinate systems.....	18
FIGURE 3.19: Transponder’s acoustic signals from VICTOR	21
FIGURE 3.20: Incorrect acoustic navigation.....	21
FIGURE 3.21: Incorrect POSIDONIA navigation.	22
FIGURE 4.1: Borders and zones of Irish waters.....	23
FIGURE 4.2: Mounds localities in Irish waters.....	24
FIGURE 4.3: Research vessel POLARSTERN.....	27
FIGURE 4.4: Remotely operated vehicle VICTOR 6000.	28
FIGURE 4.5: Depressor of VICTOR 6000.....	28
FIGURE 4.6: Constellation of ship, depressor and underwater vehicle.	29
FIGURE 4.7: Circulation of acoustic and electric pulses.....	31
FIGURE 4.8: Erroneous microbathymetry.....	35

FIGURE 5.1: Examples of civilian applications: bathymetry sounder.....	37
FIGURE 5.2: Snell’s Law	38
FIGURE 5.3: Sound velocity profile.....	40
FIGURE 5.4: Different sound velocity profiles for deep and shallow waters	40
FIGURE 5.5: CTD sonde.....	40
FIGURE 5.6: Multibeam geometry on rough terrain.....	41
FIGURE 5.7: Transmitting part of HYDROSWEEP and surveying principle	42
FIGURE 5.8: Principal of cross-fan calibration HYDROSWEEP.....	42
FIGURE 5.9: Forward motion of the vessel.....	43
FIGURE 5.10: Different heave motions	44
FIGURE 5.11: Formation of sonar image.....	44
FIGURE 5.12: Seafloor troughs detection and respective echogram.....	45
FIGURE 5.13: Errors associated with sound velocity profile.....	45
FIGURE 5.14: Side Scan Sonar Principal.....	46
FIGURE 5.15: Parts with higher reflectivity relating to carbonate mounds.....	47
FIGURE 5.16: Side Scan image of Scarp Mounds.....	47
FIGURE 5.17: Bathymetry of Scarp Mounds	47
FIGURE 5.18: Side Scan image of Hedge Mounds.	48
FIGURE 5.19: Bathymetry of Hedge Mounds.	48
FIGURE 5.20: Profile obtained from PARASOUND system.....	48
FIGURE 5.21: Sonar SIMRAD EM 2000.....	49
FIGURE 5.22: Roll procedure.....	50
FIGURE 5.23: Ideal mapping sonar constellation - POLARSTERN and VICTOR.....	51
FIGURE 5.24: Sweeping beams of sea bottom.....	51
FIGURE 5.25: Microbathymetrical and bathymetrical determination of depths	52
FIGURE 5.26: Stable and unstable motion of VICTOR.	53
FIGURE 5.27: Rolling geometry with roll angle θ	53
FIGURE 5.28: Beginning of HM2 surveying.	54
FIGURE 5.29: Typical microbathymetric survey.	54
FIGURE 5.30: Surveying of SM2, SM3, SM4 and HM2 areas.	55
FIGURE 5.31: Mosaicking Image (right).	56

FIGURE 6.1: Processing of HYDROSWEEP data.....	58
FIGURE 6.2: Sea surface.	59
FIGURE 6.3: Editor window.....	60
FIGURE 6.4: Side, rear and single beam window.....	61
FIGURE 6.5: Swath Editor.....	61
FIGURE 6.6: Incorrect lobe beams.....	61
FIGURE 6.7: ROV VICTOR was detected	62
FIGURE 6.8: Screenshots of Subset Editor.....	63
FIGURE 6.9: Striped features.....	63
FIGURE 6.10: Gridding modes	64
FIGURE 6.11: Grazing Weight Model, Range Weight Model.....	65
FIGURE 6.12: HYDROSWEEP measurements.....	66
FIGURE 6.13: Profiles of Mounds.....	66
FIGURE 6.14: Northeast part of Porcupine Bank.....	67
FIGURE 6.15: Model of cubic B-spline	67
FIGURE 6.16: CARIS Side Scan Editor.....	69
FIGURE 6.17: Menu of SENT software.....	70
FIGURE 6.18: Scarp milli mounds	70
FIGURE 6.19: Hedge Mound	70
FIGURE 6.20: PARASOUND of Scarp Mound	71
FIGURE 6.21: Microbathymetry of Scarp Mound.....	71
FIGURE 6.22: Steps in QINSY postprocessing.....	72
FIGURE 6.23: Cuts of raw and corrected data	73
FIGURE 6.24: 30 meters of terrain mapped from ROV VICTOR 6000.....	73
FIGURE 6.25: Roll error.....	74
FIGURE 6.26: Navigation jumps	74
FIGURE 6.27: Overlaps.....	74
FIGURE 6.28: Discontinuity caused by turning.....	75
FIGURE 6.29: Artefacts.....	75
FIGURE 6.30: Standard deviations of EM 2000 measurements.	76
FIGURE 6.31: Visualisation of uncorrected microbathymetric data.....	77
FIGURE 6.32: Roll and pitch movement.....	77

FIGURE 6.33: Before and after pitch correction.....	78
FIGURE 6.34: Doubling effect.....	78
FIGURE 6.35: Mosaicking.....	79
FIGURE 7.1: Data density	82
FIGURE 7.2: Distribution of data.....	82
FIGURE 7.3: Scarp Mound SM3	83
FIGURE 7.4: Difference grids.....	85
FIGURE 7.5: Histograms of difference grids.....	86
FIGURE 7.6: Profiles of certain parts of HM2 area	87
FIGURE 7.7: The lines of profiles in the SM4 area	88
FIGURE 7.8: Profiles of the SM4 area	88
FIGURE 7.9: Difference profiles.....	89
FIGURE 7.10: Broadness of a detected.....	90
FIGURE 7.11: Regression of depth values.	91
FIGURE 7.12: Coherence graphs.	92
FIGURE 7.13: Porcupine Bank.....	93

LIST OF TABLES

TABLE 3.1: Local coordinates of several facilities	8
TABLE 3.2: VICTOR sensors	13
TABLE 3.3: Coordinates of sensors.....	13
TABLE 3.4: Commonly used underwater vehicle navigation sensors.....	16
TABLE 4.1: Technical parameters of sonars.....	30
TABLE 4.2: Overview of sonar data from the different depths.....	32
TABLE 4.3: Part of NMEA file.....	33
TABLE 4.4: Microbathymetric measurement of Hedge and Scarp Mounds.....	36
TABLE 6.1: Sensors and selected filters.....	72
TABLE 7.1: Parameters of grids and their differences.	84
TABLE 7.2: Parameters of grids and their dimensions.	84
TABLE 7.3: Features in difference grids and their explanations.	87
TABLE 7.4: Correlation and coherence coefficients.	92

REFERENCES

- Anderson, D. Z. 1986 Optische Gyroskope, in *Spektrum der Wissenschaft*, Juni 1986, 68-74
- Bellier, F. 2002 User Manual for POSIDONIA system, Oceano Technologies, Brest, France
- Bergmann, U. 1996 Interpretation of digital Parasound echosounder records of the eastern Arctic Ocean on the basis of sediment physical properties, *Reports on Polar Research* 183, AWI Bremerhaven
- Bishop R. 2004 The Bay of Fundy's Minas Basin - Highest Tides in the World, Our Annapolis Valley, Nova Scotia [Accessed 12/5/2004], in *Frontier Technologies* [web page]: <http://www.valleyweb.com/fundytides/>
- Büchenschütz-Nothdurft, O. 2002 Entwicklung eines Ausgleichungsalgorithmus zur Verbesserung der Kreuzkalibrierung des Fächerecholotes HYDROSWEEP DS-2, Diploma thesis, Bremerhaven
- CARIS HIPS 2001 User's Guide 5.1
- Christen, S. 1999 Aufbereitung, Visualisierung und Interpretation einer bathymetrischen Vermessung im Süd Sandwich Tiefseeegraben, Diploma thesis, Hamburg
- Costello, M. J. 1998 "Coral reefs in Irish Waters", *Technology Ireland* 30 (7), 28-33 [Accessed 24/1/2004], in *Ecological Consultancy Services Ltd* [web page]: <http://www.ecoserve.ie/projects/coral/>
- Currie, A. (n.d.) The history of robotics [Accessed 26/1/2004] [web page]: <http://cache.ucr.edu/~currie/roboadam.htm>
- De Mol, B.; Van Rensbergen, P.; Pillen, S.; Van Herreweghe, K.; Van Rooij, D.; McDonnell, A.; Huvenne, V.; Ivanov, M.; Swennen & R., Henriët, J.P. 2002 Large deep-water coral banks in the Porcupine Basin, southwest Ireland, in *Marine Geology* 188, 193-231
- Deacon, M. 2003 Knowledge of the deep ocean by the end of the 19th century, leading up to the decision in 1899 to compile a word series of bathymetric charts series, in *Charting the Secret World of the Ocean Floor. The GEBCO Project 1903-2003, GEBCO Centenary Conference 2003, Monaco*
- Drogou, J.F. (n.d.) Victor 6 000 [Accessed 26/1/2004] [web page]: <http://www.equipement.gouv.fr/recherche/rst/uk/maritime/m31.htm>
- Christian Edy, Hervé Bisquay and al. 2003 Cruise report ARK XIX 3/b onboard R/V Polarstern, Microbathymetry on ROV Victor 6000
- EM 2000 Multibeam echosounder, Operator manual – Base version 2002 Kongsberg Simrad AS

Encyclopedia.com 2004 Copyright Alacritude LLC., Early Navigational Techniques and Introduction of Navigational Instruments, updated 21 Feb 2002 [Accessed 26/1/2004] [web page]: <http://www.encyclopedia.com/html/s1/submersi.asp> 26/1/2004

Encyclopædia Britannica 1987 Gwinn, R.P.; Norton, P.B.; Goetz, P.W. The New Encyclopædia Britannica, MICROPAEDIA and MACROPAEDIA, Chicago

ESI/IE 2003 Victor 6000 - Système Informatique: Interfaces de Communication – Messages réseau, IFREMER

European Communities 1995-2003 2000 Environment and Sustainable Development: 165 new research projects to be launched [Accessed 8/2/2004], in Annex to Press release – Brussels, 16 February 2000 [web page]: <http://europa.eu.int/comm/research/press/2000/pr1602en-annex.html>

Evans, F. 2001 Porcupine History [Accessed 24/1/2004], in Porcupine Marine Natural History Society [web page]: <http://www.pmnhs.co.uk/>

Expeditionsprogramm Nr.66 2003 ARK XIX/3: in Summary and Itinerary, FS "Polarstern" ARKTIS XIX/3, AWI, Bremerhaven

Dpa (Deutsche Presseagentur) 2002 „Polarstern“ bricht Eis für die Forschung, in Frankfurter Rundschau, Dec 10th 2002, 38

Garcia, R.; Batlle, J.; Cufí, X.; Amat, J. "Positioning an Underwater Vehicle through Image Mosaicking" IEEE International Conference on Robotics and Automation (ICRA), vol. 3, pp. 2779-2784, Seoul, Rep.of Korea, 2001 [Accessed 20/4/2004] [web page]: <http://eia.udg.es/~rafa/papers/icra-2001.pdf>

Garrison,R. 1999 Lesson 7 : Dead Reckoning,in course presentations from Naval Science 301, Rice University [Accessed 25/2/2004] [web page]: <http://www.owl.net.rice.edu/~nava301/presentations/Lesson07.ppt>

Geughegan, M. 2003 Ireland's Seabed Survey – Mapping the Irish Seabed 2003, prospect of Geological Survey of Ireland

Gourley M.; Hughes Clarke J. E. 2000 Integrating Time and Spatial Domains During Multibeam Data Cleaning, 15th Hydrographer's Conference, German Hydrographic Society

Gutberlet, M.; Schenke H. W. 1989 HYDROSWEET: New Era in High Precision Bathymetric Surveying in Deep and Shallow Water, Marine Geodesy 13, 1-23

Hampacher, M.; Radouch V. 1998 Teorie chyb a vyrovnávací počet – Příklady a návody ke cvičení, TU Prague

Hampacher, M.; Radouch V. 2003 Teorie chyb a vyrovnávací počet 10, TU Prague

- Hempel, G. 2002 Around the ship, in RV Polarstern – Twenty years of research in polar seas, presentation prospect, AWI, Bremerhaven
- Henderson, T. (n.d.) Interference and Beats, in The Physics Classroom; Glenbrook South High School in Glenview, Inc. [Accessed 22/2/2004], in The Physics Classroom and Mathsoft Engineering & Education [web page]:
<http://www.physicsclassroom.com/Class/sound/U11L3a.html>
- Hohmann, C. 2002 Qualitative und quantitative Untersuchung von Eisbergflugspuren im Bereich der Austaasenbank (Antarktischer Schelf), Diploma thesis, Bremerhaven
- Huvenne, V.A.I., De Mol, B. & Henriët, J.P. 2003 A 3D seismic study of the morphology and spatial distribution of buried coral banks in the Porcupine Basin, SW of Ireland, *Marine Geology* 198, 5-25
- Jacobs, M. 2002 Analyses of High Resolution Bathymetric Data in the Eltanin Impact area, Master's thesis, Bremerhaven
- Kenyon, N.H., Akhmetzhanov, A.M., Wheeler, A.J., van Weering, T.C.E., de Haas, H. & Ivanov, M.K. 2003 Giant carbonate mud mounds in the southern Rockall Trough, in *Marine Geology* 195, 5-30
- Kinsey, J.C.; Whitcomb, L.L. 2003 Preliminary field experience with the DVLNAV integrated navigation system for manned and unmanned submersibles, in *Proceeding of the 1st IFAC Workshop on Guidance and Control of Underwater Vehicles, GCUV '03, 9 - 11 April 2003, Newport, South Wales*
- Laughton, A. S. 2003 The impact on ocean mapping of the post war revolution in marine geology and the work of SCOR working group 41 The GEBCO Project 1903-2003, GEBCO Ceternary Conference 2003, Monaco
- Lurton, X. 2002 *An Introduction to Underwater Acoustics: Principles and Applications*, Praxis Publishing Ltd, Chichester, 2002, Springer publisher
- Macmillan Publishers 2003 *The Onestop Magazine: The exotic roots of English vocabulary* [Accessed 19/1/2004] [web page]:
<http://www.onestopenglish.com/News/Magazine/Vocab/storyword3.htm>
- MathPages (n.d.) [Accessed 7/4/2004] [web page]: <http://www.mathpages.com>
- Maul, G.A. and Bishop, J.C. 1970 Mean sounding velocity a brief review, *International Hydrographic Review*.
- Maury, M.F. 1893 *The Physical Geography of the Sea*, London: Nelson
- Merriam-Webster Online Dictionary [Accessed 27/1/2004], in Merriam-Webster, Incorporated [web page]:
<http://www.m-w.com/cgi-bin/dictionary?book=Dictionary&va=bathymetry>

- McLauchlan J. 2000 ROV world - Subsea Information Portal [Accessed 27/1/2004], in PHP-Nuke [web page]:
http://rovworld.com/phpnuke/modules.php?name=FAQ&myfaq=yes&id_cat=8&categories=About+ROV%27s+and+AUV%27s
- Ng'ang'a, S; Nichols, S.; Monahan (n.d.) The Role of Bathymetry Data in a Marine Cadastre: Lessons from the Proposed Musquash Marine Protected Area [Accessed 11/4/2004], in The Hydrographic society of America [web page]: http://www.thsoa.org/hy03/9a_1.pdf
- Nielsen, R. O. 1991 Sonar signal processing, Artech House, Boston
- Nokin, M. 1999 Sea Trials of the Deep Scientific System VICTOR 6000, in Proceeding of the Ninth(1999) International Offshore and Polar Engineering Conference, Brest, France, May 30-June 4,1999
- Ommanney, F. D. 1961 The Ocean, London Oxford University Press
- Peyronnet, J.P.; Person, R. ; Rybicki, F. 1998 POSIDONIA 6000 : A new Long Range Highly Accurate Ultra Short Base Line Positioning System, IEEE
- Raytheon Company 2001 Marine Inertional Navigational System (MINS) – Palett, in Sea going vessel's navigation [Accessed 20/2/2004] [web page]:
http://www.raytheon-marine.de/highseas/products/surface/navigation/mins_pallet.html
- Raytheon Electronics (n.d.) MINS, Marine Inertial Navigational System, prospect
- Sager, W. W.; MacDonald I. R.; Hou R. 2003 Geophysical signatures of mud mounds at hydrocarbon seeps on the Louisiana continental slope,northern Gulf of Mexico, in Marine Geology 198, 97-132.
- Sarradin, P.M.; Olu, K.; Ondréas, H.; Sibuet, M.; Klages, M.; Fouquet, Y.; Savoye, B.; Drogou, J.F.; Michel, J.L. 2002 Evaluation of the first year of scientific use of the French ROV Victor 6000, Congrès UT 16-19 April 2002, Tokyo
http://www.ifremer.fr/flotte/systemes_sm/images/victor6000/UT%202002.pdf
- Schenke, H.W. 1992 GPS und Fächersonarmessungen mit Hydrosweep auf FS „Polarstern“, Zeitschrift für Vermessungswesen (ZfV), Volume 8/9 1992, Stuttgart, 599 - 615
- Schenke, H.W. 2001 Eiskalte Entdeckungen – Forschungsreisen zwischen Nord- und Südpol, Lange, G. (eds.) publisher Delius Klasing, Bielefeld
- Seeber, G. 2001 Lectures on Marine Geodesy, University of Hannover
- Seeber, G. 2003 Satellite Geodesy, 2nd Edition, Walter de Gruyter, Berlin
- Smee, J. 2003 Hydrocarbon potential of parcels 1-12, C-NOPB call for bids NF 03-1, Report prepared for Department of mines and energy government of Newfoundland and Labrador, [Accessed 24/1/2004] [web page]: <http://www.gov.nf.ca/mines&en/oil/callforbids/basin.pdf>

Soukup, R.J.; Gragg, R.F. 2003 Roughness-Induced Ocean Bottom, in 2003 NRL (Naval Research Laboratory) Review, Washington, [Accessed 18/4/2004] [web page]: <http://www.nrl.navy.mil/content.php?P=RESEARCHHILITES>

The Irish National Seabed Survey (INSS) (n.d.) Progress of survey, 2003 Summary Review, updated 3 Feb 2004 [Accessed 14/2/2004] [web page]: <http://www.gsiseabed.ie/>

The MathWorks 2000 [Accessed 11/5/2004] [web page]: https://tagteambserver.mathworks.com/ttserverroot/Download/647_8517v04_Spline3_DS.pdf

USGS (n.d.) U.S. Geological Survey Open-File Report 00-410, maintained by Eastern Publications Group, updated 21 Dec 2001, [Accessed 14/5/2004] [web page]: <http://pubs.usgs.gov/of/of00-410/mapdisc.htm>

Verplaetse, C. 1995 "Strapdown Systems", in Can A Pen Remember What It Has Written Using Inertial Navigation?: An Evaluation Of Current Accelerometer Technology, University of Leeds: updated May 26 1995 [Accessed 20/2/2004] [web page]: <http://xenia.media.mit.edu/~verp/projects/smartpen/node8.html>

Ward, C. ROV.net (n.d.) "The origins of the ROV a discussion": updated 10 Dec 2002 [Accessed 26/1/2004] [web page]: <http://www.rov.net/>

Wessel, P.; Smith W. H. F. 2002 The Generic Mapping Tools – GMT, Version 3.4.1, Technical Reference and Cookbook, School of Ocean and Earth Science and Technology University of Hawai'i at Manoa & Laboratory for Satellite Altimetry NOAA/NESDIS/NODC: updated 27 Feb 2002, [Accessed 16/5/2004] [web page]: http://www.earth.rochester.edu/ees254/gmt/doc/html/GMT_Docs/GMT_Docs.html

Weisstein E. W.; "Bicubic Spline." From MathWorld--A Wolfram Web Resource [Accessed 26/1/2004] [web page]: <http://mathworld.wolfram.com/BicubicSpline.html>

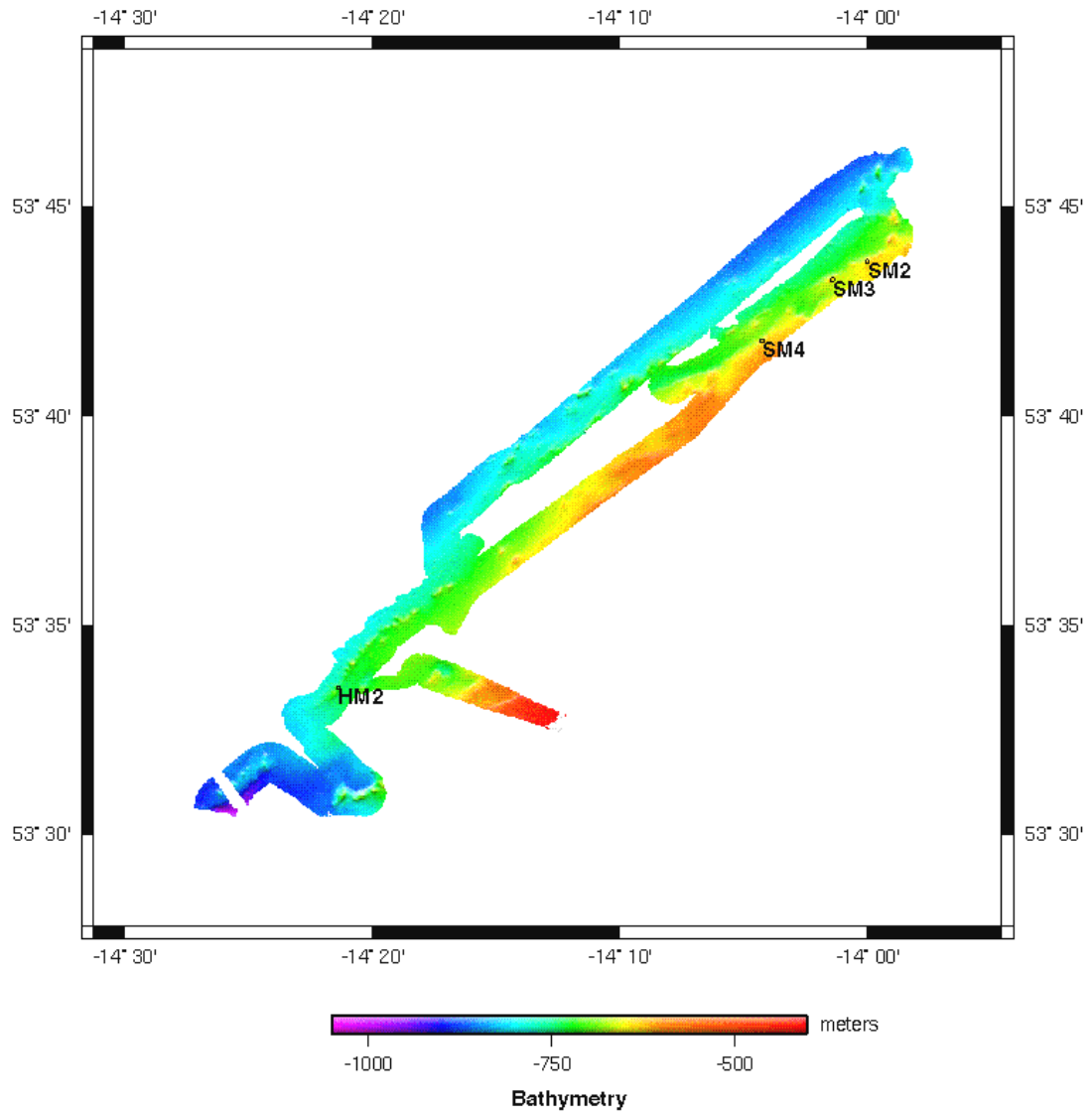
Wheeler, A.J., Beck, T. , Thiede, J. , Klages, M. , Foubert, A. , Grehan, A. , Berov, D. , Beyer, A., Brennan, C. , Buldt, K. , Dabrowski, P. , Devanathan, V. , Dorschel, B. , Gault, J. , Guinan, J. , Gutt, J. , Hall-Spencer, J. , Kozachenko, M. , Kroker, R. , Kulaksiz, S. , Möller, H-J. , Monteys, F.X. , Opderbecke, J. , Pfannkuche, O.12 , Pokorná, M. , Rathlau, R. , Roberts, J.M. , Sharma, P. , Sumoondur, A.D. , Thomsen, L. , Tseu, G. , Unnithan, V. , Wilson, M. 2004 (in press) Deep-water Coral Mounds on the Porcupine Bank, Irish Margin: Preliminary Results from the Polarstern ARK-XIX/3a ROV cruise.; In: A. Freiwald & J.M. Roberts (eds). Deep-water corals and Ecosystems: Proceedings of the 2nd International Symposium on Deep-water Corals, Springer-Verlag

GEOMOUND, The Internal Mound Factory (n.d.) The Geomound Webserver, The Department of Geology University College Dublin, updated 19 Nov 2002 [Accessed 10/8/2003] [web page]: <http://geomound.ucd.ie/>

APPENDIX A

Digital terrain models - overview

Scarp and Hedge Mounds – SM2, SM3, SM4, HM2



(GMT)

Scarp and Hedge Mounds



(CARIS)

APPENDIX B

Sound velocity profiles used

CTD measurement, sound velocity profiles from 16. and 19.6. 2003

16.6.2003			19.6.2003	
Section 2003-167 08:00 (m, m/s)	Section 2003-167 16:00 (m, m/s)	Section 2003-168 08:00 (m, m/s)	Section 2003-170 00:00 (m, m/s)	Section 2003-170 08:00 (m, m/s)
11.50 1500.30	11.50 1500.30	11.50 1500.30	11.50 1500.40	11.50 1500.40
29.00 1500.20	29.00 1500.20	29.00 1500.20	33.00 1500.40	33.00 1500.40
33.00 1500.00	33.00 1500.00	33.00 1500.00	59.00 1498.20	59.00 1498.20
46.00 1500.10	46.00 1500.10	46.00 1500.10	81.00 1497.00	81.00 1497.00
53.00 1498.40	53.00 1498.40	53.00 1498.40	158.00 1497.30	158.00 1497.30
101.00 1497.10	101.00 1497.10	101.00 1497.10	248.00 1498.30	248.00 1498.30
134.00 1497.50	134.00 1497.50	134.00 1497.50	355.00 1498.80	355.00 1498.80
196.00 1497.50	196.00 1497.50	196.00 1497.50	439.00 1499.40	439.00 1499.40
329.00 1498.70	329.00 1498.70	329.00 1498.70	487.00 1499.60	487.00 1499.60
409.00 1499.90	409.00 1499.90	409.00 1499.90	519.00 1500.70	519.00 1500.70
468.00 1499.90	468.00 1499.90	468.00 1499.90	566.00 1501.10	566.00 1501.10
561.00 1500.70	561.00 1500.70	561.00 1500.70	637.00 1499.40	637.00 1499.40
626.00 1500.30	626.00 1500.30	626.00 1500.30	732.00 1498.90	732.00 1498.90
688.00 1498.00	688.00 1498.00	688.00 1498.00		
721.00 1498.40	721.00 1498.40	721.00 1498.40		
743.00 1497.80	743.00 1497.80	743.00 1497.80		
874.00 1499.80	874.00 1499.80	874.00 1499.80		

APPENDIX C

Tidal flow applied on microbathymetric measurements

Scarp Mound SM2

June 2003 5344N01400W UT +0.0

day height every 10 minutes in centimetres

Mon	16	41	40	40	41	44	47	51	56	61	68	75	83
		92	101	110	120	131	141	152	163	174	185	196	206
		216	226	236	245	253	261	268	274	280	285	289	292
		294	295	295	295	293	291	287	283	278	272	266	259
		251	242	233	224	214	204	194	183	173	162	151	141
		131	121	112	103	94	86	79	73	67	62	58	55
	12h	52	51	50	51	52	54	58	62	67	73	79	87
		95	103	113	123	133	144	155	166	178	189	201	212
		224	235	246	256	266	276	284	293	300	307	313	318
		322	325	328	329	330	329	328	325	322	318	313	307
		300	292	284	275	265	255	245	234	223	212	200	188
		177	165	154	143	132	121	111	102	93	85	77	70

Scarp Mound SM3

June 2003 5343N01402W UT +0.0

day height every 10 minutes in centimetres

Mon	16	41	40	40	41	44	47	51	56	62	68	75	83
		92	101	111	121	131	142	152	163	174	185	196	206
		217	226	236	245	253	261	268	274	280	285	288	291
		294	295	295	294	293	290	287	283	278	272	265	258
		250	242	233	223	213	203	193	183	172	161	151	141
		130	121	111	102	94	86	79	73	67	62	58	55
		52	51	50	51	52	55	58	62	67	73	80	87
		95	104	113	123	134	144	155	167	178	190	201	213
		224	235	246	256	266	276	285	293	300	307	313	318
	18h	322	325	328	329	329	329	327	325	322	317	312	306
	20h	299	292	283	274	265	255	244	234	222	211	199	188
		176	165	153	142	131	121	111	102	93	84	77	70

Scarp Mound SM4

June 2003 5342N01404W UT +0.0

day height every 10 minutes in centimetres

Tue	17	64	59	55	51	49	47	47	47	48	50	53	57
		61	66	72	79	87	94	103	112	121	131	140	150
		161	171	181	191	200	210	219	228	236	243	250	257
	6h	263	268	272	276	278	280	281	281	281	279	277	273
	8h	270	265	259	253	247	239	232	223	215	206	196	187
		177	168	158	149	139	130	122	113	105	98	91	85
		79	74	70	66	64	62	61	61	62	64	66	70
		74	79	85	91	98	106	114	123	133	142	152	163
		173	184	195	206	216	227	237	247	257	266	274	282
		290	297	303	308	312	316	319	321	322	322	321	320
		317	314	310	305	299	293	285	278	269	260	251	241
		231	221	210	199	188	178	167	157	146	136	127	117

Hedge Mound HM2

June 2003 5333N01421W UT +0.0

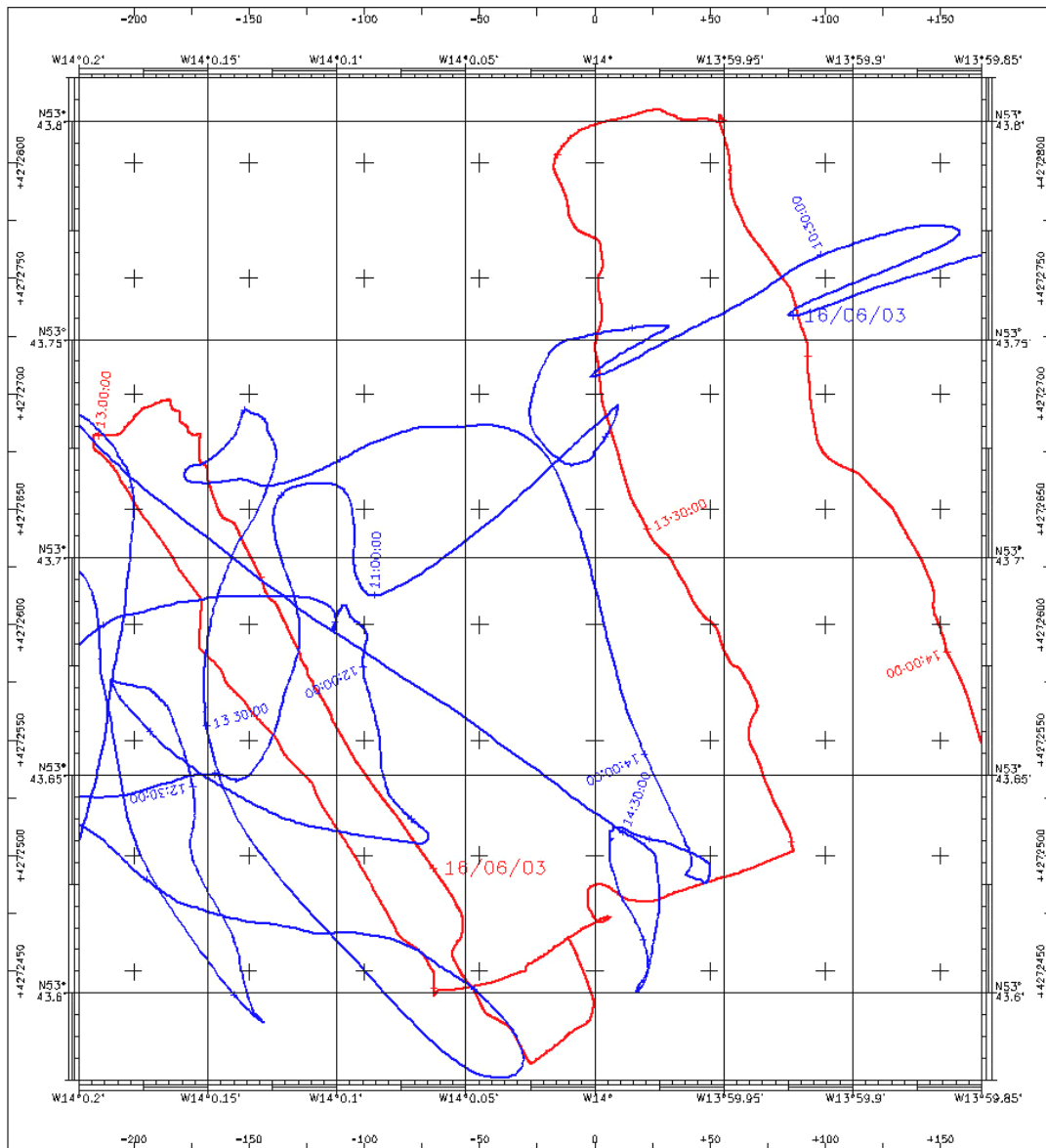
day height every 10 minutes in centimetres

		0h	10	20	30	40	50	1h	10	20	30	40	50
Th	19	154	145	137	128	120	112	105	99	93	87	83	78
	2h	75	72	70	69	69	69	70	71	74	77	80	84
	4h	89	94	100	106	113	120	127	134	142	150	157	165
	6h	173	180	188	195	202	208	215	220	226	230	235	238
	8h	241	244	246	247	248	247	247	245	244	241	238	234
	10h	230	225	220	215	209	202	196	189	182	175	168	161
	12h	154	147	140	134	128	122	116	111	106	102	98	95
	14h	93	91	89	89	89	89	91	92	95	98	102	106
	16h	111	117	123	129	136	143	151	159	167	175	183	191
	18h	200	208	216	224	232	239	247	253	260	266	271	276
	20h	280	284	287	290	291	293	293	293	292	290	288	285
	22h	281	277	272	267	261	255	248	241	233	225	217	209

APPENDIX D

Track plots of R/V POLARSTERN and ROV VICTOR 6000

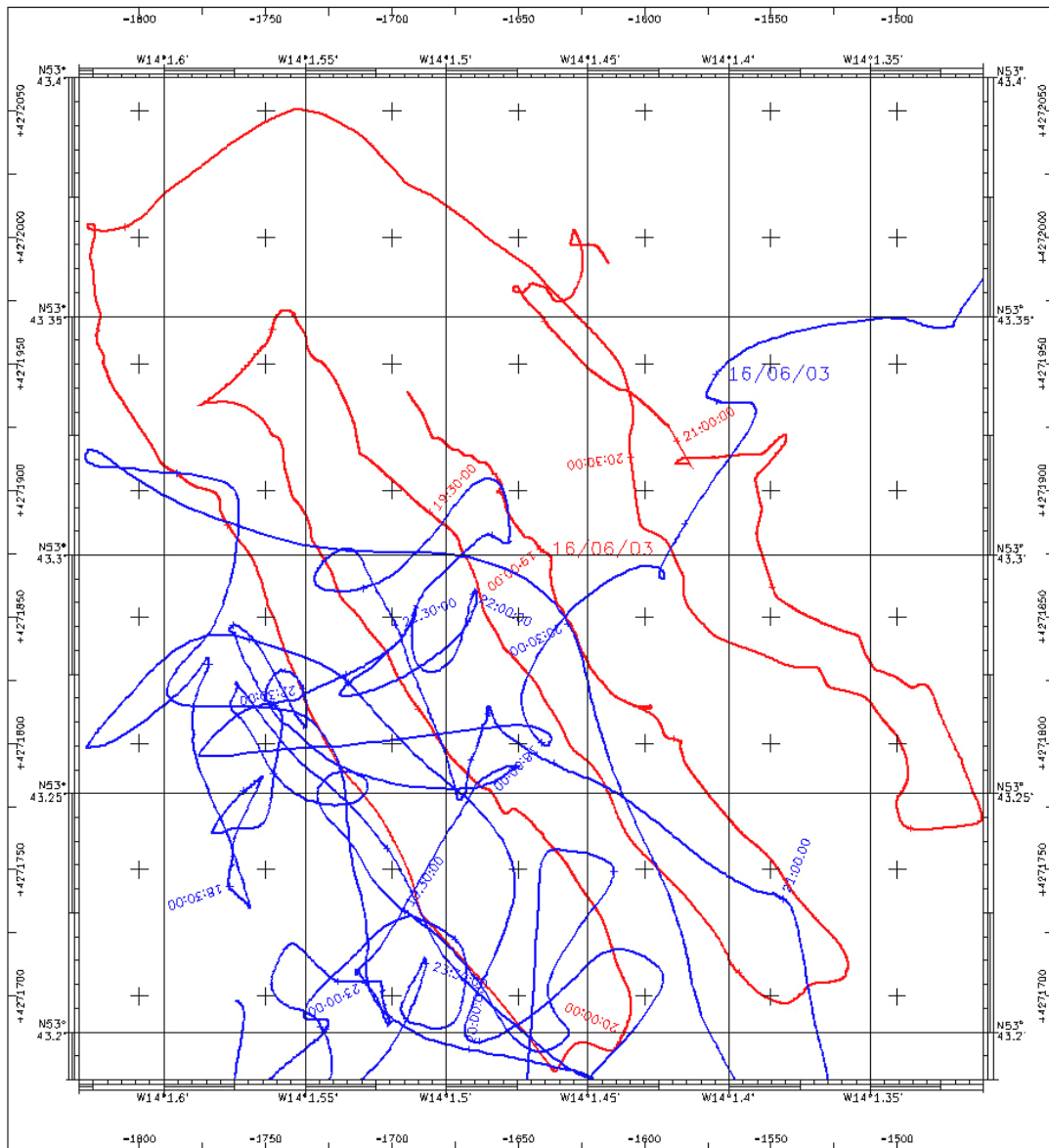
Scarp Mound SM2



— ROV VICTOR 6000
— R/V POLARSTERN

(CARAIBES)

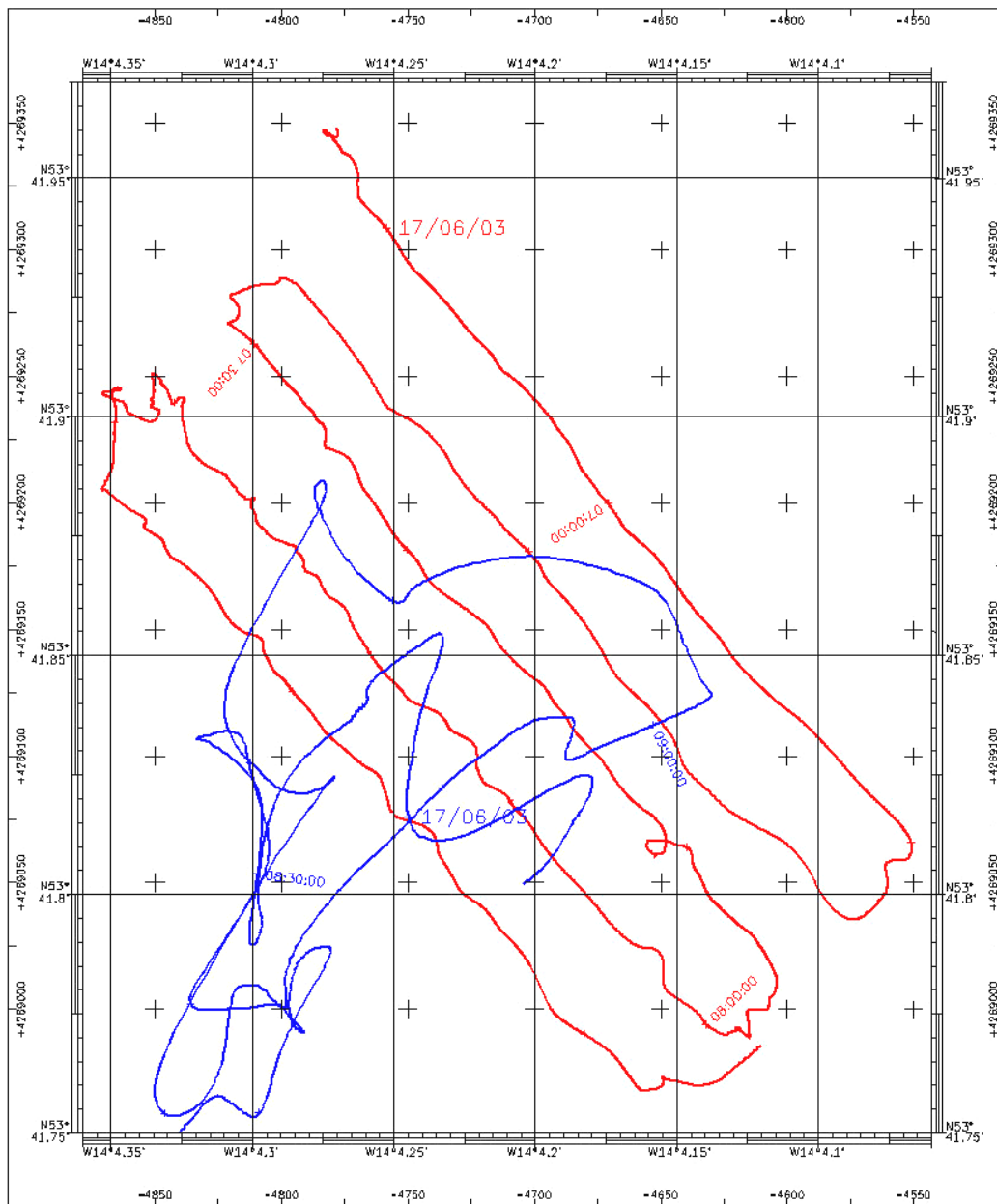
Scarp Mound SM3



— ROV VICTOR 6000
— R/V POLARSTERN

(CARAIBES)

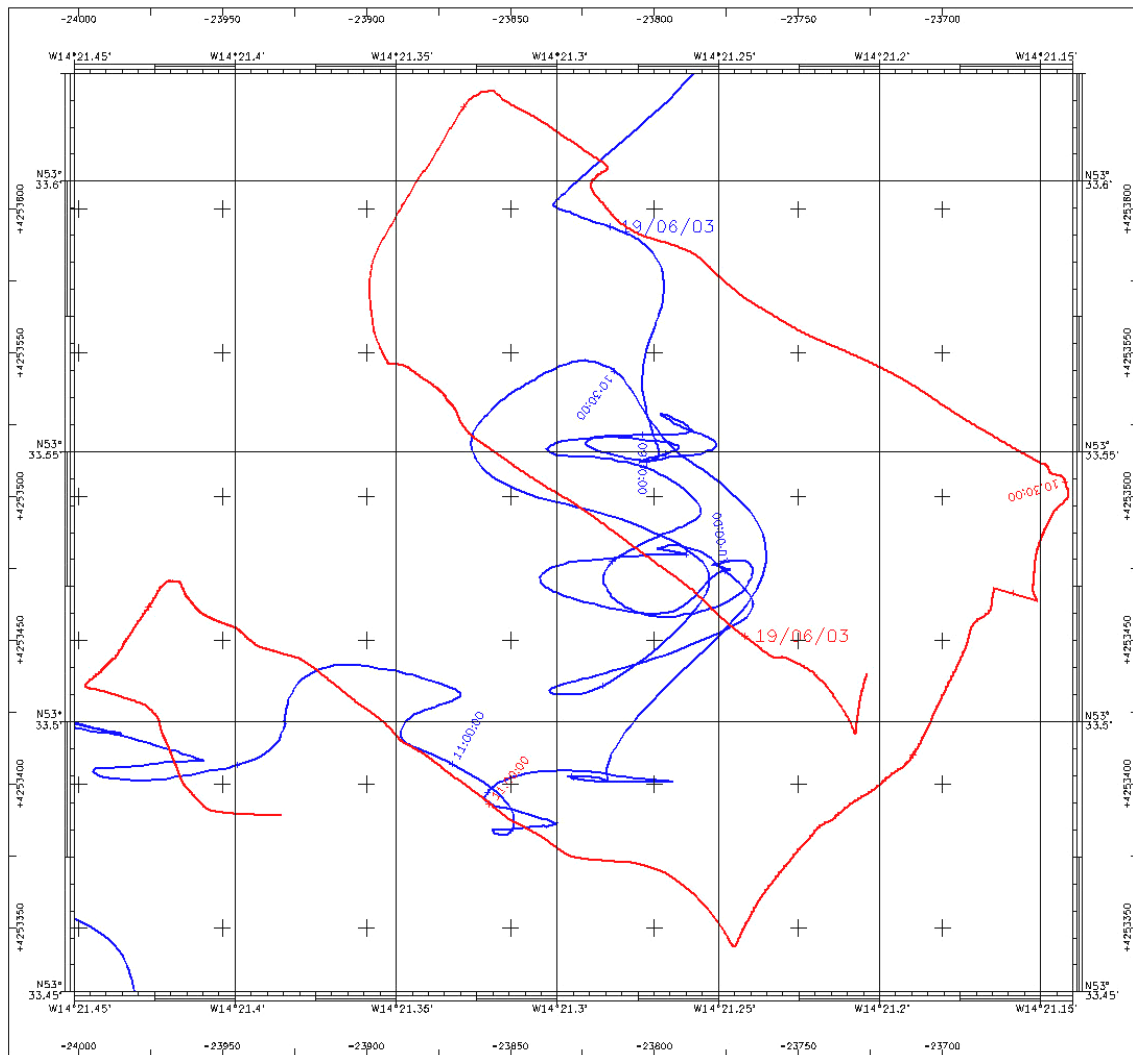
Scarp Mound SM4



— ROV VICTOR 6000
— R/V POLARSTERN

(CARAIBES)

Hedge Mound HM2



- ROV VICTOR 6000
- R/V POLARSTERN

(CARAIBES)

APPENDIX E

POLARSTERN & VICTOR parameters

Technical data – R/V POLARSTERN

Construction	Howaldtswerke/Deutsche Werft, Kiel
Shipyard	Nobiskrug, Rendsburg
Ice-breaker design	Hamburg Ship Model Basin
Total length	118 m
Breadth of frame	max. 25 m
Height to main deck	13.6 m
Draught	max. 11.2 m
Displacement at maximum draught	17 300 t
Empty weight	11 820 t
Engine capacity(4 engines)	ca. 14 000 kW(20 000 hp)
Maximum speed	16 kn

(Hempel, 2002)

Systems specifications – ROV VICTOR 6000

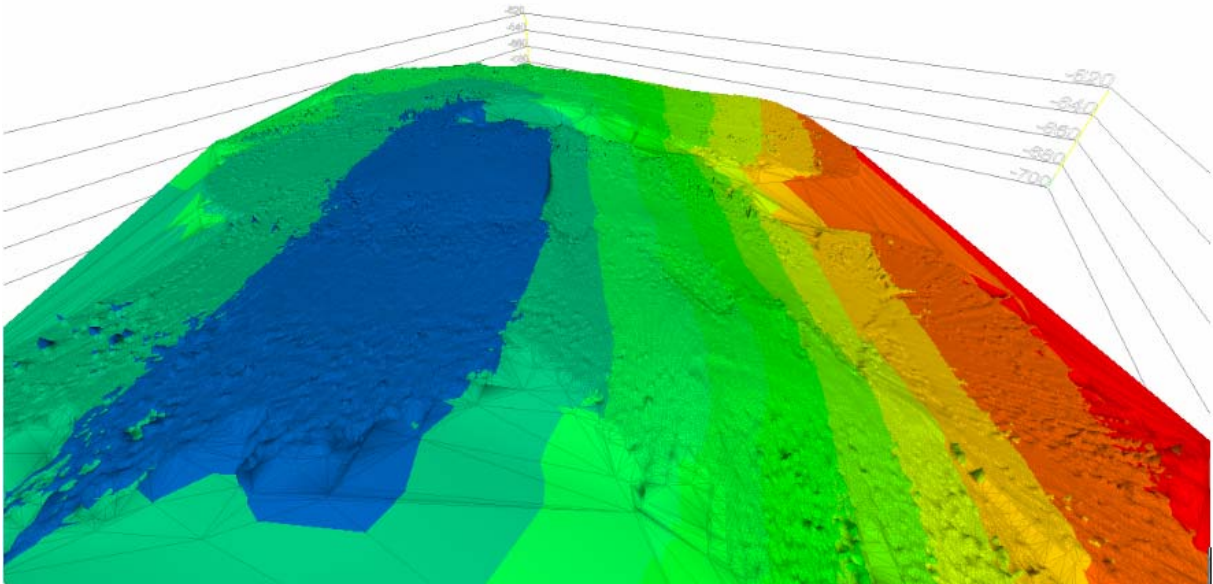
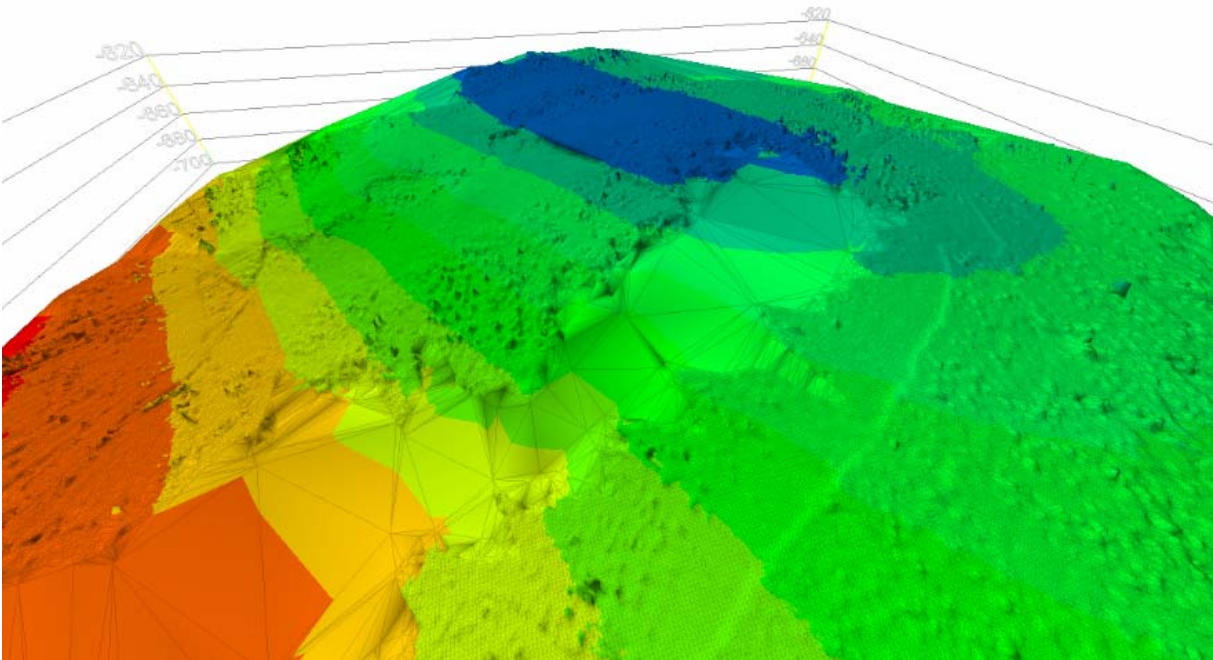
	VICTOR System	Specifications
Power requirement	Hydraulic winch	2x160kW, 380V
	Vehicle	50kW, 380V
Primary cable	Length	8 500 m
	Diameter	35 mm
	Breaking strength	20 t
Tether	Length	100 or 300m
	Diameter	35 mm
	Breaking strength	9 t
Vehicle	Depth rating	6 000 m
	Dimensions	3.1(L) x 1.8(W) x 2.0(H) m
	Mass in air	4 000 kg
	Power	20 kW
	Thrust	200 kg in all directions
	Main video camera	3CDD with zoom lens
	Additional cameras	5 colour cameras
	Lights	5kW max, 8 units
Sensors	Sensors	MRU6, depth, altitude, OAS
	Manipulator (MAESTRO)	7 fct ME, 100 kg lift capacity
	Grabber	5 fct
	Reversible buoyancy system	701.21/mn at 600 bars
	Payload	100 kg in water, 600 kg in air
Depressor	Weight in air	1.2 t
	Dimensions	1.5m(L)x0.8m(W)x0.5m(H)
	Sensors	heading, depth

(Nokin, 1999)

APPENDIX F

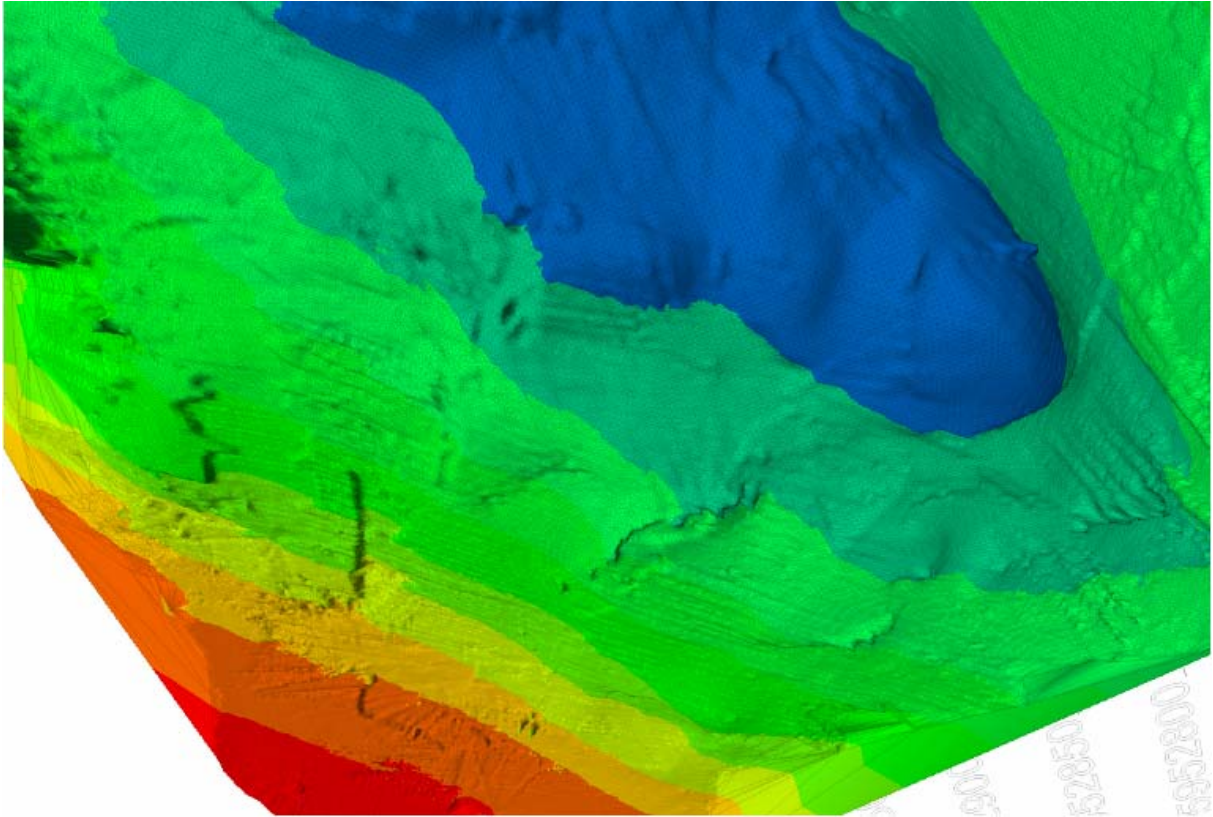
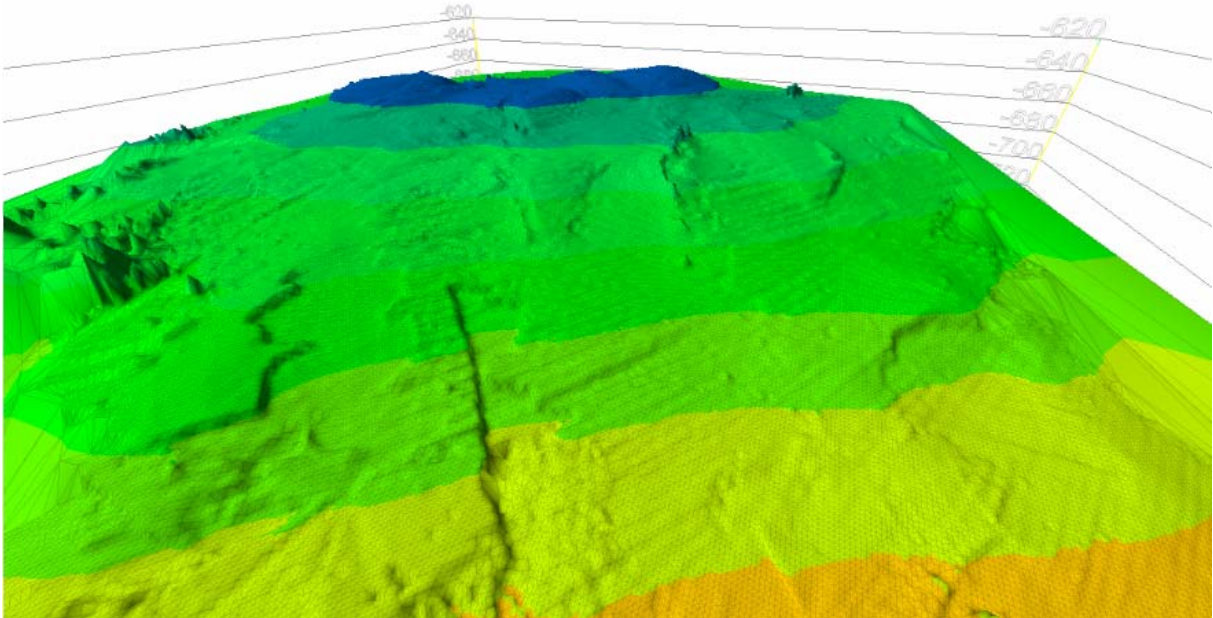
Digital terrain models - RAW data

Scarp Mound SM2



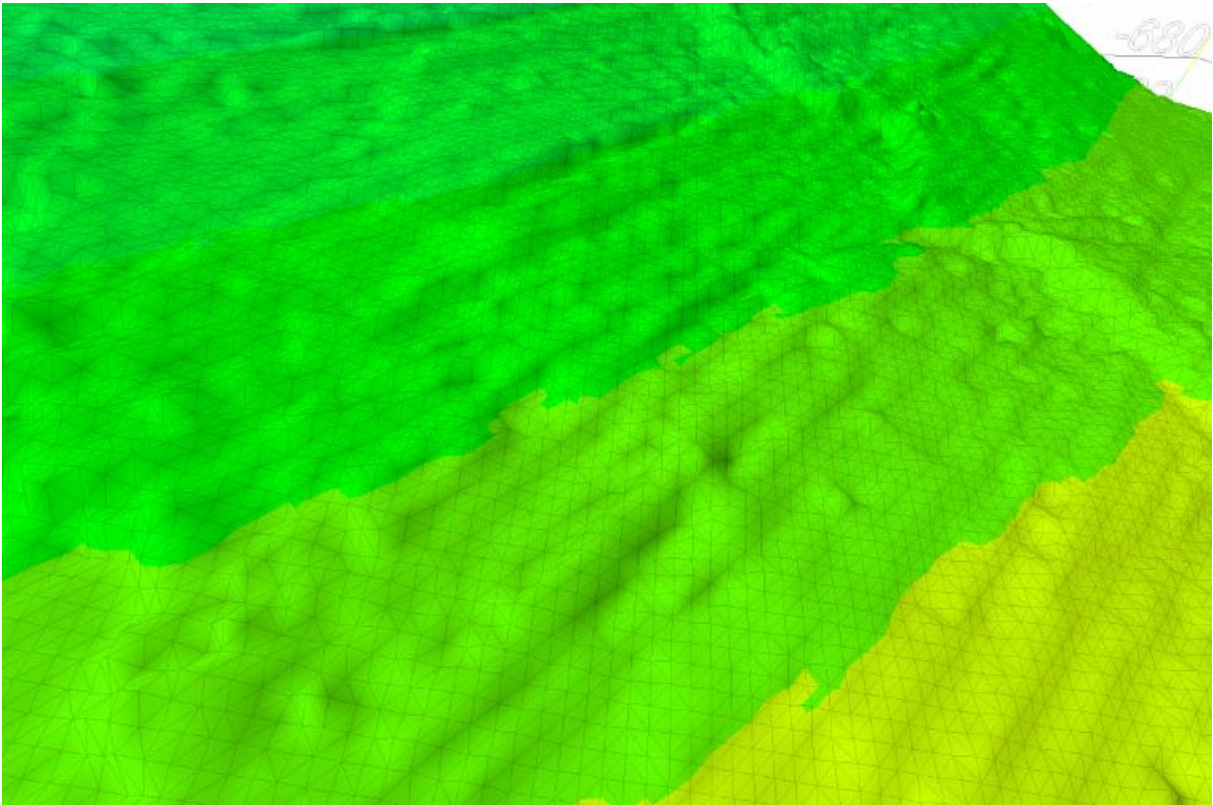
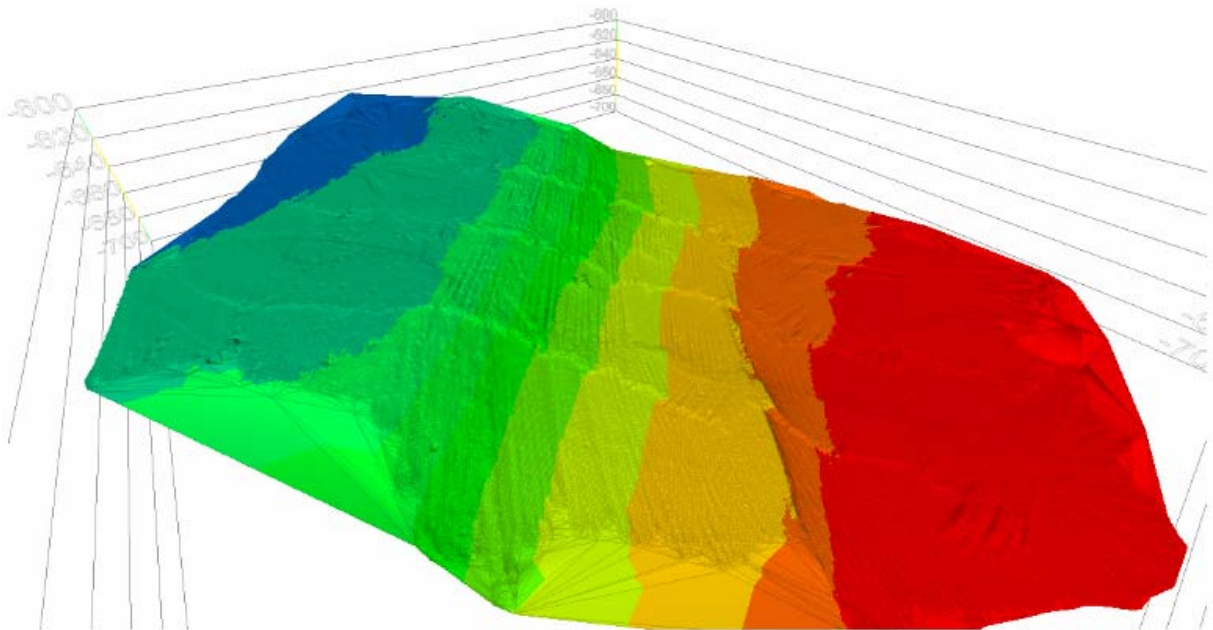
(TERRAMODEL)

Scarp Mound SM3



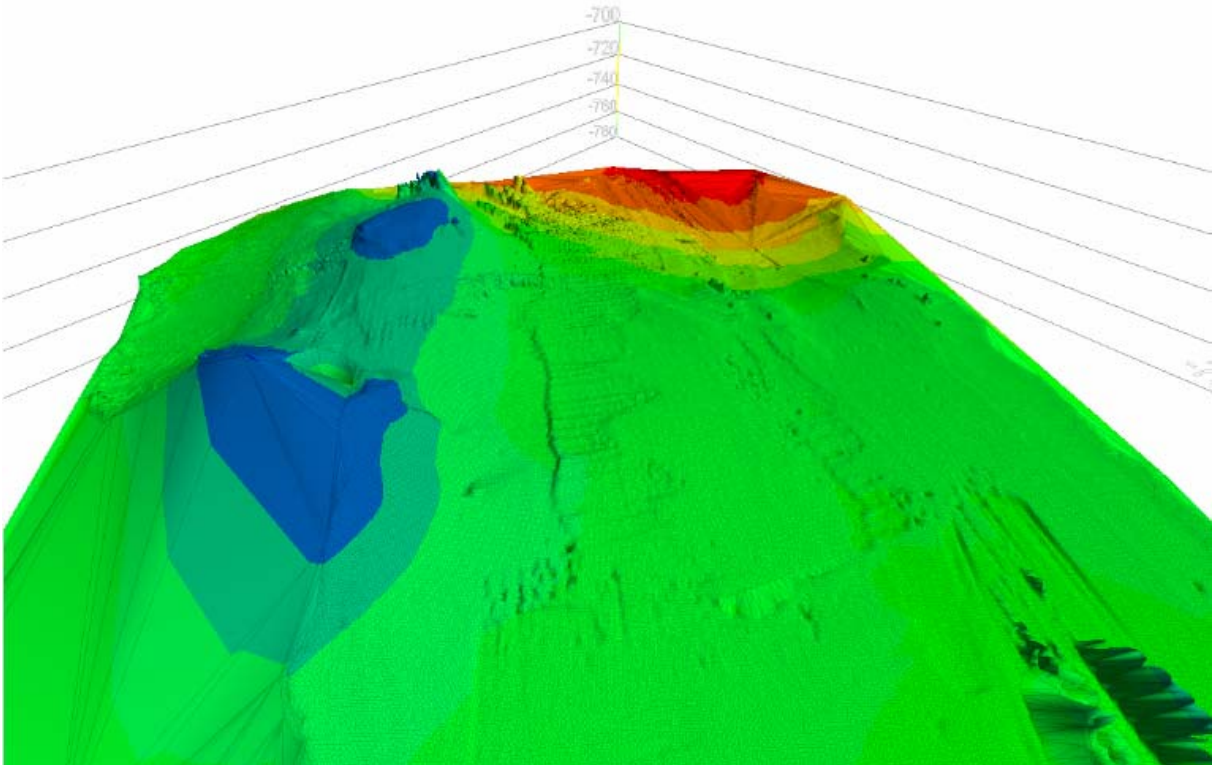
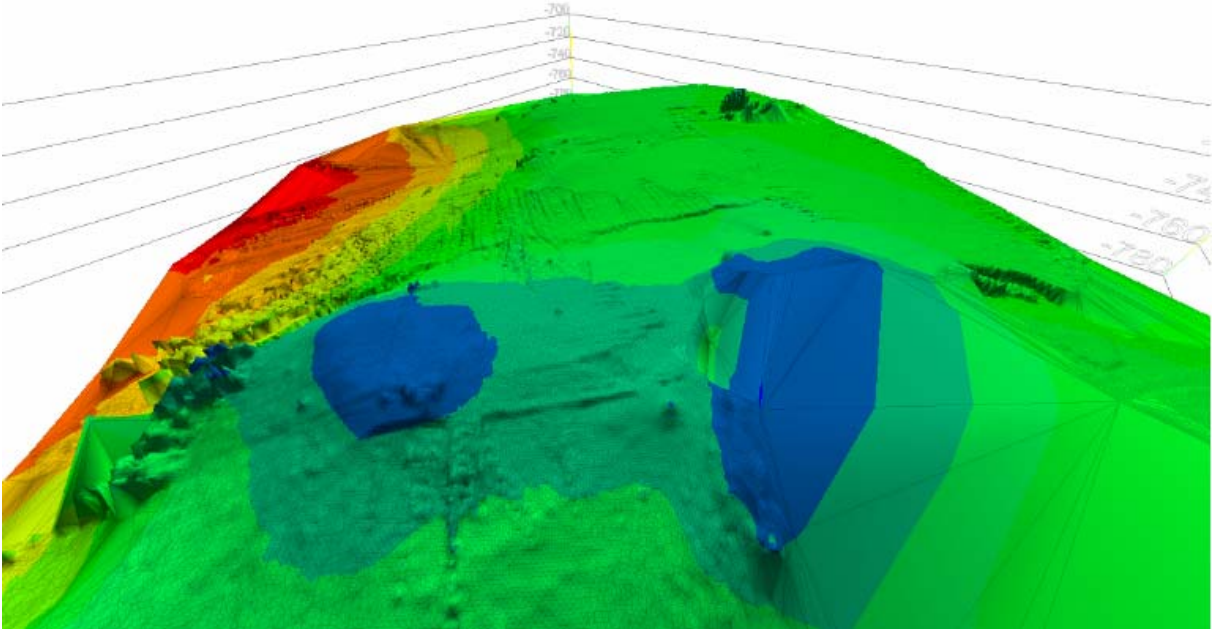
(TERRAMODEL)

Scarp Mound SM4



(TERRAMODEL)

Hedge Mound HM2

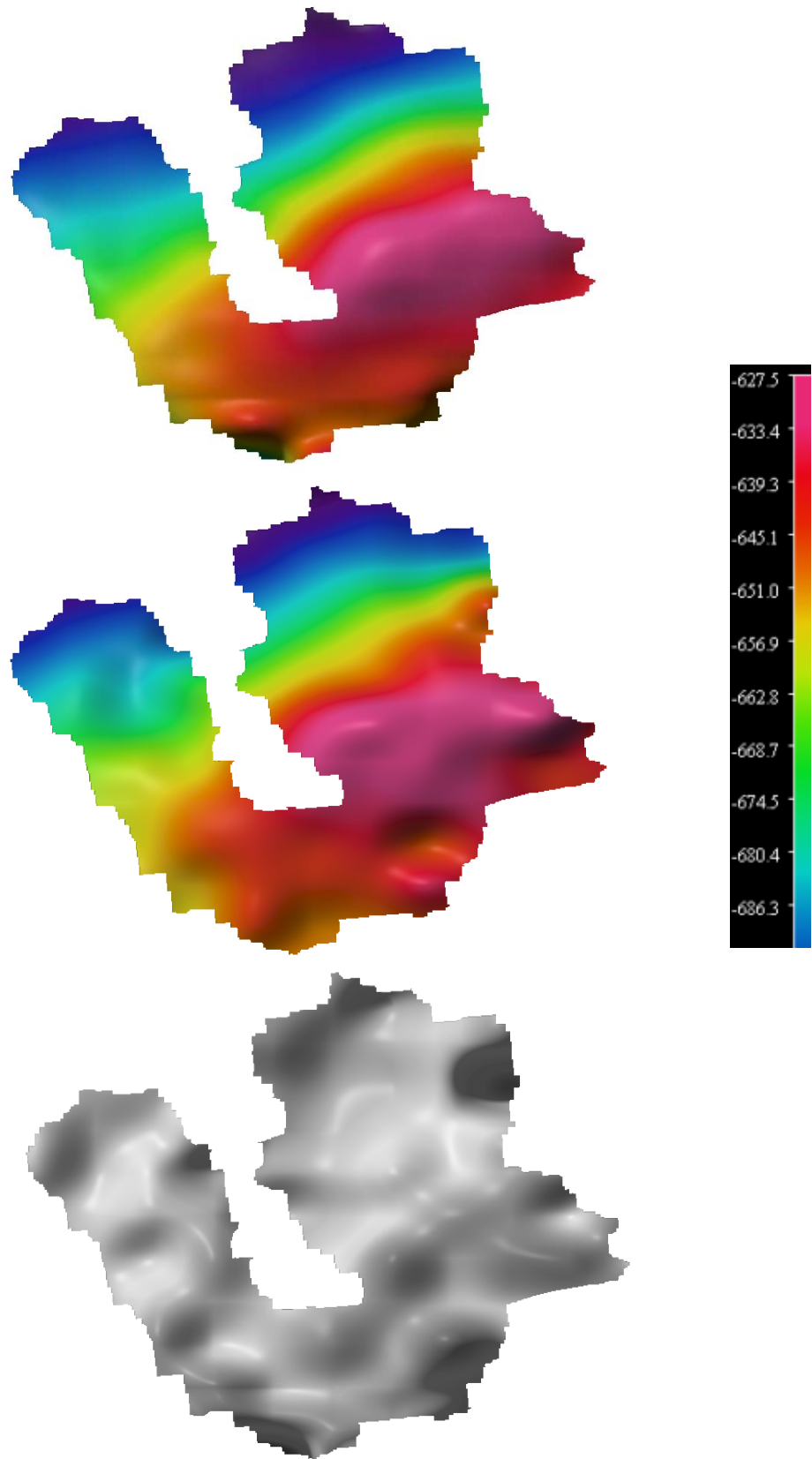


(TERRAMODEL)

APPENDIX G

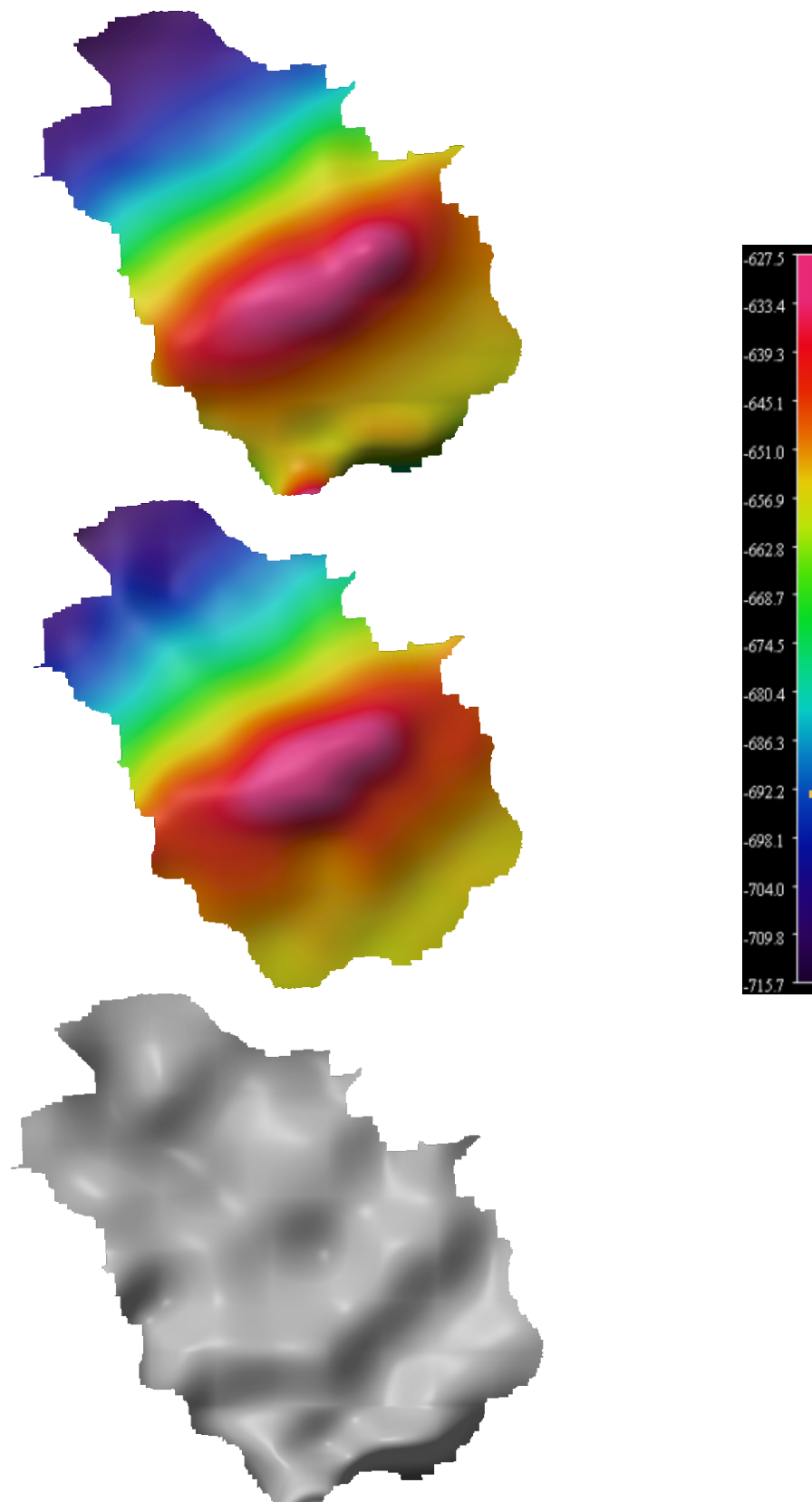
Visualisation of digital terrain models and their differences

SM2 – from top to bottom: EM 2000, HYDROSWEEEP, DIFFERENCE



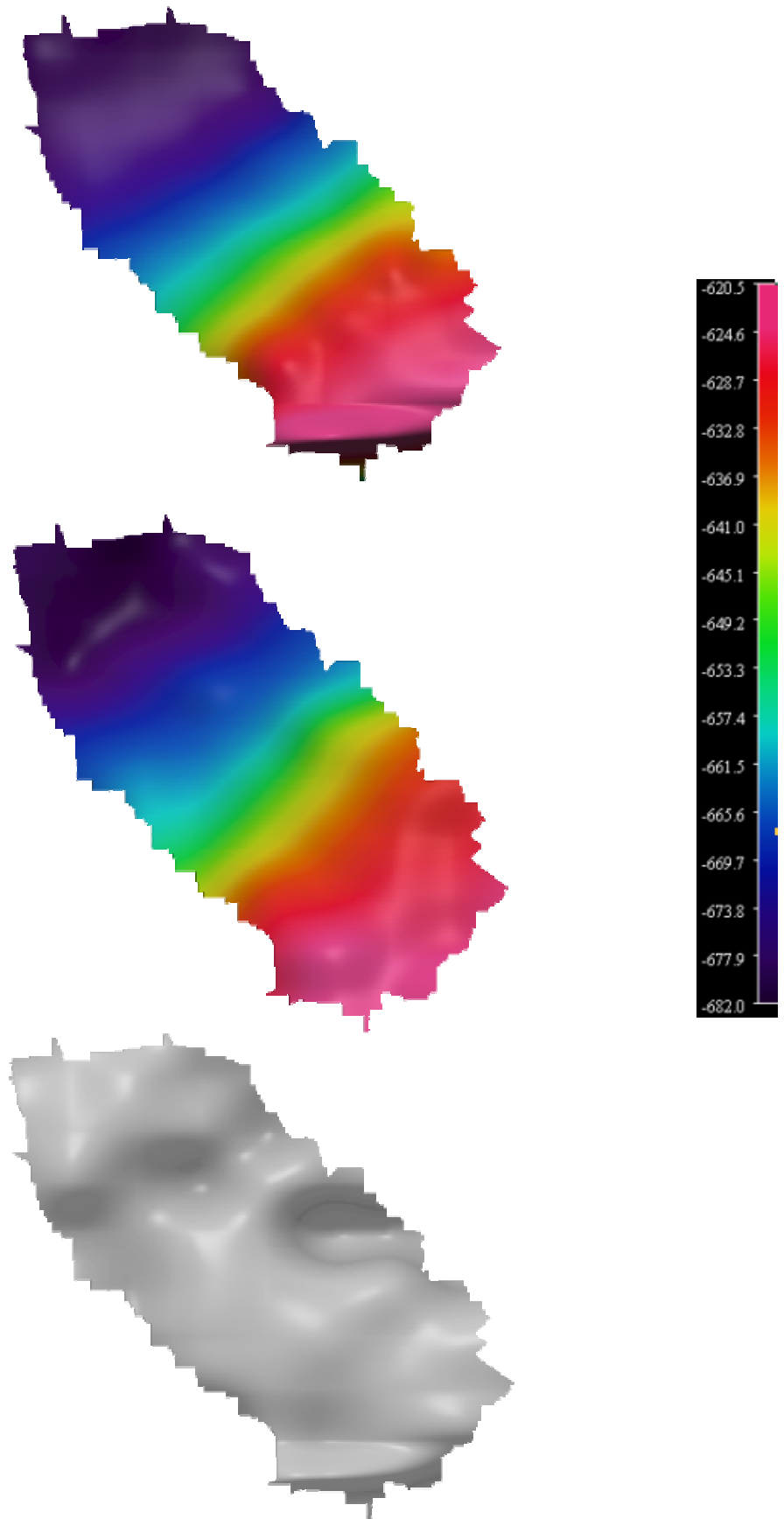
(FLEDERMAUS)

SM3 – from top to bottom: EM 2000, HYDROSWEEP, DIFFERENCE



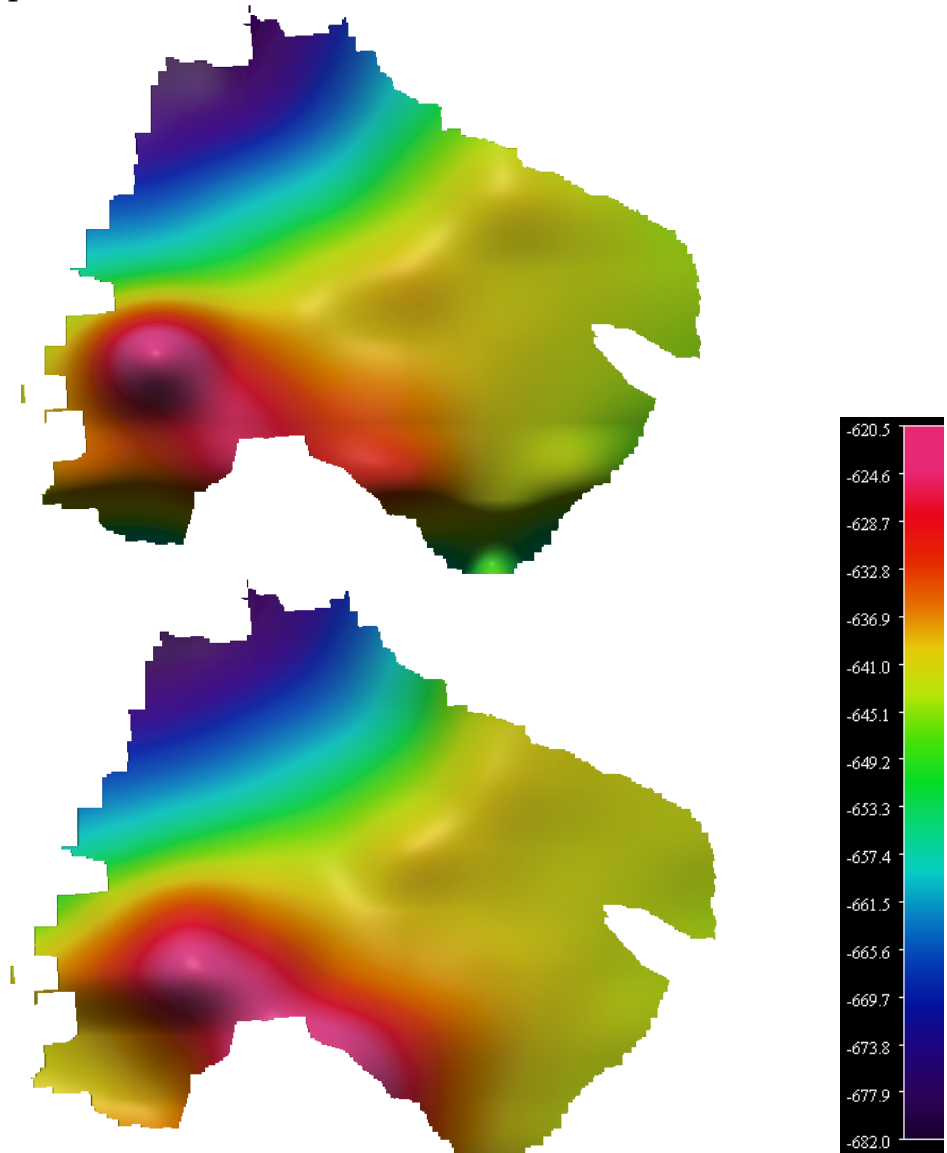
(FLEDERMAUS)

SM4 – from top to bottom: EM 2000, HYDROSWEEP, DIFFERENCE



(FLEDERMAUS)

HM2 – from top to bottom: EM 2000, HYDROSWEEEP, DIFFERENCE



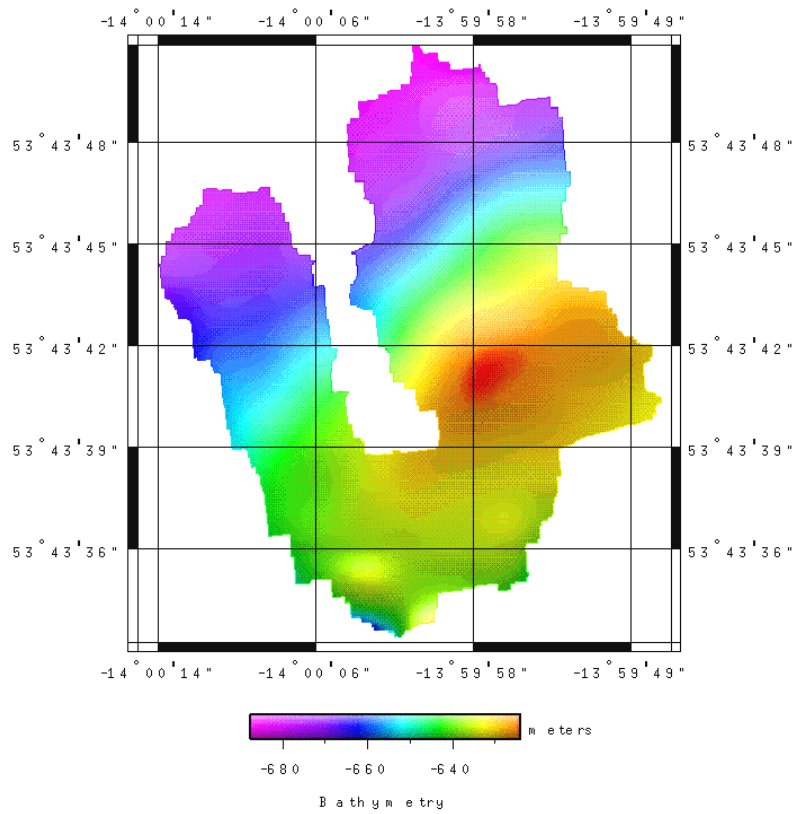
(FLEDERMAUS)

APPENDIX H

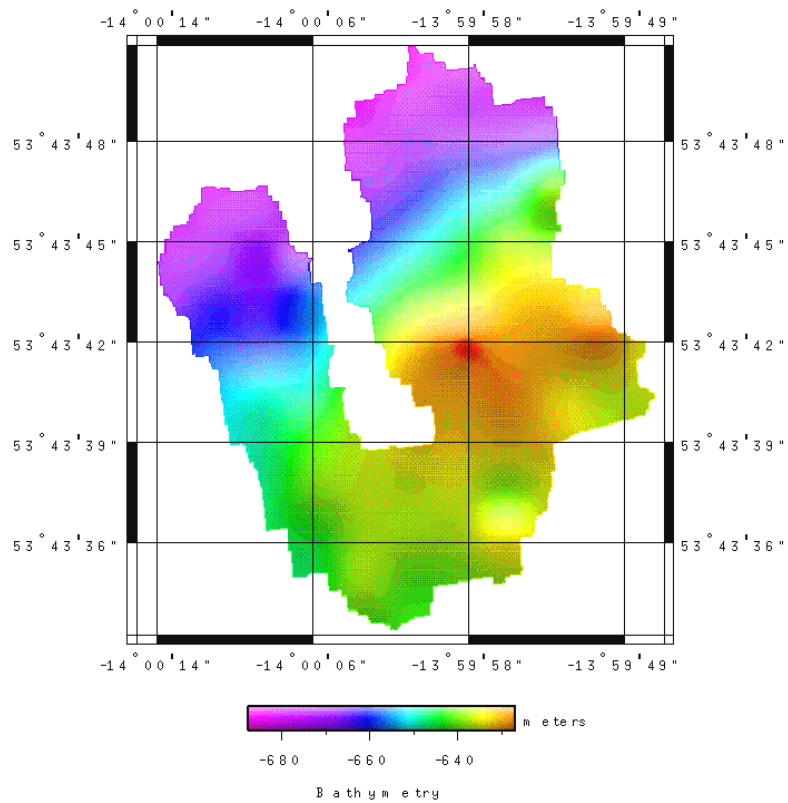
Digital terrain models – GMT software

Scarp Mound SM2

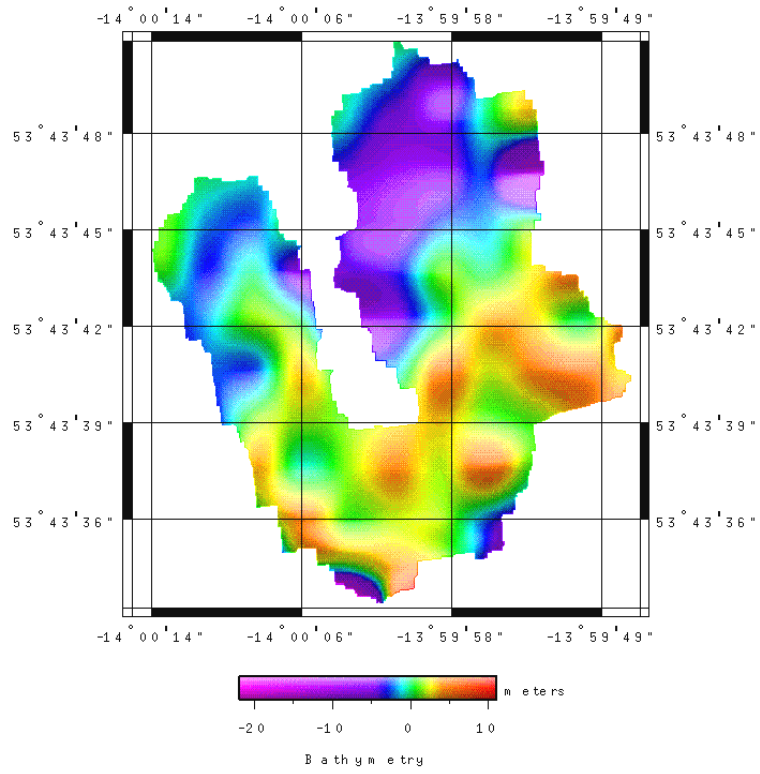
EM 2000



HYDROSWEEP DS-2

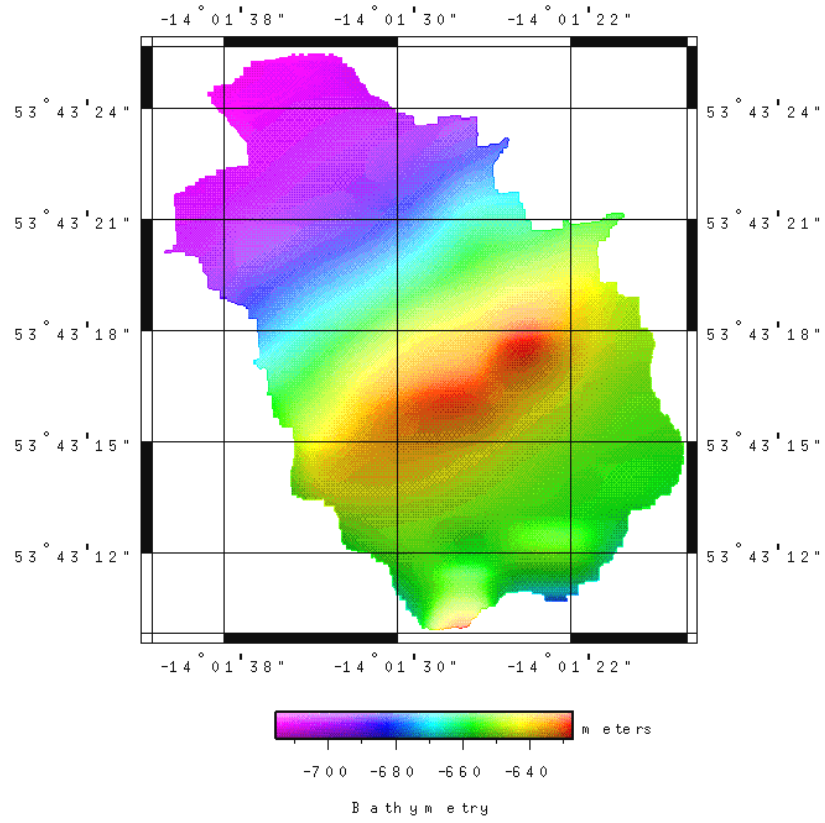


Difference SM2

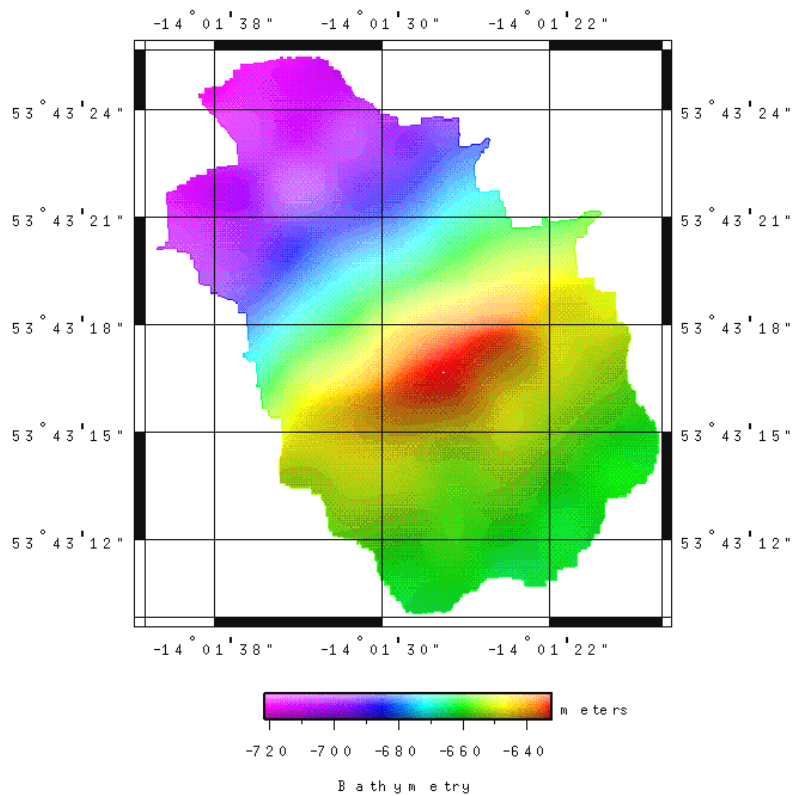


Scarp Mound SM3

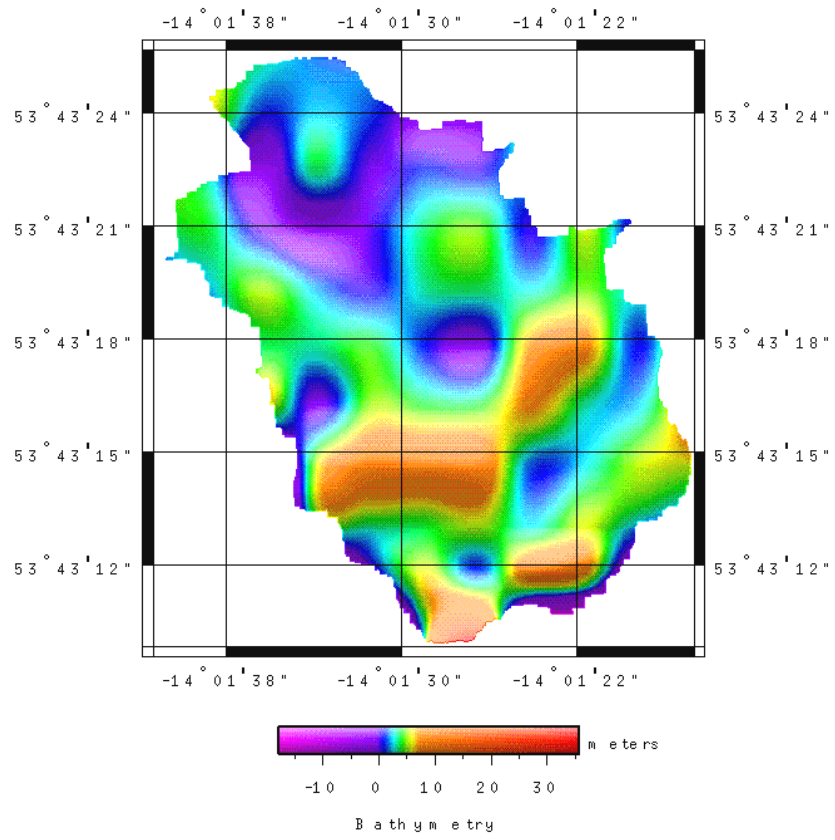
EM 2000



HYDROSWEEP DS-2

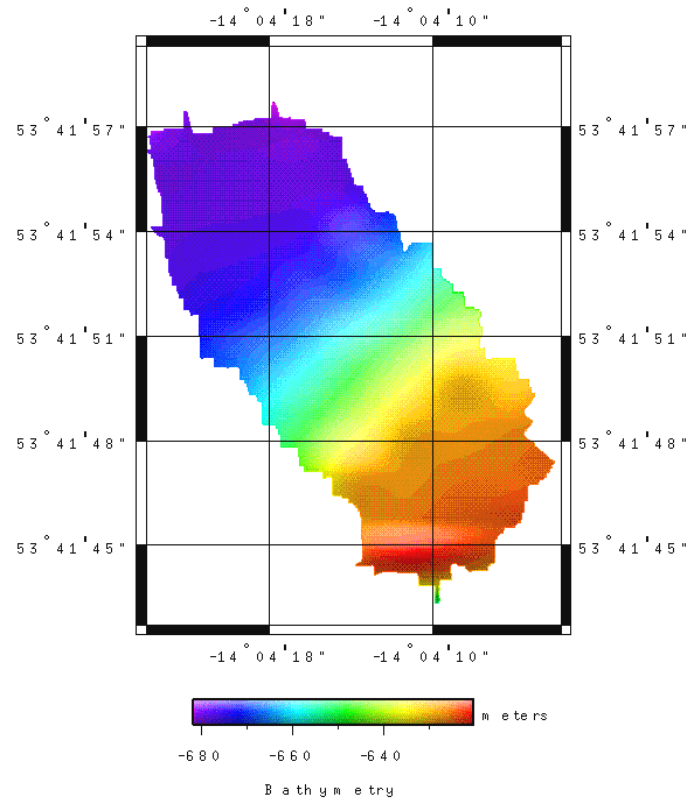


Difference SM3

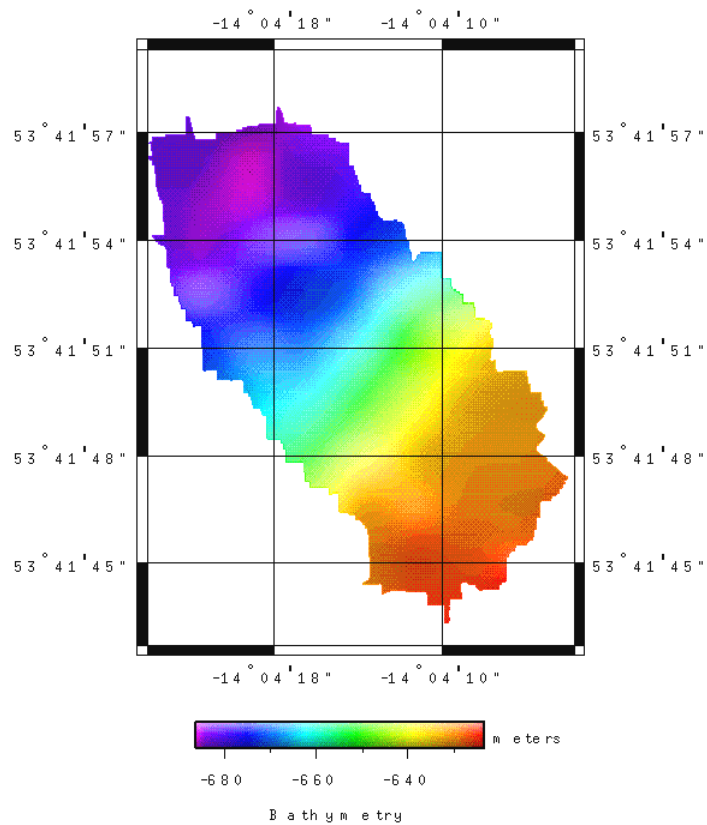


Scarp Mound SM4

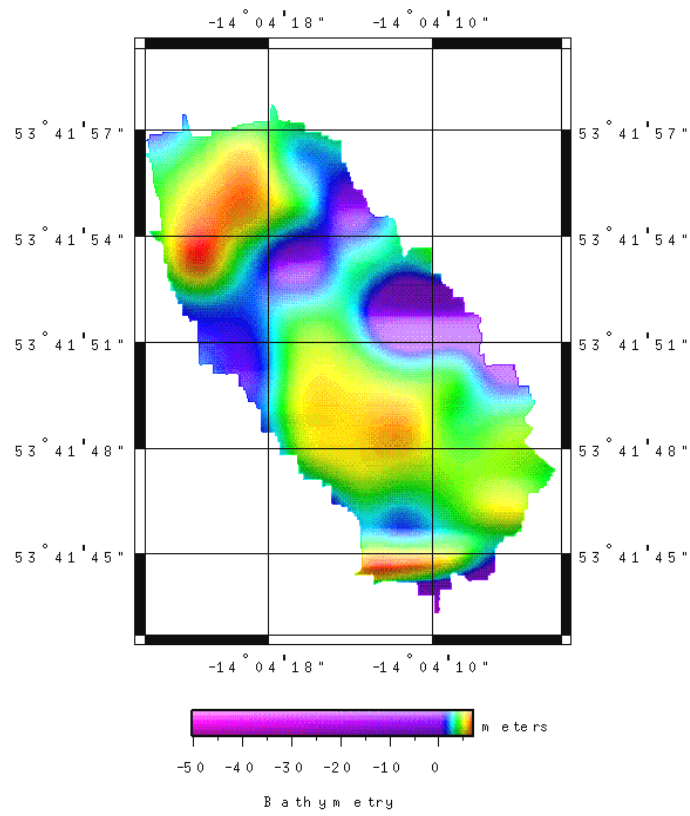
EM 2000



HYDROSWEEP DS-2

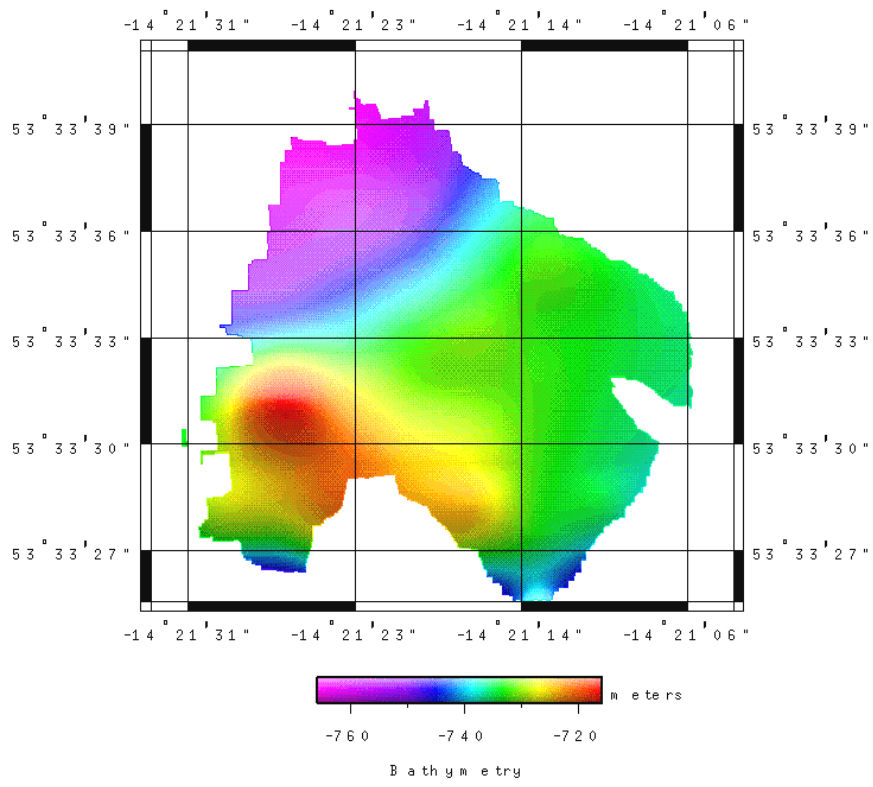


Difference SM4

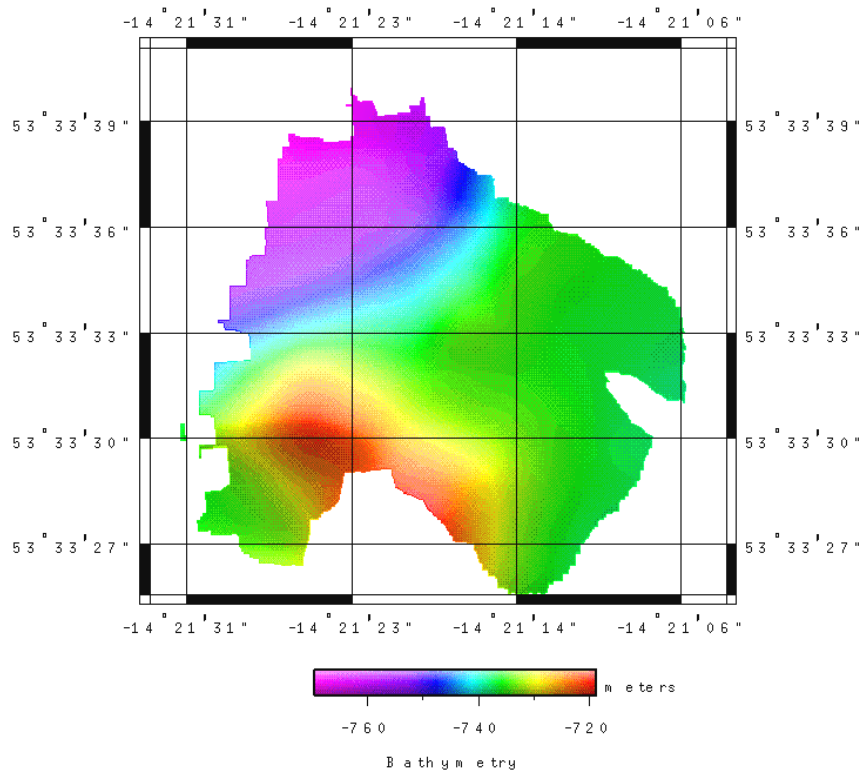


Hedge Mound HM2

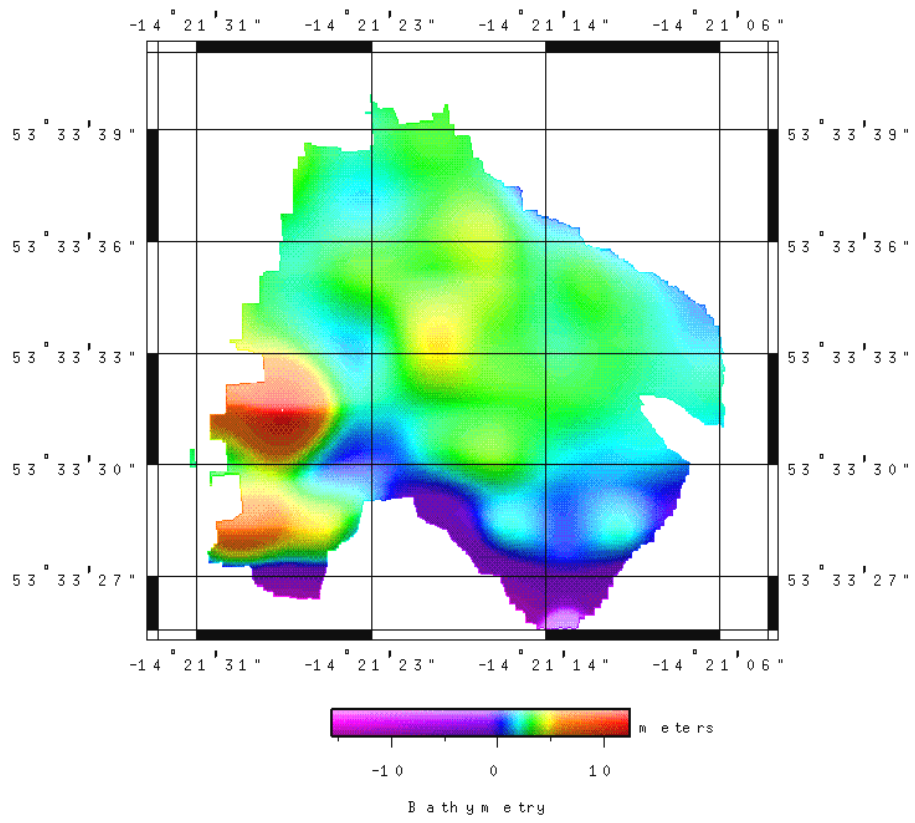
EM 2000



HYDROSWEEP DS-2



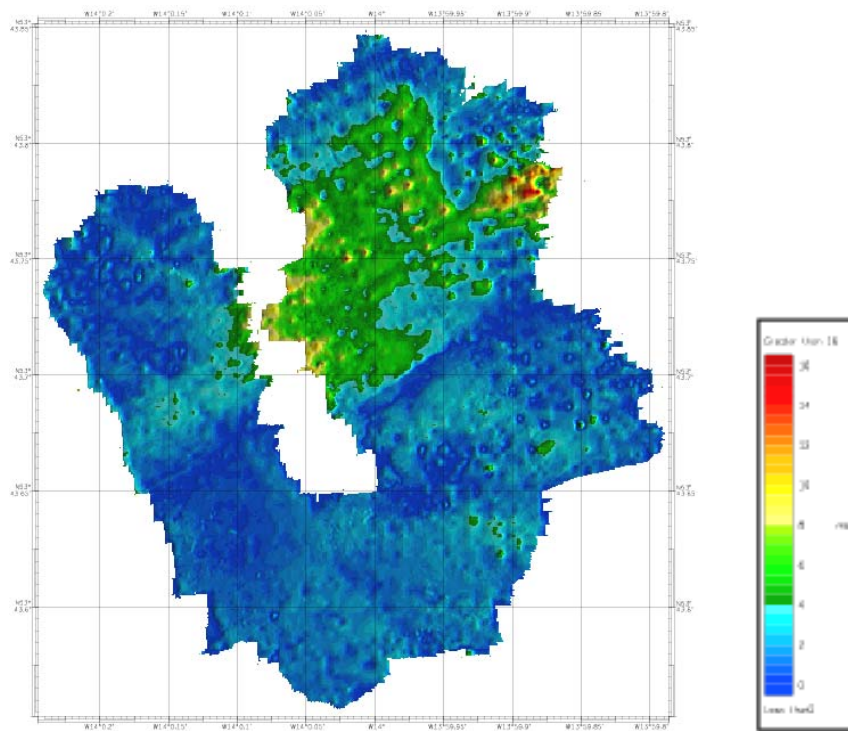
Difference HM2



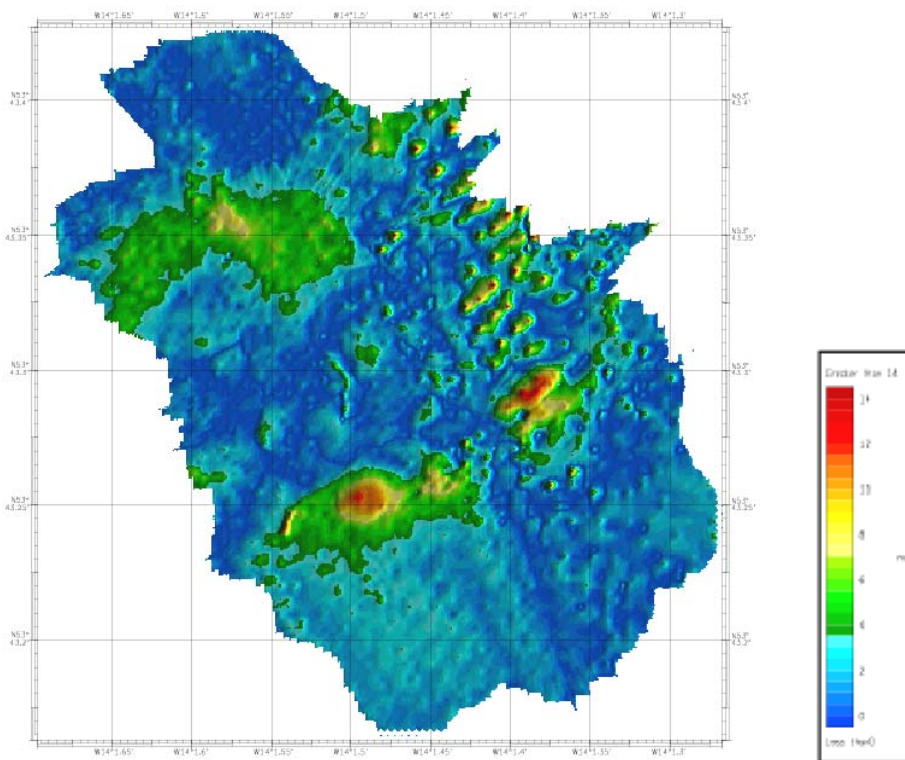
APPENDIX I

Difference grids - CARAIBES software

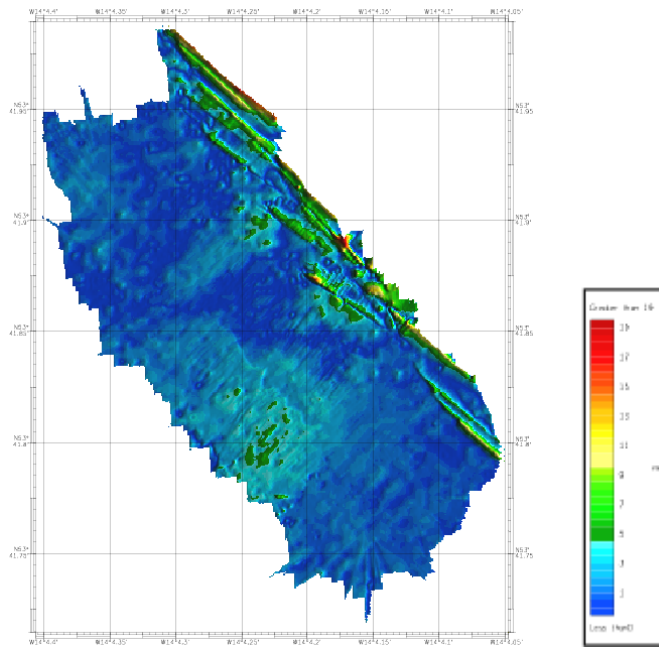
Difference SM2



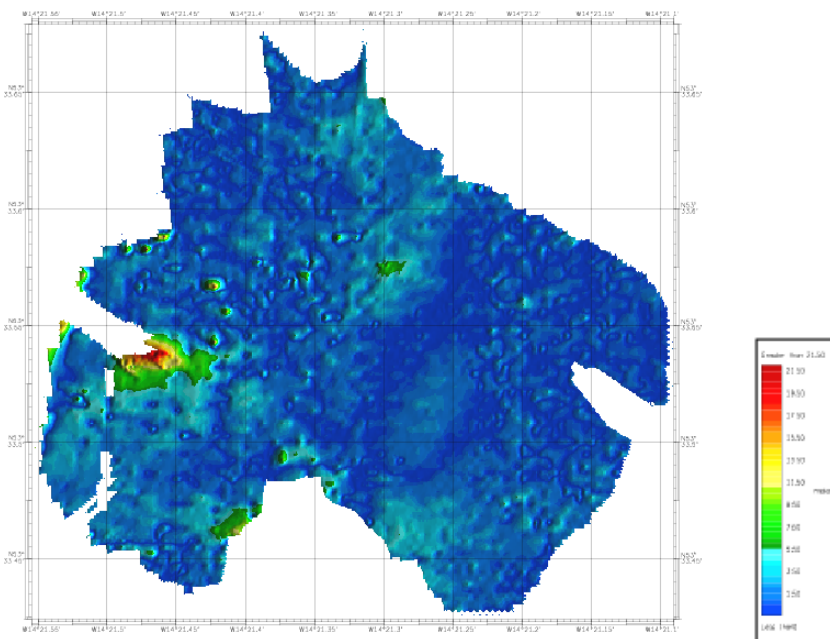
Difference SM3



Difference SM4



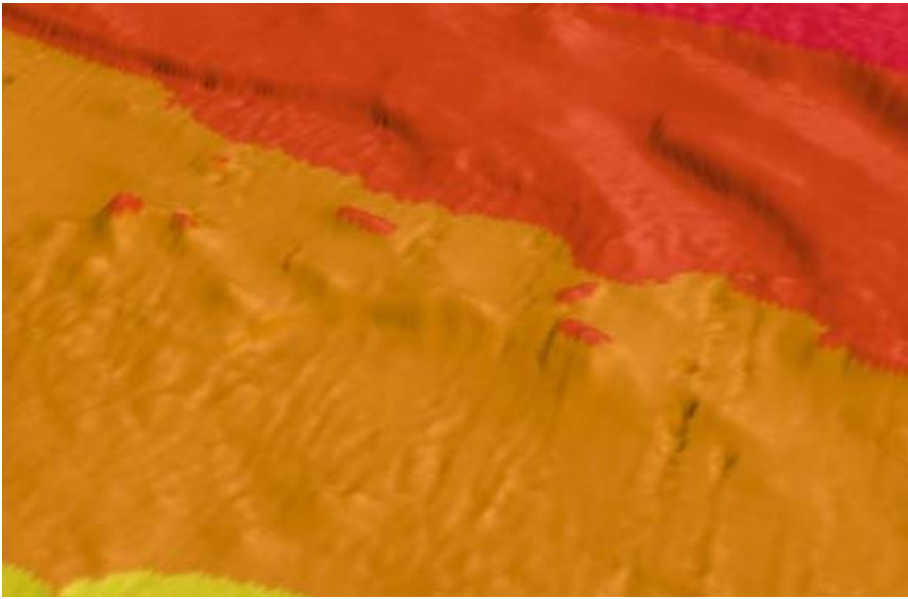
Difference HM2



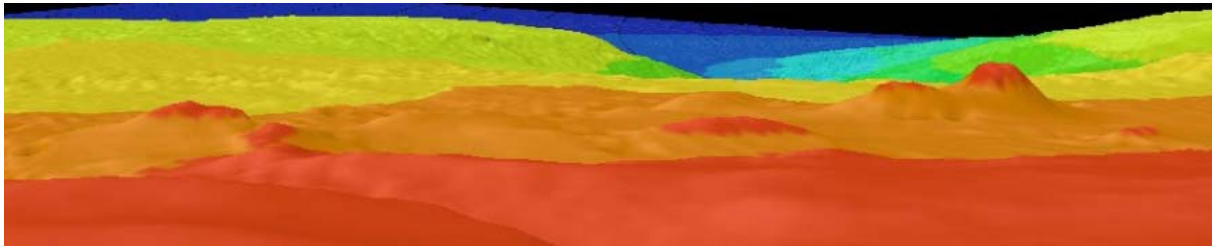
APPENDIX J

Digital terrain models provided by GSI

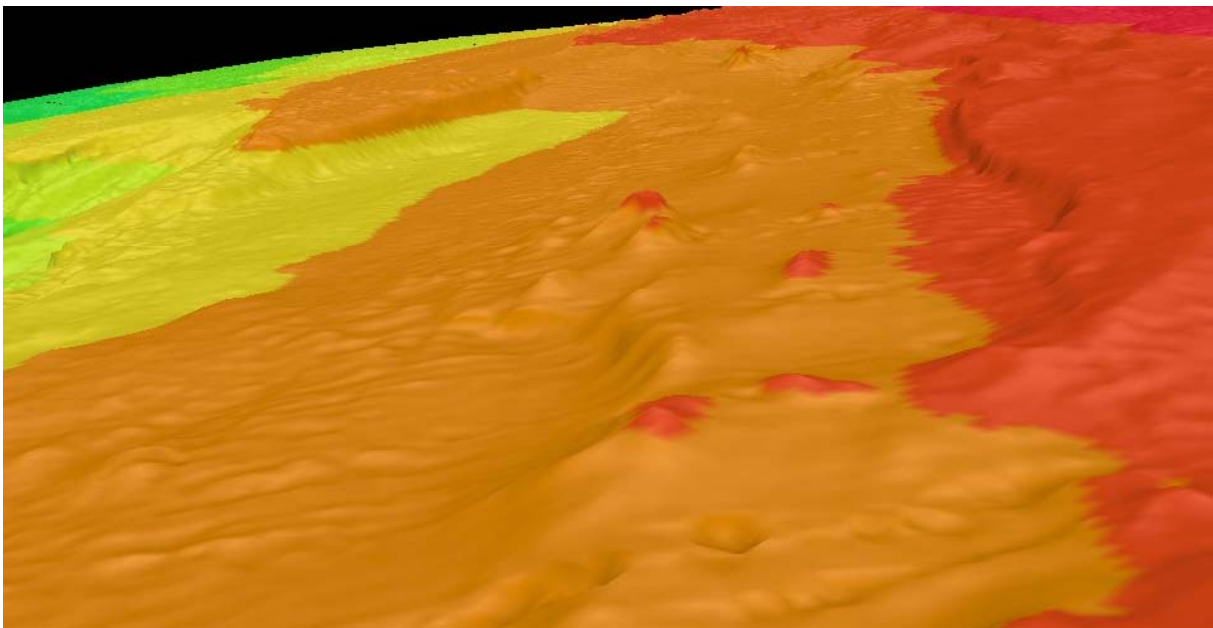
Scarp Mounds



Scarp Mounds from west



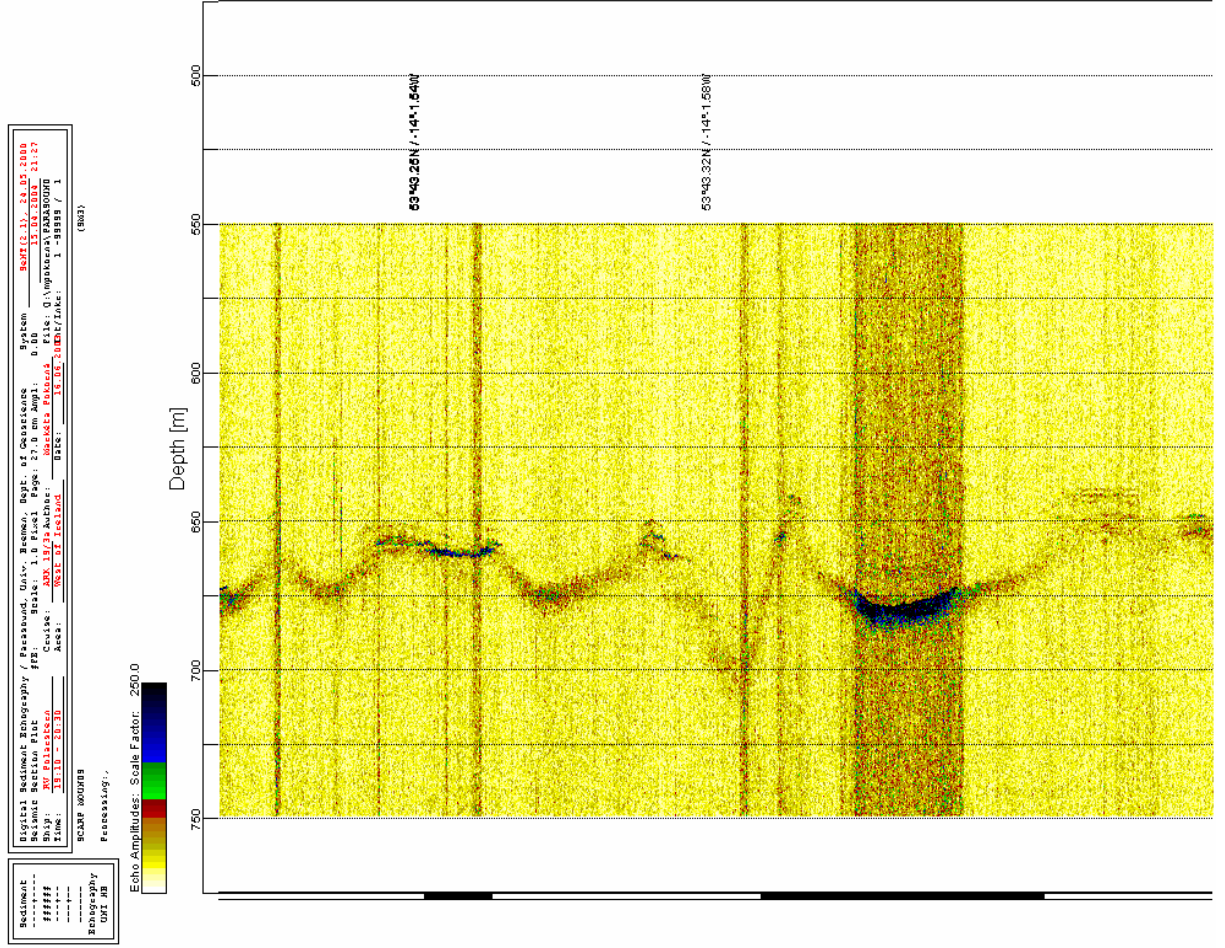
Scarp Mounds from south



APPENDIX K

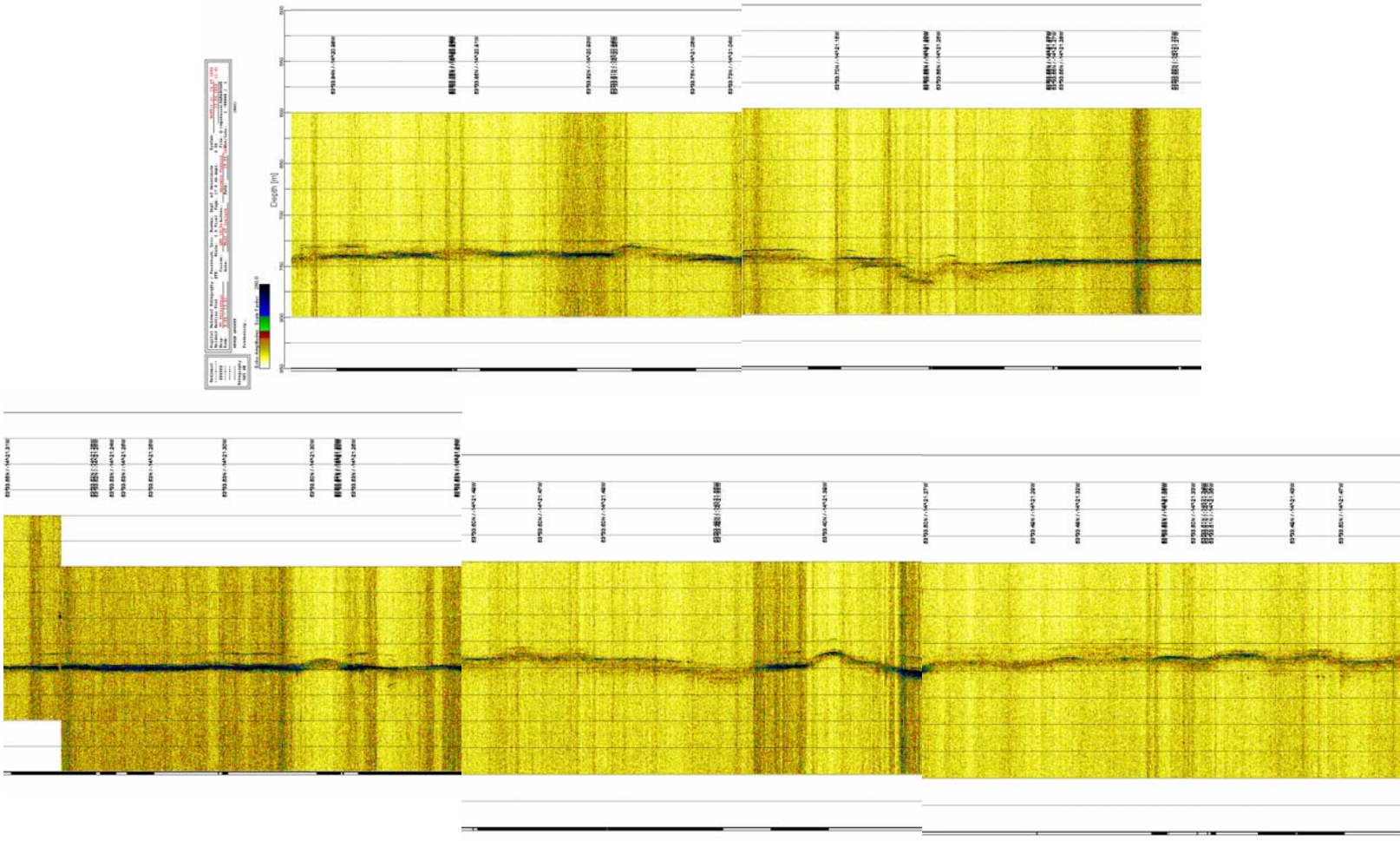
PARASOUND data images

Scarp Mound SM3



(SENT)

Hedge Mound HM2 – I,II,III,IV,V

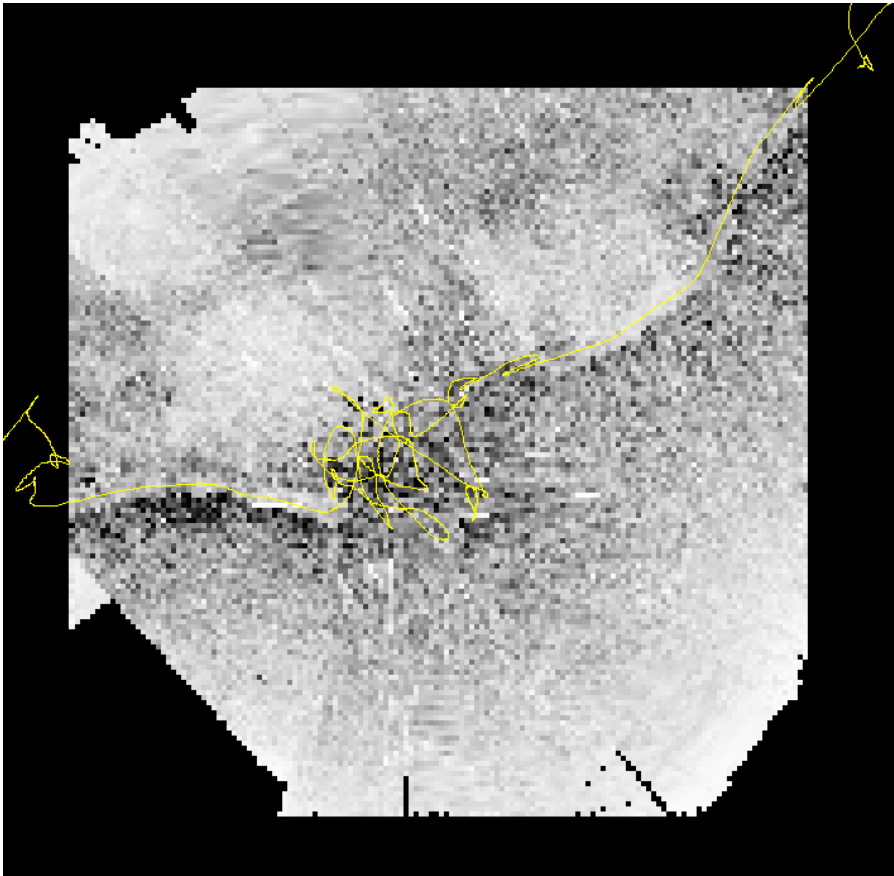


(SENT)

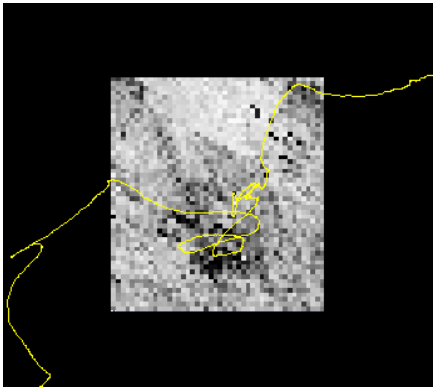
APPENDIX L

Sidescan images

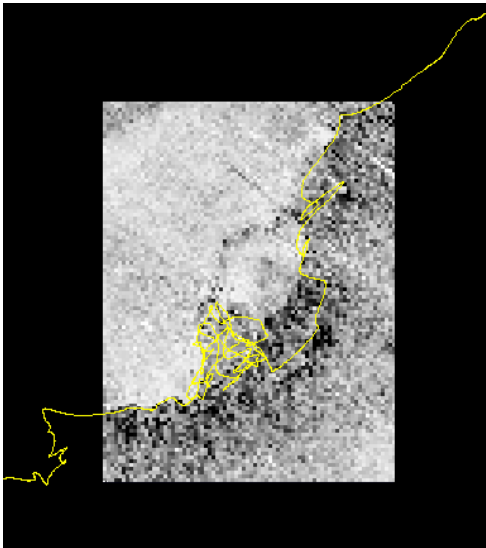
Scarp Mound SM2



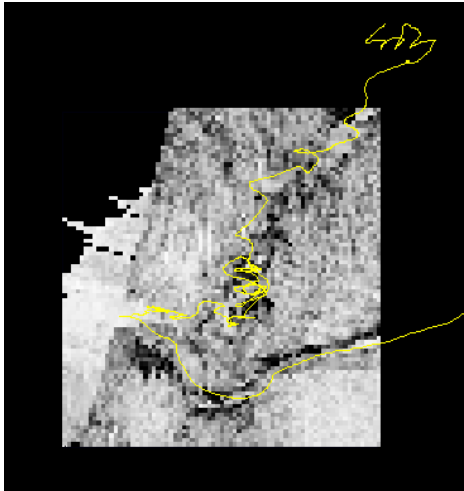
Scarp Mound SM3



Scarp Mound SM4



Hedge Mound HM2



APPENDIX M

Mosaicking images

Scarp Mounds

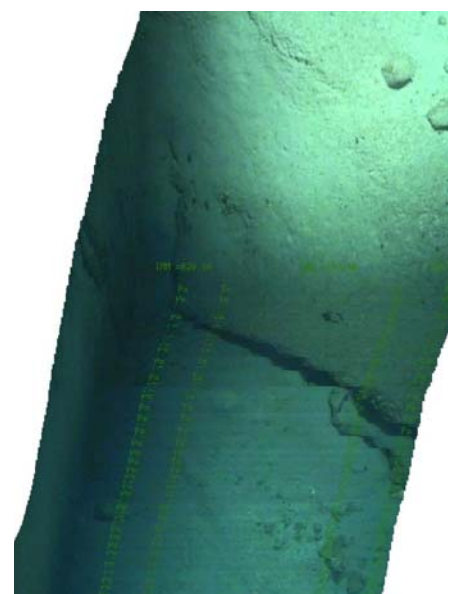
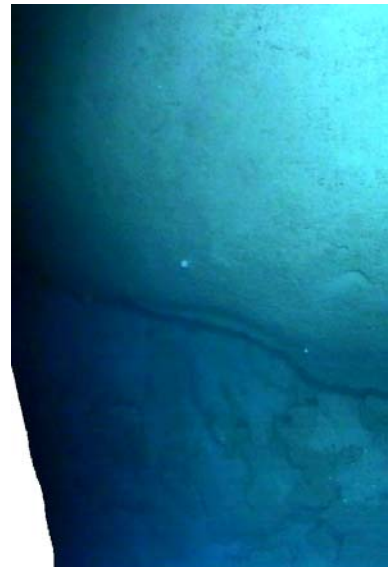
16.6.03, dive 217, S10s, 14:33UTC
(first)

16.6.03, dive 217, S10s, 5:02UTC
(second)

16.6.03, dive 217, S10s, 14:13UTC
(third)

L = length in minutes

S = snapshot every X second



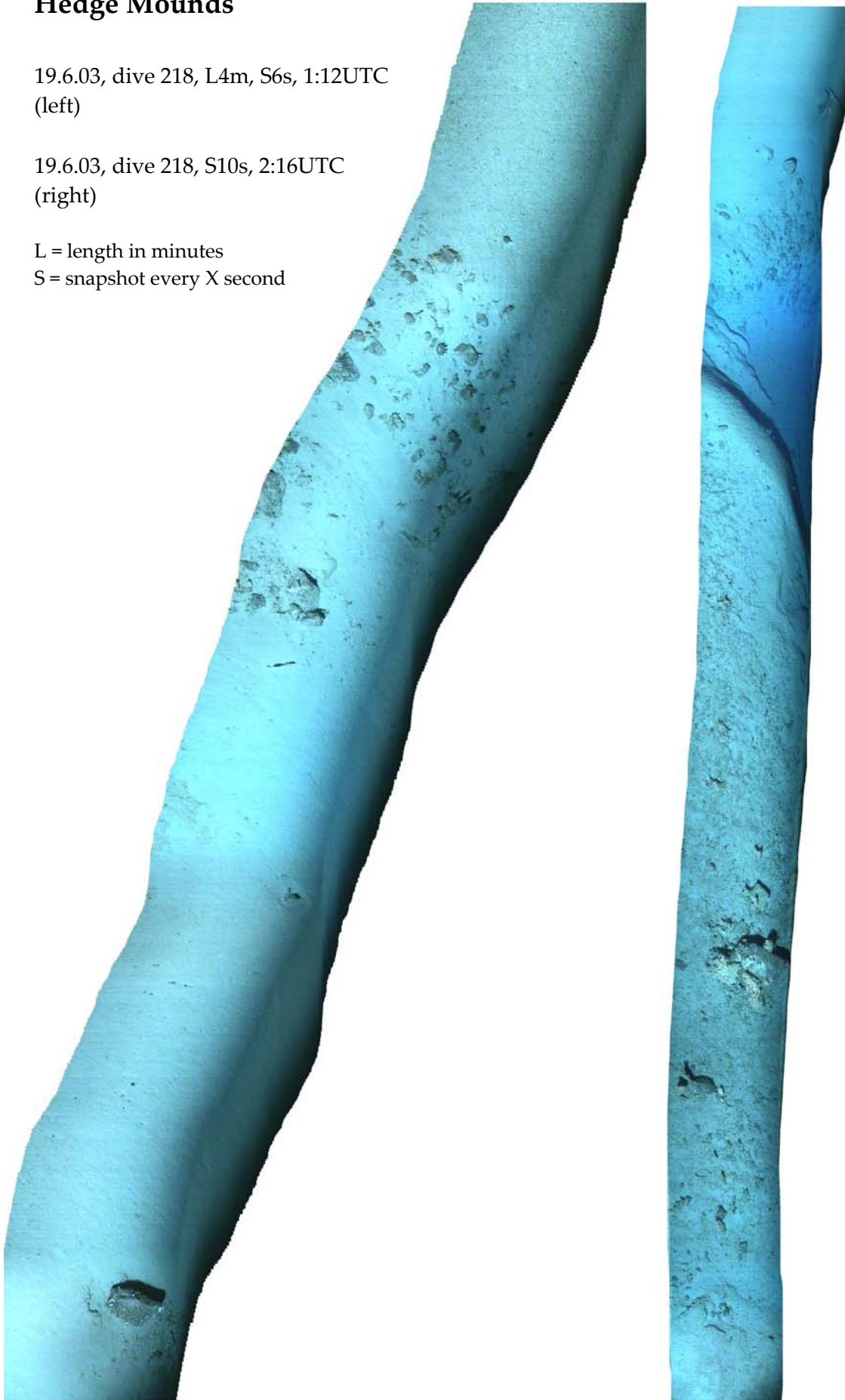
Hedge Mounds

19.6.03, dive 218, L4m, S6s, 1:12UTC
(left)

19.6.03, dive 218, S10s, 2:16UTC
(right)

L = length in minutes

S = snapshot every X second



Hedge Mounds

19.6.03, dive 218, L3m,S10s, 1:49UTC
(left)

19.6.03, dive 218, S10s, 2:15UTC
(right)

L = length in minutes
S = snapshot every X second



